JAEA-Conf 2013-002
INDC(JPN)-198

JAEA-Conf

Proceedings of the 2012 Symposium on Nuclear Data

November 15-16, 2012, Research Reactor Institute, Kyoto University, Kumatori, Japan

(Eds.) Ken NAKAJIMA, Osamu IWAMOTO, Jun-ichi HORI, Nobuyuki IWAMOTO
Shoji NAKAMURA and Hiroyuki KOURA

Nuclear Science and Engineering Directorate

October 2013

Japan Atomic Energy Agency

日本原子力研究開発機構

本レポートは独立行政法人日本原子力研究開発機構が不定期に発行する成果報告書です。
本レポートの入手並びに著作権利用に関するお問い合わせは、下記あてにお問い合わせ下さい。
なお、本レポートの全文は日本原子力研究開発機構ホームページ（http://www.jaea.go.jp）
より発信されています。

独立行政法人日本原子力研究開発機構　研究技術情報部　研究技術情報課
〒319-1195　茨城県那珂郡東海村白方白根 2 番地 4
電話 029-282-6387, Fax 029-282-5920, E-mail:ird-support@jaea.go.jp

This report is issued irregularly by Japan Atomic Energy Agency.
Inquiries about availability and/or copyright of this report should be addressed to
Intellectual Resources Section, Intellectual Resources Department,
Japan Atomic Energy Agency.
2-4 Shirakata Shirane, Tokai-mura, Naka-gun, Ibaraki-ken 319-1195 Japan
Tel +81-29-282-6387, Fax +81-29-282-5920, E-mail:ird-support@jaea.go.jp

JAEA-Conf 2013-002
INDC(JPN)-198

Proceedings of the 2012 Symposium on Nuclear Data November 15-16, 2012, Research Reactor Institute, Kyoto University, Kumatori, Japan

(Eds.) Ken NAKAJIMA[*] , Osamu IWAMOTO, Jun-ichi HORI[*], Nobuyuki IWAMOTO, Shoji NAKAMURA and Hiroyuki KOURA[+]

Nuclear Science and Engineering Directorate
Japan Atomic Energy Agency
Tokai-mura, Naka-gun, Ibaraki-ken

(Received July 8 , 2013)

The 2012 symposium on nuclear data organized by the Nuclear Data Division of Atomic Energy Society of Japan (AESJ) and Research Reactor Institute, Kyoto University (KURRI) was held at Kumatori, KURRI on Nov. 15th and 16th, 2012 in cooperation with Nuclear Science and Engineering Directorate of Japan Atomic Energy Agency. The symposium was devoted for presentations and discussions on the four topics: " Nuclear Power after Fukushima Nuclear Plant Accident", "Application of Nuclear Data", "How Should We Deal with Covariances of Nuclear Data? " and " Validation of JENDL-4.0 and Future ", as well as poster sessions on various research fields. Tutorials on neutron resonance capture and transmission analysis, international trend of nuclear data research were also given in the symposium. Talks as well as posters presented at the symposium aroused lively discussions among approximately 83 participants. This report consists of total 35 papers including 13 oral presentations and 22 poster presentations.

Keywords: Nuclear Data Symposium 2012, Nuclear Power after Fukushima Nuclear Plant Accident, Application of Nuclear Data, Covariances of Nuclear Data, Validation of JENDL-4.0

[+]Advanced Science Research Center
[*]Kyoto University

Organizers: K. Nakajima (Kyoto Univ., Chair), O. Iwamoto (JAEA, Vice-Chair), K. Kato (Hokkaido Univ.), Y. Miki (TEPSYS), J. Hori (Kyoto Univ.), I. Murata (Osaka Univ.), T. Hazama (JAEA), N. Iwamoto (JAEA), H. Koura (JAEA), S. Chiba (Tokyo Institute of Technology), S. Nakamura (JAEA), H. Harada (JAEA)

JAEA-Conf 2013-002
INDC(JPN)-198

2012年度核データ研究会報告集

2012年11月15日~ 11月16日、
京都大学原子炉実験所、大阪府泉南郡熊取町

日本原子力研究開発機構 原子力基礎工学研究部門

(編) 中島健[*] 、岩本修、堀順一[*]、岩本信之、中村詔司、小浦寛之[+]

(2013 年 7月 8日受理)

2012年度核データ研究会は、2012年11月15日から16日にかけて、熊取町の京都大学原子炉実験所にて開催された。本研究会は日本原子力学会核データ部会と京都大学原子炉実験所の主催、日本原子力研究開発機構原子力基礎工学研究部門の共催の下、4つのトピックス:「福島原発後の原子力」、「核データの応用」、「核データ誤差にどう取り組むか」、「JENDL-4.0の検証と今後に向けて」に関する講演・議論が行われるとともに、幅広い分野のポスター発表が行われた。さらに、中性子捕獲反応及び透過分析法や核データに係わる国際動向に関するチュートリアルも実施された。参加総数は83名で、盛況のうちに全日程を終えた。レポートは、同研究会における口頭発表13件とポスター発表22件を含む35件の全論文を纏めたものである。

原子力科学研究所(駐在) :〒319-1195 茨城県那珂郡東海村白方白根2-4
[+] 先端基礎研究センター
[*] 京都大学

Contents

目 次

This is a blank page.

1. Program of 2012 Symposium on Nuclear Data

Date : November 15(Thu) 13:00～16(Fri)17:15, 2012
Venue : Kyoto University Research Institute (Kumatori-cho, Sennan-gun, Osaka)
Host : Nuclear Data Division, Atomic Energy Society of Japan
& Kyoto University Research Reactor Institute
Co-host : Nuclear Science and Engineering Directorate of JAEA

Nov. 15 (Thursday)

11:00 – 12:00 Facility tour Registrants

13:00 –13:15 Opening Session K.Nakajima (Kyoto U.)

13:15 – 15:15
Session 1: **Nuclear Power after Fukushima Nuclear Plant Accident** 【Chair: I.Murata(Osaka U.)】

1.1 Electricity Planning in Japan by 2030 through Scenario Analysis [60] K.Ishihara (Kyoto U.)
1.2 Nuclear Data for Severe Accident Analysis and Decommissioning of Nuclear Power Plant [40] K.Okumura (JAEA)
1.3 Present Status of Research Reactor and Future Prospects [20] K.Nakajima (Kyoto U.)

15:15 – 15:35 Coffee Break & Group Photo [20]

15:35 – 17:20 Poster Presentation

17:30 – 19:30 Convivial Gathering

Nov. 16 (Friday)

09:00 – 10:30
Session 2: Application of Nuclear Data 【Chair: T.Hazama (JAEA)】

2.1 Present Status of BNCT at Kyoto University Research Reactor Institute [30] H.Tanaka (Kyoto U.)
2.2 Nondestructive Assay using Nuclear Resonance Fluorescence with Laser Compton Scattering Gamma-ray Beam for Safeguards and Key Nuclear Data [30] T.Hayakawa (JAEA)
2.3 Experiments on Accelerator Driven Subcritical System (ADS) and Nuclear Data for ADS Design [30] T.Misawa (Kyoto U.)

10:30 – 10:40 Coffee Break [10]

10:40 – 12:10
Tutorial 1: Neutron Resonance Analysis 【Chair: H.Harada (JAEA)】
Neutron Resonance Capture and Transmission Analysis P.Schillebeeckx (EC/JRC/IRMM)

12:10 –13:00 Lunch [50]

13:00 – 14:00
Tutorial 2: Trends of Foreign Nuclear Data Activity 【Chair: O.Iwamoto (JAEA)】

Research Experience in LANL [30] S.Kunieda (JAEA)
Introduction of Status of International Collaboration on Nuclear Data[30] T.Fukahori (JAEA)

14:00 – 14:05 Coffee Break [5]

14:05 – 15:25
Session 3: How should We Deal with Covariances of Nuclear Data? 【Chair: S.Nakamura (JAEA)】

3.1 Evaluation of Covariance Data of JENDL [20] O.Iwamoto (JAEA)
3.2 On the Uncertainty of Experimental Nuclear Data -Taking a lesson form the other- [20] H.Harada (JAEA)
3.3 Application of the Cross Section Covariance Data to Fast Reactor Core Design [20] K.Sugino (JAEA)
3.4 Uncertainty Evaluation for ^{244}Cm Production in Spent Fuel of Light Water Reactor by using Burnup Sensitivity Analysis [20] A.Oizumi (JAEA)

15:25 – 15:40 Coffee Break [15]

15:40 – 16:55
Session 4: Validation of JENDL-4.0 and Future 【Chair: S.Chiba (TIT)】

4.1 Validation of JENDL-4.0 and Future: Reactor Integral Test Working Group [25] G.Chiba (Hokkaido U.)
4.2 Activities of Covariance Utilization Working Group [25] K.Tsujimoto (JAEA)
4.3 A Working Group for Japanese Nuclear Data Measurement Network [25] Y.Watanabe (Kyushu U.)

16:55 – 17:15 Closing Session
Poster Award Nuclear Data Division, AESJ
Closing Address N.Yamano (Fukui U.)

Poster Presentation
Date : November 15 (Thursday), 15:35 – 17:20

1. New Extension of CCONE Code for Calculation of Deuteron-induced Reactions
   S.Nakayama (Kyushu U.)
2. Neutron Cross Section Sensitivity Analysis on UO_2 and MOX Cores in the MISTRAL Program
   T.Sakai (JNES)
3. Analysis of Nucleon and Triton Emissions via Breakup Process in Nucleon-induced Reactions on ^{6,7}Li H.Guo (Kyushu U.)
4. Neutron Total Cross-section Measurements on Sn and Ni using Pohang Neutron Facility
   A.Makinaga (Hokkaido U.)
5. Activation Analysis for Accelerator Structural Materials by the 5-9MeV Deutron Beam Loss
   S.Maebara (JAEA)
6. Activation Analysis of Air in the Accelerator Vault of LIPAc Building by Deuteron Beam at 5 MeV and 9 MeV H.Takahashi (JAEA)
7. Validation of CBZ Code System for Post-Irradiation Examination Analysis and Sensitivity Analysis of (n,γ) Branching Ratio Y.Kawamoto (Hokkaido U.)
8. GEANT4 Simulation Study of a Gamma-ray Detector for Neutron Resonance Densitometry
   H.Tsuchiya (JAEA)
9. Asian Collaboration on Nuclear Reaction Data Compilation M.Aikawa (Hokkaido U.)
10. JENDL-4.0 Benchmarking For Effective Delayed Neutron Fraction with a Continuous-energy Monte Carlo Code MVP Y.Nagaya (JAEA)
11. Measurement of Neutron Capture Cross Section of ^{142}Nd with the Accurate Neutron-Nucleus Reaction Measurement Instrument (ANNRI) at J-PARC T.Matsuhashi (TIT)
12. Measurement of 100 MeV/u Carbon Incident Neutron Production Cross Sections on a Carbon Target N.Shigyo (Kyusyu U.)
13. Evaluation of Neutron Induced Reaction Cross Sections on Re Isotopes N.Iwamoto (JAEA)
14. Influence of Difference in Nuclear Data Libraries on Important Back-end Parameters
    S.Yoshida (Hokkaido U.)
15. Study on keV-neutron Capture Cross Sections and Capture Gamma-ray Spectra of Pd Isotopes
    K.Terada (TIT)
16. Measurements and Simulations of the Responses of the Cluster Ge Detectors to Gamma Rays
    K.Y.Hara (JAEA)
17. Development of keV Region Neutron Spectrometer using ^{3}He Proportional Counter
    T.Obata (Osaka U.)
18. Cross section Measurement of ^{117}Sn(n,γ) using ANNRI-NaI(Tl) Spectrometer at J-PARC
    K.Hirose (JAEA)
19. Estimation of Reaction Rate in Subcritical System by Gamma Ray Spectrum Measurement
    Y.Nauchi (CRIEPI)
20. Target Dependency of Light Mass Fragment Production DDX for 6 MeV/u Carbon Induced Reaction T.Sanami (KEK)
21. Validity of Covariance Data of ^{232}Th in JENDL-4.0 and ENDF/B-VII.1
    T.Kojima (Osaka U.)
22. Measurement of High Energy Neutron Induced Cross Sections for Terbium H.Suzuki (Kyoto U.)

This is a blank page.

2. Electricity Planning in Japan by 2030 through Scenario Analysis

Keiichi N. Ishihara[1], Zhang Qi[1], Benjamin C. Mclellan [1],
and Tetsuo Tezuka[1]

[1] Graduate School of Energy Science, Kyoto University, Yoshida Honmachi, Sakyo-ku, Kyoto 606-8501, Japan
E-mail: Ishihara@energy.kyoto-u.ac.jp

Under continuing policies of the mitigation of GHG (Green House Gases) emission, it is crucial to consider scenarios for Japan to realize a safe and clean future electricity system after the Fukushima nuclear accident. The development plans of nuclear power and renewable energy - mainly PV and wind power - need to be reconsidered. Therefore, in the present study, three electricity supply scenarios in 2030 are proposed according to different future nuclear power development strategies: (1) negative nuclear power; (2) conservative nuclear power; and (3) active pursuit of nuclear power. On the other side, three electricity demand scenarios are also proposed considering energy saving. The purpose of the study is to propose electricity supply systems with maximum renewable energy penetration under different nuclear power development strategies and demand situations through scenario analysis. The scenario analysis is conducted using an input-output hour-by-hour simulation model subject to constraints from technological, economic and environmental perspectives. The obtained installed capacity mix, power generation mix and CO_2 emissions of the scenarios were compared and analyzed with each other and with historical data. The results show that (1) penetration level of renewable energy is subject to the share of nuclear power as base load; (2) it is very difficult to remove nuclear power absolutely from the electricity system even when a high level of penetration of renewable energy is realized; (3) high level penetration of renewable energy can reduce the dependence on nuclear and thermal power, but there is a need for more flexible power sources to absorb fluctuations; (4) CO_2 emissions reduction compared to 1990 levels can be readily achieved with the help of renewable energy, nuclear power and energy saving in 2030. This is a revised version of the paper that was published in [1].

1. Introduction

Electricity supply in Japan was highly dependent on nuclear power, which provided about 31% of their electricity demand in 2010 using a total of 54 nuclear power plants (NPP). Nuclear power was expected to reach 68GW installed capacity and contribute 40% electricity generation by 2030 under the Strategic Energy Plan (SEP) released by the government in 2010 [2]. However, all of the nuclear power reactors in the Kanto and Tohoku areas stopped when they were hit by the 9.0-magnitude earthquake and subsequent tsunami on March 11, 2011. Subsequent coolant losses in the reactors and spent fuel ponds at the Fukushima Daiichi power plant led to hydrogen explosions, fuel rod meltdown, contamination of the local environment and evacuation of local residents. It is quite certain that at least four of the six nuclear reactors at Fukushima Daiichi will be closed permanently, and the remaining stopped reactors are unlikely to resume operation in the near future in light of public concern [3]. After the accident, it takes more time for the regular inspections in every nuclear power plant in Japan. It leads to serious electricity shortage in Kansai, Chubu and Kyushu areas. The Fukushima nuclear accident changed the electricity supply structure dramatically.

However, from a long-term viewpoint, apart from the safety issues of nuclear power, Japan also faces very serious energy security problem, global warming pressure and renewable energy penetration bottlenecks from technological, systemic and economic perspectives. Energy supply in Japan is 96% dependent on imports [4],

and the price of energy resources is still increasing in international markets [5]. The domestic CO_2 emissions in Japan have increased by 20% compared to 1990 levels in the electricity generation sector up to 2009 [6]. Therefore, building new coal-fired and oil-fired power plants seems to be an undesirable choice even in an electricity shortage situation. On the other hand, renewable energy - mainly including PV and wind power - the potential is limited in Japan due to physical-geographic reasons and constraints in technology and system integration [7]. Therefore it is crucial to reconsider the energy policy across the whole country in the mid-to-long term to realize a future clean and safe electricity system considering constraints from various perspectives.

Some previous studies focused on the impact of the phase-out of nuclear power in the energy system in Japan [8][9], however renewable energy penetration and subsequent excess electricity issues were not considered. The excess power issue with renewable energy penetration has been studied particularly in Europe, however, excess power in those studies has been mainly due to a large proportion of combined heat and power (CHP) being used to supply heat and electricity simultaneously during cold weather [10][11]. Furthermore, there is good inter-connectivity in the European electricity grid which can buffer the effects of excess electricity production. In Japan, the situation is quite different, there is no inter-connection with other countries and even inside, the grid is separated into two parts by its frequency (50 and 60Hz). Then, excess power occurrences with high penetration of renewable energy are due to the electricity system being based on nuclear power without load-following operation.

This study presents scenario analysis of the Japanese electricity system in 2030, after the Fukushima nuclear accident using a model, which incorporates aspects of resource availability, technology, economy and environment. The study focuses on the electricity demand-supply balance, and all the scenarios are analyzed and compared from multiple aspects. Nuclear reactors considered in this study would be new generation technology that incorporates “passive” safety features intended to avoid disasters like the one in Fukushima. In the event of an accident, the reactor relies on natural forces such as gravity and condensation to help keep its nuclear fuel from dangerously overheating—features the Fukushima plant lacked. Furthermore, very high standard anti-earthquake (and tsunami) technologies will be employed in nuclear power plants in the future.

2. Scenario Analysis Methodology

In the scenario analysis on supply-demand in electricity system, installed capacities of nuclear power and thermal power are decided by their development strategy and their stipulated lifetime, and thus given as preconditions, which will be introduced in the following section in details.

In this study, the scenario analysis is conducted based on both supply and demand sides. And the matches between different supply and demand options are discussed based on the obtained simulation results and the values of performance indicators.

In details, the purpose of the comparative analysis on multiple electricity supply-demand scenarios in Japan in this study is to understand the following issues:

(1) the constraints of the penetration of renewable energy from system integration aspect in term of the occurrence of excess electricity;

(2) the role of nuclear power in the whole system and whether or not it can be removed;

(3) contribution of renewable energy in different scenarios;

(4) CO_2 emissions reduction compared to 1990 level in environmental aspect.

The scenario analysis was conducted by the following scheme. It is organized in an “Input-Output” framework and realized by hour-by-hour demand-supply balance computer simulation. The arrows in the figure show the data flow direction. Main data inputs are demand, solar irradiation, wind speed, fuel supply, installed capacity, CO_2 emission factor and basic cost information (for full list see tables in following sections). Main rules inputs are classed into technological, economic and environmental perspectives, with emphasis on

prohibition of blackout, generation priority of power sources, upper limitation of excess electricity, range of capacity factor, cost and CO_2 emission constraints respectively. Outputs are mainly energy balances and resulting annual productions, fuel consumption, total/average cost, total/average CO_2 emission, etc. The explanations of the main contents in "Data" and "Rule" will be given in details in the following sections.

Previously, many models have been proposed and developed for the energy (electricity) mix with renewable energy penetration [12][13]. Some of them are based on hour by hour simulation [14][15]. However, the model used in the present study is unique in that focuses on nuclear power based electricity system to integrate renewable power in Japan, and the purpose of analysis is not only economic (investment) performance, but also CO_2 emissions and energy supply security are considered.

The methodology has been developed as operable computer software using Visual Studio C#.net 2008 [16], and the database is managed using Microsoft Excel 2007. In the developed software platform, the data can be easily read from and written in database through ADO.net [17]. When the hour-by-hour simulation is finished, the obtained simulation results of supply-demand balance and the outputs of various power generation technologies can be shown in figures in annual, monthly and daily intervals.

3. Main input preconditions

The hourly distribution of electricity demand in 2001 is shown in [18]. The electricity production increased by about 30% in the last 20 years from 740TWh in 1990 to 960TWh in 2009 [18]. However, on the demand side, energy saving has been notable because of the electricity shortage after the Fukushima accident [2], and possible population reduction is also predicted. Therefore, we assume that demand remains at 2009 level in the first demand scenario (D1); 15% reduction is realized in the second demand scenario (D2); and a 30% reduction is realized in the third scenario (D3).

Three supply scenarios are proposed according to different nuclear power development strategies in light of the Fukushima nuclear accident: (1) negative nuclear power; (2) conservative nuclear power; and (3) active pursuit of nuclear power as shown in **Fig.1**. In the negative nuclear scenario (S1), the stopped NPPs in this earthquake will be closed permanently, all NPPs under construction and in planning will be canceled and the NPPs in operation will be closed in their early lifetime 35-40 years. On the other hand, in the conservative nuclear power (S2) and active pursuit of nuclear power (S3), all NPPs under construction and in planning will be continued according to the schedule and all NPPs will operate for a long lifetime 40-50 years and very long lifetime 50-60 years, furthermore, in S3 Fukushima Daiichi NPPs will be rebuilt before 2030.

If all the thermal power plants (coal, LNG, oil) are stipulated to have 45 year lifetimes, and there will be no new construction of thermal plants up till 2030, the installed capacities of thermal power plants are shown in **Fig.2** based on historical installed capacity data [19]. This is the basic installed capacity for thermal power, and in the scenario analysis, new LNG power plants can be built when necessary to provide sufficient capacity.

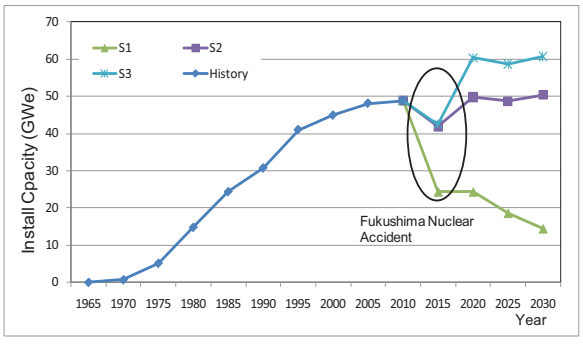

Fig.1 Three scenarios of nuclear power development in Japan up till to 2030 [1]

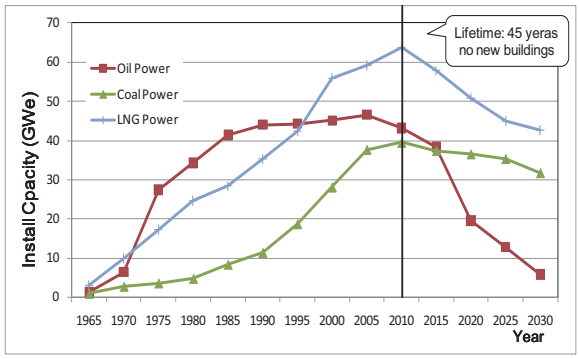

Fig.2 Installed capacities of thermal power in Japan up till to 2030 [1]

Therefore, in 2030, the installed capacities of nuclear power and thermal power in the three proposed scenarios are shown in **Table 1**. In the table, biomass power is assumed to remain at 2GW as it was in 2009 [17].

Table1 Installed capacities of nuclear power and thermal power in 2030 (GWe)

Scenarios	Nuclear	Coal	LNG	Oil	Biomass
S1	14.34	31.8	42.6	5.8	2
S2	50.35	31.8	42.6	5.8	2
S3	60.75	31.8	42.6	5.8	2

Japan will have to increase substantially the amount of electricity provided by renewable sources, especially ‘‘new’’ sources such as wind, solar, and biomass, because the country’s hydroelectric potential has already been largely exploited. At present, the installed capacity of hydropower is 21GWe and pumped storage hydropower is 27GWe [20]. We assume both values will remain constant. The potential of renewable energy in Japan is listed in the following **Table 2**. Here, we didn’t consider the constraints from production, cost, policy etc aspects, because the purpose of this study is to integrate renewable energy as much as possible.

Table2 Renewable energy and hydropower potential [7][21][22]

Renewables	Potential
PV	100GWp
Wind	50GWp
Biomass	2GWe
Hydro	21GWe
Pumped Hydro	27GWe

It is very difficult for traditional electricity mix models to integrate renewable energy sources because of the intermittency of solar and wind energy. Intermittent sources of electricity are expected to have technical and economic limitations in reaching a high level of penetration. The hour by hour simulation model is therefore vital here to test the supply-demand balance of the electricity system [23-25].

The solar irradiation and wind speed historical data in 2001 provided by JMA (Japan Meteorological Agency) is used [26]. The more PV and wind penetration in the system, the less net power will be and more excess power will appear when the base load power source level is stipulated. The “net power” means the difference of the normal load minus output of PV and wind power.

The CO_2 emissions factors of various power generation technologies are shown in [30]. According to the calculations, in 2030, most coal-fired power plants will be the advanced supercritical technology with 600ºC input temperature, and LNG-fired power plants will be in steam turbine combined cycle mode in Japan. CO_2 emissions can be reduced by about 5% and 20% respectively due to the efficiency improvements in advanced coal-fired and LNG-fired power generation technologies.

4. Main Defined Rules

The main defined rules for the hour-by-hour simulation are shown in **Table 3**, and the detailed explanations follow.

Table 3 Summary of main defined rules

	Defined Rules
Supply-demand	1. Blackouts is not allowed 2. Only PV&wind power can become excess power 3. Excess power ratio must be less than 5% in total electricity and 30% in PV&wind power 4. New building of LNG power plant is allowed 5. New buildings of coal and oil power plant are not allowed
Power generation and storage	1. Generation priority sequence: hydro, Nuclear, coal, PV&Wind, LNG, biomass, oil, pumped-hydro 2. Capacity factor of coal-fired power can be lowered to zero for more renewable energy penetration 3. LNG power is used to pump up hydro as electricity storage during night in case of peak demand periods
Resource Availability	1. Renewable energy penetration must be less than its physical potential 2. Fossil fuel demand must be less than Max. supply capability 3. Power generation facilities can be imported from overseas
Capacity factor and load-following	1. Capacity factor of Nuclear is between 75-100%, coal power less than 85% 2. LNG power, oil power, pumped hydropower operates in load-following mode
Generation cost and CO_2 emission	1. Average annual power generation cost can't exceed upper limitation (10 yen/kWh) 2. Average annual CO_2 emission per kWh can't exceed 1990 level

The installed capacities of nuclear power and thermal power are decided by the development policy and their stipulated lifetime. The purpose of the scenario is to integrate renewable energy as much as possible. When renewable energy is integrated into the electricity system as much as possible, if the supply is still not enough, new LNG power plants are possible to be built. However, when renewable energy penetration is still less than its potential, but much excess power happened, firstly the capacity factor of coal fired-power will be lowered; however, when the capacity factor of coal-fired power is lowered to be zero, if excess power is still over its upper limitation, the further penetration of renewable power will be not allowed.

In order to evaluate the performance and reliability of the obtained optimized electricity mix, two parameters are employed. One is the deficiency of power supply probability (DPSP), the other is the relative excess power ratio (REPR). DPSP is used to evaluate the possibility of a deficiency in the power supply which can be calculated as shown in eq. (1), and the REPR is given as a ratio of the total annual excess power generated by the system, as expressed in Eq.(1). Here the TEL is the annual total electrical load; The Output and Load are the hourly electrical production and load respectively.

$$DPSP = \frac{DPS}{TEL} = \frac{\sum_{i=1}^{8760}(Load_i - (Output_i + StorElectricity_i))}{\sum_{i=1}^{8760} Load_i} \quad (1)$$

$$REPR = \frac{REP}{TEL} = \frac{\sum_{i=1}^{8760}(Output_i - (Load_i + Storage_i))}{\sum_{i=1}^{8760} Load_i} \quad (2)$$

In the present study, blackouts are not permitted; therefore, the DPSP must be zero at all times. Electricity generated by solar and wind is used as much as possible in the study, however, when excess power happens, it is difficult to lower the output of nuclear power as base load, so PV panels and wind turbines are controlled to lower their outputs in this situation, thus, any excess electricity is generated by PV and wind power. In the study, the maximum excess electricity ratios in the total generation and PV and wind generation are defined. Furthermore, of the carbon-based fuels, only new build of LNG power plant is permitted due to its good performance in CO_2 emissions reduction and the absorption of intermittent electricity as a kind of flexible power source.

Hydropower, nuclear power and coal power is used to supply base load, gas for middle load and oil and pumped storage hydro power are used for peak load. If the pumped up hydro power has more than half of its storage capacity, only surplus based load power and PV, wind power are stored, however, when its capacity becomes less than one third, gas power is operated dedicated to pump up hydro for storage to ensure capacity. With the penetration of PV and wind power, if too much excess power is being produced annual capacity factor of coal power plants can be lowered even to zero.

Renewable energy penetration must be less than physical potential of renewable energy sources, and the fossil fuel demand must be less than overseas import capacity. Power generation facilities such as PV panel and wind turbine can be made domestically in Japan, but can also be supplied from overseas. For example, 100 GWp PV power can be reached by installing 5GWp per year from 2010 to 2030. Today approximately 2.5 GWp PV power can be produced in Japan [31], however the global production capacity is 15GWp [32]. Furthermore, the production capacities in domestic and in the world are expected to increase quickly in the future.

Hydropower operates with 45% capacity factor to supply based load. The capacity factor of nuclear power is stipulated to be about 90% in average but has different monthly values from 75%-100% according to periodic inspection and maintenance. Coal-fired power follows nuclear power also work as a based load follow the nuclear power, however its maximum capacity factor is 85% and its annual average capacity factor can be lowered even to zero in order to integrate more renewable energy. All the base load power cannot change their outputs very quickly, and thus do not operate in load-following mode. Gas, oil and hydropower can change their outputs by 100% within one hour, and therefore can operate in load-following mode. The outputs of PV and wind are determined by solar radiation and wind speed respectively, and change continuously every hour.

In 1990, CO_2 emission is 392g/kWh per unit electricity generation and 290 million tonnes in total. The CO_2 emission levels in 1990 will be used as a standard to evaluate the reduction in the electricity system scenarios. In the Strategic Energy Plan (SEP) 2030 released by the government in 2010, total CO_2 emission reduction is expected to be 15% comparing with 1990 level. One the other hand, the average generation cost per unit electricity is an economic parameter, which is regulated to avoid the scenario becoming too expensive. At present, renewable energy is much more expensive than traditional electricity; however its cost is expected to be reduced greatly to the competitive level of present traditional electricity [29].

5. Results

The maximum renewable energy penetration scenarios in 2030 are obtained based on the three supply scenarios (S1, S2, and S3) and three demand scenarios (D1, D2 and D3) subject to various input preconditions and defined rules introduced above. The results will be shown and discussed in technological and environmental perspectives.

The obtained results of installed capacity mix, electricity mix and key performance indicators are shown in **Fig.3**, **Fig.4** and **Table 4**. The results show that:

(1) In S1 with only 14.3GWe nuclear power, even though a high level penetration of renewable energy is realized, a maximum of about 40GWe new LNG power plants need to be built by 2030, and maximum about 40% more LNG needs to be imported from overseas in 2030 comparing with 2009 levels. Furthermore, coal-fired power has to operate at a high capacity factor of about 75% in S1.

(2) In S2 and S3 with 50.3GWe and 60.7GWe nuclear power respectively, no new LNG power plants need to be built, and at least 20% LNG fuel is saved in 2030 compared to 2009 levels. Coal-fired power can be removed from the electricity system absolutely with the help of renewable energy and energy saving in S2 and S3 to reduce CO_2 emission.

(3) Comparing with S1 with S2 and S3 introduced in (1) and (2), we can understand that it is very difficult to remove nuclear power absolutely in an available, clean and safe future electricity system in

Japan even renewable energy penetrates as much as possible and energy saving is realized.

(4) In S2 and S3, the penetration level of renewable energy reduces from D1 to D3 with the demand reduction, because it is hindered by the increasing share of nuclear power as base load supply. It is proven that when power generation capacity become big enough relative to the demand, energy saving is optional and it is difficult for new renewable energy to penetrate into the whole system; and there will be more excess electricity even when the capacity factor of coal-fired power is lowered.

(5) Penetration of renewable energy can reduce the dependence on nuclear power and thermal power, but it needs flexible power sources such as LNG power to compensate for its supply variability.

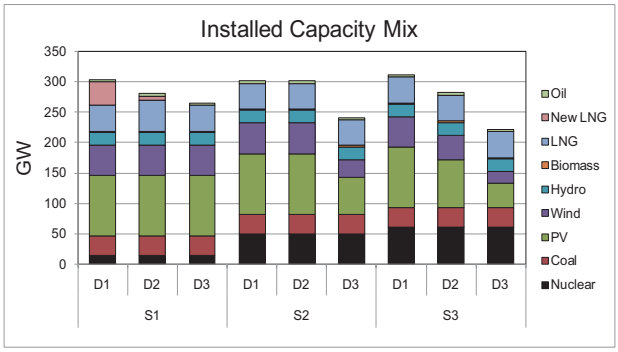

Fig. 3 Installed capacity mix of the supply-demand scenarios [1]

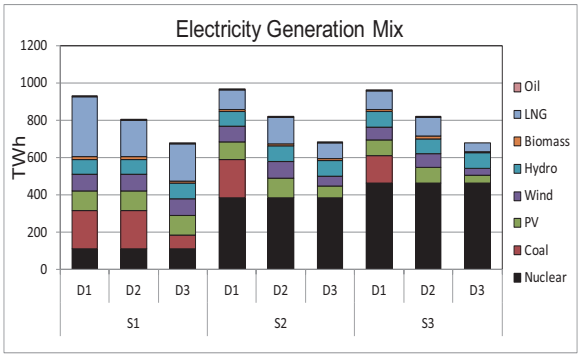

Fig.4 Electricity generation of the supply-demand scenarios [1]

Table 4 Analysis results of key performance parameters

	Excess electricity share			Renewable share			Capacity factor of Coal-fired power		
	S1	S2	S3	S1	S2	S3	S1	S2	S3
D1	0.9%	4.9%	4.5%	20.9%	18.1%	16.1%	74.1%	74.1%	52.3%
D2	2.7%	4.2%	4.2%	24.0%	23.7%	19.0%	74.1%	0%	0%
D3	3.5%	3.9%	4.3%	28.6%	17.1%	11.4%	27.9%	0%	0%

CO_2 emission information is shown in **Fig.5** and **6**. The CO_2 emissions per unit electricity are also affected by many factors. More shares of renewable energy and nuclear power and less shares of thermal power can improve CO_2 emissions reduction. In the three demand scenarios, the first supply scenario-S1 has much more CO_2 emissions per unit electricity comparing with S2 and S3 although the renewable energy share in S1 is higher, because more thermal power (mainly LNG) is introduced in the electricity system to compensate for energy shortages and to absorb fluctuations of renewable energy. However, compared to 1990 levels, the scenarios can all achieve an emissions reduction with the help of nuclear power, renewable power and energy saving.

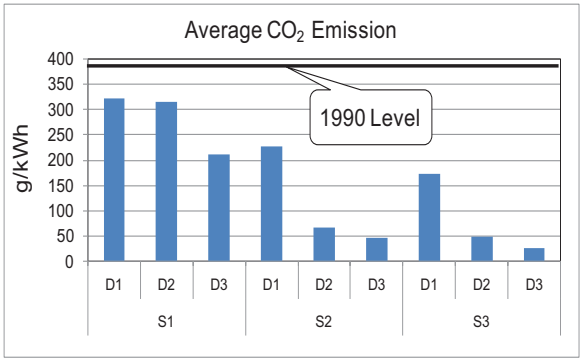

Fig.5 Average CO_2 emission per unit electricity production in the scenarios [1]

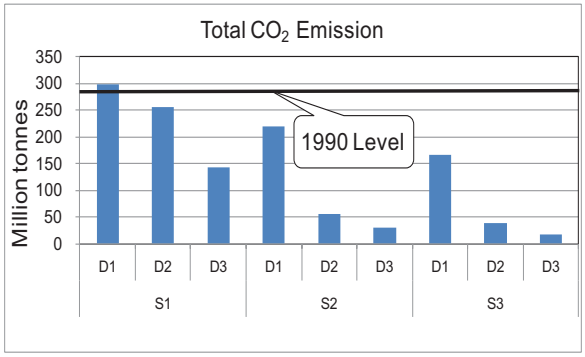

Fig.6 Total CO_2 emission in the scenarios [1]

6. Discussions

If the "negative nuclear power" scenario is selected, even renewable is developed as much as possible; Japan will have to face unstable fossil fuel availability in global market, CO_2 emission/climate change pressure and possibly slow economy development due to electricity shortage. On the other hand, if the country is still dependent on nuclear power as in S3, the people and country have to face potential dangers of nuclear power, even the most advanced technology is used. The authors provide several scenarios, of which D2S2 seems to be most practical and performs well from technological, economic and environmental perspectives. However, the scenarios - especially the nuclear development policy - will ultimately be self-selected by the people, government and industry in Japan.

In the further study, electricity supply-demand will be studied in different regions and the interconnection between different regions will be the focus. Furthermore, electricity storage using battery and smart grid technologies with more new controllable load such as electric vehicle and heap pump will be involved into the future electricity system.

7. Conclusions

The study focused on the balance and match of supply-demand of the future electricity system in Japan. Scenario analysis on the electricity system was conducted from technological, and environmental perspectives using an input-output hour-by-hour simulation model.

The obtained results show that:

- penetration level of renewable energy is subject to the share of nuclear power as base load due to the occurrence of excess electricity, for example, renewable energy share is lowered from 20% in D2S3 to 10% in D3S3;
- it is very difficult to remove nuclear power absolutely from the electricity system even though high level penetration of renewable energy is realized, because the renewable energy contribute maximum about 30% in D3S1 with maximum energy saving and maximum renewable energy penetration;
- renewable energy contribute 10-30% in the scenarios, and the high level penetration of renewable energy can reduce the dependence on nuclear and thermal power, but needs more flexible power sources to absorb fluctuations;
- CO_2 emissions reduction compared to 1990 level can be realized easily with the help of nuclear power, renewable energy and energy saving in 2030, in D2 and D3, CO2 emissions are 10 million tonnes to 250 tonnes comparing with 290 million tonnes in 1990.

References

[1] Qi Zhang, K. N. Ishihara, B. McLellan and T. Tezuka, Scenario Analysis of Future Electricity Supply and Demand in Japan, Energy, 2012, 38: pp.376-385

[2] METI (Ministry of Economy, Trade and Industry of Japan), The Strategic Energy Plan of Japan, 2010, available at <http://www.meti.go.jp/english/press/data/pdf/20100618_08a.pdf>.

[3] TEPCO Homepage, Graph which shows Use of Electric Power, accessed May 2011, available at <http://www.tepco.co.jp/en/forecast/html/index-e.html>.

[4] IEA , Energy Balance of OECD Countries (2010 Edition), Paris, 2010.

[5] IEA, Energy Price and Taxes, Quarterly Statistics, First Quarter 2011, Paris, 2011.

[6] Greenhouse Gas Inventory Office of Japan, The GHG Emissions Data of Japan (1990-2009), April 2011, available at< http://www-gio.nies.go.jp/index.html >.

[7] ME (Ministry of Environment of Japan), study of Potential for the Introduction of Renewable Energy (FY 2010), 2011 [in Japanese].

[8] T. Nakata, Analysis of the impacts of nuclear phase-out on energy systems in Japan, Energy 2002; 27: pp.363–377.

[9] K. Takase, T. Suzuki, The Japanese energy sector: Current situation, and future paths. Energy Policy (2010), doi:10.1016/j.enpol.2010.01.036.

[10] H. Lund, E. Munster, Modelling of energy systems with a high percentage of CHP and wind power, Renewable energy 2003; 28:pp.2179-2193.

[11] H. Lund, Large-scale integration of optimal combinations of PV, wind and wave power into the electricity supply, Renewable Energy 2006;31:pp.503–515.

[12] D. Connolly, H. Lund, B.V. Mathiesen, M. Leahy, A review of computer tools for analysing the integration of renewable energy into various energy systems, Applied Energy 2010; 87:pp.1059–1082.

[13] T. Nakata, D. Silva, M. Rodionov, Application of energy system models for designing a low-carbon society, Progress in Energy and Combustion Science 2011; 37: pp.462-502.

[14] G. J. Dalton, D. A. Lockington, T. E. Baldock, Feasibility analysis of stand-alone renewable energy supply options for a large hotel, Renewable Energy 2008;33:pp.1475–1490.

[15] H. Lund, Renewable energy strategies for sustainable development, Energy 2007;32(6):pp.912-919.

[16] A. Troelsen, Pro C# 2008 and the .Net 3.5 Platform, Apress, 2007.

[17] D. Sceppa, Programming Microsoft ADO.Net 2.0 Core Reference, Microsoft Press, 2006.

[18] FEPC (The Federation of Electric Power Companies of Japan), Accessed May, 2011, Electricity power statistic information, available at < http://www.fepc.or.jp/library/data/tokei/index.html>.

[19] H. Moritsuka, Study on the Reduction of Carbon Dioxide Emission from the Electric Power Industries on 2050, CRIEPI 2009. [in Japanese]

[20] IEA, Energy Policies of IEA Countries: Japan 2008 Review. Paris, 2008.

[21] JWPA (Japan Wind Power Association), 2011, Roadmap of long-term introduction of wind power in Japan, available at <http://log.jwpa.jp/content/0000289019.html>.

[22] NEDO (New Energy and Industrial Technology Development Organization), PV potential in Japan, accessed in May. 2011, available at < http://www.nedo.go.jp/ >.

[23] H. Lund, Large-scale integration of wind power into different energy systems. Energy 2005; 30: pp.2402–2412.

[24] A. R. Prasad, E. Natarajan, Optimization of integrated photovoltaic-wind power generation systems with battery storage, Energy 2006; 31:pp.1943-1954.

[25] P. Denholm, M. R. Margolis, Evaluating the limits of solar photovoltaics (PV) in traditional electric power systems, Energy policy 2007; 35: pp.2852-2861.

[26] JMA (Japan Meteorological Agency), Amedas data 2001-2004, 2005.
[27] FEPC (The Federation of Electric Power Companies of Japan), Cost comparison of various power generation technologies, 2004.
[28] NEDO, Technology white book of renewable energy, 2010. [in Japanese]
[29] PV Power in Japan, Cost examples of PV power install, accessed June 2011 Available at < http://www.taiyokohatuden.jp/solar/ex.html>.[in Japanese]
[30] E. Imamura, K. Nagano, Evaluation of Life Cycle CO_2 emissions of Power Generation Technologies, CRIEPI, p. 34, 2010 [in Japanese].
[31] JPEA (Japan Photovoltaic Energy Association), Statistic data, accessed June 2011, available at <http://www.jpea.gr.jp/04doc01.html>.
[32] Renewable energy focus, solar-pv-panel-production-above-15-gw-in-2010, accessed June 2011, available at < http://www.renewableenergyfocus.com/view/13492/ >.

3. Nuclear Data for Severe Accident Analysis and Decommissioning of Nuclear Power Plant

Keisuke OKUMURA, Kensuke KOJIMA, Tsutomu OKAMOTO, Hiroyuki HAGURA, Kenya SUYAMA
Nuclear Science and Engineering Directorate, Japan Atomic Energy Agency
Tokai-mura, Naka-gun, Ibaraki-ken 319-1195 Japan
e-mail: okumura.keisuke@jaea.go.jp

Three-dimensional nuclide inventory and decay heat distributions at the time of the nuclear accident in Fukushima-Daiichi power plants were evaluated on the basis of the detailed burnup calculation with JENDL-4.0. Total decay heat of the unit-2 after the accident was compared with the decay heats obtained by simple evaluation formulas used in the safety analyses of ECCS and in the severe accident analyses. As a result, applicability of the formulas to the Fukushima-Daiichi accident was quantitatively clarified. At the end, we briefly introduce our recent activities on the development of the basic database for decommissioning of light water reactors.

1. Introduction

Accurate information on nuclide inventory is necessary to understand progression of the Fukushima-Daiichi nuclear accident and to make a plan of radioactive wastes management in future. Generally, one-point burn-up calculation codes such as ORIGEN2 [1] are widely used for nuclide inventory calculation. However, for accurate inventory calculation for large amounts of fuels in a BWR, we have to pay attention not to averaged values of burn-up and void fraction but to their distributions in the core. In addition, reliable nuclear data and method should be used. Then, three-dimensional nuclide inventory and decay heat analysis was performed for the Fukushima-Daiichi power plants (1F1, 1F2, 1F3) by using a modular code system for reactor analyses MOSRA [2,3] and nuclear data library based on JENDL-4.0 [4]. The result for unit-2 (1F2), in which core meltdown after shutdown was delayed among the plants, is shown.

2. Method of Three-Dimensional Nuclide Inventory Calculation

In the analysis, each of cores is divided into horizontal five or six regions corresponding to refueling batches, and each region is furthermore divided into 25 axial nodes. Information on region-wise radial burn-up and operating power history was derived from a JAEA report by Nishihara et al.[5]. Since there was no published information on axial power distribution, we used a γ-scanning data ($^{134}Cs/^{137}Cs$ radioactivity ratio) obtained in the post-irradiation examination [6] for a spent fuel rod of the Fukushima-Daini-2 power plant. Assuming it is a representative axial power distribution during burnup, the node-wise power density and burn-up were determined to be consistent with the region-wise burn-up. Then, axial void distribution was calculated by one-dimensional thermal-hydraulic calculation module MOSRA-Hydro [2] based on the forced-convection sub-cooled boiling model.

For each node, atomic number densities for about 1400 nuclides were obtained by the burnup calculation module MOSRA-SuperBacon [3] adopting matrix exponential method and neutron spectrum calculation by 200-group collision probability method. Finally, decay heat distribution was directly obtained by summation of all nuclide-wise contributions.

3. Results and Discussions

(1) Nuclide inventory

Table 1 shows an example of the obtained inventories for some nuclide in 1F2. The existing result of the ORIGEN2 calculation [5] using the JENDL-3.3 library (ORLIBJ33) is also shown for comparison. In the ORGEN2 calculation, axial burn-up and void distributions are not considered. In the Table 1, Sr-90 and Cs-137 show good agreements between both results. This is because that these inventories are not sensitive to cross sections and neutron spectra, and they increase in proportion to burn-up [6]. On the other hand, other nuclides especially Am-241 and Cm-244 show large differences due to the differences of nuclear data and of the consideration of the axial distributions. From the post irradiation examination analyses, it is known that JENDL-3.3 gives underestimation for Cm isotopes [7]. In addition, no consideration of burn-up and void distribution results in the systematic underestimation [6].

Table 1 Nuclide Inventory (g/core) in 1F2 at the time of accident

Calculation code	SuperBacon	ORIGEN2*	Difference (SuperBacon−ORIGEN2)/ORIGEN2
Number of regions	5(X−Y)×25(Z)	5(X−Y)	
Nuclear data	JENDL−4.0	JENDL−3.3	
Am−241	2.70×10^{3}	3.42×10^{3}	−20.9%
Cm−244	1.45×10^{3}	1.07×10^{3}	35.2%
Sr−90	3.75×10^{4}	3.73×10^{4}	0.4%
Cs−134	6.08×10^{3}	5.78×10^{3}	5.2%
Cs−137	7.90×10^{4}	7.95×10^{4}	−0.6%
Sm−152	7.29×10^{3}	7.42×10^{3}	−1.8%
Eu−154	1.18×10^{3}	1.04×10^{3}	13.4%

*ORIGEN2.2 with ORLIBJ33 [5]

(2) Decay heat distribution

Figure 1 shows the fuel loading pattern assumed in this study and the obtained decay heat distribution in 1F2. From the power history shown in the same figure, region-wise power density has a tendency to decrease as burn-up increase. As a result, the decay heat at the time of the accident is larger in newer fuel region (e.g. #1) rather than older one (e.g. #5). After core shutdown, the distribution of the decay heat gradually becomes flatter due to the decay of fission products with short half-lives. As shown in Eq.(1), the decay heat distribution P_d at the time of core shutdown (t_0) is approximately proportional to the power density distribution q'''.

$$P_d(\vec{r},t_0)\approx\sum_{i\in FP}E_i\lambda_i N_i(\vec{r},t_0)\approx\left(\sum_{i\in FP}E_i\Gamma_i\right)\Sigma_f(\vec{r},t_0)\phi(\vec{r},t_0)=c\cdot q'''(\vec{r},t_0) \quad (1)$$

where, i: identification of nuclide, E_i: average decay heat from β or γ decay of nuclide i, λ_i: decay constant, Γ_i: cumulative fission yield, c: constant value.

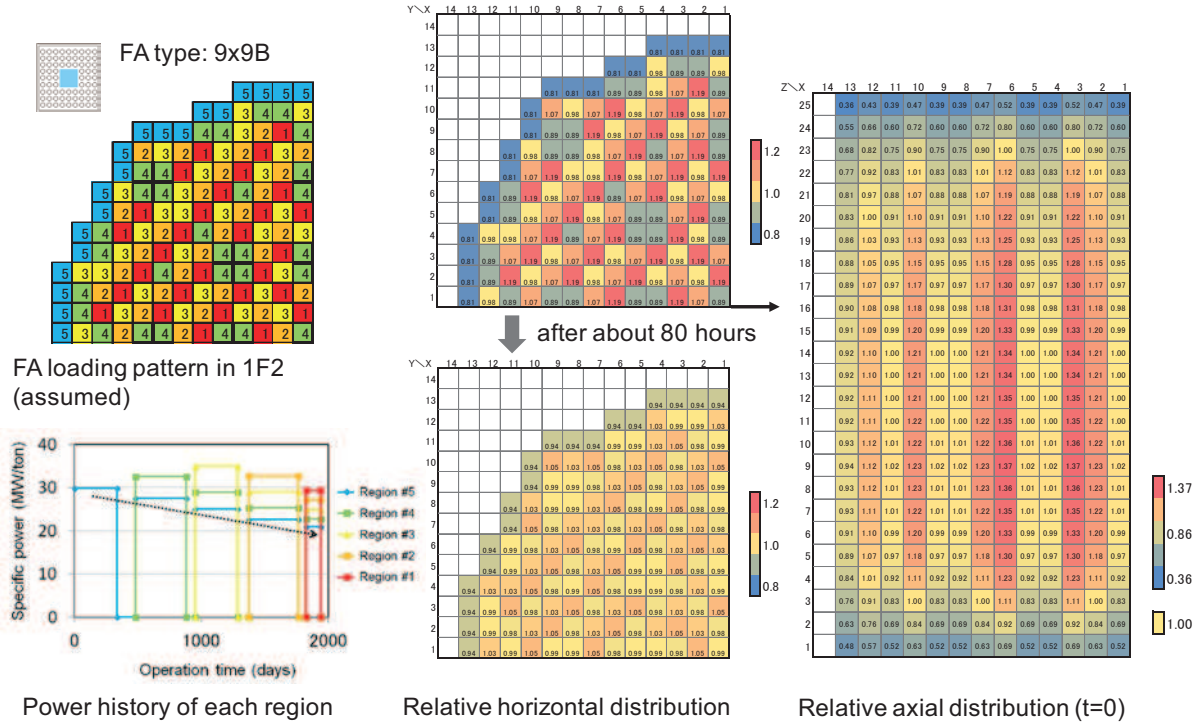

Fig. 1 Fuel loading pattern, power history, and three-dimensional decay heat distribution in 1F2

(3) Time-dependent total decay heat

Figure 2 shows the time-dependence of total decay heat and major contributing nuclides. The total decay heat was obtained by summation over all nuclides in all nodes.

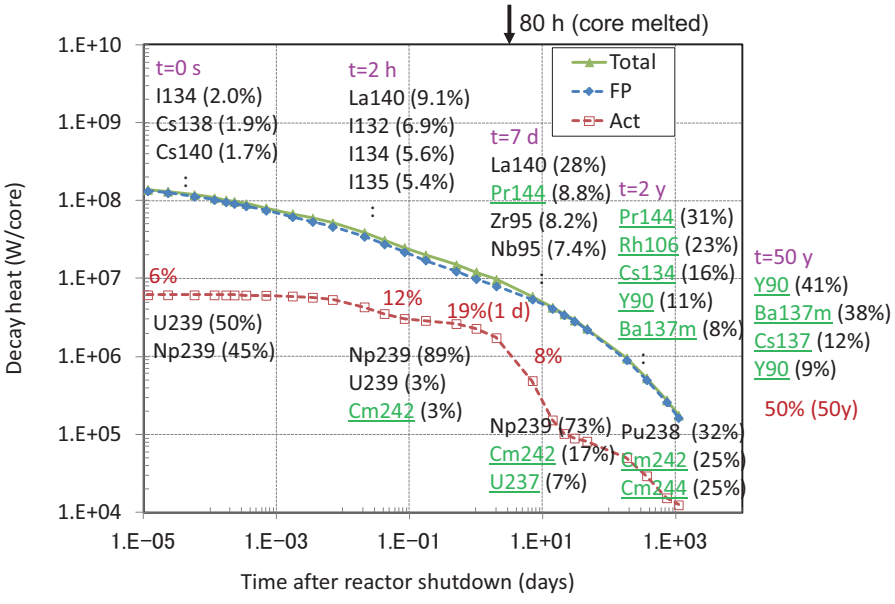

Fig.2 Time-change of total decay heat and major contributing nuclides (1F2)

The melting time of the 1F2 core is estimated about 80 hours later after the core shutdown. Up to about 80 hours, the total decay heat is almost determined by the inventories of nuclides with short half-lives less than a few days (e.g. I-132, I-134, I-135, Cs-138, Cs-140, U-239, Np-239, etc.). After that, contribution of nuclides whose inventories strongly depend on burnup increases. They are Pr-144 (radioactive equilibrium to Ce-144), Rh-106, Cs-134, Y-90 (equilibrium to Sr-90), Ba-137m (equilibrium to Cs-137), Cm-242, Cm-244 and so on. Among them, inventories and decay heats of Sr-90, Y-90, Cs-137 and Ba-137m are easy to be evaluated because they are generated in proportion to burnup.

The time-dependent total decay heat for 1F2 was compared with those obtained by using the AESJ recommendation[8] and by using the following simple formula, which is an old ANS standard (ANS-5.1-1971) based on Shure's formula for infinite irradiation [9,10].

$$P_d^{total}(t_0 + t_s) = A t_s^{-\alpha} \times P_0 \ , \tag{2}$$

where, t_s is an elapsed time after the core shutdown, P_0 is a total thermal power, A and α are fitting coefficients: A=0.0603, α =0.0639 $(0.1 \le t_s \le 10)$, A=0.0766, α =0.1807 $(10 \le t_s \le 1.5 \times 10^2)$, A=0.1301, α=0.2834 $(1.5 \times 10^2 \le t_s \le 4.0 \times 10^6)$, A=0.2659, α=0.3350 $(4.0 \times 10^6 \le t_s \le 2.0 \times 10^8)$.

The formula of the AESJ recommendation consists of the FP decay term considering 33-groups of fission products yielded from five fissionable nuclides (U-235, U-238, Pu-239, Pu-240, Pu-241) and the actinide decay terms considering U-239 and Np-239. To apply this formula to the 1F2 core with different refueling regions, we need information on the region-wise power history because the formula of the AESJ recommendation is a function of thermal power, irradiation time, cooling time, etc. This kind of decay heat formula has been used for the safety evaluation guide of ECCS in Japan and for some severe accident (SA) analysis codes such as MELCOR[11]. On the other hand, the simple formula of ANS-5.1-1971 has an advantage that it can be immediately applied to the SA analyses even when detailed information on core specifications and fuel irradiation histories are unavailable.

Figure 3 shows the differences of the total decay heats obtained with the AESJ recommendation and ANS-5.1-1971 from the three-dimensional calculation result by MOSRA-SuperBacon. Any prescribed corrections (e.g. +3σ for the AESJ recommendation, 1.2× P_0 for ANS-5.1-1971) for the conservative safety evaluation were not employed here.

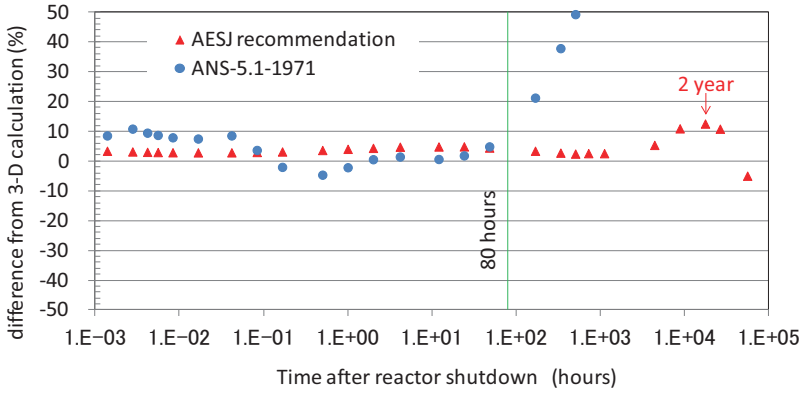

Fig.3 Differences of total decay heats with existing formulas from 3-dimensional calculation result (1F2)

Up to 80 hours, the simple formula of ANS-5.1-1971 gives good agreement with the three-dimensional calculation result within about 10%. As shown in Eq. (3), the total decay heat can be simply approximated by P_0 and an appropriate fitting function $f(t)$ for a while after the core shutdown. After that the difference rapidly increases due to no consideration of decay characteristics of individual nuclide.

$$P_d^{total}(t_0 + t) \approx \left(\sum_i c_i e^{-\lambda_i t} \right) \cdot \int_{core} q'''(\vec{r}, t_0) dV = f(t) \cdot P_0 \quad (3)$$

In the case of the AESJ recommendation, the difference is less than 6% up to 4400 hours (about a half-year) after the core shutdown. After that, the difference shows the maximum peak at about t=2×10^4 hours, then it gives negative values (i.e. underestimation) from t=5×10^4 onward due to no contribution of decay heats from minor actinides except for U-239 and Np-239. To improve the accuracy of the AESJ recommendation for $t > 2 \times 10^4$, more precise treatment is necessary for the inventory of nuclides depending on neutron spectra and burn-up, they are Pr-144 (Ce-144), Cs-134, Rh-106, Pu-238, Cm-242, Cm-244 and so on. However, for the short-term decay heat evaluation up to 80 hours, both of the AESJ recommendation and the simple formula of ANS-5.1-1971 are useful enough.

4. Development of Database for Decommissioning of LWRs

In 2011, JAEA started a research program to develop the basic database for radioactivity inventory evaluation for nuclear facilities in collaboration with the Japan Atomic Power Company [12]. The primary purpose of the program is to develop the data and method optimized for decommissioning of Japanese light water reactors by reflecting the most recent findings. From JAEA, three groups are taking part in the research program. The Nuclear Data Center at JAEA is now in the process of evaluating new cross section data not included in JENDL-4.0. The Research Group for Corrosion Resistant Materials is developing a material composition database optimized to Japanese nuclear power plants. Our group, Research Group for Standard Nuclear Engineering Software Development, is in charge of the following activities.

- Study to obtain appropriate neutron spectra for condensation of activation cross sections in representative regions such as core internals, pressure vessel, biological shield wall, etc.
- Development of processing tools to produce the activation cross section libraries for the existing activation calculation codes (e.g. ORIGEN2, ORIGEN-S) and also for more sophisticated codes (e.g. MOSRA-SuperBacon).
- Validation of the data and method by comparison with assay data of irradiated samples.

It is expected that these activities will contribute to the decommissioning of Fukushima-Daiichi power plants in future.

5. Conclusion

In order to contribute to understanding of progression of the Fukushima-Daiichi nuclear accident and to making a plan of radioactive wastes management in future, three-dimensional nuclide inventory and decay heat calculation was carried out. From this study, detailed information was obtained on radioactivity inventory and decay heat in Fukushima-Daiichi power plants at the time of the accident. In addition, we showed the following findings.

- For accurate inventory calculation, distributions of burnup and void fraction in a core should be considered, especially for the nuclides which are not generated in proportional to burnup (e.g. Cs-134, Cm isotopes, etc).
- Decay heat distribution within about 80 hours after the core shutdown is independent of burn-up distribution and it is mainly determined by the power distribution at the time of the core shutdown.
- Total decay heat evaluated by the AESJ recommendation agrees with the result of the three-dimensional summation calculation using MOSRA-SuperBacon and JENDL-4.0 within 6% up to 4400 hours (about a half-year) after the core shutdown.
- Total decay heat evaluated by the ANS-5.1(1971) formula agrees with the result of the three -dimensional summation calculation within 10% up to 80 hours, which is the melting time of 1F2. This simple formula is effective for the severe accident analysis when detailed information on core specifications and power history are unavailable.

JAEA started a collaboration study with the Japan Atomic Power Company to develop the basic database for decommissioning of LWRs including Fukushima NPPs. One of the key issues of the study is to develop accurate activation cross section library and its validation using assay data.

References

[1] A.G. Croff, "ORIGEN2: A Versatile Computer Code for Calculating the Nuclide Compositions and Characteristics of Nuclear Materials", Nucl. Technol. 62, 335 (1983).
[2] K. Okumura, T. Kugo, H. Nakano, *et al*., "Development of Modular Reactor Analysis Code System MOSRA", 2008 annual meeting of the Atomic Energy Society of Japan (2008), [in Japanese].
[3] K. Okumura, K. Kojima, T. Okamoto, "Development of Burn-up Calculation Modules in the MOSRA System", 2012 autumn meeting of the Atomic Energy Society of Japan (2012) , [in Japanese].
[4] K. Shibata, O. Iwamoto, T. Nakagawa, *et al*., "JENDL-4.0: A New Library for Nuclear Science and Engineering", J. Nucl. Sci. Technol. 48[1], 1 (2011).
[5] K. Nishihara, H. Iwamoto, K. Suyama, "Estimation of Fuel Compositions in Fukushima-Daiichi Nuclear Power Plant", JAEA-Data/Code 2012-018 (2012), [in Japanese].
[6] K. Okumura, T. Okamoto, "Nuclide Inventories of Spent Fuels from Light Water Reactors", JAEA-Data/Code 2011-020 (2012), [in Japanese].
[7] G. Chiba, K. Okumura, K. Sugino, *et al*., "JENDL-4.0 Benchmarking for Fission Reactor Applications", J. Nucl. Sci. Technol. 48[2], 172 (2011).
[8] S. Iijima, T. Yoshida, K. Tasaka, *et al*., "Fission Product Decay Power – AESJ Recommendation", Proc. of Int. Conf. on Nuclear Data for Science and Technology, 13-17 May 1991, Julich, Germany, pp.542-544, (1992).
[9] K. Shure, J. Dudziak, "Calculating energy released by fission products", WAPD-T-1309, Bettis Atomic Power Laboratory, Pittsburgh, Pennsylvania, USA (1961).
[10] Subcommittee ANS-5, Proposed ANS Standard, "Decay Energy Release Rates Following Shutdown of Uranium-Fueled Thermal Reactor", ANS Standards Committee, (1971).
[11] R. M. Ostmeyer, "An Approach to Treating Radionuclide Decay Heating for Use in the MELCOR Code System", NUREG/CR-4169, SAND84-1404, Sandia National Laboratories, Albuquerque, NM (1985).
[12] K. Tanaka, T. Fukahori, M. Yamamoto, *et al*.: "The development of the database for radiological characterization for nuclear facilities (1) The purpose and the plan for the study," 2012 annual meeting of the Atomic Energy Society of Japan, E18 (2012), [in Japanese].

4. Present Status of Research Reactor and Future Prospects

Ken Nakajima
Research Reactor Institute, Kyoto University
Kumatori-cho, Sennnan-gun, Osaka 590-0494
e-mail: nakajima@rri.kyoto-u.ac.jp

Abstract

Research reactors have been playing an important role in the research and development of the various fields, such as physics, chemistry, biology, engineering, agriculture, medicine, etc. as well as human resource development. However, the most of them are older than 40years, and the ageing management is an important issue.

In Japan, only two research reactors are operational after the Great East Japan Earthquake in 2011. JAEA's reactors suffered from the quake and they are under inspections. Kyoto University Research Reactor, one of the operational reactors, has been widely used for research and human resource development, and the additional safety measures against the station blackout were installed.

Besides the affect of the quake, the disposal or treatment of spent fuel becomes an inevitable problem for research reactors. The way of spent fuel disposal or treatment should be determined with the nation-wide and/or international coalition.

1. Introduction

Research reactors have been playing an important role in the research and development of the various fields, such as physics, chemistry, biology, engineering, agriculture, medicine, etc. as well as human resource development. According to the IAEA's Research Reactor Database[1], 244 research reactors (RRs) are operational or temporary shutdown in the world, and 17 of them are in Japan. (Note that those numbers include the critical assemblies.)

In this paper, the present status and future prospects of RRs, in particular those in Japan are presented.

2. Research Reactors in the World

The IAEA's Research Reactor Database (RRDB) contains administrative, technical and utilization information on over 670 research reactors including critical and sub-critical assemblies in 69 countries and the European Union. The information in the database is updated directly by facility or national representatives officially nominated as facility data providers, reviewed and accepted by the IAEA.

Using the RRDB, the present status of RRs in the world is summarized in **Table 1**. As shown in the table, about 444 RRs of total 696 (except the canceled RRs) are shutdown or decommissioned. In contrast, only 4 are under construction and 4 are planned.

Table 1 Present status of Research Reactors

Region	OPERA-TIONAL	TEMPORARY SHUTDOWN	UNDER CONSTRUC-TION	PLANNED	SHUT DOWN	DECOM-MISSIONED	CANCELLED
N/A					1		
North America	49				61	146	1
Latin America	17	1		2	2	3	
Western Europe	39	3	2	1	42	90	
Eastern Europe	67	5	1		9	50	
Africa	7	2				1	1
Middle East and South Asia	14		1	1	4	5	
South East Asia and the Pacific	5	1			1	2	2
Far East	31	3			11	16	1
Total	**229**	**15**	**4**	**4**	**131**	**313**	**5**

The age of the operational RRs can also be found in the RRDB. **Figure 1** shows the age distribution of the operational RRs using the data of the RRDB. It is found from the figure that the aged reactors are dominant in the world. In fact, about 60% of RRs are older than 40 years. Thus, the ageing management is one of the most important issues in the RR community, and the IAEA creates the Ageing Database, which is intended to assist interested Member States share information and experiences specific to the management of technical issues related to ageing as well as the development and implementation of comprehensive ageing management programs.

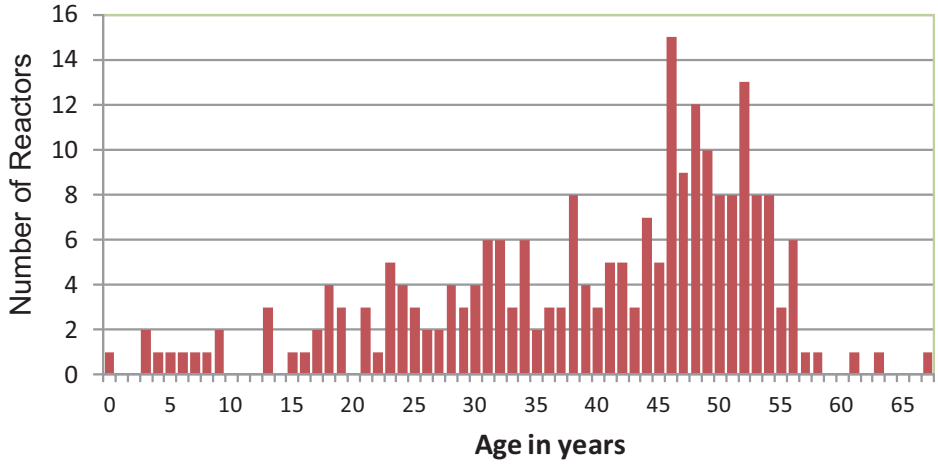

Figure 1 Age distribution of Operational Research Reactors

3. Research Reactors in Japan

3.1 Present Status of RRs in Japan

In Japan, there are 9 RRs in **Figure 2**, 6 of them owned by Japan Atomic Energy Agency

(JAEA) and others by universities[1]. After the Great East Japan Earthquake on 11th March, 2011, only two research reactors, KUR at Kyoto University and UTR-KINKI at Kinki University, have been operating. Tokyo University has determined to decommission Yayoi before the quake and it was shut down after the quake. All the other reactors suffered from the quake and they are under inspections because the integral safety examinations are necessary to re-start.

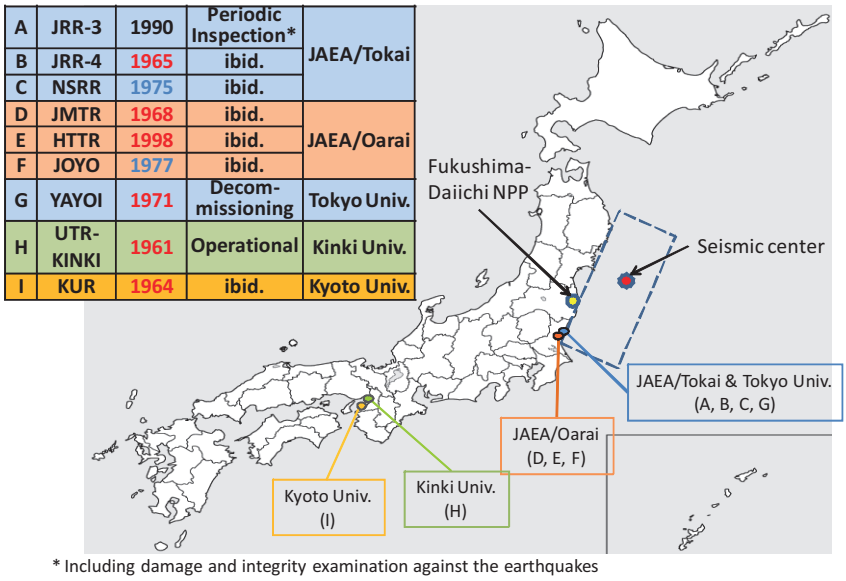

Figure 2 Present Status of Research Reactors in Japan

For the RRs of JAEA at Tokai and Oarai, no significant damage was observed for the main facilities, although the several auxiliary facilities were damaged[2]. To the present, the damaged facilities were restored and the seismic analyses have been performed to confirm that the reactors have the resistant with the quake. JAEA has submitted the report on 'Check & Test' and 'Seismic Analysis' of JRR-3 to the Nuclear Regulation Authority (NRA) on 2nd November, 2012[3]. Hereafter, NRA will check and confirm the report and approve it, although the schedule is not yet fixed.

3.2 Status of Kyoto University Research Reactor (KUR)

3.2.1 Safety evaluation of KUR

For KUR, there was no physical effect/damage by the quake. However, MEXT[2] (Regulatory body) has dictated to evaluate the soundness of research reactors against the long-term SBO (Station Blackout) in April, 2011. Then, Kyoto University Research Reactor Institute (KURRI) has made the evaluation and submitted the report with the following results.

---

[1] In this section, critical and sub-critical assemblies are not included in the research reactors.
[2] Ministry of Education, Culture, Sports, Science and Technology, Japan.

- The core (fuels) can be cooled by the natural convection when the core is immersed in the cooling water.
- The cooling water in the core tank has enough volume that the core is immersed over than 30 days.
- About 3 days of cooling is enough for the KUR core. (No water is necessary after 3 days.)
- Spent fuels in the pool have less decay heat than those in the core and the pool has larger volume of water, hence those fuels have no damage.

In addition to the present safety measures, a 40-ton water tank was settled near the reactor room, a mobile fire pump and a mobile power generator were prepared to enhance the safety of KUR as shown in **Figure 3**.

Figure 3 Additional Safety Measures for KUR

3.2.2 Modification of Beam Ports

For the improvement of research capability, the modifications of irradiation beam ports are in progress.

a) B-2 port

The B-2 port, which was used as a triple-axis neutron diffractometer, was fully modified to a neutron irradiation facility in 2011. This facility is capable to irradiate a large and/or heavy sample including a liquid sample. The maximum size and weight of the sample are 60 mm x 60 mm x 100 mm and 4 kg.

The modification of the port has been already finished and the experiments to measure the basic characteristics of the facility are being conducted.

b) B-1 port

The B-1 port, where the iron neutron filter is installed, will be modified to a positron beam irradiation facility. By using a positron beam, researchers can measure the non-uniformity of elements distributions in the material and lattice defects which cannot be observed by an electron microscope. In particular, the experimental study on the brittle fracture of reactor vessel material will be performed using the facility.

The modification of the port will be initiated in 2012, and the design of the facility is being conducted.

3.2.3 Human Resource Development

KUR is also used for the human resource development. In 2011, the Reactor Physics Course using KUR has started after 2 years' trial experiences. The course is intended for the non-nuclear students or beginners to understand the basic concept of nuclear reactors. Two courses are offered, 2-day course and 1-day course, in this year. These courses consist of the following subjects;

1) Approach-to-critical experiment,
2) Control rod worth measurement,
3) Observation of KUR inherent safety characteristics.

The third subject is to observe the negative reactivity effect due to moderator temperature rise and it is conducted by operating KUR at about 100kW with natural convection operation. In the 2-day course, in addition to the above subject, participants also experience the inspections for start-up and shutdown of the reactor under the guidance of operators, as well as the daily safety inspection.

4. Spent Fuel Take Back Program

The spent fuel of Japanese research reactors is returned to the US in the framework of the US take-back program. The program will terminate in 2016/2019 as described below[4].

The international activities in the back-end of the RR nuclear fuel cycle are dominated by the RR spent fuel take back programs, the United States of America Foreign Research Reactor Spent Nuclear Fuel (FRRSNF) acceptance program and the Russian Research Reactor Fuel Return (RRRFR) program. The major goal of the separate take-back programs for USA and Russian origin fuels is to eliminate inventories of Highly Enriched Uranium (HEU) by returning RR spent nuclear fuel to the country where the fuel was originally enriched. The US FRRSNF acceptance program, also known as the US take-back program, is a longstanding initiative launched originally in 1996 to accept US enriched fuel irradiated by May 2006, and returned by May 2009. Then, a revised record of decision extended these dates to May 2016, and May 2019, respectively.

At present, another extension of the US take back program seems to be difficult, and the international framework of the RR spent fuel disposal or treatment is under discussion. As well as in Japan, the alternative way of disposal or treatment of spent fuel should be determined to continue the operation of research reactors beyond 2016.

5. Summary

- Research reactors (RRs) are useful and indispensable tools for the R&D in the various fields.
- However, most of RRs are older than 40 years, and the ageing management is an important issue for RRs.
- In Japan, only two RRs are operational and all of JAEA's RRs are temporary shutdown because they suffered from the Great East Japan Earthquake on 11th March. To re-start the JAEA's RRs, the approval of the safety report by NRA is necessary, although the schedule is not yet fixed.
- For KUR, one of the operational RRs, the additional safety measures against the station blackout were installed. KUR has been widely used for research and human resource development, and the modifications of irradiation beam ports are in progress to improve the research capability.
- Spent fuels of Japanese research reactors are returned to the US in the framework of the US take-back program. The program will terminate in 2016/2019. To continue the operation of RRs beyond 2016, the way of spent fuel disposal or treatment should be determined with the nation-wide coalition.

Reference

[1] IAEA Research Reactors Database, http://nucleus.iaea.org/RRDB/RR/ReactorSearch.aspx?rf=1.
[2] http://www.jaea.go.jp/jishin/shisetsu.html
[3] http://jrr3.jaea.go.jp/8/images/20121102.pdf
[4] IAEA-TECDOC-1593 (2008).

5. Present status of BNCT at Kyoto University Research Reactor Institute

Hiroki TANAKA, Yoshinori SAKURAI, Minoru SUZUKI, Shin-ichiro MASUNAGA, Yuko KINASHI, Masaru NARABAYASHI, Natsuko KONDO, [1]Toshinori MITSUMOTO,Akira MARUHASHI,Koji ONO

Kyoto University Research Reactor Institute
Asashironishi, Kumatori-cho, Sennan-gun, Osaka 590-0458 Japan
e-mail:h-tanaka@rri.kyoto-u.ac.jp
[1] Sumitomo Heavy Industries, Ltd
Osaki, Shinagawa-ku, Tokyo 141-6025 Japan

At Kyoto University Research Reactor Institute, we have two facilities for BNCT such as a reactor-based and an accelerator-based neutron source. In this article, we will present the characteristics overview of both facilities.

1. Introduction

At Kyoto University Research Reactor Institute, over 400 patients have been treated by BNCT using Heavy Water Neutron Irradiation Facility (HWNIF)[1] of KUR up to the present. The effectiveness of BNCT for treating not only malignant melanoma, and brain tumor but also recurrent head and neck tumor, liver cancer[2], mesothelioma[3] has been demonstrated. On the other hand, we have developed and installed Cyclotron-Based Epithermal Neutron Source (C-BENS) on December 2008[4]. On March 2009, the sufficient intensity of neutron flux for clinical application was successfully obtained. In this article, we introduce current status of HWNIF and C-BENS.

2. Heavy Water Neutron Irradiation Facility (HWNIF)

In **Fig.1**, schematic layout of HWNIF is shown. This facility has a heavy water tank adjacent to the KUR core. In the heavy water tank, a moderator composed of aluminum and heavy water, and a neutron-energy spectrum shifter of heavy water whose thickness changed from 0 to 90cm, were installed. Outside of the spectrum shifter, two thermal neutron filters of 1mm-thick cadmium plate were installed. The energy spectrum of the neutron beam can be changed from almost pure thermal to epi-thermal energy region. The neutron spectrum of epithermal and mixed mode is shown in **Fig.2**. Mixed mode was used for an irradiation of small animal and cell experiments. Epithermal mode was used for clinical studies.

3. Cyclotron-Based Epithermal Neutron Source (C-BENS)

In **Fig.3**, schematic layout of C-BENS is shown. C-BENS consists of a cyclotron accelerator producing protons with the energy of 30 MeV, a beam transports with two scanning magnets to expand proton beam, a moderator, a collimator and an irradiation bed. The moderator consists of two kinds of components. One is the moderator such as iron and lead for reducing the energy of high energy neutron up to 28 MeV emitted from Be(p,n) reaction. The other is the filter such as

aluminum and calcium fluoride producing the several tens keV neutrons.

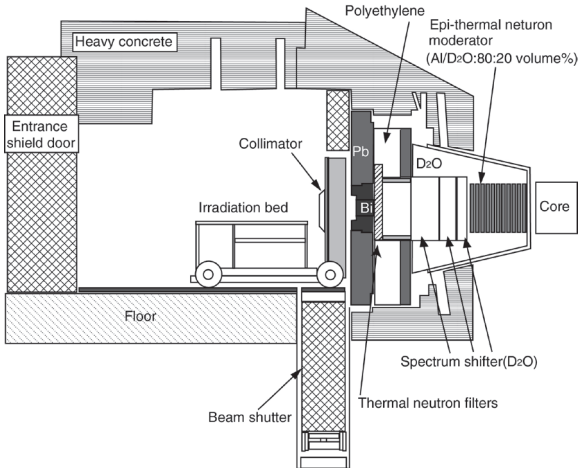

Figure 1 Schematic layout of Heavy Water Neutron Irradiation Facility (HWNIF) of KUR.

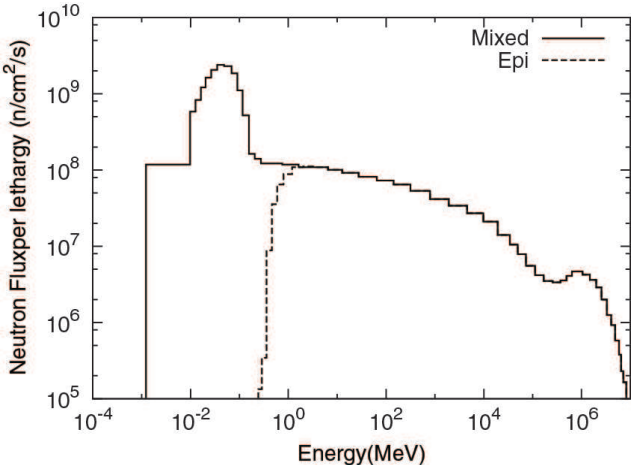

Figure 2 Neutron energy spectrum of HWNIF for mixed and epithermal mode.

Figure 4 shows the neutron spectrum at the surface of gamma-shield of C-BENS. Neutron spectrum of C-BENS has the peak of around 10 keV which is most efficient for giving dose at deeper sited tumor.

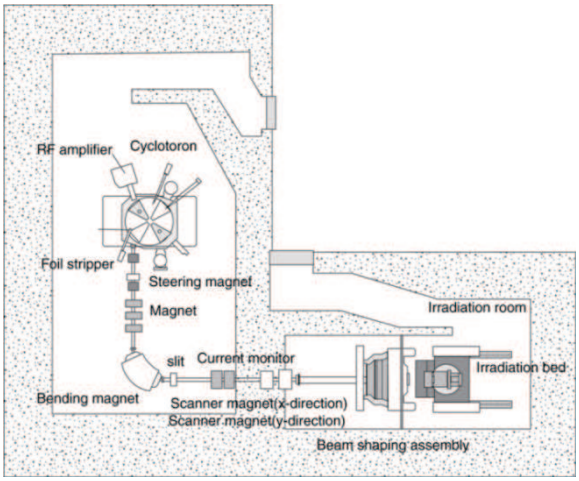

Figure 3 Schematic layout of Cyclotron-Based Epithermal Neutron Source (C-BENS).

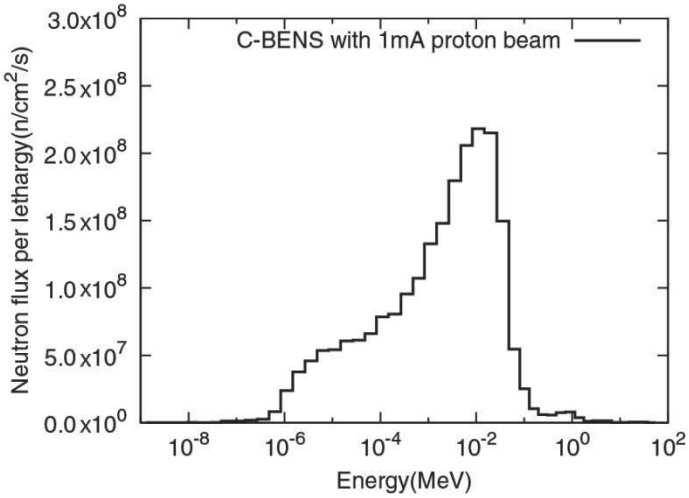

Figure 4 Neutron spectrum of C-BENS.

Epithermal neutron flux of C-BENS is about 1.5 times higher than that of HWNIF. On the other hand, the contamination of gamma dose for HWNIF and C-BENS in treatment beam is 2.4×10^{-13} and 7.6×10^{-14} (Gy/cm^2), respectively. The contamination of fast neutron dose in treatment beam is 9.1×10^{-13} and 5.8×10^{-13} , respectively. It was found that the characteristic of treatment beam of C-BENS is superior to HWNIF.

4. Conclusion

HWNIF and C-BENS have the different source of neutron production with the different neutron energy. Therefore, the optimal moderator, that produces epithermal neutron flux of around 10^9 (n/cm^2/s) for BNCT clinical application, was designed using the suitable nuclear data. Characteristics of treatment beam of both facilities were evaluated. C-BENS has the good beam characteristic compared with HWNIF.

Reference

[1] Y. Sakurai, T. Kobayashi : "Characteristics of the KUR Heavy Water Neutron Irradiation Facility as a neutron irradiation field with variable energy spectra", Nuclear Instruments and Methods in Physics Research A **453**,pp.569-596(2000).

[2] M. Suzuki, Y. Sakurai, S. Hagiwara, S. Masunaga, Y. Kinashi, K. Nagata, A. Maruhashi and K. Ono:" First attempt of boron neutron capture therapy(BNCT) for hepatocellular carcinoma", Jpn J Clin Oncol ,**37**(5), pp.376-381(2007).

[3] M. Suzuki, Y. Sakurai, S. Masunaga, Y. Kinashi, K. Nagata, A. Maruhashi and K. Ono : "Feasibility of boron neutron capture therapy(BNCT) for malignant pleural mesothelioma from a viewpoint of dose distribution analysis", Int. J. Radiation Oncology Biol. Phys., **66**, No. 5, pp.1584-1589(2006).

[4] H. Tanaka, Y. Sakurai, M. Suzuki, S. Masunaga, Y. Kinashi, G. Kashino, Y. Liu, T. Mitsumoto, S. Yajima, H. H. Tsutsui, A. Maruhashi, K. Ono : "Characteristics comparison between a cyclotron-based neutron source and KUR-HWNIF for boron neutron capture therapy", Nuclear Instruments and Methods in Physics Research B **267**, pp.1970-1977(2009).

This is a blank page.

6. Nondestructive Assay using Nuclear Resonance Fluorescence with Laser Compton Scattering Gamma-ray Beam for Safeguards and Key Nuclear Data

Takehito HAYAKAWA[a#], Ryoichi HAJIMA[a], Michio SEYA[b]

[a]Quantum Beam Science Directorate, Japan Atomic Energy Agency
Shirakata-Shirane 2-4, Tokai-mura, Naka-gun, Ibaraki-ken 319-1195 Japan
[b]Integrated Support Center for Nuclear Nonproliferation and Nuclear Security,
Japan Atomic Energy Agency
Funaishikawa 3-1-1, Tokai-mura, Naka-gun, Ibaraki-ken 319-1118 Japan
[#]E-mail: hayakawa.takehito@jaea.go.jp

We review nondestructive assay of plutonium and other fissionable isotopes in spent nuclear fuel using nuclear resonance fluorescence with laser Compton scattering gamma-ray and the nuclear data for this method.

1. Introduction

Nondestructive assay (NDA) of plutonium and other fissionable isotopes in spent nuclear fuel is a key technology for safeguards in the world. One of safeguards issues is the shipper receiver difference (SRD), which is the difference between the quantity of a fissionable nuclide such as ^{239}Pu before a shipping from a nuclear plant (or a facility with nuclear materials) to a reprocessing plant and the quantity that is measured after the fuel reprocessing. The SRD is sometimes not zero, suggesting a possibility that a part of a nuclide of interest might be lost in the reprocessing or in the transportation between two plants. This is, however, considered to originate from a fact that the quantity before the reprocessing is only calculated with a nuclear fuel burn-up simulation code. The method to measure the quantity of fissionable isotopes in nondestructive manner should be developed to resolve fundamentally the SRD problem. In the next generation safeguards initiative (NGSI) program of United States department of energy (DOE), NDA of Pu in the spent nuclear fuel is the top priority in technology development.

For the NDA of Pu in the spent fuel, many techniques, for example X-ray resonance fluorescence or differential die-away analysis with neutrons, have been

studied. However, the NDA of ^{239}Pu in the nuclear fuel assembly has not been well established yet. The spent fuel is often kept in a cooling water pool, since the spent nuclear fuel is heated up due to the decay of the residual radioactivities, and the water absorbs or scatters neutrons and low energy X-rays. In addition, the high-Z element such as uranium in the nuclear fuel absorbs detection probes such as low-energy X-rays. These methods cannot measure practically all isotopic abundances for these heavy elements. Therefore, one should develop a new nondestructive assay for individual fissionable isotopes in the spent nuclear fuel.

Nuclear resonance fluorescence with laser Compton scattering gamma-rays has been proposed as a nondestructive assay of nuclides. In this report we review this method and the relevant nuclear data.

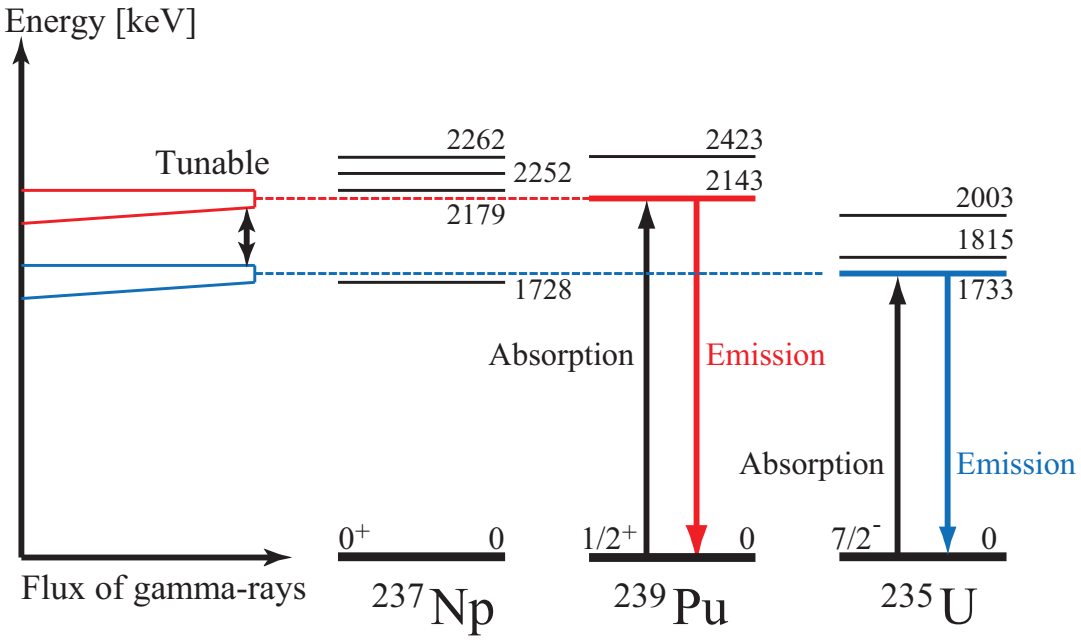

Fig.1 Schematic view for the NRF assay.

2. Nuclear resonance fluorescence with laser Compton scattering gamma-ray beam

Bertozzi *et al.* have proposed a new method to detect a hidden fissionable materials using nuclear resonance fluorescence (NRF) with Bremsstrahlung gamma-rays [1]. However, the Bremsstrahlung gamma-rays generally produce large background at the low-energy side. The NRF measurement in conjunction with energy tunable monochromatic gamma-ray beam generated by laser Compton scattering (LCS) has been proposed for nuclear security [2] and analysis of nuclear wastes [3]. **Figure 1** shows a schematic view of this method. An object is irradiated by a LCS gamma-ray beam. If the energy of the incident gamma-ray beam is

identical with a transition energy from the ground state to an excited state of a nucleus of interest, the incident gamma-rays are effectively absorbed in the nucleus and the excited state is populated. The populated state de-excites subsequently by gamma-ray emission. The energies of the states excited by NRF are inherent in the atomic number and mass of the nucleus of interest. With measuring directly the scattering gamma-rays or measuring the absorption of the incident monochromatic gamma-ray beam, one can know the quantity of the nuclide of interest.

This method has following advantages. First, one can measure materials through heavy shields such as metal plates with thickness of several cm or water with thickness of several ten cm since the energies of the LCS gamma-rays are of the order of several MeV. This gives an advantage for measuring, in particular, nuclear materials in a water cooling canister or fuel assembly kept inside a water pool. Second, one can detect the NRF scattering gamma-rays with a high signal to noise (S/N) ratio since the background in the measured gamma-ray spectrum appears in the energy region lower than the NRF energy. Third, this method is in principal applicable to the non-destructive detection of all the isotopes of all the elements for atomic number $Z > 2$. In other words, unstable isotopes as well as stable isotopes can be detected.

3. Proof-of-principle experiment using available LCS gamma-ray beam

Kikuzawa *et al.* carried out a proof-of-principle experiment to measure an isotope of interest concealed inside a heavy shield using an available LCS gamma-ray beam [4]. A lead block was hidden by iron plates with the thinness of 15 mm and the position of the lead block was detected by measuring a 5512-keV gamma-ray of ^{208}Pb with the LCS gamma-rays generated at the National Institute of Advanced Industrial Science and Technology (AIST). This method can be extended to measure different two nuclides with the same time using a wide energy spread gamma-ray beam, whose energy covers the NRF energies of two nuclides. Hayakawa *et al.* demonstrated a detection of two isotopes at the same time [5]. They detected two nuclides of ^{12}C and ^{14}N in a chemical compound, melamine ($C_3H_6N_6$), through a 15-mm thick iron plate and a 4-mm thick lead plate using the LCS gamma-ray beam at AIST. A similar demonstration to detect hidden materials has been subsequently carried out using a LCS gamma-ray beam produced by the T-REX source at the Lawrence Livermore National Laboratory [6]. Toyokawa *et al.* presented two-dimensional imaging of a lead triangular prism in a material, which is hidden by a 15-mm iron plate box at AIST [7]. An advantage of NRF is that we

can distinguish several isotopes of an element. It was demonstrated to measure two lead isotopes, ^{206}Pb and ^{208}Pb, in the iron shield box with two different energy LCS gamma-ray beams at AIST [8].

4. Next generation of LCS gamma-ray source for safeguards

A key technology for the NRF assay is the high-flux LCS gamma-ray source. Hajima *et al.* has proposed a high-flux gamma-ray facility utilizing a 350-MeV energy recovery linac (ERL) equipped with a superconducting accelerator [3]. The ERL accelerator is the next generation of accelerator to generate a high-quality electron beam with a high-intensity average-current. This gamma-ray source can measure 1% fraction ^{239}Pu in all the fuel rods in a BWR fuel assembly with statistical error lower than 2% with the measurement time of 4000 s [9].

5. Nuclear Data

The most important nuclear data for the NRF assay is excitation energies and resonance widths of exited states in nuclei of interest. The spins and parities of NRF levels are useful for calculation of the angular distribution of the scattered gamma-rays in viewpoint of practical measurement technique. The resonance width (or mean lifetime) of an excited state has been usually measured using in-beam gamma-ray spectroscopy technique with nuclear reactions. Among all nuclear reactions, direct photon excitation reactions are most effective to measure the resonance width and energy for each excited state populated directly from the ground state. The NRF assay can measure in principle all actinide, for example ^{241,243}Am and ^{244,245,247}Cm. The nuclear data for these nuclides have not been, however, studied well.

Recently, it becomes clear that the NRF for the actinide is of importance for the NRF assay as well as nuclear physics and thus excited states on ^{235}U [10], ^{239}Pu [10,11], ^{240}Pu[12], and ^{237}Np[13] have been measured using NRF with Bremsstrahlung gamma-rays. Two nuclides of ^{235}U [14] and ^{238}U [15] have been also studied using laser Compton scattered gamma-rays. Strong M1 resonances are systematically observed in these nuclides. These resonances can be understood by the scissors mode of nuclear collective motions in viewpoint of the nuclear physics. This suggests that there are probably M1 resonances around 2 MeV in all actinide isotopes. There is a discrepancy between the results for ^{235}U in Refs. [10] and [11]. This indicates that we should perform further nuclear experiments and evaluate the nuclear data systematically for the NRF method.

References

[1] W. Bertozzi and R.J. Ledoux: Nucl. Instr. and Meth. B **241**, 820 (2005).

[2] J. Pruet, D.P. McNabb, C.A. Hagmann, F.V. Hartemann, C.P.J. Barty: J. Appl. Phys. **99**, 123102 (2006).

[3] R. Hajima, T. Hayakawa, N. Kikuzawa and E. Minehara: J. Nucl. Sci. Technol., **45**, 441 (2008) .

[4] N. Kikuzawa, R. Hajima, N. Nishimori, E. Minehara, T. Hayakawa, T. Shizuma, H. Toyokawa, H. Ohgaki: Appl. Phys. Express, 2, 036502 (2009).

[5] T. Hayakawa, H. Ohgaki, T. Shizuma, R. Hajima, N. Kikuzawa, E. Minehara, T. Kii, H. Toyokawa: Rev. Sci. Instr., **80**, 045110 (2009).

[6] F. Albert, *et al.*: Optics Letters, **35**, 354 (2010).

[7] H. Toyokawa, H. Ohgaki, T. Hayakawa, T. Kii, T. Shizuma, R. Hajima, N. Kikuzawa, K. Matsuda, F. Kitatani and H. Harada: Jpn. J. Appl. Phys. **50**, 100209 (2011).

[8] T. Shizuma, T. Hayakawa, R. Hajima, N. Kikuzawa, H. Ohgaki and H. Toyokawa: Rev. Sci. Instr. **83**, 015103 (2012).

[9] T. Hayakawa, N. Kikuzawa, R. Hajima, T. Shizuma, N. Nishimori, M. Fujiwara and M. Seya: Nucl. Instrum. Methods Phys. Res. A **621**, 695 (2010).

[10] O. Yevetska, J. Enders, M. Fritzsche, P. von Neumann-Cosel, S. Oberstedt, A. Richter, C. Romig, D. Savran, and K. Sonnabend: Phys. Rev. C **81**, 044309 (2010).

[11] W. Bertozzi, J. A. Caggiano, W. K. Hensley, M. S. Johnson, S. E. Korbly, R. J. Ledoux, D. P. McNabb, E. B. Norman, W. H. Park, and G. A. Warren: Phys. Rev. C **78**, 041601(R) (2008).

[12] B.J. Quiter, T. Laplace, B.A. Ludewigt, S.D. Ambers, B.L. Goldblum, S. Korbly, C. Hicks, and C. Wilson: Phys. Rev. C **86**, 034307 (2012).

[13] C.T. Angell, R. Yee, T.H. Joshi, E. Swanberg, E.B. Norman, C.L. Hicks, Jr., A. Klimenko, S. Korbly, C. Wilson, W. D.Kulp, G.A. Warren, T.H. Bray, R. Copping, P.A. Glans, T. Tyliszczak and D.K. Shuh: Phys. Rev. C **82**, 054310 (2010).

[14] E. Kwan *et al.*, Phys. Rev. C **83**, 041601(R) (2011).

[15] S.L. Hammond *et al.*, Phys. Rev. C **85**, 044302 (2012).

This is a blank page.

7. Experiments on Accelerator Driven Subcritical System (ADS) and Nuclear Data for ADS Design

Tsuyoshi Misawa

Research Reactor Institute, Kyoto University, Kumatori, Osaka 590-0494, Japan

E-mail: misa@rri.kyoto-u.ac.jp

Basic experiments for an accelerator driven subcritical system (ADS) have been carried out at Kyoto University Critical Assembly (KUCA) combined with FFAG (Fixed Field Alternating Gradient) proton accelerator from 2009 for developing ADS for transmutation or for an innovative neutron source which can be utilized like a present research reactor.

1. Introduction

An accelerator driven subcritical system (ADS) is a new hybrid system combined with nuclear fuel and an accelerator which can inject neutrons into a reactor. Because a core in ADS is operated in subcritical state and its steady state can be achieved by injected neutrons from an accelerator, energetic reactivity accidents hardly occur at ADS and its operation can be terminated by simply stopping the accelerator operation without using control rods. It has attracted worldwide attention in recent years for transmuting nuclear wastes such as minor actinides and long-lived fission products due to its superior safety characteristics and potential for burning nuclear wastes because of using high energy neutrons.

At Kyoto University Research Reactor Institute (KURRI), a new project for research on ADS has been performed using a multi-core type research reactor, Kyoto University Critical Assembly (KUCA) whose maximum power is 100 W, combined with a Cockcroft-Walton type accelerator to produce 14 MeV neutrons by D-T reactions or an up to date FFAG (Fixed Field Alternating Gradient) accelerator to produce proton beam with 100 to 150 MeV. The purposes of ADS basic research in KURRI are to develop a new system for transmutation of minor actinides or for an innovative neutron source which can be utilized like a present research reactor.

2. Basic experiment at KUCA with FFAG accelerator

The KUCA A-core, which is a solid-moderated one with highly enriched uranium fuels and the polyethylene moderator among the three cores (A, B and C) of the KUCA, has been used for ADS experiments. A polyethylene moderated and reflected core loaded with 93% uranium-aluminum (U-Al) alloy fuel was assembled at the A-core. The fuel rod was consisted of polyethylene and U-Al plates with the upper and lower polyethylene reflector of more than 50cm, respectively. The neutron spectrum of the core can be varied by changing combination of approximately 1.6-mm (1/16-inch) thick U-Al plates and approximately 3.1-mm (1/8-inch) thick polyethylene plates piled up in the fuel rod. Before starting ADS experiments with FFAG proton accelerator, a Cockcroft-Walton type accelerator which is installed at KUCA building to accelerate deuteron beam up to around 300keV and make collision with a tritium target located outside the core generate 14MeV pulsed neutrons by D-T reaction was utilized for basic experiments.

In 2009, the world's first experiments on ADS with KUCA and the FFAG proton accelerator shown in **Figs. 1** and **2** were successfully started by producing high energy neutrons generated by bombarding a tungsten target [1].

These ADS experiments at KUCA include various kind of reactor physics measurements to investigate basic characteristics of ADS; (1) subcriticality measurement by pulsed neutron method or other methods mentioned below, (2) neutron flux distribution measurement by using optical fiber detectors or by foil and wire activation method in subcritical core, (3) neutron spectrum measurement by irradiated activation foil or unfolding method using a liquid scintillator, (4) neutron noise analysis such as new variance to mean ratio method with pulsed neutron source to measure core properties, (5) reactor dynamics measurements caused by perturbation. Since one of the features of KUCA is that it is easy to change the core configuration or fuel composition for altering neutron energy spectrum, those ADS experiments have been carried out at various cores. These experimental data were also analyzed by Monte Carlo code, such as MCNPX, or other deterministic calculation codes to investigate various reactor physics parameters.

Fig.1 FFAG proton accelerator

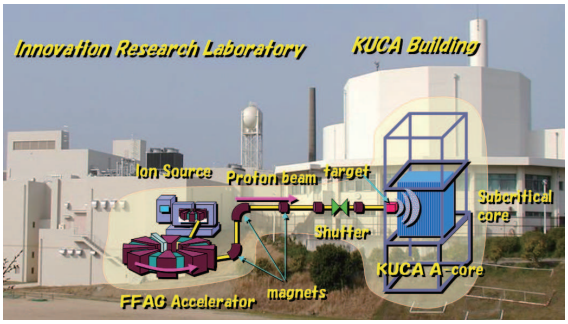

Fig. 2. KUCA and FFAG complex for ADS research

To confirm the produced neutron energy from the Tungsten (W) target which was set at the end of proton beam line from FFAG accelerator as shown in **Fig. 3**, Bismuth (Bi) foil was irradiated in front of the target because Bi has several capture reactions such as Bi(n,xn) reactions with different threshold energy. **Figure 4** shows gamma-ray spectrum from irradiated Bi foil and more than 50 MeV energy neutrons were detected by this method.

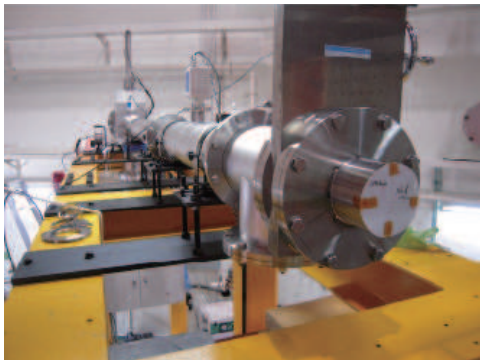

Fig. 3 End of proton beam line with W target

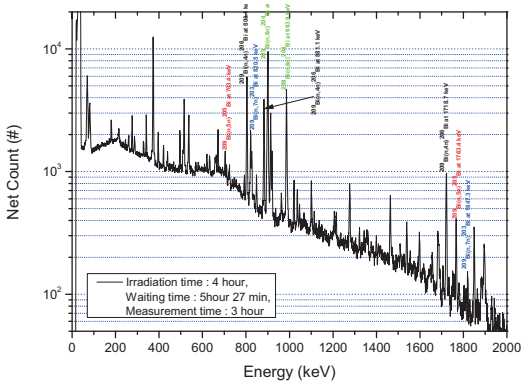

Fig. 4 Gamma-ray spectrum from irradiated Bi foil

Figures 5 and **6** show measured indium reaction rate (^{115}In(n,g)^{116m}In) distribution at A3/8"P36EU(3) core which has soft neutron spectrum core in horizontal (Fig. 5) and vertical (Fig. 6) distribution with calculated results. In these calculations, MCNPX was adopted in the fixed source calculations, where the external source was modeled at the subcritical states by a homogeneous 100 MeV proton circular surface source of 40 mm diameter (spot size) injected onto the tungsten target. High-energy neutrons and protons over 20 MeV were transported using LA150N library in which the ENDF/B-VI.8 data is extended from 20 to 150 MeV, if available, otherwise the LAHET physics model was used. The number of histories used in the fixed source calculations was approximately 10^8 and the statistical error in the reaction rate was 2.7% in average. Those results show good agreement within the given statistical error [2].

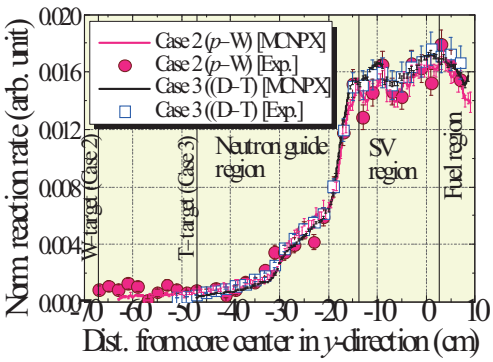

Fig. 5 Indium reaction rate at outer region

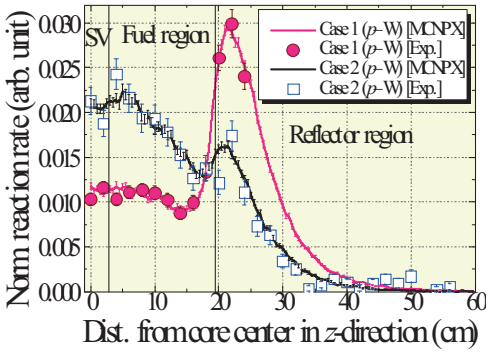

Fig. 6 Indium reaction rate in vertical direction

Subcriticality measurement in real time at ADS is one of the important research subjects in ADS development to assure safety operation under subcritical state, and several experimental techniques have been applied for this purpose at KUCA; pulsed neutron method [3], neutron source multiplication method, and neutron noise analysis methods including time domain analysis and frequency domain analysis methods. Among those methods, neutron noise analysis method is thought to be an appropriate method for this purpose because of its accuracy and reliability. The ADS system, neutron counts are fluctuated not only by the effect of chain reaction that is observed in a critical reactor, but also by the periodic operation of external neutron source from the accelerator. Including these effects, new formulation based on the variance-to-mean ratio method (Feynman-alpha method) and new noise data acquisition system were developed, which have been adopted in KUCA experiments [4]. Through the experiments, it was found that subcriticality of the system that was obtained from the prompt neutron decay constant (alpha value) can be observed in a real time by analyzing neutron noise data acquired during operation of ADS.

Since thorium fueled reactor experiments have been one of the important research topics at KUCA and the usage of thorium in ADS to produce ^{233}U fissile fuel has been the attractive purpose for ADS operation, KUCA core loaded with thorium metal fuel was also used for ADS research combined with FFAG proton accelerator and various static and kinetic parameters including thorium reaction rate such as capture reaction rate has been measured and those results were compared with MCNPX calculation results to confirm the accuracy of nuclear data of thorium in high energy region because of lack of enough experimental date [5]. At the preset stage of experiments at KUCA, beam power from FFAG, namely neutron production rate from proton target, is not enough to measure the fission reaction rate of thorium, however, those researches will be continued for the future with continual effort to increase the proton beam current of the accelerator. Now, the proton beam current of FFAG main ring is approximately 1 nA and it is possible to increase up to 10 nA in the near future, and moreover, hopefully up to 100 nA through minor improvement of the system.

3. ADS neutron source

A research reactor such as KUR (Kyoto University Reactor, whose thermal power is 5 MW) at KURRI has been widely used as a steady state strong neutron source for research activities such as neutron activation analysis, neutron diffraction analysis, neutron radiography, production of radioisotopes and so on. Recently, safety demand for nuclear reactor operation has become much more severe, which is also applied even to research reactors whose thermal power level is much less than conventional power reactors because of the Fukushima NPP accident of 2011, then construction of new research reactors has become difficult especially in Japan. On the other hand, research fields with use of neutrons have become wider and intense neutron source such as a big research reactor is expected to be constructed. On the other hand, the advantage of ADS is its safety operation characteristics and ability to produce various energy neutrons of high energy neutrons from accelerator target and thermalized neutrons by moderator, which means that ADS has a great potential to be used as an intense neutron source like a research reactor.

A design of ADS strong neutron source has been carried out with MCNP Monte Carlo code, and **Fig. 7** shows an example. It is assumed that this system can be replaced by KUR reactor with using the existing same reactor building, biological shielding concrete, irradiation holes and control room, and fuel assemblies are settled at the bottom of the core tank inside the shielding concrete. It uses pin type UO_2 fuels with low enriched uranium fuel (less than 5 wt%) like conventional power reactor because it is possible to fabricate at Japanese nuclear fuel companies and to be reprocessed in Japan without complicated technical problem. It uses light water as moderator material like KUR reactor without forcing water circulation cooling system, which means that the maximum power level should be less than 100 kW with safety point of view. Proton beams are injected horizontally from outside into the core and are bombarded into beryllium metal target located at the center of the core to produce high energy neutrons. The performance of ADS such as thermal power and neutron intensity largely depends on power of proton beam, namely, the performance of accelerator, and in this design, it is assumed to use a compact cyclotron accelerator (30 MeV proton beam in 2 mA) for BNCT cancer therapy which has been recently developed and available at KURRI. Note that in the present design of ADS, basic concept is that it can be constructed without research and development works, namely, all system should be established with existing technologies, and for this reason, the above compact cyclotron accelerator was selected as the present ADS. This system has several neutron irradiation holes at inner region of the core to insert irradiation materials from outside by using such as a pneumatic system. To increase thermal neutron flux at those irradiation holes, the core consisted of two regions; inner hard neutron spectrum region near the proton target region with tight fuel pitch lattice and outer soft neutron spectrum region with loose fuel pitch lattice to increase k-eff, and the core was surrounded by outer graphite reflector region where outer neutron irradiation holes are possible to be installed.

Neutron multiplication factor (k-eff) of ADS is very important parameter in ADS design. If k-eff approaches unity, the power level will increase, however, the safety margin which is important feature of ADS operation becomes small. On the other hand, if k-eff becomes less than 0.95, which is upper criteria

in nuclear fuel treatment facility such as a fuel storage facility or a spent fuel transport cask, ADS construction and operation is expected to become much easier in the view point of receiving admission from safety authority because safety margin until super critical state becomes much larger. In the present design, k-eff was set to be less than 0.9 to ensure large safety margin and, hopefully, to be controlled by the safety authority not under existing reactor regulations.

The results of thermal neutron flux distribution in horizontal direction is shown in **Fig. 8**, and it is found that neutron flux shows maximum value at the irradiation holes of 5-cm-diam. which are located at the boundary of the inner and outer core regions. In this design, total thermal neutron power is approximately 30 kW and the peak value of thermal neutron flux at inner irradiation hole is about 1.2×10^{12} (n/sec/cm^2), which is comparable to the value at the pneumatic irradiation hole (Pn-2) of KUR at 400 kW operation. This fact indicates that the performance of the present ADS neutron source, namely the intensity of maximum thermal neutron flux, is comparable to a low power (400 kW) research reactor. This fact indicates that the amount of spent fuel produced by its operation is less than 10% compared with conventional reactor operation with same amount of thermal flux level. Researchers who have used the neutron irradiation holes at KUR require much higher thermal neutron intensity for neutron source, however, since this is a preliminary design of new ADS, more improved results will be expected through detailed investigation, for example, arrangement of fuel pins or irradiation holes, and improvement of the performance of accelerator.

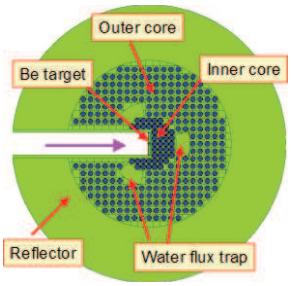

Fig. 7 Horizontal cross section of the core

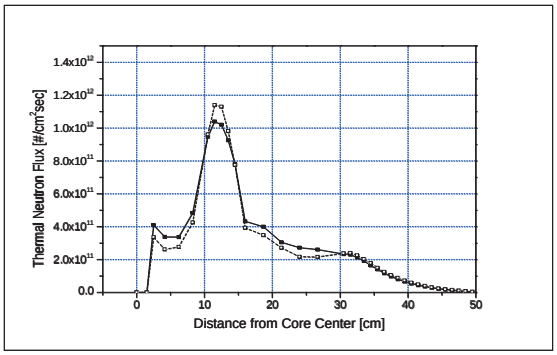

Fig. 8 Horizontal thermal flux distribution

4. Conclusions

The basic experimental research on ADS has just been started using KUCA combined with FFAG proton accelerator, and other worldwide ADS research project will be followed from now. We will continue the project on ADS research for development of the future nuclear system for transmutation of minor actinides or for an innovative intense neutron source which can replace research reactor.

References

[1] C. H. Pyeon *et al.*, "First Injection of Spallation Neutrons Generated by High-Energy Protons into the Kyoto University Critical Assembly," *J. Nucl. Sci. Technol.*, **46**, 1091 (2009).
[2] C. H. Pyeon *et al.*, "Experimental Analyses of External Neutron Source Generated by 100 MeV Protons at the Kyoto University Critical Assembly," *Nucl. Eng. Technol.*, **45**, 81 (2013).
[3] T. Yagi *et al.*, "Application of Wavelength Shifting Fiber to Subcriticality Measurements," *Appl. Radiat. Isot.*, **72**,11 (2013).
[4] Y. Kitamura *et al.* "Application of Variance-to-mean Technique to Subcriticality Monitoring for Accelerator-Driven Subcritical Reactor," *Int. J. Nucl. Energy Sci. and Technol.*, **2**, 266 (2006).
[5] C. H. Pyeon *et al*., "Reaction Rate Analyses in the Thorium-Loaded Accelerator-Driven System at the Kyoto University Critical Assembly," *Trans. Am. Nucl. Soc.*, **105**, 792 (2011).

8. Evaluation of Covariance Data of JENDL

Osamu Iwamoto
Nuclear Data Center, Japan Atomic Energy Agency
Tokai-mura, Ibaraki 319-1195
e-mail: iwamoto.osamu@jaea.go.jp

1. Introduction

An advance of covariance data is one of main topics on the latest version of Japanese Evaluated Nuclear Data Library, JENDL-4.0[1]. The covariance data indicate uncertainties of the evaluated nuclear data with correlations between the different data, e.g. the data at different neutron energies; they were represented by matrices. A large amount of efforts was focused on evaluating the covariance data, resulting in provision of enhanced covariance data covering over all reactions for all actinides in JENDL-4.0[1,2]. They include those for resonance parameters, reaction cross sections, fission neutron spectra, and neutron numbers per fission, which are required for fission reactor applications.

Recently, an important revision of covariance data has been made for the covariance data at resonance energy ranges for major actinides of $^{233, 235, 238}$U and ^{239}Pb. It might make significant impacts on uncertainty estimation for thermal reactors. The revised data were released as JENDL-4.0 Updated File on September 2012 and are available from a website.

Since more covariance data would be needed in nuclear reactor applications, further attempt to evaluate new covariance data for non-actinides was started after the release of JENDL-4.0. The new evaluation has been planned to cover the 17 elements from C to Bi whose needs arose from thermal and fast reactors as well as advanced reactors. Preliminary results for Sm and Pb were obtained up to now and are in progress for other elements.

In this article, overview of the methods and result of the covariance evaluations for JENDL-4.0 are shown. The updated covariance data for major actinides and the preliminary results for non-actinides, which have been evaluated after the release of JENDL-4.0, are also mentioned.

2. Evaluation Method of JENDL-4.0 covariance

The covariance information of the nuclear data in JENDL-4.0 was estimated based on the experimental data and the evaluation methodology applied to each of the nuclear data. The covariance evaluations were performed for 1) number of fission neutron, 2) resonance parameter, 3) cross section, 4) angular distribution of elastic scattering (1st order Legendre coefficient), and 5) fission spectrum. The methods applied for the minor actinides are mainly described in this section. Details of the covariance evaluation for JENDL-4.0 are reported in

references[1,2].

The covariance information at the resonance region of minor actinides was provided as a sum of contributions from resonance parameter uncertainties without correlations and long range cross section uncertainties which were introduced to compensate the ignored correlations between resonance parameters. The resonance parameter uncertainties were obtained from results of resonance analyses in literatures or the recommendation of Mughabghab[3]. For unknown cases, resonance energy uncertainties were assumed to be 0.1% and those for widths of neutron, fission and gamma to be 10-50% depending on uncertainties of the other resonances. Thermal cross section uncertainties were evaluated based on experimental data. Uncertainties of negative resonance parameters were adjusted or cross section uncertainties were added so as to reproduce the evaluated uncertainties at thermal energy.

For fast neutrons, the fission cross sections, for which experimental data were abundant, were evaluated by least-square fitting with GMA code[4]. In this case, the covariance matrices were obtained at the same time as the cross section evaluation. They were adopted in JENDL-4.0 with modification by taking account of consistencies with the experimental data. For major actinides, covariance data were obtained from simultaneous evaluation by SOK code at the same time of the cross section evaluation.

For other cross sections and elastic scattering angular distributions, which were evaluated by nuclear model calculations, the covariance matrices were obtained by using the CCONE-KALMAN code system, in which sensitivities of data to nuclear model parameters were calculated by the CCONE code[5] and least squares fittings to experimental data were performed by the KALMAN code[6] with the calculated sensitivities. On the evaluation with CCONE-KALMAN, three different evaluation procedures were employed. They were categorized by adoption of the experimental data. For capture cross section, the covariance matrices were obtained by applying all reliable experimental data with correlations among experimental data sets to the analyses (hereafter referred as “high fidelity”). For other cross section with experimental data, covariance was evaluated by using the uncertainties estimated form experimental data at

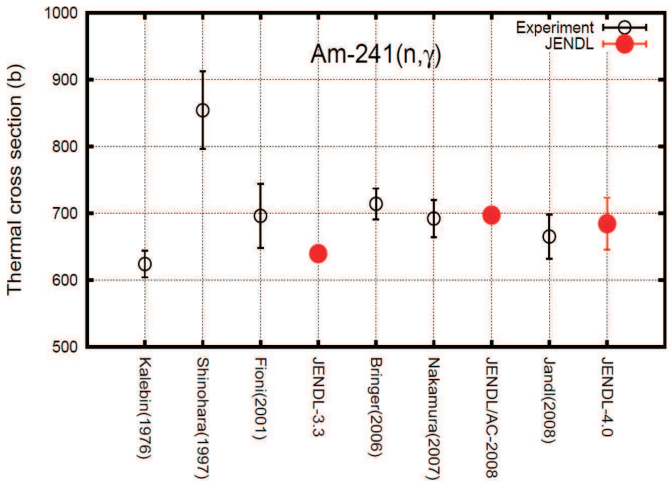

Fig. 1. Thermal cross section for ^{241}Am. A partial cross section to ground state (620 ± 25) measured by Nakamura *et al.* (2007) is converted to total one using JENDL-4.0 isomeric ratio of 0.896.

several energy points ("middle fidelity"). If no experimental data were available, their covariance matrices were obtained from model parameter uncertainties which were decided so as to reproduce experimental data spreading ("low fidelity"). The sensitivities of the cross sections were calculated for approximately 50 parameters such as those for optical model potentials, level densities, gamma strength functions, and fission barriers.

3. Evaluated Results

The evaluated results are shown for a few cases of minor actinides in this section.

Figure 1 shows thermal capture cross sections of ^{241}Am plotted in chronological order. Experimental and evaluated data are shown by open and closed circles, respectively. The cross section uncertainty (±1σ) of JENDL-4.0, which is calculated from the resonance parameter covariance, is shown by an error bar. The JENDL-4.0 agrees with measured data within the uncertainty except the data of Shinohara.[7]

Figure 2 shows the result of GMA evaluation for ^{242m}Am fission cross section. While the data of JENDL-3.3 was evaluated based on a experimental data set of Browne *et al,* much more data sets measured by several authors were included in the analysis for JENDL-4.0. Within the resulting evaluated uncertainty, JENDL-4.0 agrees with JENDL-3.3.

In **Fig. 3**, the ^{237}Np capture cross section of JENDL-4.0, whose covariance data were evaluated by

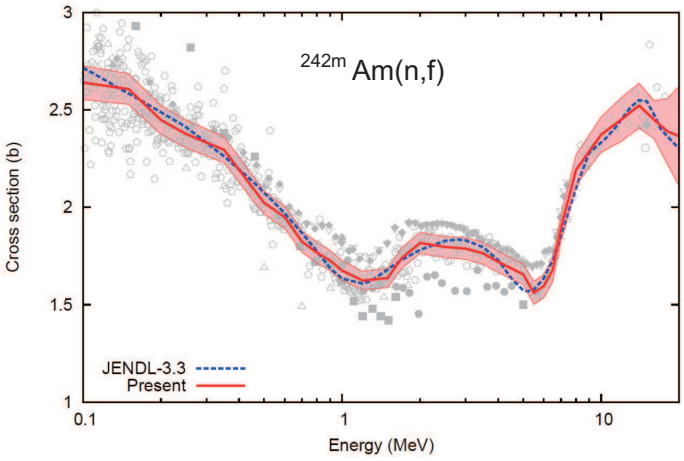

Fig. 2. Fission cross section for ^{242m}Am. Solid and dashed lines show data of JENDL-4.0 and JENDL-3.3, respectively. Shaded area shows evaluated uncertainties of JENDL-4.0.

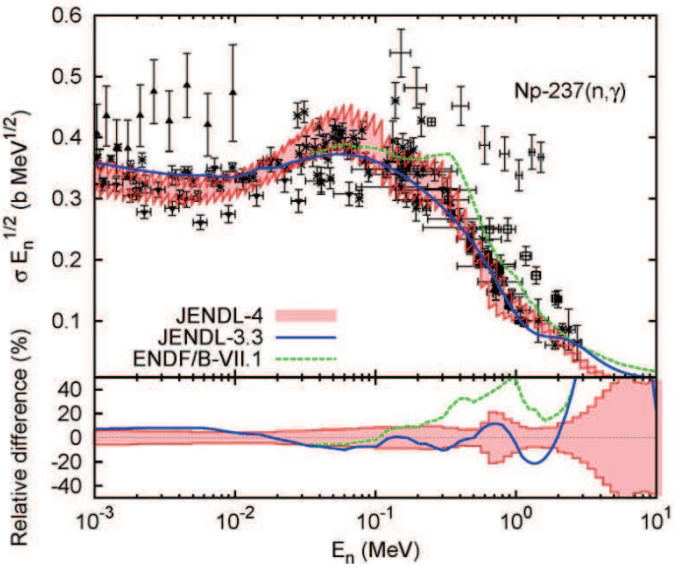

Fig. 3. ^{237}Np capture cross section. Cross sections and relative differences are shown in upper and lower panels, respectively. JENDL-4.0 is shown by shaded area which means uncertainties. In the upper panel, cross sections are multiplied by $E_n^{1/2}$ for visualization, where E_n is incident neutron energy. Experimental data are shown by various symbols.

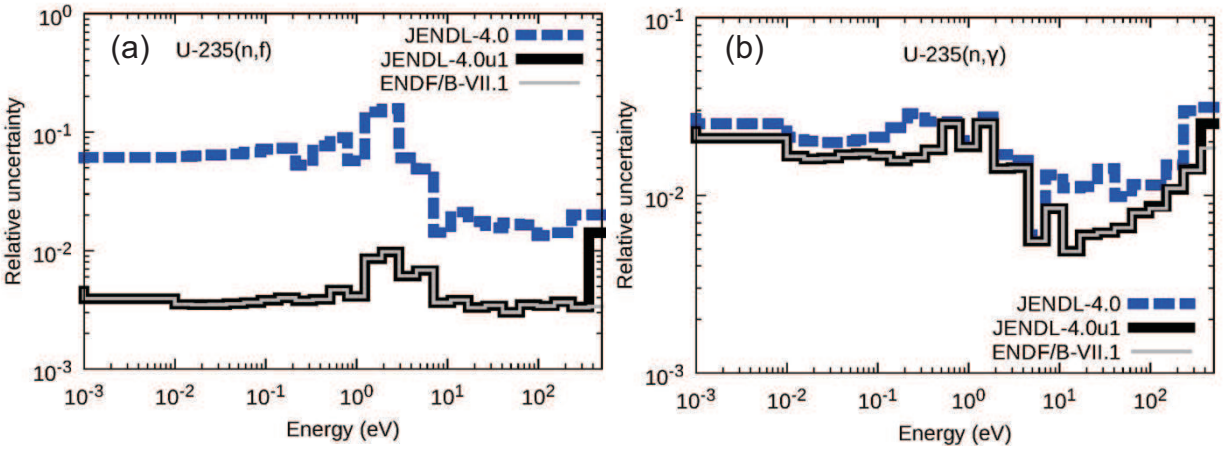

Fig. 4. Uncertainties of ^{235}U (a) fission and (b) capture cross sections. Thick solid line and dashed lines show JENDL-4.0 and JENDL-4.0u, respectively. Data of ENDF/B-VII.1 is indicated by thin gray lines.

CCONE-KALMAN with high fidelity, is compared with measured and evaluated data. The cross section with uncertainty (±1σ) of JENDL-4.0 is shown by the shaded area. JENDL-4.0 agrees with JENDL-3.3 and ENDF/B-VII.0 below 1 MeV and 200 keV, respectively, within the uncertainty. Above 3 MeV, where no experimental data are available, deviations become much larger. However, it might give only a small impact on reactor applications because the cross section becomes small significantly.

4. Progress in covariance evaluation for JENDL-4.0

4.1 JENDL-4.0 Update File

It was found that the covariance data for major actinides of ^{233}U, ^{235}U, ^{238}U and ^{239}Pu in JENDL-4.0 had a problem in the resolved resonance region, which was attributed to the truncation of the original covariance matrix of the original resonance parameters derived by the SAMMY analysis at ORNL. The covariance matrices of the cross sections for ^{233,235,238}U and ^{239}Pu have been recalculated with the full covariance matrices of the resonance parameters by the NJOY-99 code applying a patch provided by G. Chiba[8]. The NJOY results have been adopted as covariance data of cross section in the library. The largest impact appears in the ^{235}U(n,f) cross section in thermal energy region as shown in Fig. 4(a). On the other hand, that of capture cross section is not so significant (Fig.4(b)). The updated data are now available as JENDL Updated Files from a web site[9].

4.2 New evaluation of covariance data for JENDL-4.0

To meet needs of covariance data, new evaluation of covariance is in progress for the elements of C, N, Zr, Mo, Tc, Ru, Rh, Ag, Cd, In, Cs, Nd, Sm, Eu, Gd, Pb, and Bi. Preliminary results have been obtained for some of the elements such as Sm and Pb.

Figure 5 shows the evaluated uncertainties of total cross sections for Sm isotopes and

natural Sm. They were evaluated by CCONE-KALMAN code system with sensitivities to optical model parameters so as to reproduce uncertainties of the experimental data for natural Sm; the data of s-wave neutron strength function for each isotopes[3] were also taken into account. The calculated result without cross correlation between isotopes significantly underestimates the cross section uncertainty for natural Sm as shown in **Fig. 5**. Therefore it is needed to include cross correlations in the evaluated files so as to reproduce the uncertainties for natural Sm which is expected from experimental data.

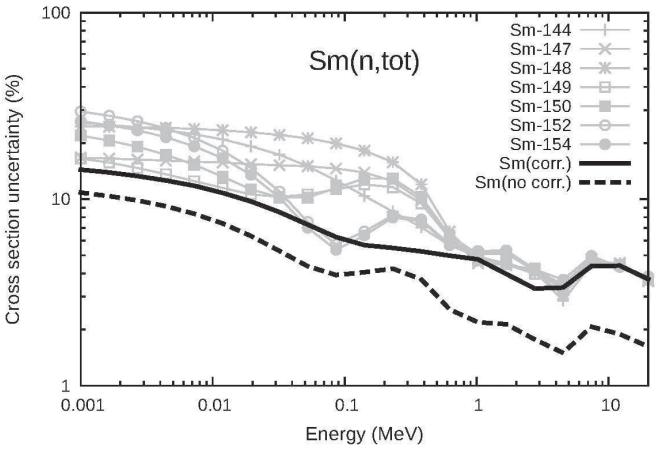

Fig. 5. Evaluated uncertainties of Sm total cross sections. Those of Sm isotopes are shown by various symbols connected by lines. Thick solid and dashed lines are those for natural Sm with and without cross isotope correlations, respectively.

5. Summary

Covariance data associated with the nuclear data required for reactor applications had been evaluated for all actinides in JENDL-4.0 until its release date. An overview of the methods and results of the covariance evaluation was described mainly for minor actinides.

Progresses on evaluation of covariance data after the release were shown. One of them is the revision of the data in resonance region for the major actinides. The largest change was appeared for fission cross sections for ^{235}U. For capture cross section, it was not so significant. The revised data were released as JENDL-4.0 Updated Files, which are available on a website[9]. New evaluations of covariance for the non-actinide data of JENDL-4.0 are in progress for 17 elements from C to Bi. Some preliminary results have been obtained. The results of Sm total cross sections were shown with indicating an impact of the cross correlations between the isotopes.

Reference

[1] K. Shibata *et al.*, "JENDL-4.0: A New Library for Nuclear Science and Engineering," *J. Nucl. Sci. Technol.*., **48**(1), pp.1-30 (2011).

[2] O. Iwamoto, T. Nakagawa, N. Otuka, and S. Chiba: "Covariance Evaluation for Actinide Nuclear Data in JENDL-4," Proc. the 2010 International Conference on Nuclear Data for Science and Technology (ND2010), *J. Korean. Phys. Soc.*, **59**(23), pp.1224-1229 (2011).

[3] S. F. Mughabghab, “Atlas of Neutron Resonances, Resonance Parameters and Thermal Cross Sections, Z=1-100,” Elsevier, Amsterdam (2006).

[4] W. P. Poenitz, "Data interpretation, objective evaluation procedures and mathematical techniques for the evaluation of energy-dependent ratio, shape and cross section data," Proc. Conf. Nuclear Data Evaluation Methods and Procedures, Upton, USA, Sep. 22–25, 1980, BNL-NCS-51363, Vol. I, 249 (1981).

[5] O. Iwamoto, “Development of a comprehensive code for nuclear data evaluation, CCONE, and validation using neutron-induced cross sections for uranium isotopes,” *J. Nucl. Sci. Technol.,* **44**[5], pp.687-697 (2007).

[6] T. Kawano, K. Shibata, “Covariance Evaluation System,” JAERI-Data/Code 97-037, Japan Atomic Energy Research Institute (JAERI) (1997), [in Japanese].

[7] N. Shinohra, Y. Hatsukawa, K. Hat, N. Kohno, “Radiochemical Determination of Neutron Capture Cross Sections of ^{241}Am”, *J. Nucl. Sci. Technol,* **34**[7], pp.613-621 (1997).

[8] G. Chiba, private communication (2011).

[9] JENDL-4.0 Update Files, http://wwwndc.jaea.go.jp/jendl/j40/update/.

9. On the Uncertainty of Experimental Nuclear Data
- Taking a lesson from the other -

Hideo HARADA

Nuclear Science and Engineering Directorate, Japan Atomic Energy Agency
Tokai-mura, Naka-gun, Ibaraki-ken 319-1195 Japan
e-mail: harada.hideo@jaea.go.jp

Possible paths to obtain the nuclear data with the required target accuracy are discussed based on the lessons from the research field of fundamental physical constants and recent advancements on nuclear data measurement techniques.

1. Introduction

The nuclear data needs for advanced reactor systems have been identified by the activities of WPEC Subgroup 26 (SG-26) “Uncertainty and Target Accuracy Assessment for Innovative Systems Using Recent Covariance Data Evaluations”. The target accuracies on selected important nuclear data were deduced for each selected nuclear system [1]. The current uncertainties of relevant nuclear data were also evaluated. It was systematically shown that there exist significant gaps between the current uncertainties and the target accuracies.

It is recognized that it is a hard task to obtain the nuclear data with the required target accuracy. In order to take lessons for approaching the accurate and precise data, some experiences in the research field of fundamental physical constants are discussed, where the fundamental physical constants were consistently determined with extremely small uncertainties, less than ppm (parts per million) order.

The evaluations and experiments on ^{241}Am capture cross section are reviewed as an example of nuclear data, and are compared with the examples on fundamental physical constants. With the lessons from the research field of fundamental physical constants and the recent advancements on nuclear data measurement techniques, possible paths to obtain the nuclear data with the required target accuracy are discussed.

2. Lessons from other fields

Each nuclear data has a unique value, as the fundamental physical constants such as electron mass, speed of light, etc. have. These constants have been revised periodically by the Committee on Data for Science and Technology (CODATA), and have been determined with extremely small uncertainty, less than ppm order, as tabulated in Appendix-II-a of ref. [2].

For an example, the recommended value of the electron mass in 1965 [3] was 9.109 08 (13) × 10^{-31} [kg]. The up-to-date revision of CODATA in 2006 [7] gave the value as 9.109 382 15 (45) × 10^{-31} [kg]. The uncertainty of the recommended value decreased from 14 [ppm] in ref. [3] to 0.05 [ppm] in ref. [7]. The other example is the recommended value of the elementary charge. The uncertainty of the recommended value also decreased from 12 [ppm] in ref. [3] to 0.025 [ppm] in ref. [7]. The chronological tables on the improvements are shown in **Tables 1** and **2**.

Table 1: Recommended value of electron mass

Publication year	Electron mass [kg]	Uncertainty [ppm]	Reference
1965	9.109 08 (13) × 10^{-31}	14	Ref. 3
1987	9.109 389 7 (54) × 10^{-31}	0.6	Ref. 4(CODATA1986)
2000	9.109 381 88 (72) × 10^{-31}	0.08	Ref. 5 (CODATA1998)
2005	9.109 382 6 (16) × 10^{-31}	0.18	Ref. 6 (CODATA2002)
2008	9.109 382 15 (45) × 10^{-31}	0.05	Ref. 7 (CODATA2006)

Table 2: Recommended value of elementary charge

Publication year	Elementary charge [C]	Uncertainty [ppm]	Reference
1965	1.602 10 (2) × 10^{-19}	12	Ref. 3
1987	1.602 177 33 (49) × 10^{-19}	0.3	Ref. 4(CODATA1986)
2000	1.602 176 462 (63) × 10^{-19}	0.04	Ref. 5 (CODATA1998)
2005	1.602 176 53 (14) × 10^{-19}	0.09	Ref. 6 (CODATA2002)
2008	1.602 176 487 (40) × 10^{-19}	0.025	Ref. 7 (CODATA2006)

What are the lessons to be learned from Tables 1 and 2. During the first two decades (1965-1987), the uncertainty of the electron mass was decreased by 24 times and that of the elementary charge by 41 times. During the next two decades (1987-2008), both of those uncertainties were again decreased by 12 times. Although the uncertainties of these quantities were extremely small even in 1965, further improvements have been demonstrated to be achieved. The improvement factor (previous uncertainty / new uncertainty) is also impressive; ***the averaged improvement factor is about 4 to 5 for each decade.*** It is also noticed that these recommended data were almost immediately challenged by several new measurements, and data are constantly appearing that affect the knowledge of these constants.

The difference of the evaluated electron mass between ref. [3] and ref. [7] is only 33 [ppm]. However, the uncertainty in ref. [3] is too small to explain the discrepancy. In case of the elementary charge, the difference is 47 [ppm]. This is about 4 times larger than the evaluated uncertainty in ref. [3].

In the process of their achievement mentioned above, there are important lessons; how they have misevaluated. For example, in the review of ref. [3], authors illustrated an experiment of misevaluation, and stated their lesson as "blind weight averaging of a mass of data without critical examination of how the items were determined is to be deplored".

The other lesson in this field worth mentioning is the following important remark; Birge [8] wrote that E. O. Lawrence stated that "In any highly precise experimental arrangement there are initially many instrumental difficulties that lead to numerical results far from the accepted value of the quantity being measured. It is, in fact, just such wide divergences that are the best indication of instrumental errors of one kind or another. Accordingly, the investigator searches for the source or sources of such errors, and continues to search until he gets a result close to the accepted value. *Then, he stops!*" This dangerous tendency is called as "intellectual phase locking". R. Feynman also described the intellectual phase locking effect as revealed in measurement of the charge of the electron in his unique style book [9]. This effect has also been used to explain next patterns of data [10].

Pattern 1: In an idealized world, one would expect early experiments to show means (with large error bars) that varied unsystematically and then the later experiments of some physical properties follow that ideal pattern.

Pattern 2: One common pattern is for earliest measurement to be quite far from the current value; then the mean of subsequent experiments move up over time until some point they level off.

Pattern 3: Another pattern is to have the measurements cluster over a period of time, then suddenly an experiment gives a measurement that is many standard of deviations outside the previous means, and the later measurements cluster around the new measurement.

3. Review of evaluations and experiments on ^{241}Am capture cross section

In order to compare the achieved precision of nuclear data with that of fundamental physical constants, evaluations and experiments on ^{241}Am capture cross section for thermal neutron are briefly reviewed here as an example of nuclear data. Lynn *et al.* reported their evaluation on the ^{241}Am thermal neutron capture cross section with careful and logical discussions in 1980 [11]. They recommended the value with its uncertainty as 600 ± 20 [b]. The uncertainty is 3 [%] or 3 × 10^4 [ppm]. At that age, the evaluated value was 581.5 [b] in ENDF/B-IV and 832 [b] in JENDL-1, where no uncertainty was given in both evaluated nuclear libraries. The difference of those evaluated values in two different nuclear libraries was about 30 - 40 [%].

After three decades, Bernard *et al.* reviewed the cross sections of ^{241}Am in 2012 [12]. The

updated list of recent capture measurements cited in ref. [12] and the current value in the evaluated library [13] are summarized in **Table 3**.

Table 3: Recent measurements and evaluated data on thermal neutron capture cross section of ^{241}Am (note: references of experimental data are given in ref. [11] and [12])

Year	First Author or Library name	σ_0 [b]	Uncertainty [%]
2011	**JENDL-4.0**	**684 (15)**	**2**
2011	Letourneau	677 (20)	3
2008	Jandel	665 (33)	5
2007	Nakamura	688 (22)	3
2007	Bringer	704 (32)	5
1980	**Lynn**	**600 (20)**	**3**
1976	Gavrilov	853 (52)	6
1973	Harvour	832 (20)	2
1969	Dovbenko	647 (104)	16
1967	Bak	740 (60)	8
1955	Pomerance	625 (35)	6

The up-to-date evaluated cross section in JENDL-4.0 is 684 [b]. The uncertainty improvement factor (uncertainty of Lynn's evaluation / that of JENDL-4.0) achieved by three decades is only 1.5. On the other hand, the discrepancy of the evaluated values is 84 [b], that is, about 12-14 [%]; this is about 4 times larger than the evaluated uncertainty by Lynn [11]. This gives an example of similarity on the relation between the discrepancy and the uncertainty with the case discussed in ch. 2. On the other hand, there is a large gap on the improvement factor!

4. Possible paths to obtain the nuclear data with the required target accuracy

The ratios between evaluated current uncertainties and target accuracies on ^{241}Am related nuclear data are picked up from the OECD/NEA SG-26 report [1] as examples, and listed in **Table 4**. The ratio is defined here as "the target improvement factor". The improvement factors in Table 4 vary from 2 to 10, and their averaged value is about 4. If the speed of improvement in the field of the fundamental physical constants is used, uncertainties of nuclear data would be almost less than the required target accuracy within one decade. If the speed of improvement in the case of ^{241}Am during last three decades is used, one century will be required to satisfy the target accuracy.

Table 4: The target improvement factor

Reactor#	Reaction	Energy range	Evaluated uncertainty [%]	Target accuracy [%]	Target improvement factor
ADMAB	capt	1.35 MeV-0.454 keV	8	2	4
GFR	capt	183-2.03 keV	8	3	3
ADMAB	fiss	6.07-0.183 MeV	10	1	10
GFR	fiss	6.07-0.498 MeV	10	3	3
LFR	fiss	1.35-0.498 MeV	10	5	2
SFR	fiss	6.07-0.498 MeV	10	6	2
ADMAB	inel	6.07-0.183 MeV	25	4	6
ADMAB	nu	6.07-1.35 MeV	2	1	2

#: definition of reactor type is given in ref. [1].

In the recent advancements on nuclear data measurement techniques, utilization of spallation neutron sources is one of the most significant breakthroughs. At n_TOF in CERN, LANCE in LANL, and ANNRI in J-PARC, nuclear data measurements have been started using spallation neutrons. For examples, neutron capture cross sections of some highly radioactive nuclei have been measured at these facilities [14-16]. Their neutron fluxes are more than two orders of magnitude high [17] compared to those obtained by historically used electron accelerator based neutron sources, such as GELINA in IRMM, ORELA in ORNL and electron linac in KURRI. Therefore, statistical uncertainty is expected to be reduced by more than one order of magnitude if these high flux neutron beams could be used with the same beam time. Efforts of systematic measurements using the high intensity neutron beams are surely expected to contribute to improving the uncertainty.

On the other hand, the study of systematic uncertainty is also indispensable, including the effort of identifying unrecognized systematic uncertainty. For the study of systematic uncertainty, the cross check measurements are essentially important. For examples,

Cross check 1: spallation neutrons vs. photo neutrons
Cross check 2: differential measurements vs. integral measurements

Efforts of decreasing statistical and systematical uncertainties should be encouraged, and the progress should be reviewed periodically as was done in the field of the fundamental physical constants.

References

[1] OECD/NEA WPEC Subgroup 26 Final Report: “Uncertainty and Target Accuracy Assessment for Innovative Systems Using Recent Covariance Data Evaluations”, 2008.

[2] J. K. Tuli, “Nuclear Wallet Cards”, National Nuclear Data Center, October 2011.

[3] E. R. Cohen and J. W. M. DuMond, Rev. Mod. Phys. **37**, 537 (1965).

[4] E. R. Cohen, B. N. Taylor, Rev. Mod. Phys. **59**, 1121 (1987).

[5] P. J. Mohr, B. N. Taylor, Rev. Mod. Phys. **72**, 351 (2000).

[6] P. J. Mohr, B. N. Taylor, Rev. Mod. Phys. **77**, 1 (2005).

[7] P. J. Mohr, B. N. Taylor, D. B. Newell, Rev. Mod. Phys. **80**, 633 (2008).

[8] R. T. Birge, Nuovo Cimento, Suppl. **6**, 39 (1957).

[9] R. P. Feynman, R. Leighton, E. Hutchings, “Surely you’re joking, Mr. Feynman!”, W. W. Norton (1985).

[10] W. F. Brewer, Ch. 13 in ““Psychology of Science: Implicit and Explicit Processes”, R. W. Proctor, E.J. Capaldi (Eds.) (2012) Oxford University Press.

[11] J. E. Lynn, B. H. Patrick, M. G. Sowerby, E. M. Bowey, Progress in Nucl. Eng., **5**, 255 (1980).

[12] D. Bernard, O. Bouland, J. Nucl. Sci. Technol., **49**, 132 (2012).

[13] K. Shibata, et al., J. Nucl. Sci. Technol., **48**, 1 (2011).

[14] S. Marrone et al., Phys. Rev. , C**73**, 034604 (2006).

[15] E. –I. Esch et al., Phys. Rev. , C**77**, 034309 (2008).

[16] A. Kimura et al., J. Nucl. Sci. Technol., **49**, 708 (2012).

[17] K. Kino et al., Nucl. Instru. Meth., A 626, 58 (2011).

10. Application of the Cross Section Covariance Data to Fast Reactor Core Design

Kazuteru SUGINO
Advanced Nuclear System Research and Development Directorate,
Japan Atomic Energy Agency
4002, Narita-cho, Oarai-machi, Higashi-Ibaraki-gun, Ibaraki, 311-1393, Japan
E-mail: sugino.kazuteru@jaea.go.jp

In order to contribute to the validation of the cross-section covariance data, an equality was investigated between uncertainties of core characteristics evaluated by the conventional mock-up experimental approach and the current uncertainty quantification one.

1. Introduction

In Japan, as fast reactor (FR) technology has been under development and FR plant operation experiences have been quite less in comparison with those of light water reactors, actual core characteristics data of power reactors have not been sufficient. Therefore, core neutronics design systems for "Joyo" and "Monju" were validated with the core characteristics data measured in the real-scale engineering mock-up experiments by using the critical facilities, with large conservative uncertainty or design margin from engineering judgments, considering such extrapolation errors as differences in fuel cell structures and composition changes due to the depletion in a power reactor core.

However, this conventional approach which relies on the real-scale engineering mock-up experiments is not realistic particularly in terms of expenses for neutronics designs of middle- or large-scale reactor cores being studied in the fast reactor cycle technology development (FaCT) project[1].

Recently, Japanese evaluated nuclear data library JENDL-4.0 has been produced[2], being improved by accumulating the measured data and adopting the new nuclear model codes. In addition, JENDL-4.0 has high accuracy in terms of application to the core neutronics design because it was validated with rigorously qualified experimental data documented in the IRPhEP and ICSBEP handbooks and with MA irradiation tests data[3-5]. Furthermore, cross-section induced uncertainty can be calculated with high fidelity as covariance data are evaluated with accumulated experiences and given for most of nuclides included in fast reactor cores. Therefore, an alternative uncertainty quantification approach is promising: quantifying not uncertainty of core characteristics themselves directly but existing uncertainty components of core characteristics, e.g. those induced by

cross-section data, calculation modeling and others, subsequently combining all components considering their correlations. Thus, the present approach has a potential to predict nuclear characteristics with high quality and reliability without conventional real-scale engineering mock-up experiments.

In the present approach, one of the major issues is to validate the cross-section covariance data. Therefore, the present paper is aiming at contributing to the validation of the cross-section covariance data, observing an equality in uncertainties of core characteristics evaluated by both the conventional and the uncertainty quantification approaches.

2. Core design methods and uncertainty evaluation schemes

2.1 Conventional method and scheme

In the "Monju" core neutronics design, a real-scale engineering mock-up bias-factor method was basically applied, which was based on the MOZART experimental analyses results with the ZEBRA experimental facility. The uncertainties were evaluated based on the ratios of calculation to experiment (C/E) values, treating the systematic discrepancy of C/E values from the unity and fluctuations of C/E values among mock-up cores or experimental patterns like positions or types. **Figure 1** presents a sample of the conventional uncertainty evaluation on worth of the "Monju" coarse control rod, whose absorber was made of B-10 enriched boron carbide. The uncertainty of the core design method on the coarse control rod worth was estimated as 5% of the statistical uncertainty, considering the trends due to the difference in the B-10 enrichment of the boron absorber used in the mock-up experiments. Finally, design margin was specified as 10% by including such an extrapolation error as the difference in the fuel composition.

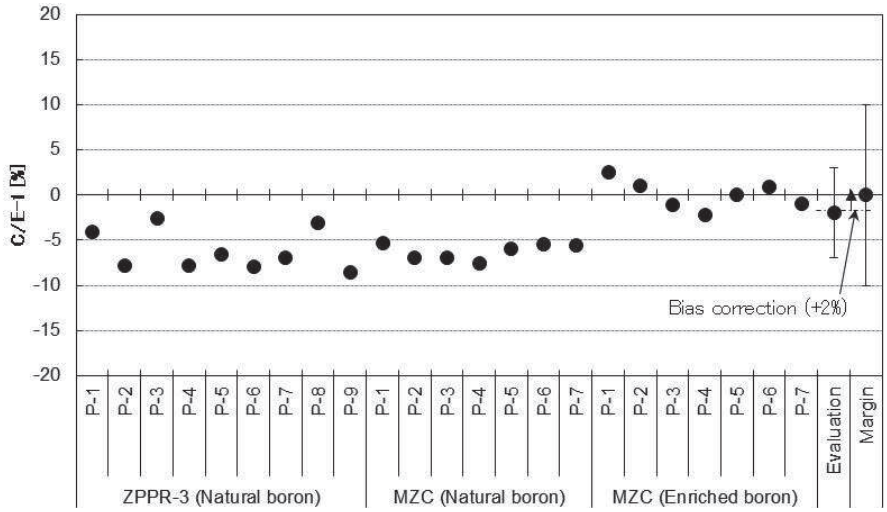

Fig. 1 Specification of design margin on the "Monju" coarse control rod worth

2.2 Alternative uncertainty evaluation scheme

Table 1 shows the comparison in major specifications of the large- and middle-scale advanced FRs in the FaCT project and "Monju". In order to improve the economics, outputs of the advanced FRs have been increased in comparison with "Monju". Core sizes of advanced FRs have also been enlarged. In detail, core equivalent diameter of middle-scale core is about twice and that of large-scale core is around three times as much as that of "Monju". Real-scale mock-up experiments for such a core scale as the advanced FRs core are impossible by using the existing critical experimental facilities and construction of a new critical experimental facility is not realistic.

Table 1 Comparison in major specifications

Item	Advanced FR (Large-scale)	Advanced FR (Middle-scale)	Monju
Electric / thermal output	1500MWe / 3530MWt	750MWe / 1765MWt	280MWe / 714MWt
Reactor inlet / outlet temperature	550℃ / 395℃	←	529℃ / 397℃
Core equivalent diameter	540cm	380cm	180cm
Core height	100cm	100cm	93cm
Operation cycle length	26months	18months	5months
Breeding ratio	1.10	1.10	1.20
Core discharge burnup	150GWd/t	150GWd/t	80GWd/t
Burnup reactivity	2.7%Δk/kk'	1.9%Δk/kk'	2.6%Δk/kk'

Therefore, it can be important to perform core neutronics design of advanced FRs by applying a combination of best estimation and qualified uncertainty, utilizing the basic data and calculation code system which are sufficiently verified, validated and quantified in their uncertainty. The present paper focuses on the uncertainty quantification. An uncertainty is quantified by deriving any causes, evaluating uncertainty/covariance on each cause and combining all uncertainty/covariance components. Major causes of uncertainty/covariance in core characteristics are cross-section and calculation modeling. The present paper is aiming at comparing the quantified uncertainty of combination with the conventional uncertainty estimated from the C/E distribution.

3. Evaluation of uncertainties

3.1 Evaluation conditions

Uncertainties of core characteristics were evaluated by using the latest Japanese evaluated nuclear data library JENDL-4.0[2] with its covariance data[7] and standard fast reactor core calculation code system. Details of evaluations were described in Ref. [8].

Core neutronics designs are normally carried out by utilizing or reflecting the accumulated integral data obtained by critical experiments and power reactor tests. In the present study, three design methods were treated: no correction with integral data indexed

as Method (1), bias-factor correction method as Method (2) and cross-section adjustment method[9] as Method (3).

In addition, two uncertainty evaluation schemes were treated: conventional estimation from C/E distribution indexed as Scheme (a) and alternative covariance combination as Scheme (b).

In Scheme (a), systematic uncertainty component is estimated from discrepancy of C/E values from the unity and statistical uncertainty component is from fluctuation of C/E values, which are adequately synthesized. Further, extrapolation error due to fuel composition, which is contributed from nuclides excluded in critical experiments like high order plutonium, minor actinides and fission products, is estimated by multiplying the cross-section covariance data with sensitivity coefficients of core characteristics like following scheme.

In Scheme (b), cross-section induced uncertainty, calculation modeling one and integral experimental one, which is related to Method (2) only, are calculated. Cross-section induced uncertainty is obtained by multiplying the cross-section covariance data with sensitivity coefficients of core characteristics. Calculation modeling uncertainty is empirically estimated by statistical sum of a half of correction amount for model detailing like transport theory and ultra-fine energy group corrections.

Table 2 presents a summary of above description. Uncertainty is evaluated for core characteristics of 750MWe middle-scale advanced FR core. Uncertainty of criticality, control rod worth, sodium (Na) void reactivity, Doppler reactivity and power distributions in core region and blanket region are evaluated.

Table 2 Combination of core design method and uncertainty evaluation

Item		(1) No correction	(2) Bias-factor correction method	(3) Cross-section adjustment method
Nominal design value		JENDL-4.0 base	JENDL-4.0 base ×E/C value	Adjusted set based on JENDL-4.0
(a) C/E distribution	Basic	Discrepancy of C/E values from 1.0 and fluctuation of C/E values by each method		
	Composition extraporation	$\sqrt{\mathbf{GMG}^t}$ of high order Pu, MA and FP*1		
	Integral experiment	Excluded	Included	Excluded
(b) Covariance combination	Cross-section induced	$\sqrt{\mathbf{GMG}^t}$*1	$\sqrt{\mathbf{\Delta GM\Delta G}^t}$*1	$\sqrt{\mathbf{GM'G}^t}$*1
	Calculation modeling	Design core	Design and mock-up cores	Design core
	Integral experiment	Excluded	Included	Excluded*2

*1 $\mathbf{G}$: Sensitivity of design core $\mathbf{M}$: Covariance of JENDL-4.0 $\mathbf{M}'$: Adjusted covariance
$\mathbf{\Delta G}$: Difference of sensitivity between design and mock-up cores
*2 Affecting nominal design value and covariances of cross section and calculation modeling

3.2 Evaluation results

Table 3 presents the results of uncertainty evaluation. It is found that both evaluation schemes (a) and (b) produce almost equal uncertainties in general. Thus, obvious inconsistency between integral data and cross-section covariance is not observed and a certain degree of reliability can be confirmed.

Followings are consideration for the discrepancy of uncertainty between schemes (a) and (b).

Criticality by Method (1)

Uncertainty of (1)-(b) is quite larger than that of (1)-(a). The reason is considered that cross-section covariance data was not modified, though some cross-sections of JENDL-4.0 were adjusted so as to improve the criticality as well as evaluation of ENDF/B-VII.1[10]. In other words, result of (1)-(a) shows the reflection of integral data as well as those in Methods (2) and (3), however, result of (1)-(b) presents no explicit reflection of integral data.

Na void reactivity by Methods (1) and (3)

Results of analyses or C/E values had a room for an improvement in all methods, which was considered to be due to the systematic error in calculation modeling for the integral experiments or mock-up experiments. Concerning Scheme (b), Methods (1) and (2) cannot treat this kind of error and only Method (2) can take into account as shown in Table 2. That would be reason why Scheme (b) by Methods (1) and (3) underestimate uncertainties in comparison with Scheme (a).

Power distribution in the blanket region by Methods (1) and (3)

Results of analyses or C/E values had a room for an improvement in Methods (1) and (3), which was considered to be due to the systematic error in calculation modeling for the integral experiments as well as Na void reactivity analysis. The reason for underestimation in Scheme (b) by Methods (1) and (3) may be the same as that for Na void reactivity.

On the other hand, Method (2) can reduce such error and treat calculation modeling error of mock-up experiments. Therefore, uncertainty of Scheme (b) was almost equal to that of Scheme (a).

Table 3 Comparison in the uncertainty evaluations among combinations of core design methods and uncertainty evaluation schemes

Core characteristics		(1) No correction		(2) Bias-factor		(3) X-sec adjustment	
		(a) C/E distribution	(b) Cov. combination	(a) C/E distribution	(b) Cov. combination	(a) C/E distribution	(b) Cov. combination
Criticality		0.30	0.96	0.31	0.55	0.30	0.31
Control rod worth		3.1	2.9	2.8	2.6	2.1	1.3
Na void reactivity		7.9	4.6	8.0	9.3	7.0	2.0
Doppler reactivity		3.5	4.7	8.6	9.1	5.1	2.1
Power distribution	Core region	1.2	2.3	1.8	2.6	1.1	1.6
	Blanket region	4.4	1.4	3.6	3.7	4.2	1.4

Unit: % (1σ)

4. Conclusions

The present paper introduced a methodology to rationally perform core neutronics design for FRs, whose plant operation experiences are quite less in comparison with those of light water reactors. It is found that higher priority on the solution of the calculation modeling issues would lead to promote the verification and validation with uncertainty quantification of FR core neutronics design system with higher efficiency.

Acknowledgments

The author wishes to express his deep gratitude to following collaborators: K. Numata, T. Iwai, T. Jin, A. Soga, and H. Komoda of NESI Inc., G. Chiba, of Hokkaido University, M. Ishikawa, T. Hazama, K. Yokoyama, Y. Nagaya, T. Kugo, S. Ohki and T. Okubo of JAEA.

References

[1] Advanced Nuclear System Research and Development Directorate of Japan Atomic Energy Agency and Research and Development Department of the Japan Atomic Power Company, Fast Reactor Cycle Technology Development Project (FaCT Project) - Phase I Report -, JAEA-Evaluation 2011-003, 2011 [in Japanese].

[2] K. Shibata, O. Iwamoto, et al., JENDL-4.0: A New Library for Nuclear Science and Engineering, J. Nucl. Sci. Technol., Vol. 48, No. 1, 2011, pp. 1-30.

[3] G. Chiba, K. Okumura, et al., JENDL-4.0 Benchmarking for Fission Reactor Applications, J. Nucl. Sci. Technol., Vol. 48, No. 2, 2011, pp. 172-187.

[4] International Handbook of Evaluated Reactor Physics Benchmark Experiments (IRPhE), NEA/NSC/DOC(2006)1, OECD/NEA, 2010.

[5] NEA Nuclear Science Committee, International Handbook of Evaluated Criticality Safety Benchmark Experiments, NEA/NSC/DOC(95)03, 2009.

[6] T. Naganuma, T. Kobayashi, et al., Evaluation of MONJU Neutronics Parameters on the Basis of the Analysis of Mockup Experiment, PNC TJ206 76-14, 1976 [in Japanese].

[7] Iwamoto, O., Nakagawa, T., N. et al., Covariance Evaluation for Actinide Nuclear Data in JENDL-4, Proc. the 2010 International Conference on Nuclear Data for Science and Technology (ND2010), J. Korean. Phys. Soc., 59(23), 2011, pp. 1224-1229.

[8] K. Sugino, M. Ishikawa, et al., Development of a Standard Data Base for FBR Core Design (XIV) - Analyses of Extensive FBR Core Characteristics Based on JENDL-4.0 -, JAEA-Research 2012-013, 2012 [in Japanese].

[9] J. B. Dragt, J. W. M. Dekker, et al., Method of Adjustment and Error Evaluation of Neutron Capture Cross Sections; Application to Fission Product Nuclides, Nucl. Sci. Eng., 62, pp. 117-129, 1977.

[10] P. Talou, P. G. Young, et al., Quantification of Uncertainties for Evaluated Neutron-Induced Reactions on Actinides in the Fast Energy Range, Nucl. Data Sheets 112, 2011, pp. 3054-3074.

11. Uncertainty Evaluation for ^{244}Cm Production in Spent Fuel of Light Water Reactor by using Burnup Sensitivity Analysis

Akito OIZUMI, Kenji YOKOYAMA, Makoto ISHIKAWA, Teruhiko KUGO
Nuclear Science and Engineering Directorate, Japan Atomic Energy Agency (JAEA)
Tokai-mura, Naka-gun, Ibaraki-ken 319-1195 Japan
e-mail: ohizumi.akito@jaea.go.jp

The uncertainty evaluation for the minor-actinide production is important to assure the reliability of the basic database of heat generation and radioactivity from reactor spent fuel. To identify the cross-section improvement priority for nuclide, reaction and energy range, the present paper describes the evaluation methodology for effective uncertainty reduction of target nuclide production by using the burnup sensitivity coefficients and the covariance of nuclear data. As a typical instance, the ^{244}Cm production is focused on. The objects of uncertainty analysis are MOX and UO_2 of a pressurized water reactor, so that we can clarify the difference of the uncertainties between them. From the result, it is found that the nuclides near ^{244}Cm on the burnup chain such as ^{243}Am and ^{242}Pu are important to produce ^{244}Cm in both fuel types. In addition, it is confirmed the priority of ^{243}Am, ^{242}Pu and ^{241}Pu is higher than ^{235}U and ^{239}Pu. Finally, the accuracy improvement of ^{243}Am capture in the thermal and resonance regions should take a higher-priority than in the fast region.

1. Introduction

Basic database of heat generation and radioactivity from reactor spent fuel is indispensable in the fields of reactor decommissioning, fuel transportation, storage, processing and disposal. These physical quantities depend on the amount of nuclides such as minor actinides (MAs) and fission products (FPs) in the reactor spent fuel. Therefore, it is extremely important to evaluate the uncertainty of production of such nuclides to ensure the reliability of the basic database. In the present study, we describe the uncertainty evaluation methodology by using the burnup sensitivity coefficients and the covariance of nuclear data.

First, we analyze the sensitivity of the nuclide production in the spent fuel of light water reactors (LWRs). Second, the physical mechanism of the resulted sensitivity is considered in detail. Finally, from the sensitivity analysis results and the nuclear data covariance based on JENDL-4.0, we identify the nuclide, reaction and neutron energy range which are effective in reducing the uncertainty.

2. Burnup sensitivity coefficient

We first summarize the definition of burnup sensitivity coefficient that is important to assess the uncertainty of nuclide production. The burnup sensitivity coefficient G is calculated with Equation (1), which consists of five terms, that is, the direct term T_D, the number density term T_N, the flux term T_ϕ, the adjoint flux term T_{ϕ^*} and the power normalization term T_P,

$$G(\sigma_x^g) = \frac{\sigma_x^g}{R}\left\{T_D + T_N + T_\phi + T_{\phi^*} + T_P\right\} \quad . \quad (1)$$

The first term T_D is a direct effect of the cross-section (XS) change on a neutronic integral parameter R. The second term T_N is an impact of the XS change on R through the burnup chain. The third term T_ϕ gives the influence on R via the neutron flux change due to the XS change. The fourth term T_{ϕ^*} represents an effect on R via the adjoint neutron flux change. The term T_{ϕ^*} has a non-zero value only if the targeted integral parameter is reactivity. The last term T_P gives an effect through the correlation between fission XSs and neutron flux to keep the reactor thermal power constant under the quasi-static approximation. In the present analysis, T_D and T_{ϕ^*} have no effects since the targeted integral parameter is nuclide production.

Table1 Calculating condition

			Unit	MOX	UO_2
^{235}U enrichment			wt%	0.23	3.9
Pu-total enrichment				6.3	-
Pu-fissile ratio				68	-
Initial number density	Fuel	^{234}U	#/barn/cm	1.0829E-07	8.1095E-06
		^{235}U		4.7572E-05	8.8436E-04
		^{236}U		5.4739E-07	5.4914E-06
		^{238}U		2.0828E-02	2.1503E-02
		^{238}Pu		1.8542E-05	-
		^{239}Pu		8.4377E-04	-
		^{240}Pu		3.3808E-04	-
		^{241}Pu		1.1555E-04	-
		^{242}Pu		6.8382E-05	-
		^{241}Am		1.1236E-05	-
		^{16}O		4.4544E-02	4.4802E-02
	Cladding	Zr-nat		3.7860E-02	
		Fe-nat		2.3820E-04	
		Cr-nat		6.7700E-05	
		^{1}H		8.7300E-05	
		^{12}C		7.9120E-05	
	Moderator	^{1}H		5.6593E-02	
		^{16}O		2.8296E-02	
Liner heat rate			W/cm	176.12288	176.98673
Temperature	Fuel		K	973.15	
	Cladding			603.15	
	Moderator			573.15	
Burnup			GWd/t	50	
Irradiation time			day	1333	
Cooling time				0	

3. Calculating condition

The sensitivity coefficients are evaluated with a burnup sensitivity calculation module of a multi-purpose reactor analysis code MARBLE [1]. The burnup chain includes 21 MAs (^{234}U-^{246}Cm), 104 FPs and 12 Burnable Poisons (BPs). Neutron transport calculation and burnup chain analysis are based on the 107 energy-group collision probability method and the matrix exponential method, respectively. The sensitivity coefficients of the atomic number density N after burnup are calculated on the basis of the generalized perturbation theory [2, 3]. The fuel types treated here are UO_2 and MOX of a pressurized water reactor (PWR). The cell model is shown in **Figure 1**. **Table 1** shows ^{235}U enrichment, Pu-total enrichment, Pu-fissile ratio of fresh fuels, the End-of-Life (EOL) burnup and so on. Sensitivity analysis for the number density after burnup without cooling is done. The uncertainty of the final nuclide production is evaluated by multiplying the sensitivity by covariance of nuclear data based on JENDL-4.0. In the present paper, we concentrate on the production of ^{244}Cm as a typical instance since the nuclide is important due to its high decay heat.

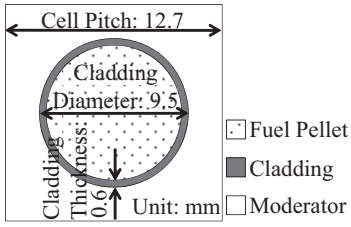

Fig.1 Cell model

4. Reaction rates for ^{244}Cm production

We predict the result of sensitivity analysis from reaction rates for ^{244}Cm production on the paths of the burnup chain. **Figure 2** summarizes reaction rates for MOX and UO_2 at EOL. All the reaction rates in the figure are normalized so that the sum of capture reaction rates of ^{243}Am and ^{243}Cm generating directly ^{244}Cm has a value of 100 in MOX. In the both fuel types, the reaction rates on the path through ^{243}Am and plutonium isotopes, as shown by solid arrows, are larger than the others such as those through ^{243}Cm and ^{241}Am with dotted arrows.

Therefore, ^{243}Am and plutonium isotopes are important in the ^{244}Cm production. Their sensitivity coefficients are also expected to be large, as confirmed later.

5. Calculated result of burnup sensitivity

Figure 3 shows isotope- and reaction-wise sensitivities of ^{244}Cm production. First, we focus on the capture reaction of ^{244}Cm. It has a negative sensitivity, since the number density of ^{244}Cm decreases if its XS becomes large. Second, the sensitivities to ^{243}Am, ^{242}Pu and ^{241}Pu capture XSs are largely positive. This is consistent with the expectation from the reaction rates in Fig.2. Third, the sensitivities to ^{243}Cm, ^{242}Cm and ^{241}Am capture XSs on the minor paths, are almost zero. Finally, the sensitivities to ^{235}U, ^{238}U, ^{239}Pu and ^{241}Pu fission XSs are negative, the reason of which is discussed below. In addition, there are XSs showing difference in sensitivity values between MOX and UO_2. These facts could be interpreted mainly as the effects of terms T_N and T_P.

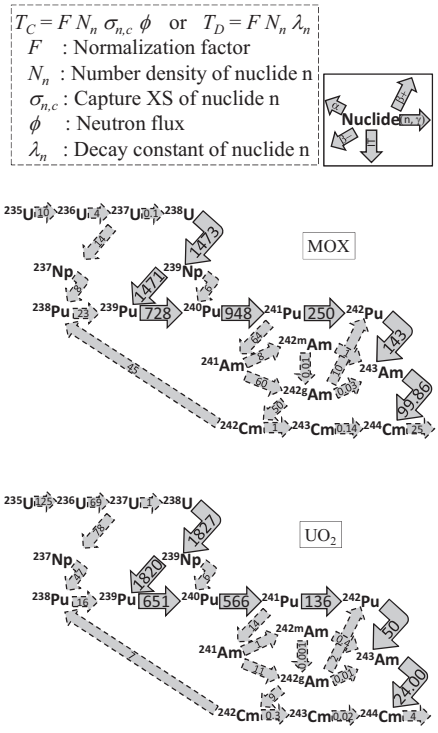

Fig.2 Reaction rate for ^{244}Cm production

Figure 4 shows the contributions of each term in Eq. (1) to the total sensitivity. In the case of the fission reaction, the term T_P is dominant. The reason is discussed with Equations (2) and (3).

$$T_P = \sum_{i=1}^{I+1}\left[P_i^* \frac{\partial P_i}{\partial \sigma_x^g}\right]_{E,V} \quad , \quad (2)$$

$[\ ]_{E,V}$: Integral for all neutron energy groups and whole space,

σ_x^g: Microscopic XS of reaction type x and energy range g,

P_i^*: Adjoint reactor power at the burnup step i,

P_i: Reactor power at the burnup step i as described in Eq. (3).

$$P_i = \left[\varepsilon_f \sigma_f N \phi_i\right]_{E,V} \quad , \quad (3)$$

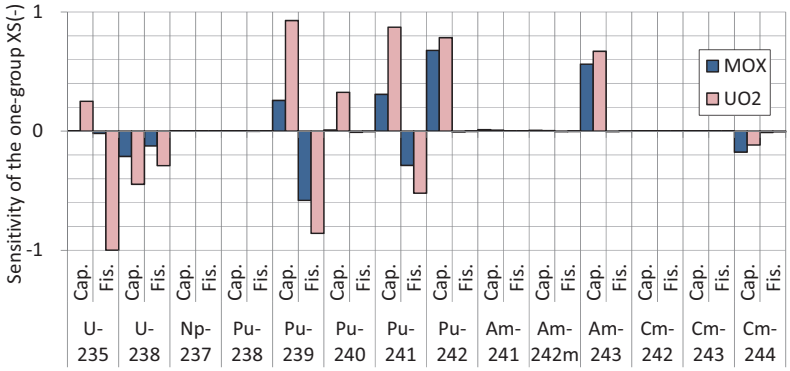

Fig.3 Sensitivity of ^{244}Cm production

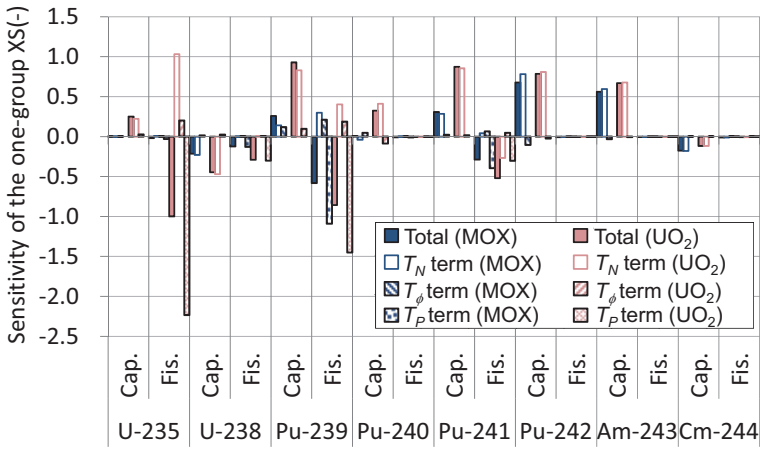

Fig.4 Term-wise contributions to the total sensitivity of ^{244}Cm production

ε_f: Production of energy per fission reaction,

σ_f: Microscopic XS of fission reaction,

N: Number density,

ϕ_i: Neutron flux at the burnup step i.

The value of ϕ_i decreases with increasing σ_f, since the reactor power P_i is assumed to be constant during the whole irradiation period. This leads to decrease of the ^{244}Cm production and, consequently, the sensitivity to fission XS is negative.

Concerning the nuclides on the main path such as ^{243}Am, ^{242}Pu, ^{241}Pu and so forth, the term T_N is dominant. The difference in the sensitivities of capture reactions of ^{241}Pu and ^{240}Pu is seen between MOX and UO_2 and is discussed by T_N which is evaluated by:

$$T_N = \sum_{i=1}^{I} \int_{t_i}^{t_{i+1}} \left[N^* \frac{\partial M}{\partial \sigma_x^g} N \right]_{E,V} dt \quad . \quad (4)$$

The number density term T_N depends on N, σ_x^g, the transmutation operator of burnup chain M and the adjoint number density N^*. The operator M is composed of the microscopic capture reaction rate ϕC and the decay constant D as follows:

$$\frac{\partial}{\partial t} N = \{[\phi C]_E + D\} N = MN \quad . \quad (5)$$

The adjoint number density N^* means the importance that one atom of the nuclide at time t contributes to the ^{244}Cm production at EOL, and is obtained with the backward calculation of the adjoint burnup chain [2, 3]. As shown in **Figures 5 and 6**, in the case of the target nuclide ^{244}Cm, N^* has a value of unity at EOL, and decreases with going back in time. In the case of the other nuclides, N^* has a value of zero at EOL, and increases with dating back to the Beginning-of-Life (BOL). By comparing the N^*s between nuclides, we can guess the important isotopes in the target nuclide production. To discuss the importance of each nuclide quantitatively, however, we have

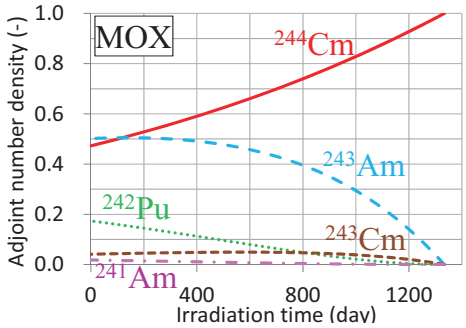

Fig.5 Adjoint number density (MOX)

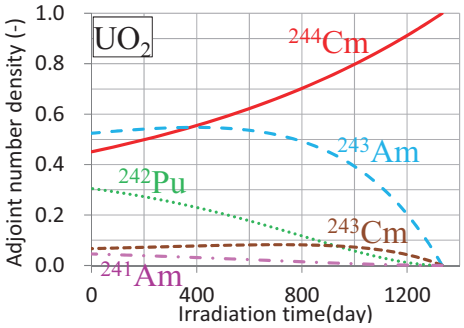

Fig.6 Adjoint number density (UO_2)

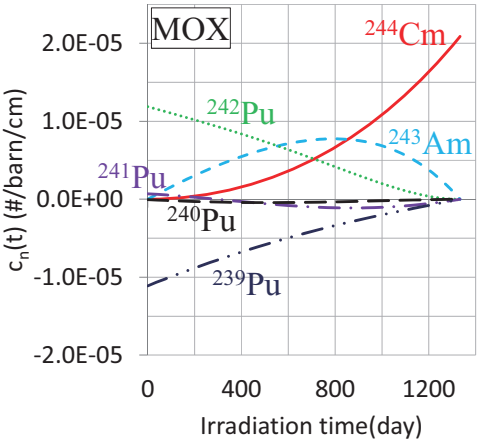

Fig.7 Nuclide contribution density (MOX)

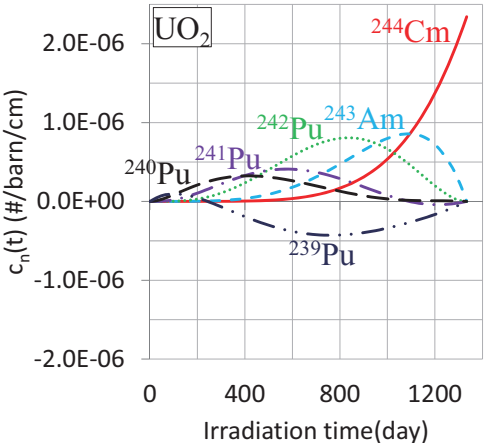

Fig.8 Nuclide contribution density (UO_2)

to consider the nuclide contribution density c_n including number density N as follows:

$$c_n(t) = N_n(t)N_n^*(t) \quad . (6)$$

Figures 7 and 8 show burnup dependences of c_n for the ^{244}Cm production. Note that, the time integral of c_n through the burnup is equivalent to the sensitivity coefficient. First, we compare the entire trends of c_n between MOX and UO_2. In MOX, the nuclide contribution densities c_n of ^{243}Am and ^{242}Pu are dominant ones. In UO_2, however, the nuclide contribution densities are large in sequence from ^{239}Pu to ^{243}Am. Thus, the difference in the sensitivity is caused by the different ^{244}Cm producing mechanism that comes from initial fuel composition. As seen in the vertical axes of Figs.7 and 8, the point we should notice is that nuclide contribution densities of UO_2 are an order of magnitude smaller than those of MOX because of the difference in the amount of nuclides production. Next, c_n of ^{239}Pu that is negative contribution to the ^{244}Cm production in the both fuel types. This is because ^{239}Pu is fissile. By the definition mentioned above, the adjoint number density N^* cannot be negative if we consider only burnup chain. However, the adjoint number density N^* can be negative if we take account of the power normalization term [2, 3]. Hence, the nuclide contribution density c_n has the potential to be negative.

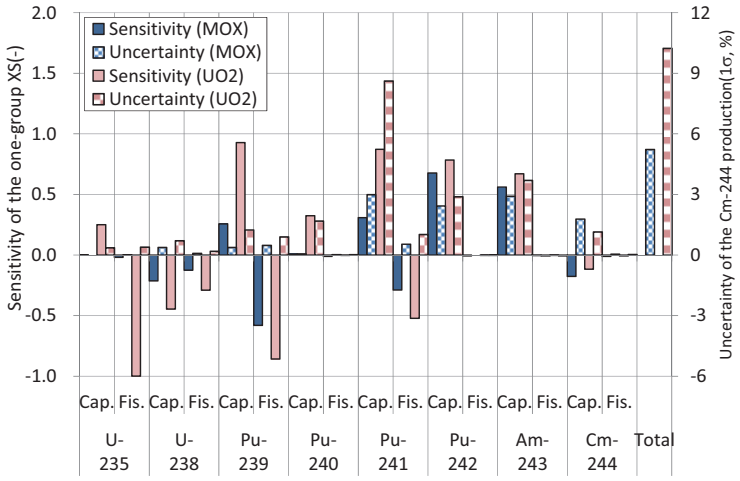

Fig.9 Sensitivity and uncertainty for ^{244}Cm production

6. Uncertainty of ^{244}Cm production

Figure 9 shows the sensitivity of the one-group XS and the uncertainty of ^{244}Cm production. The sensitivities to ^{235}U fission XS, ^{239}Pu capture and fission XSs in UO_2 are large with the values of about ± 1.0, however, those uncertainties are small with the values of about 1.5%. This means that these major nuclide XSs have the highly accurate nuclear data. Hence, in order to lower the uncertainty of the ^{244}Cm production, the reduction of the uncertainties of these XSs has a lower-priority. On the other hand, ^{243}Am, ^{242}Pu and ^{241}Pu capture XSs have large sensitivities as about 0.7-0.9 in UO_2. In addition, their uncertainties are as large as about 3-9% since their nuclear data have the low accuracy. In MOX, the situation is similar to UO_2. Therefore, regarding these capture XSs, the priority to reduce the uncertainties of nuclear data is high.

7. Energy dependence of sensitivity and covariance for ^{243}Am capture cross-section

We here examine the energy dependency of the sensitivity and standard deviation. We take the ^{243}Am capture XS, as an example, since the XS was determined as one of the higher-priority XS in the previous chapter. **Figure 10** shows energy dependences of the sensitivity of ^{244}Cm production to the ^{243}Am capture XS and the standard deviation of the nuclear data. First, in the fast neutron region from 100keV to 1MeV, the standard

deviation is the largest values of around 12-44%. However, the maximum sensitivity is about 10^{-3} in the region. On the other hand, in the thermal and resonance region from 0.5 to 300 eV, the standard deviation ranges from 5 to15% and is smaller than that in the fast region. The sensitivity has a value of 2.0 at the maximum in these regions and is much larger than that in the fast region. To reduce the uncertainty of the ^{244}Cm production efficiently with the ^{243}Am capture XS, therefore, it can be said that the accuracy improvement in the thermal and resonance regions should take a higher-priority than in the fast region.

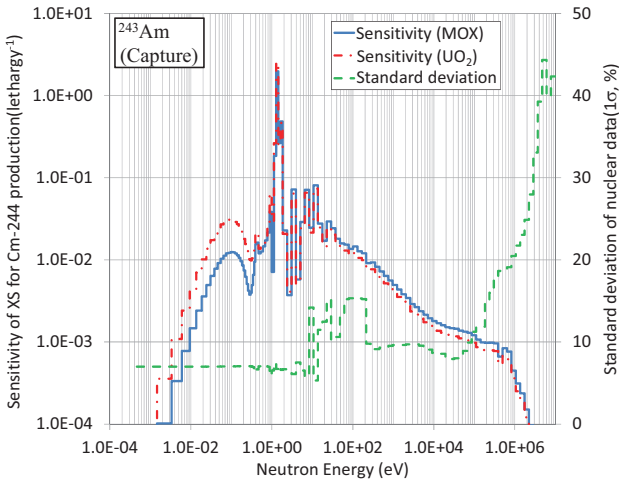

Fig.10 Sensitivity and standard deviation of nuclear data

8. Conclusions

We evaluate MA production uncertainty with burnup sensitivity and covariance of nuclear data. In the present study, we focus on ^{244}Cm production. First, the sensitivity analysis is done. Concerning the capture XS, the nuclides of upstream on the burnup chain have larger ones than ^{244}Cm. As for the fission XS, the major fissile nuclides have negative sensitivities. Second, the result of the sensitivity analysis is discussed. The negative sensitivities to the fission XSs are due to the power normalization. From the discussion of nuclide contribution density, the difference in sensitivities to capture XSs between MOX and UO_2 is caused by the different ^{244}Cm producing mechanism coming from initial fuel composition. As a result, the nuclides near ^{244}Cm on the burnup chain such as ^{243}Am and ^{242}Pu are important to produce ^{244}Cm in both fuel types. Finally, the XS improvement priority is identified by analyzing the uncertainty of ^{244}Cm production. The priority of ^{243}Am, ^{242}Pu and ^{241}Pu is higher than ^{235}U and ^{239}Pu, since the nuclides ^{243}Am, ^{242}Pu and ^{241}Pu have less accurate nuclear data and larger sensitivities. From the energy dependences of sensitivity and XS uncertainty for ^{243}Am capture, for instance, it can be said that the accuracy improvement in the thermal and resonance regions should take a higher-priority than in the fast region. Thus, we provide the methodology to identify the XS improvement priority for nuclide, reaction and energy range, to reduce uncertainty effectively in target nuclide production.

【Reference】

[1] K. Yokoyama, et al., MARBLE: next generation neutronics analysis code system for fast reactors, *Proc. of Int. Conf. on the Physics of Reactors, PHYSOR2008*, Sep. 14-19, Interlaken, Switzerland (2008). [CD-ROM]

[2] M. L. Williams, Development of Depletion Perturbation Theory for Coupled Neutron/Nuclide Fields, *Nucl. Sci. Eng.*, **70**, p.20-36 (1979).

[3] T. Takeda and T. Umano, Burnup Sensitivity Analysis in a Fast Breeder Reactor –part I: Sensitivity Calculation Method with Generalized Perturbation Theory, *Nucl. Sci. Eng.*, **91**, p.1-10 (1985).

12. Validation of JENDL-4.0 and Future: Reactor Integral Test Working Group

Go CHIBA
Graduate School of Engineering, Hokkaido University, Sapporo, Hokkaido, 060-8628
e-mail: go_chiba@eng.hokudai.ac.jp

Recent activity of the reactor integral test working group under the JENDL committee is summarized.

1. Introduction

The reactor integral test working group (RIT-WG), which is one of working groups organized under the JENDL committee, has worked on integral data testing for nuclear data files, such as JENDL and others, in order to obtain beneficial information for the JENDL development. At the beginning of April in 2011, RIT-WG was re-organized and the following short-term (two-year) targets were set up: (1) to examine JENDL-4.0 for light-water reactor (LWR) application and give feedback to JENDL evaluators, (2) to promote utilization of sensitivity analysis tools for nuclear data benchmark calculations, and (3) to promote communication among specialists on cross section processing with the NJOY code. To accomplish these targets efficiently, many specialists on the LWR core analyses participate in RIT-WG. In the first fiscal year 2011, we have focused on the JENDL-4.0 examination for LWR application. The present paper summarizes activities done in the fiscal year 2011.

2. Venus International Program (VIP) experimental analysis using JENDL-4.0

The performance of JENDL-4.0 has been examined through the experimental analysis for the Venus International Program (VIP) critical data. **Figure 1** shows the configuration of the critical assembly. A MOX assembly at the core center is surrounded by four UO2 assemblies and outer driver regions. Using an advanced lattice physics code AEGIS [1] and various nuclear data libraries, errors in pin-wise fission rate have been evaluated. **Table1** shows root-mean-square and maximum values of these errors. There is no significant difference in the errors of fission rate among different nuclear data libraries.

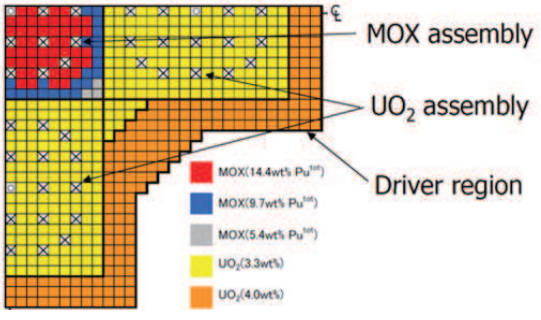

Fig. 1 Configuration of VIP experiment

Table 1 Errors in fission rate

	UO2 assembly		MOX assembly	
	RMS	MAX	RMS	MAX
JENDL-4.0	1.09%	4.20%	0.76%	-1.66%
JENDL-3.3	1.09%	4.20%	0.77%	-1.73%
ENDF-B7.0	1.11%	4.14%	0.82%	-1.98%
ENDF-B6.8	1.09%	4.16%	0.78%	-1.77%

3. Testing for Am-241 thermal capture revision

Several authors have pointed out through integral data testing that Am-241 thermal capture cross section of JENDL-3.3 is underestimated.[2][3] In the JENDL-4.0 development, these suggestions were taken into consideration and the Am-241 thermal capture cross section was re-evaluated as shown in **Fig. 2**. Reference [4] shows that this revision partially improves the problem raised by Nakajima.

A validation test for this revision has been carried out with a set of critical data obtained through the FUBILA critical experiment program.[5] **Figure 3** shows predicted critical eigenvalues for various core configurations, which are different from each other in the number of MOX rods in the driver region. All the calculations have been performed by the continuous-energy Monte Carlo code MVP-II. Since driver MOX fuels contain more Am-241 than MOX fuels in test region (6 and 2 at%, respectively), the number of MOX rods in driver region has a strong correlation with neutron capture contribution by Am-241. As shown in Fig. 3, C/E dependence on Am-241 capture contribution in the JENDL-4.0 result is smaller than that in the JENDL-3.3 result. Detail sensitivity analysis has been also performed and its result is shown in Ref. [6]. Note that ENDF/B-VII.0 (ENDF-VII in Fig.3) shows similar trend as JENDL-3.3 and that the revised library ENDF/B-VII.1 solve this problem by adoption of the JENDL-4.0 evaluation for resolved resonance parameters of Am-241.[7]

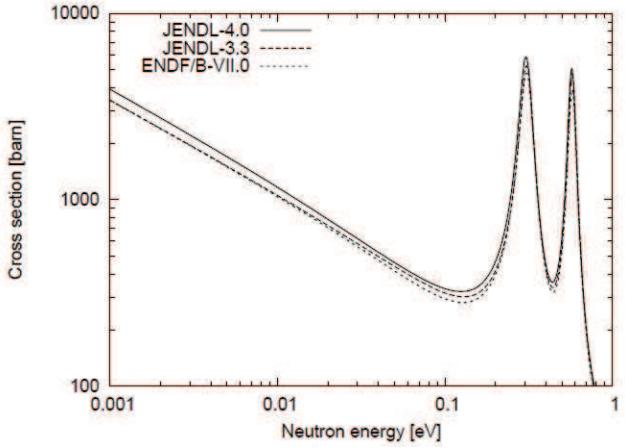

Fig. 2 Am-241 capture cross section

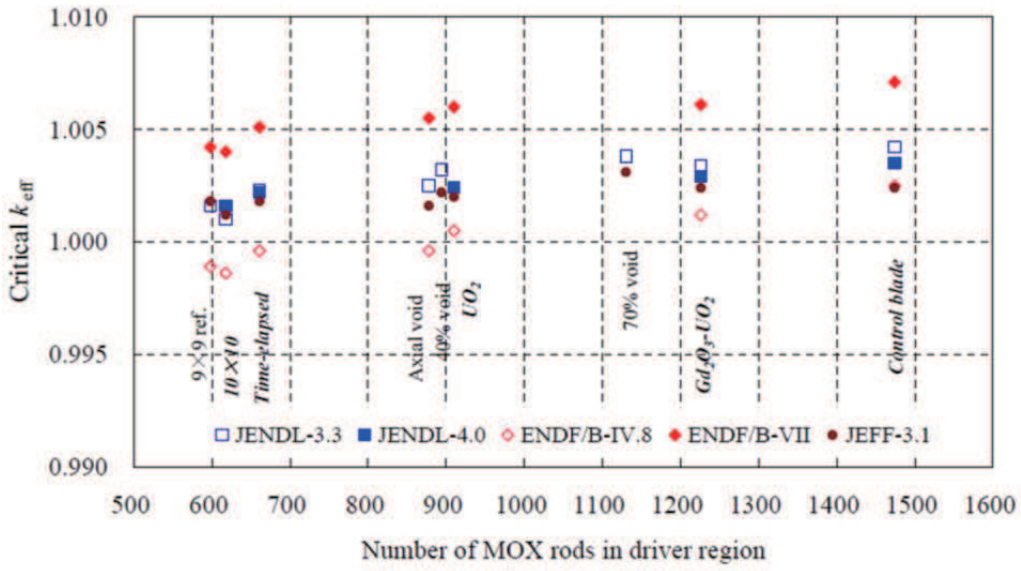

Fig. 3 Predicted criticalities for the FUBILA assemblies[5]

4. Testing for Gd-157 thermal capture revision

It has been reported that pin power of Gd_2O_3-UO_2 fuel is underestimated in comparison with that of normal UO_2 fuel.[8][9] **Figuire 4** shows C/E values of pin-wise fission rate in the FUBILA experiment obtained with JENDL-3.3.[9] Underestimation in Gd-loaded fuels is easily found. Recently Leinweber et al. have conducted new nuclear data measurement on gadolinium isotopes and have yielded new evaluated data for Gd-157 thermal capture.[10] Jatuff et al. have reported that this new Gd-157 data has a potential to solve the aforementioned problem.[8] As shown in **Fig. 5**, the underestimation observed in the FUBILA experiment is improved when the new Gd-157 data is used.[5] On the other hand, this new Gd-157 data significantly overestimate criticalities of specific water-moderated systems, such as those given in the ICSBEP handbook as LEU-COMP-THERM-005 and LEU-COMP-THERM-052, in which gadolinium is dissolved in water.[4] Thus JENDL-4.0 adopts the new Gd-157 data and considers additional background cross section in a thermal energy range.

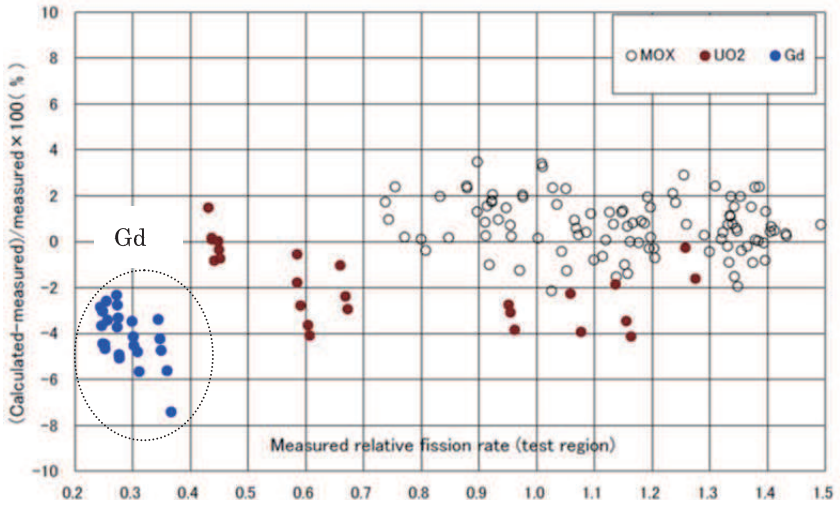

Fig. 4 C/E values of pin-wise fission rate in FUBILA[9]

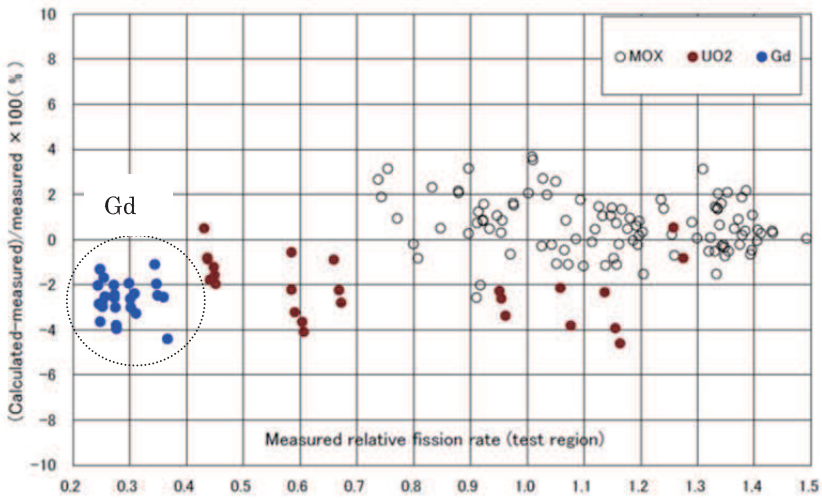

Fig. 5 C/E values of pin-wise fission rate in FUBILA (new Gd-157 data is used) [5]

We have newly conducted calculations for the FUBILA experiment with JENDL-4.0, and have found that the improvement of the underestimation in Gd-loaded pins is moderated.

We have conducted another calculation to validate the Gd-157 revision using different critical experiment data. In this experiment, Gd-bearing fuel rods, whose Gd concentration varies from 0 to 15%, are loaded in a water-moderated system. **Figure 6** shows calculated critical eigenvalues. Among three different Gd-157 data, JENDL-4.0 gives the best results. Different validation test for the Gd-157 revision has been also reported in Ref. [11].

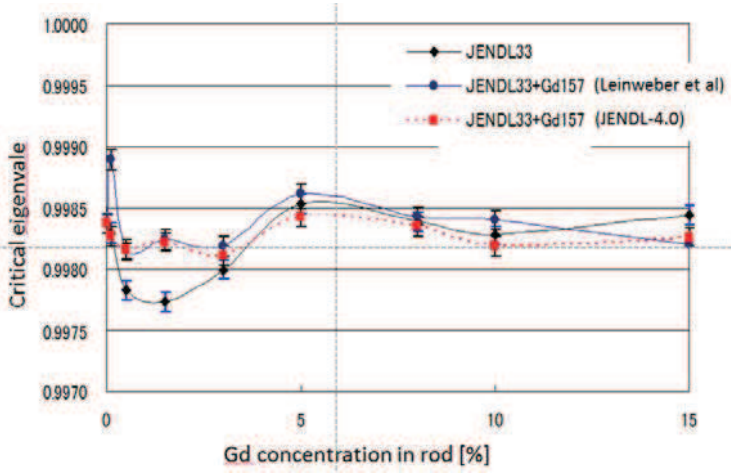

Fig. 6 Calculated k-eff in Gd-loaded systems

Pin-power calculations for a realistic PWR fuel assembly have been conducted with the next generation code GALAXY[12]. JENDL-4.0 results in about 1.3% smaller fission rate in Gd-bearing fuel rod than ENDF/B-VII.0, whose Gd-157 evaluation is conventional.

5. Difference in burnup characteristics between JENDL-4.0 and ENDF/B-VII.0

Burnup calculations for PWR fuels have been carried out with JENDL-4.0 and ENDF/B-VII.0, and differences between these two libraries have been investigated.

The first examination has treated PWR single pin-cells of 4.8 wt% UO_2 fuel and 14.4 wt% (Pu-total) MOX fuel. **Figure 7** shows nuclide-wise differences in infinite multiplication factor (k-inf) between two libraries: k-inf changes induced by replacement of focused nuclide's nuclear data of JENDL-4.0 by that of ENDF/B-VII.0.

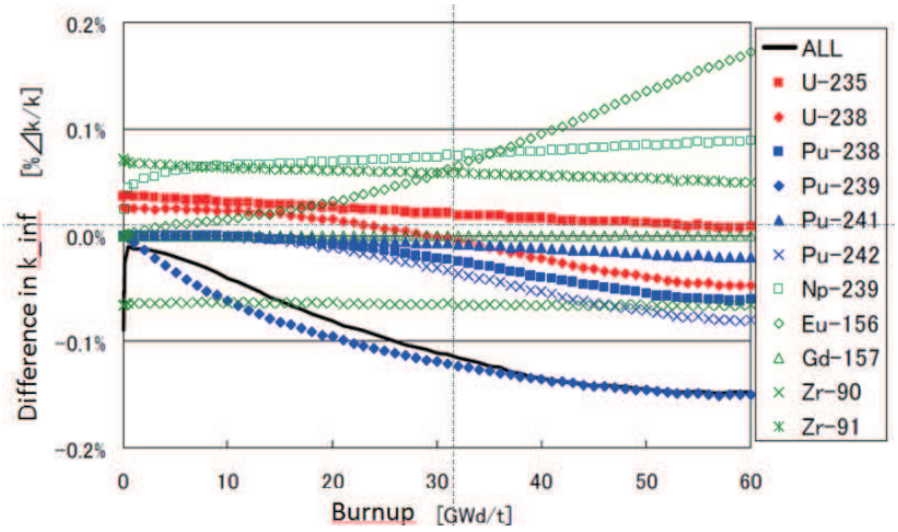

Fig. 7 Nuclide-wise k-inf difference

While differences in several nuclides' nuclear data contribute to the k-inf difference, those in Pu-239 and Eu-156 are notable. The difference in Eu-156 has been discussed in detail in Ref. [13],

and influence of the Eu-156 revision on isotopic composition after fuel depletion has been reported in Ref. [14]. Recently, update file of Eu-156 of JENDL-4.0 has been released.

The second examination has treated 17x17 assemblies of 4.1 wt% UO_2 fuel, 4.1 wt% UO_2 fuel with 6 wt% Gd_2O_3-UO_2 fuel, and MOX fuel. All the calculations have been conducted with AEGIS. Differences in k-inf between two libraries are shown in **Fig. 8**. Nuclide-wise differences have been also quantified as shown in **Fig. 9**. Differences in Pu-239, Gd-155, -157 and Am-241 have relatively large impacts on burnup characteristics. Note that differences in k-inf at the very beginning cycle come from a difference in Xe-135 thermal capture cross section. Similar exercise has been also performed using the GALAXY code and consistent results have been obtained.

6. Conclusion

Performance of JENDL-4.0 for LWR application has been tested through various integral data. In addition, difference in PWR burnup characteristics between JENDL-4.0 and ENDF/B-VII.0 has been quantified. These information has been provided to JENDL nuclear data evaluators, and these will be successfully utilized for the next version of JENDL.

This manuscript has been prepared through cooperation with all the members of RIT-WG.

References

[1] N. Sugimura, et al.: *Trans. Am. Nucl. Soc.*, **97**, 559 (2007).

[2] K. Nakajima, et al.: "Analysis of criticality change with time for MOX cores," *Proc. of Int. Conf. on Physics of Reactors, PHYSOR2004,* April 25-29, 2004, Chicago, IL, (2004).[CD-ROM]

[3] T. Yamamoto: "Analysis of core physics experiments of high moderation full MOX LWR," JAEA-Conf 2006-009, p.7 (2006).

[4] G. Chiba, et al.: *J. Nucl. Sci. Technol.,* **48**[2], 172 (2011).

[5] T. Yamamoto, et al.: *J. Nucl. Sci. Technol.* **49**[1], 103 (2012).

[6] T. Sakai, et al.: "Neutron cross section sensitivity in keff analysis of FUBILA-MOX core physics experiments," *Proc. of 2012 annual meeting of AESJ*, F10, (2012).[CD-ROM][in Japanese]

[7] M. B. Chadwick, et al.: *Nucl. Data Sheets*, **112**, 2887 (2011).

[8] F. Jatuff, et al.: "Impact of newly-measured gadolinium cross sections on BWR fuel rod reaction rate distributions," *Proc. of Int. Conf. on Physics of Reactors, PHYSOR2008*, Sep. 14-19, 2008, Interlaken, Switzerland (2008).[CD-ROM]

[9] T. Yamamoto, et al.: "Analysis of core physics experiments on MOX assemblies loaded with Gd_2O_3-UO_2 and UO_2 rods," *Proc. of Int. Cong. on Advances in Nuclear Power Plants, ICAPP'09*, May 10-14, 2009, Tokyo, Japan (2009).[CD-ROM]

[10] G. Leinweber, et al.: *Nucl. Sci. Eng.*, **154**, 261 (2006).

[11] H. Matsumiya, et al.: "Analyses of critical experiments for LWR configurations with containing Gd rods by JENDL-4", *Proc. of 2011 fall meeting of AESJ*, N33, (2011),[CD-ROM][in Japanese]

[12] K. Yamaji, et al.: *Trans Am. Nucl. Soc.*, **97**, 573 (2007).

[13] H. Tagawa, et al.: "Validation of JENDL-4/0 in PWR pin cell geometry," *Proc. of 2012 annual meeting of AESJ*, E23, (2012).[CD-ROM][in Japanese]

[14] M. Suzuki, et al.: "Analysis of burnup and isotopic compositions of BWR 9x9 UO_2 fuel assemblies," *Proc. of Int. Conf. on Physics of Reactors, PHYSOR2012*, knowxville,(2012).[CD-ROM]

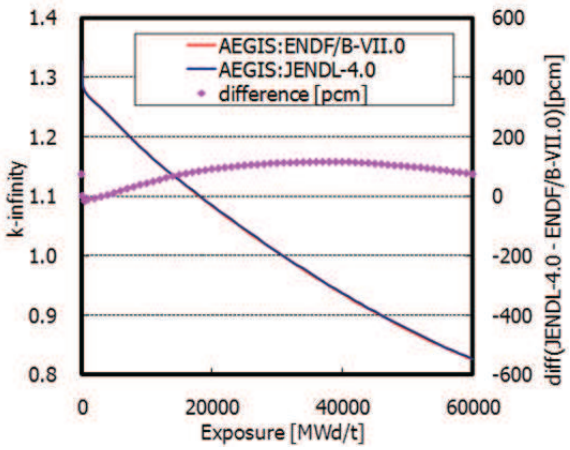

Fig. 8-1 Difference in k-inf of PWR assembly (UO_2)

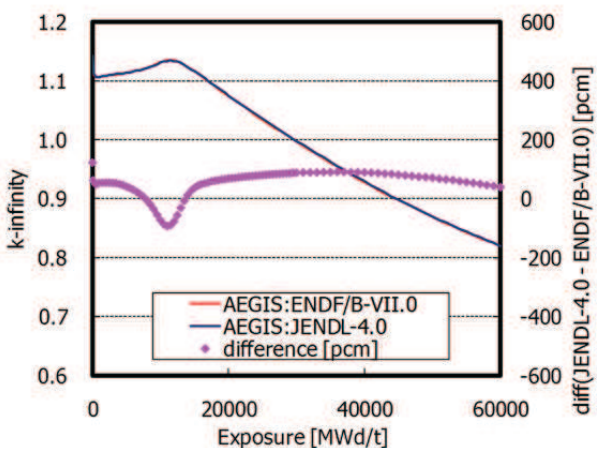

Fig. 8-2 Difference in k-inf of PWR assembly (UO_2+Gd)

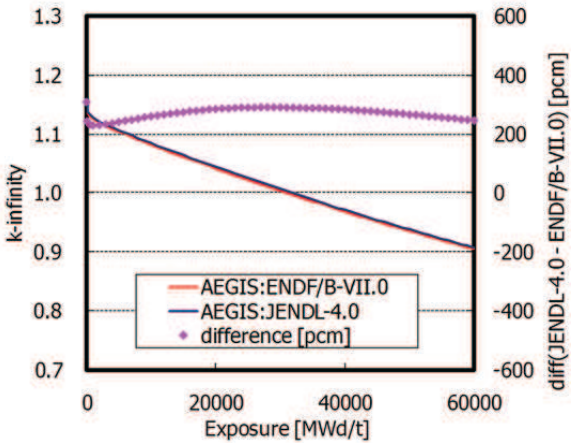

Fig. 8-3 Difference in k-inf of PWR assembly (MOX)

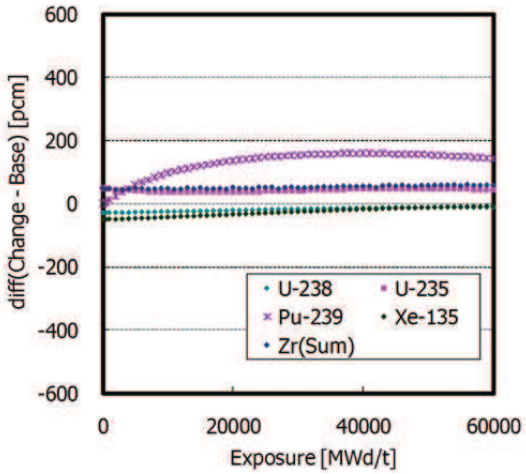

Fig. 9-1 Nuclide-wise difference in k-inf of PWR assembly (UO_2)

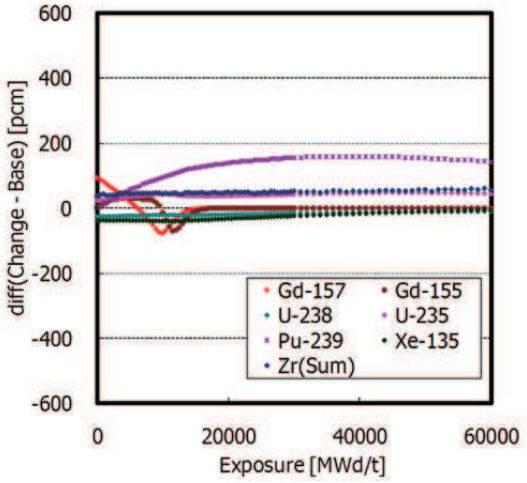

Fig. 9-2 Nuclide-wise difference in k-inf of PWR assembly (UO_2+Gd)

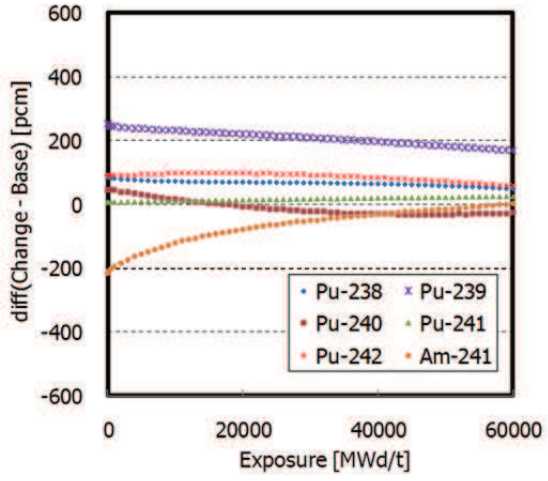

Fig. 9-3 Nuclide-wise difference in k-inf of PWR assembly (MOX)

13. Activities of Covariance Utilization Working Group

Kazufumi Tsujimoto
Nuclear Transmutation Technology Group,
Japan Atomic Energy Agency
tsujimoto.kazufumi@jaea.go.jp

During the past decade, there has been a interest in the calculational uncertainties induced by nuclear data uncertainties in the neutronics design of advanced nuclear system. The covariance nuclear data is absolutely essential for the uncertainty analysis. In the latest vesion of JENDL, JENDL-4.0, the covariance data for many nuclides, especially actinide nuclides, was substantialy enhanced. The growing interest in the uncertainty analysis and the covariance data has led to the organisation of the working group for covariance utilization under the JENDL committee.

Background of the working group

Accuracy of nuclear data, especially of minor actinides (MAs), is being concerned in designing future reactors for MA transmutation such as an Accelerator-Driven System (ADS). In order to understand current accuracy of neutronics calculation for the ADS, some benchmark activities were performed. As one of these benchmark activities, we proposed the benchmark problem for the depletion analysis of the ADS to the Coordinated Research Project on "Analytical and Experimental Benchmark Analyses of Accelerator Driven Systems" held by the International Atomic Energy Agency[1]. The benchmark calculation model based on the basic concept investigated in JAEA was adopted; namely, an 800 MWth lead-bismuth eutectic (LBE) cooled type reactor with MA nitride fuel. **Table 1** summarizes participant, code and library for the benchmark. The benchmark results by several nuclear data libraries showed that discrepancy among the

Table 1 Participant, code and library [2]

Participant	Code	Library [a]
JAEA (Japan)	PHITS, NMTC or MCNPX (MC code for proton and neutron >20MeV) SLAROM (Cross section code) TWODANT (Deterministic neutron transport code) ORIGEN (Burn-up code)	JENDL-3.3 JENDL-3.2 JENDL-4.0 ENDF/B-VI JEFF-3.0
CIEMAT (Spain)	EVOLCODE2 (MCNPX-based burnup code)	JEFF-3.0 (JEFF-3.1) (ENDF/B-VI)
KIT (Germany)	High energy particles are not analyzed. C^4P, ZMIX (Cross section code) DANTSYS (Deterministic neutron tansport code) TRAIN (Burn-up code)	ENDF/B-VII JEFF-3.1

[a] Library in parenthesis is only for the beginning of cycle (BOC).

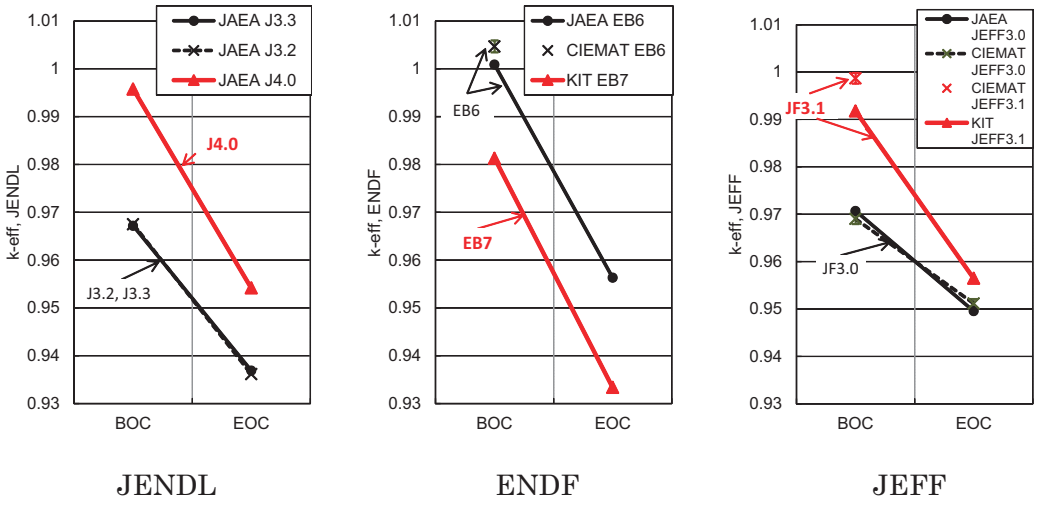

Fig.1 Calculation results of k-effective for IAEA benchmark problem of ADS (BOC=beginning of cycle, EOC=end of cycle) [2)]

libraries was as large as 3% for k-eff even for an initial criticality before burn-up[2)]. In case of JENDL, the difference between the calculated k-eff values by using JENDL-3.3 and JENDL-4.0 is approximately 3%, as shown in **Fig.1**.

On the other hand, JENDL-4.0 library provides comprehensive covariance data, especially for actinide nuclides. By using the covariance data, it is able to estimate an uncertainty for the neutronics parameters that are induced by uncertainties in nuclear data. The results of the uncertainty analysis were showed in **Table 2**. The uncertainty analysis were performed for similar ADS model based on more simplified model with single core fuel region, whether two zone-fule region adopted for the IAEA benchmark problem. As shown in Table 2, an estimated uncertainty for k-eff was about 1%[3)], which is much smaller than the discrepancy among the nuclear libraries.

Table 2 Calculational results of uncertainty analysis for k-eff and coolant void reactivity by using covariance data in JENDL-3.3 and JENDL-4.0 [3)]

	JENDL-3.3		JENDL-4.0	
Criticality (k-eff)	0.971	1.3%	0.999	1.1%
Coolant void reactivity [pcm]	5331	6.8%	3876	8.1%

Activities of the working group

Responding to this result, a meeting between JENDL evaluators and users was held to discuss about the JENDL covariance data. As a conclusion, there are certainly rooms to improve the covariance data of JENDL library, but this never means the covariance data are totally wrong or useless. The meeting members all agreed that this kind of continuous efforts to make actual data analysis and discussions between evaluators and users would improve the covariance data to be used in reactor design work.

With this purpose, a working group, named as "Covariance Utilization WG" in the JENDL committee, has been launched in 2011. The objectives of the WG activities are: to promote the conversation on the covariance of nuclear data between the users and evaluators, and finally to improve the quality of the covariance data.

References

[1] Alberto Abánades, *et al.*: “IAEA coordinated research project (CRP) on Analytical and experimental benchmark analyses of accelerator driven systems,” Proc. of International Conference on the Physics of Reactors “Nuclear Power: A Sustainable Resource”, Interlaken, Switzerland, September 14-19, 2008.

[2] K.Nishihara, T.Sugawara, H.Iwamoto, F.A.Velarde, and A.Rineiski “Investigation of Nuclear Data Accuracy for the Accelerator-Driven System with Minor Actinide Fuel”, Proc. of 11th Information Exchange Meeting on Partitioning and Transmutation, San Francisco, USA, 1-4 November 2010.

[3] H. Iwamoto, K.Nishihara, K.Tsujimoto, K.Sugino, and K.Numata, “Analysis of Transmutation System using JENDL-4.0”, JAEA-Research 2011-036 (2012).

This is a blank page.

14. A Working Group for Japanese Nuclear Data Measurement Network

Yukinobu WATANABE
Department of Advanced Energy Engineering Science, Kyushu University,
Kasuga, Fukuoka 816-8580, Japan
e-mail: watanabe@aees.kyushu-u.ac.jp

A new working group in the Japanese Nuclear Data Committee has been established to make a cooperative network among researchers involved in nuclear data measurements and to discuss the strategy for nuclear data measurements. The working group activities are reported.

1. Introduction

Nuclear data measurements are important to meet various needs of nuclear data for science and technology. However, the present situation is not necessarily satisfactory because the number of researchers involved in nuclear data measurements has been declining with decrease in the number of dedicated accelerator facilities. In addition, the experimental style has recently been changing from experiments with relatively small-scale dedicated accelerators to shared use of large-scale multi-purpose accelerators such as J-PARC, RCNP, HIMAC, etc. In the latter type of experiments, a collaborative teams are usually organized by researchers and students belonging different universities and institutes, and it is not necessarily easy to secure beam time enough for nuclear data measurements under strong competition with the other research fields. Thus, many researchers concerned in nuclear data measurements have a common recognition that it is one of the most crucial issues to develop human resources and to establish a cooperative network among researchers.

Under these situations, a new working group in the Japanese Nuclear Data Committee (JNDC) has been established to make a cooperative network among researchers involved in nuclear data measurements and to discuss the strategy for nuclear data measurements. It is called the working group for Japanese Nuclear Data Measurement Network (JNDM-net). Figure 1 shows location of experimental facilities for nuclear data measurements in Japan. Twelve members and four observers have participated in the working group from major universities and institutes.

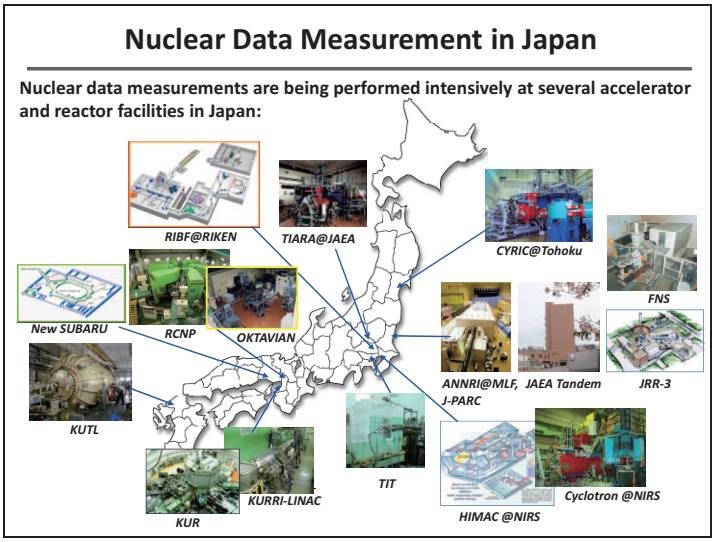

Fig.1 Experimental facilities available for nuclear data measurements in Japan

In this report, I shall mention about the action plan and working group activities in FY2012, and finally discuss future outlook on domestic nuclear data measurements.

2. Action plan

The basic action plan of the working group is as follows:

1) To establish a cooperative network among researchers involved in nuclear data measurements in Japan.
2) To explore the needs of nuclear data measurements based on constructive discussions with evaluators and users, and prepare for an effective framework to summarize a data request list.
3) To discuss the planning and proposal of new experimental projects, and make a roadmap on domestic nuclear data measurements.

3. Activities in FY2012

So far, the working group meetings have been held twice since the working group launched in FY2012. The activities in FY2012 are summarized as follows.

First, the website shown in Fig.2 was established not only to play the central role of a networking site among the members but also to offer useful information about the working group activities. Second, we have exchanged information on the present status of nuclear measurements and future plan in research group belonging to each member. Note that brief overview of the present status and perspectives of domestic measurement activities is reported in Refs.[1][2]. There are growing needs for nuclear data in many application fields: fission reactors of new generation, fusion technology, ADS, hadron therapy with proton beam or heavy-ion beam, nuclear medicine, irradiation of materials and microelectronic devices, development and characterization of new detectors, and validation of codes. In FY2012, we have conducted a preliminary request survey from the stand point of nuclear data evaluation and development of PHITS code.

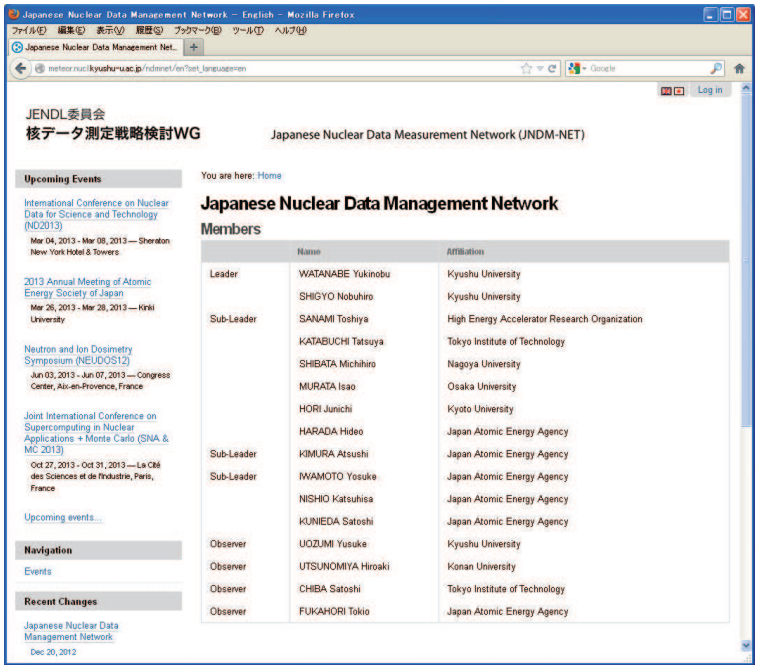

Fig.2 Web site of JNDM-net (http://meteor.nucl.kyushu-u.ac.jp/ndmnet/)

4. Summary and future outlook

The working group for Japanese Nuclear Data Measurement Network (JNDM-net) was established in FY2012. Based on the survey of nuclear data needs, we would like to start discussing the planning and proposal of new experimental projects to revitalize domestic activities of nuclear data measurements and to develop related human resources. One of the approaches is to organize a relatively large-scaled project utilizing shared-use facilities such as RCNP and RIBF@RIKEN under a unique research subject with novelty and high priority. It will be also important to make continuous efforts on measurements of systematic and high-quality data by a relatively small group because they will contribute to improvement of theoretical models. I think that it is time to discuss the strategy toward further development of our domestic community of nuclear data measurement.

Finally, it is expected that this working group will play an essential role as a system for coordination and cooperation among researchers involved in nuclear data measurements in Japan.

Acknowledgement

The author would like to thank all the working group member for their cooperation.

References

[1] M. Igashira, Proc. of the 2011 Symp. on Nuclear Data; JAEA-Conf 2012-001 (2012), pp.53-56.

[2] Y. Watanabe, Proc. of the 2011 Symp. on Nuclear Data; JAEA-Conf 2012-001 (2012), pp.57-62.

This is a blank page.

15. New extension of CCONE code for calculation of deuteron-induced reactions

Shinsuke Nakayama[1*], Shouhei Araki[1], Yukinobu Watanabe[1], Osamu Iwamoto[2]

[1]Department of Advanced Energy Engineering Science, Kyushu University, Japan
[2]Nuclear Science and Engineering Directorate, Japan Atomic Energy Agency, Japan
*E-mail: nakayama@aees.kyushu-u.ac.jp

We propose a new method of calculating the cross sections for deuteron-induced reactions and extend CCONE code in order to develop a deuteron nuclear data library. In the extension, the continuum discretized coupled-channels (CDCC) theory and the Glauber model are employed for calculations of elastic breakup and stripping reactions to continuum, respectively. Statistical decay from compound nuclei formed by nucleon stripping and deuteron absorption is calculated by the exciton and the Hauser-Feshbach models implemented in CCONE code. The calculation results reproduce double-differential (*d*,*xp*) cross sections measured at forward angles for incident energies of 65 and 100 MeV fairly well.

1. Introduction

In recent years, research and development of intensive accelerator-driven neutron sources lead to renewed interest in the study of deuteron-induced reactions. The neutron sources with deuteron-induced reactions on light nuclei (^{7}Li, ^{9}Be, ^{12}C, etc.) are proposed for various neutron beam applications such as irradiation testing of fusion reactor materials, boron neutron capture therapy (BNCT), and production of radioisotopes for medical use. For development and detailed design of accelerator-driven neutron sources, comprehensive nuclear data of deuteron-induced reactions are indispensable as fundamental data. Currently available deuteron nuclear data file is TENDL[1)] which has been developed by compiling the output of TALYS code[2)]. As shown in Fig.1, TALYS code is not necessarily adequate for calculation of deuteron-induced reactions. The calculation result underestimates considerably a characteristic broad peak observed around half the deuteron incident energy in experimental (*d*,*xp*) data[3)], which is caused by deuteron breakup processes. Thus, new comprehensive nuclear data of deuteron-induced reactions are required for accurate estimation of neutron yields and induced radioactivity in the engineering design of accelerator-driven neutron sources.

Theoretical model calculations play an important role in nuclear data evaluation, particularly, in the case where experimental data are not available. Therefore, we have started to develop a reliable calculation method for deuteron-induced reactions and an integrated code system applicable over the wide ranges of target mass number (including accelerator structure materials. e.g. Fe, Ni, Cr) and incident

energies up to 200 MeV.

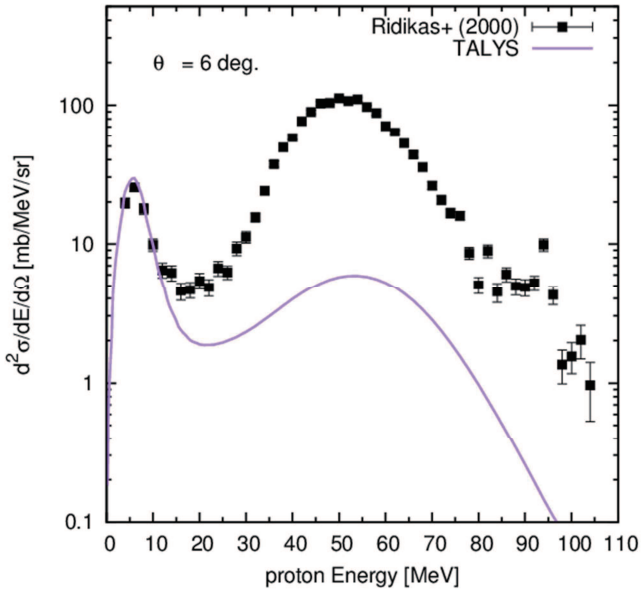

Fig.1 Comparison of double-differential cross sections calculated with TALYS code and experimental data[3] for ^{58}Ni (*d,xp*) at 100MeV.

2. Methodology

Neutron-emission data are necessary for the engineering design of neutron sources, but there are no available experimental data of double-differential cross sections (DDXs) of (*d,xn*) reactions over the wide target mass number and incident energy ranges. In the present work, we analyze DDXs of (*d,xp*) reactions measured systematically for some target nuclei at 100MeV and those for ^{58}Ni at several incident energies[3,4].

In our previous study[5], we used the continuum discretized coupled-channels (CDCC) theory for elastic breakup reaction and the Glauber model for stripping reaction to continuum in order to investigate deuteron breakup processes over the wide target mass number range. Moreover, the phenomenological moving-source model was used to estimate preequilibrium and evaporation components from highly excited compound and residual nuclei. In the present study, we employ a comprehensive code for nuclear data evaluation, CCONE[6], instead of using the phenomenological moving-source model. In this way, the statistical decay from compound nuclei formed by nucleon stripping and deuteron absorption can be calculated by the conventional exciton and Hauser-Feshbach models which are implemented in CCONE code. The DDXs of (*d,xp*) reactions are expressed by the incoherent summation of three components:

$$\frac{d^2\sigma^{(d,xp)}}{dEd\Omega} = \frac{d^2\sigma_{breakup}}{dEd\Omega} + \frac{d^2\sigma_{stripping}}{dEd\Omega} + \frac{d^2\sigma_{statistical}}{dEd\Omega} \qquad (1)$$

where $\frac{d^2\sigma_{breakup}}{dEd\Omega}$, $\frac{d^2\sigma_{stripping}}{dEd\Omega}$, and $\frac{d^2\sigma_{statistical}}{dEd\Omega}$ correspond to DDXs for elastic breakup reaction, neutron stripping reaction, and statistical decay, respectively.

DDXs for elastic breakup and neutron stripping reactions are directly calculated with the CDCC method and the Glauber model, respectively, based on the method described in Ref. [5]. Statistical decay processes from compound nuclei are relatively complicated. We cannot calculate them by using original CCONE code. This difficulty is caused by the fact that three different compound nuclei are formed by absorption of either a neutron or a proton or both in the deuteron in the case of deuteron-induced reactions. To solve this problem, we calculate DDXs for statistical decay from those compound nuclei in the following way:

$$\frac{d\sigma_{compound}}{dEd\Omega} = R^{d}_{Glauber}\left.\frac{d\sigma_{(d,xp)}}{dEd\Omega}\right|_{CCONE} + R^{n}_{Glauber}\left.\frac{d\sigma_{(n,xp)}}{dEd\Omega}\right|_{CCONE} + R^{p}_{Glauber}\left.\frac{d\sigma_{(p,xp)}}{dEd\Omega}\right|_{CCONE} \quad (2)$$

where $R^{d}_{Glauber}$, $R^{n}_{Glauber}$, and $R^{p}_{Glauber}$ denote the formation fractions of three different compound nuclei, which are calculated with the Glauber model, and $\left.\frac{d\sigma_{(d,xp)}}{dEd\Omega}\right|_{CCONE}$, $\left.\frac{d\sigma_{(n,xp)}}{dEd\Omega}\right|_{CCONE}$, and $\left.\frac{d\sigma_{(p,xp)}}{dEd\Omega}\right|_{CCONE}$ are DDXs of (*d,xp*) , (*n,xp*) , and (*p,xp*) reactions calculated with CCONE code, respectively.

In the calculation of (*n,xp*) and (*p,xp*) with CCONE code, the incident energies of neutron and proton are fixed to half the deuteron incident energy. Strictly speaking, this approximation is not correct because either neutron or proton absorbed on stripping reaction has an energy distribution. However our preliminary calculation showed that there is not so much difference between the calculation results of the approximate case and those of the case where energy distribution is considered exactly. We use this approximation for reduction of computation time. In statistical decay calculations, optical model potentials (OMPs) are necessary in all the calculations, and we use Koning and Delaroche OMPs[7] for protons and neutrons, and An and Cai OMPs[8] for deuterons. Default values in CCONE code are used for other physical parameters such as level density parameters.

3. Results and discussion

Figure 2 shows comparisons between the calculated and experimental DDXs[3] of ^{58}Ni (*d,xp*) reaction at 100MeV. The present calculations reproduce both the shape and magnitude of the experimental (*d,xp*) spectra at forward angles better than TALYS calculations. A large difference between both calculations is seen in the broad peak around half the deuteron incident energy. The characteristic peak is formed by proton emission via elastic breakup and stripping processes. These components are calculated with the Kalbach empirical formula in TALYS code, while they are calculated using physics-based CDCC

and Glauber models in the present work. This indicates that the breakup and stripping processes characteristic of deuteron-induced reactions should be taken into account using reliable theoretical models. However, our model calculation fails to reproduce several peaks in the high energy region at 6 degrees as shown in Fig.2. These peaks correspond to the transition to bound states in the residual nucleus, ^{59}Ni, via neutron stripping. Since the Glauber model cannot treat this transition properly, a conventional distorted wave Born approximation (DWBA) approach with spectroscopic factor for each bound state will be necessary to describe such the stripping reaction.

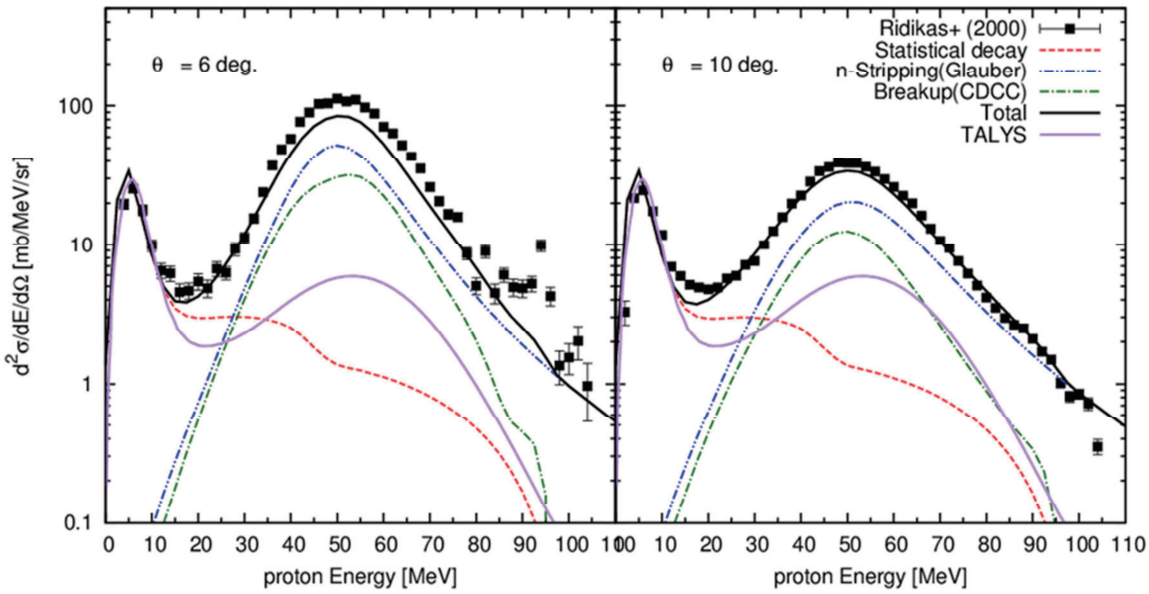

Fig.2 Calculated and experimental DDXs of ^{58}Ni (*d,xp*) at 100MeV

Our proposed calculation method is applied to other reactions. The results for ^{58}Ni (*d,xp*) reaction at 65MeV and ^{27}Al (*d,xp*) reaction at 100MeV are shown in Figs.3 and 4, respectively. Both calculations reproduce the experimental data[3, 4] fairly well. Further comparisons with available experimental data including activation cross sections will be necessary over the wide ranges of incident energy and target mass number to confirm the applicability of the present calculation method for nuclear data evaluation of deuteron induced reactions.

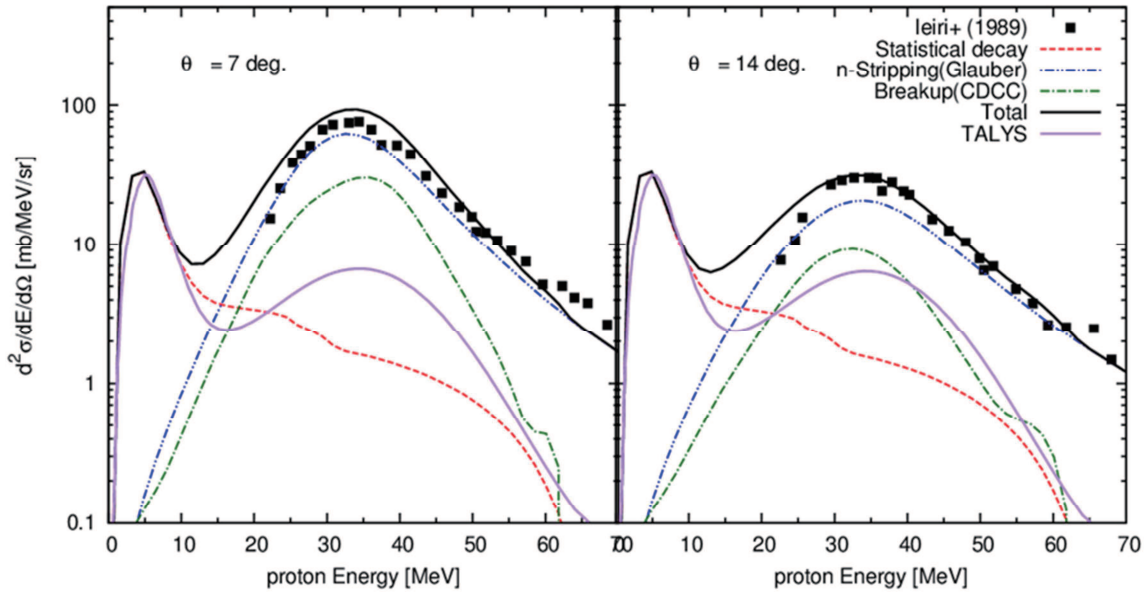

Fig.3 Same as in Fig.2 but for ^{58}Ni (*d,xp*) at 65MeV

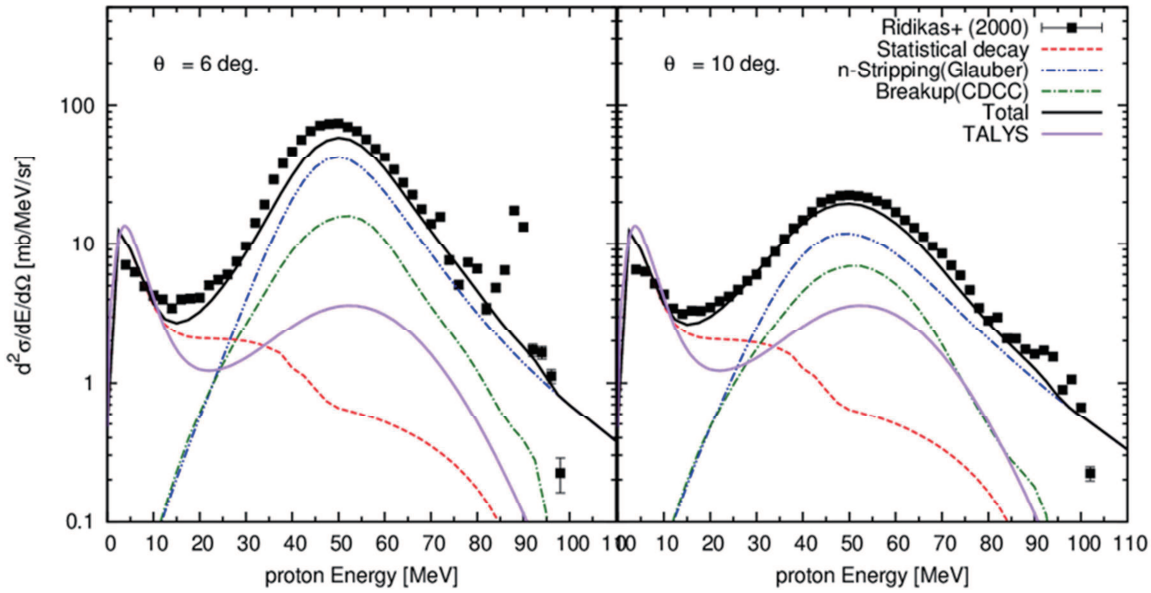

Fig.4 Same as in Fig.2 but for ^{27}Al (*d,xp*) at 100MeV

4. Conclusions and outlook

We have developed a code system with CCONE code for deuteron-induced reactions. The cross sections for elastic breakup and stripping reactions are calculated with the codes based on the CDCC and the Glauber model, and their results are inputted to CCONE code. The calculation results with the code system reproduce the experimental (*d,xp*) data at 65 and 100 MeV better than those with TALYS code.

As previously mentioned, it will be necessary to consider the stripping reaction to bound states in order to make this calculation method more reliable. Thus, we aim to develop a calculation method

including a conventional DWBA approach to calculate this component. In addition, further analysis will be necessary for quantities other than DDXs of (*d,xp*) reactions such as activation cross sections and DDXs of (*d,xn*) reactions.

Acknowledgments

The authors wish to thank S. Hashimoto of the Advanced Science Research Center, JAEA, for the several calculations with the CDCC theory.

References

1) A.J. Koning, D. Rochman, S. van der Marck et al., "TENDL-2012: TALYS-based evaluated nuclear data library," URL: www.talys.eu/tendl2012.html

2) A.J. Koning, S. Hilaire and M.C. Duijvestijn, "TALYS-1.0," Proceedings of the International Conference on Nuclear Data for Science and Technology, April 22-27, 2007, Nice, France, EDP Sciences, 211-214(2008).

3) D. Ridikas, W. Mittig, H. Savajols et al., "Inclusive proton production cross sections in (d,xp) reactions induced by 100 MeV deuterons," Phys. Rev. C 63, 014610 (2000).

4) M. Ieiri, H. Sakaguchi, M.nakamura et al., "Polarization transfer measurements for the *(d, pX)* reaction at E_d = 65 MeV and the reaction mechanism for the protons in the continuum," Nucl. Phys. A 504, 477–510 (1989).

5) T. Ye, S. Hashimoto, Y. Watanabe et al., "Analysis of inclusive (*d,xp*) reactions on nuclei from ^{9}Be to ^{238}U at 100 MeV," Phys. Rev. C 84, 054606 (2011).

6) O. Iwamoto, "Development of a comprehensive code for nuclear data evaluation, CCONE, and validation using neutron-induced cross sections for uranium isotopes," J. Nucl. Sci. Technol. 44 (5), 687 (2007).

7) A.J. Koning, J.P. Delaroche, "Local and global nucleon optical models from 1 keV to 200 MeV," Nucl. Phys. A 713, 231 (2003)

8) H. An, C. Cai, "Global deuteron optical model potential for the energy range up to 183 MeV," Phys. Rev. C 73, 054605 (2006)

16. Neutron Cross Section Sensitivity Analysis on UO_2 and MOX Cores in the MISTRAL Program

Tomohiro SAKAI and Toru YAMAMOTO
Japan Nuclear Energy Safety Organization
Toranomon Towers Office, 4-1-28 Toranomon, Minato-ku, Tokyo 105-0001, Japan
sakai-tomohiro@jnes.go.jp

The perturbation theory based on the transport calculation has been applied to sensitivity analysis of neutron multiplication factors (k_{eff}'s) to neutron cross sections in the analysis of experimental UO_2 and MOX cores of the MISTRAL program. The UO_2 core under the investigation is a MISTRAL core 1 which is a UO_2 homogeneous core consisting of UO_2 fuel rods of 3.7wt% of ^{235}U enrichment. The MOX core is a MISTRAL core 4 (full MOX core) which is a PWR mockup full MOX core which consists of MOX rods of 7.0wt% of Pu total concentration. The studied cross sections were neutron capture, fission, elastic scattering, inelastic scattering and (n, 2n) cross sections and a number of fission neutrons ν and others. The obtained sensitivities were multiplied to relative differences in cross sections between JENDL-4.0 and JENDL-3.3 in order to estimate the effect of the differences in the cross sections on the k_{eff}'s. The results show that increase in keff, 0.31% Δk, from JENDL-3.3 to JENDL-4.0 for MISTRAL core 1 is mainly attributed to the decreases in the capture cross sections of ^{238}U. On the other hand, there are various contributions from the differences in the cross sections of U and Pu isotopes for the MISTRAL core 4. The major contributors to increase in k_{eff} are the decreases in the capture cross sections of ^{238}U, ^{238}Pu, ^{239}Pu, and those to decrease in k_{eff} are the decrease in ν of ^{239}Pu and the increase in the capture cross sections of ^{241}Am. They compensate each other, and the difference in k_{eff} from JENDL-3.3 to JENDL-4.0 is -0.03 % Δk and relatively small.

1. Introduction

The new version of the Japanese evaluated nuclear data library, JENDL-4.0, has been released and publically available[1]. As part of integral tests of the new library based on experimental data, core analysis of experimental cores in the full MOX BWR core physics experiments FUBILA[2] has been performed using a continuous energy Monte Carlo calculation code coupled with the nuclear data libraries JENDL-3.3 and JENDL-4.0[3][4]. While cross sections of most of major and minor actinide nuclides were reevaluated in the new

library, it is reported that the differences in the critical neutron multiplication factors k_{eff} of the experimental cores were less than 0.1%Δk for the FUBILA experimental cores. It suggests that, since cross sections of many kinds of nuclides such as U, Pu and Am isotopes contribute to the core reactivity in the MOX cores, the changes in some of them contribute to compensating each other. The perturbation theory based on the transport calculation has been applied to the sensitivities analysis of the neutron multiplication factors (k_{eff}'s) to neutron cross sections in the analysis of an experimental MOX core of the FUBILA program[5].

The present study is to apply the method to UO_2 and MOX cores of the MISTRAL program. The UO_2 core under the investigation is a MISTRAL core 1 which is a UO_2 homogeneous core consisting of UO_2 fuel rods of 3.7wt% of ^{235}U enrichment; the MOX core is a MISTRAL core 4 (full MOX core) which is a PWR mockup full MOX core which consists of MOX rods of 7.0wt% of Pu total concentration[6].

2. Core Configurations of MISTRAL Cores 1 and 4

Figure 1 shows the core configurations of the MISTRAL cores 1 and 4[6]. The MISTRAL core 1 is a UO_2 homogeneous core consisting of UO_2 fuel rods of 3.7wt% of ^{235}U enrichment with a lattice pitch 1.32 cm. The MISTRAL core 4 is a PWR mockup full MOX core which consists of MOX rods of 7.0wt% of Pu total concentration with a lattice pitch 1.32 cm. The lattice pitch of both cores is slightly larger than that of a standard PWR 17 x 17 fuel assembly. The experiments aimed at obtaining core characteristics of an advanced core with a higher moderation ratio as a futuristic LWR core concept.

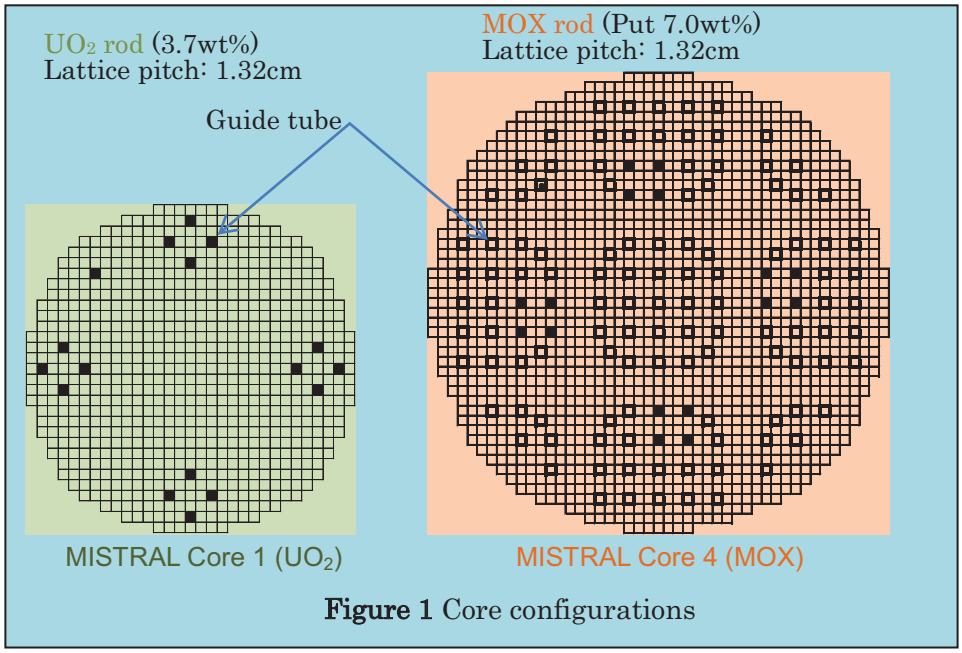

Figure 1 Core configurations

3. Cross Section Sensitivity Calculation

3.1 Sensitivity Calculation Method

The perturbation method was adopted to calculate the sensitivity of neutron cross sections[7]. The reactivity of a nuclear system is expressed as

$$\rho = \frac{\left\langle \Phi^{+}\left(\delta M - \frac{1}{k}\delta F \right)\Phi \right\rangle}{\left\langle \Phi^{+}\frac{1}{k}F\Phi \right\rangle} \tag{1}$$

here,

$$M_g\varphi_g(\Omega) = \Omega\nabla\varphi_g(\Omega) + \Sigma_t^g\varphi_g(\Omega) - \sum_{h=1}^{G}\int d\Omega'\,\Sigma_s^{h\to g}(\Omega'\to\Omega)\varphi_h(\Omega'), \tag{2}$$

$$F_g\varphi_g(\Omega) = \frac{\chi_g}{4\pi}\sum_{h=1}^{G}\int d\Omega'\,\nu_h\Sigma_f^h\varphi_h(\Omega'). \tag{3}$$

The definitions of the symbols in the above equations are common ones.

A developed calculation scheme consists of three parts: (1) fuel cell calculations, (2) core calculation, and (3) sensitivity calculation. In the process (1), a collision probability method code PIJ in a general purpose neutronics calculation code system SRAC[8] was used for cell calculations in the 107 neutron energy groups on fuel cells which compose the experimental cores to obtain space-homogenized nuclear constants for the following core analysis and sensitivity analysis. The nuclear data libraries used were based on JENDL-3.3 and JENDL-4.0. In the process (2), the core analysis in a two-dimensional geometry was performed using TWODANT code[9] to analyze the neutron multiplication factors, neutron fluxes and adjoint neutron fluxes. The axial leakage of neutrons was calculated by applying the measured axial buckling values. In the process (3), the sensitivity $(dk/k)/(d\sigma/\sigma)$ was calculated by the micro cross sections in the process (1) and the neutron fluxes in the process (2), and the reactivity contribution by replacing the cross section based of JENDL-3.3 by that of JENDL-4.0 were obtained as

$$\{(dk/k)/(d\sigma/\sigma)\}\times(d\sigma/\sigma)_{JENDL}, \tag{4}$$

here, $(d\sigma/\sigma)_{JENDL}$ is defined by (cross section of JENDL-4.0−that of JENDL-3.3)/that of JENDL-4.0.

3.2 Neutron Multiplication Factors

Difference in k_{eff} of between JENDL-4.0 and JENDL-3.3 for the MISTRAL core 1 is significant (0.28 %Δk) in Monte Carlo calculations by using MVP[10]; that for the MISTRAL core 4 is small (−0.06%Δk) as seen in **Figure 2**. The k_{eff}'s of TWODANT were not shown;

however, a similar trend was observed.

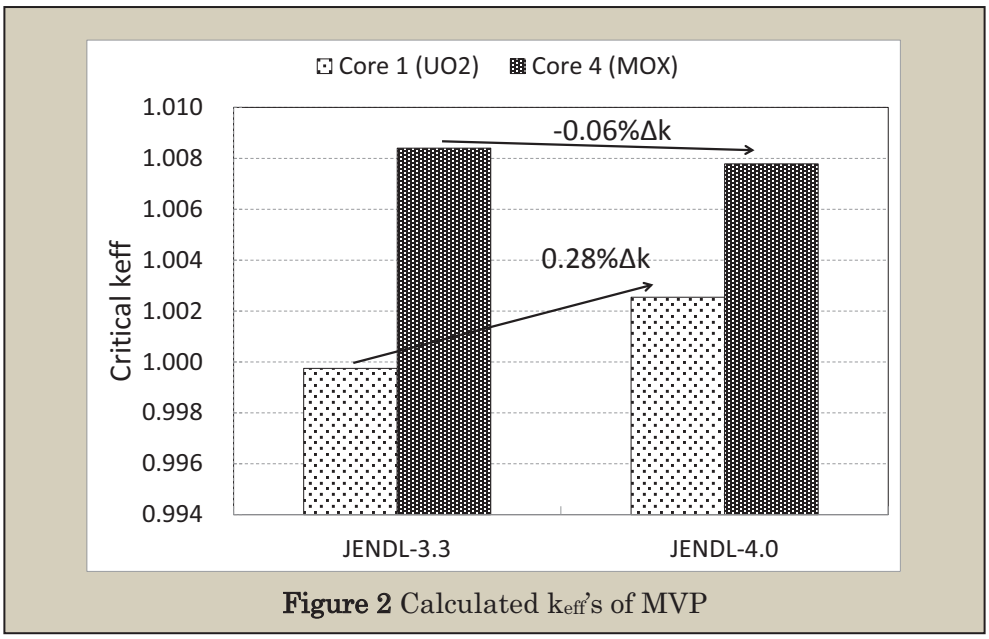

Figure 2 Calculated k_{eff}'s of MVP

3.3 Results of Sensitivity Calculation

The analysis results of the major reactivity contributions of the cross sections and the nuclides are shown in **Figure 3**. The energy dependent contributions are also shown in **Figure 4**. The results show that increase in k_{eff} from JENDL-3.3 to JENDL-4.0 for the MISTRAL core 1 is mainly attributed to the decreases in the capture cross sections of ^{238}U in thermal and resonance energy regions as seen in Figures. 3 and 4. The capture cross section (2,200m/s) was reduced by －1.3% to 2.683 b in JENDL-4.0 from 2.718 b in JENDL-3.3. The resonance integral (RI) was reduced by －0.9% to 275.6 b from 278.1 b.

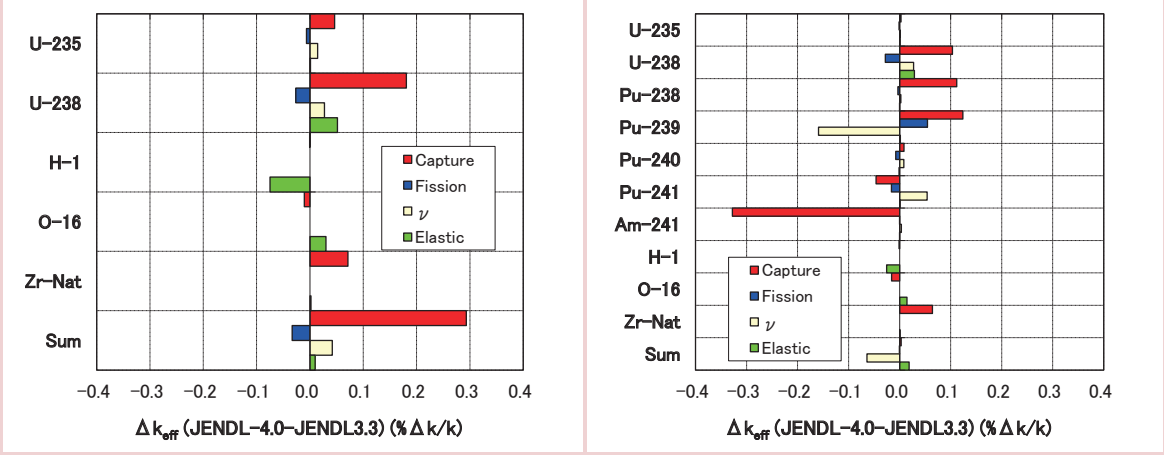

MISTRAL Core 1 (UO_2) MISTRAL Core 4 (MOX)

Figure 3 Reactivity change from JENDL-3.3 to JENDL-4.0

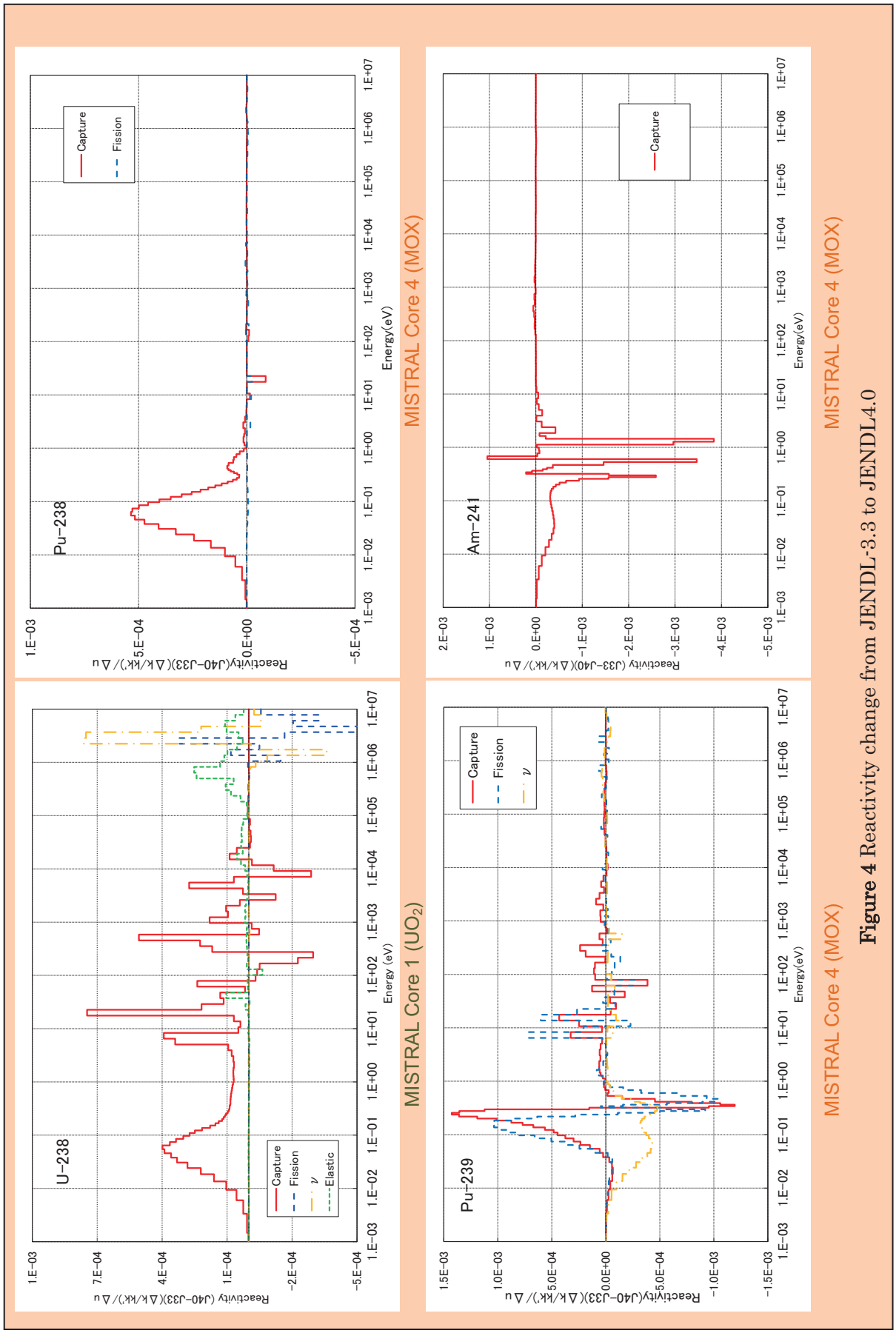

Figure 4 Reactivity change from JENDL-3.3 to JENDL4.0

On the other hand, there are various contributions from the differences in the cross sections of U and Pu isotopes for the MISTRAL core 4. The major contributors to increase k_{eff} are the decreases in the capture cross sections of ^{238}U, ^{238}Pu, ^{239}Pu. The capture cross section (2,200m/s) of ^{238}Pu was significantly reduced by －23.6% to 412.9 b in JENDL-4.0 from 540.2 b in JENDL-3.3, which gives a prominent contribution. The major contributions to decrease k_{eff} are the decreases in ν of ^{239}Pu and the increase in the capture cross sections of ^{241}Am. They compensate each other, and the difference in k_{eff} from JENDL-3.3 to JENDL-4.0 is relatively small.

4. Conclusions

The results of the cross section sensitivity analysis show that increase in k_{eff}, 0.31% Δk, from JENDL-3.3 to JENDL-4.0 for MISTRAL core 1 is mainly attributed the decreases in the capture cross sections of ^{238}U. On the other hand, there are various contributions from the differences in the cross sections of U and Pu isotopes for the MISTRAL core 4. The major contributors to increase k_{eff} are the decreases in the capture cross sections of ^{238}U, ^{238}Pu, ^{239}Pu, and those to decrease k_{eff} are the decrease in ν of ^{239}Pu and the increase in the capture cross sections of ^{241}Am. They compensate each other, and the difference in keff from JENDL-3.3 to JENDL-4.0 is －0.03 % Δk and relatively small.

References

[1] K. Shibata, O. Iwamoto, T. Nakagawa *et al.*: "JENDL-4.0: A new library for nuclear science and engineering", J. Nucl. Sci. Technol., **48**, 1 (2011).

[2] T. Yamamoto, T. Sakai, Y. Ando, S. Kikuchi and T. Umano: "Neutronics analysis of full MOX BWR core simulation experiments FUBILA", J. Nucl. Sci. Technol., **48**, 398 (2011).

[3] G. Chiba, K. Okumura, K. Sugino *et al.*: "JENDL-4.0 benchmarking for fission reactor applications", J. Nucl. Sci. Technol., **48**, 172 (2011).

[4] T. Yamamoto, H. Sakai, Y. Ando, P.H. Leim and S. Kikuchi: "Neutronics analysis of full MOX BWR core simulation experiments – FUBILA: Part 2", J. Nucl. Sci. Technol., **49**, 103 (2012).

[5] T. Sakai, T. Yamamoto and T. Nakajima: "Neutron cross section sensitivity in k_{eff} analysis of FUBILA-MOX core physics experiments", Proceedings of 2012 Annual Meeting of the Atomic Energy Society of Japan, F10, Fukui Univ., (2012) [in Japanese].

[6] T. Yamamoto: "Analysis of Core Physics Experiments of High Moderation Full MOX LWR", Proceedings of the 2005 Symposium on Nuclear Data, February 2-3, 2006, JAEA Tokai, Japan, JAEA-Conf 2006-009 (2006).

[7] M. Sasaki, Y. Tanaka, *et al.*:, "Development of reactivity calculation methods and application study," PNC Report ZJ-206 77-35 (1978) [in Japanese].

[8] K. Okumura, T. Kugo, K. Kaneko *et al.*: "SRAC2006: A Comprehensive Neutronic Calculation Code system," JAEA-Data/Code 2007-004, Japan Atomic Energy Agency (2007).

[9] R.E. Alcouffe, R.S. Baker, F.W. Brinkley *et al.*: "DANTSYS: A Diffusion Accelerated Neutral Particle Transport Code System," LA-12969-M, Los Alamos National Laboratory (June 1995).

[10] Y. Nagaya, K. Okumura, T. Mori *et al.*: "MVP/GMVP II: General Purpose Monte Carlo Codes for Neutron and Photon Transport Calculations Based on Continuous Energy and Multigroup Methods," JAERI-1348, Japan Atomic Energy Research Institute (2005).

17. Analysis of Nucleon and Triton Emissions via Breakup Process in Nucleon-induced Reactions on ^{6,7}Li

Hairui Guo[a], Kohei Nagaoka[a], Yukinobu Watanabe[a], Takuma Matsumoto[b], Kazuyuki Ogata[c] and Masanobu Yahiro[b]
[a]Department of Advanced Energy Engineering Science, Kyushu University, Kasuga, Fukuoka 816-8580, Japan
[b]Department of Physics, Kyushu University, Fukuoka 812-8581, Japan
[c]Research Center for Nuclear Physics, Osaka University, Ibaraki, Osaka 567-0047, Japan
Email: ghr@aees.kyushu-u.ac.jp

Nucleon and triton emissions via breakup processes in nucleon-induced reactions on ^{6,7}Li are analyzed with three-body Continuum Discretized Coupled Channels method (CDCC) and sequential decay model. The CDCC is applied to (n,xn) and (p,xp) reactions on ^{6,7}Li. The triton emission from n(p)+^{7}Li→t+^{5}He*(^{5}Li*) is also taken into account by the final state interaction model. In most cases, the calculated results are in good agreement with the experimental data at incident energies around 14 MeV, except for the nucleon emission with relatively low emission energy.

1. Introduction

In fusion technology, lithium is an important element relevant to not only a tritium breeding material in D-T fusion reactors but also a candidate for target material in the intense neutron source of International Fusion Materials Irradiation Facility [1]. Accurate nuclear data of nucleon and triton emission spectra for nucleon-induced reactions on ^{6,7}Li at incident energies up to 50 MeV are currently required for the design of these facilities [2]. Since ^{6}Li and ^{7}Li can easily break up, namely, ^{6}Li→ d + α and ^{7}Li → t + α, the nucleon and triton emission spectra are affected strongly by the breakup process. Therefore, the analysis of nucleon and triton emissions via breakup reaction process is of great significance.

2. Theoretical model

The nucleon production DDXs and breakup cross sections of ^{6,7}Li are analyzed with three-body continuum discretized coupled channels method (CDCC) [3-5]. ^{6}Li and ^{7}Li are considered as d+α and t+α cluster, respectively. Their discretized internal wave functions are obtained by the pseudostate method [5,6] with the interactions as Gaussian forms. The diagonal and coupling potentials between nucleon and ^{6,7}Li are obtained by folding complex Jeukenne-Lejeune-Mahaux (JLM) effective nucleon-nucleon interaction [7] with the transition densities between the corresponding discretized states. The parameters of JLM interaction are determined so as to reproduce the experimental data of total and reaction cross sections. The detailed description of the formulas of CDCC and parameters of JLM

nucleon-nucleon interaction used are given in Ref. [8].

The triton production DDX from the breakup process of ^{7}Li is calculated with the sequential decay model [9]. The triton emission is assumed to be isotropic. The formula is expressed as

$$\left(\frac{d^2\sigma}{dE_t d\Omega_t}\right)_{\mathrm{seq}}^{J^\pi} = \sum_i \frac{\sigma_i^{J^\pi}}{2\pi} \int L_1(E_N \rightarrow E_{\mathrm{Li}}) L_2(E_{\mathrm{Li}} \rightarrow E_t) \Lambda(\mu_{Nt}) dE_{\mathrm{Li}}, \quad (1)$$

where, $\sigma_i^{J^\pi}$ is the breakup cross section from the *i*th discretized state of ^{7}Li which is obtained with CDCC. L_1 denotes the probability that an incident nucleon with energy E_N produces a particle ^{7}Li with energy E_{Li}. L_2 denotes the probability that an intermediate ^{7}Li with energy E_{Li} produces a triton with energy E_{t}. $\Lambda(\mu_{Nt})$ stands for the probability of the cosine of the angle between the direction of incident nucleon and emitted triton being μ_{Nt}.

The incident energies of the existing experimental data of triton production DDX are below 20 MeV where there are other reaction processes, n(p)+^{7}Li→t+^{5}He*(^{5}Li*), contributing to triton emission. In order to compare the calculated results with experimental data, the triton emission from these reaction processes is also calculated by the final state interaction (FSI) model [10]. Here, ^{5}He* and ^{5}Li* are considered as α-n and α-p systems, respectively. The formula is expressed as

$$\left(\frac{d^2\sigma}{dE_t d\Omega_t}\right)_{\mathrm{FSI}} = N_F \cdot \sin^2\beta_l \cdot \frac{F_l^2(k_{N\alpha}a) + G_l^2(k_{N\alpha}a)}{(k_{N\alpha}a)^2} \cdot \rho_t(E_t^{lab}), \quad (2)$$

where N_F is a parameter which is determined by fitting to experimental data, F_l and G_l are the first-order spherical Bessel functions for the α-n system and the Coulomb wave functions for the α-p system, k denotes the wave number of p(n) in α-p(n) system, ρ is the phase space factor, and β_l denotes the α-p(n) phase shift .

3. Results and discussion

The neutron (proton) emission spectra for n(p)+^{6,7}Li reactions are calculated with the three-body CDCC. Figures 1 and 2 show the comparisons of the calculated results and experimental data [11,12] of neutron and proton production DDXs at incident energies around 14 MeV, respectively. The experimental data for p+ ^{6}Li reaction include the effect of contamination in target, such as ^{1}H, ^{16}O. The contributions corresponding to unbound ^{1}S, ^{1}D, ^{2}D and ^{3}D states of ^{6}Li are denoted by dash-dot-dotted, dashed, short dashed and dash-dotted lines, respectively. The three major peaks of the calculated results represent the elastic, inelastic to the 3+ resonance and 2+ resonance components, respectively, from high nucleon energy. The calculated results are in good agreement with experimental data in relatively high emission energy region, while they underestimate the experimental data in the low

emission energy region corresponding to highly exited states of ^{6}Li. One of the reasons for the discrepancy is that there are other reaction processes contributing to this energy region, such as (n,2n) and (p,2p) reactions, which cannot be calculated with the present three-body CDCC.

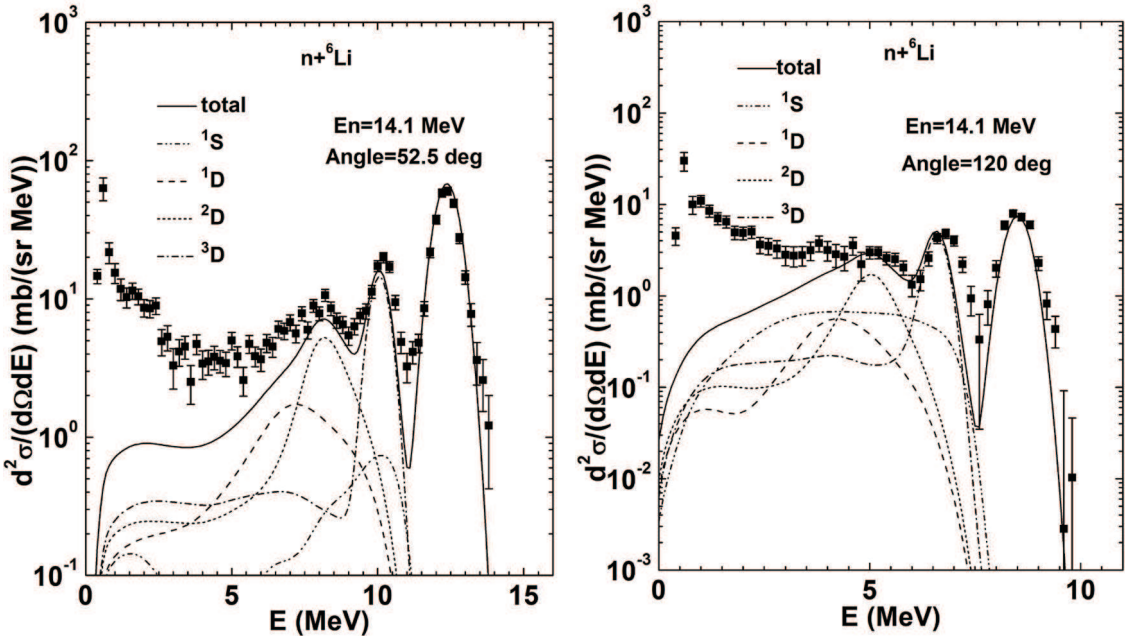

Fig. 1 The neutron production DDX (solid lines) calculated by CDCC compared with experimental data (solid squares) [11] for n+^{6}Li reaction in the laboratory system. The dash-dot-dotted, dashed, short dashed and dash-dotted lines denote the contributions corresponding to unbound ^{1}S, ^{1}D, ^{2}D and ^{3}D states of ^{6}Li, respectively.

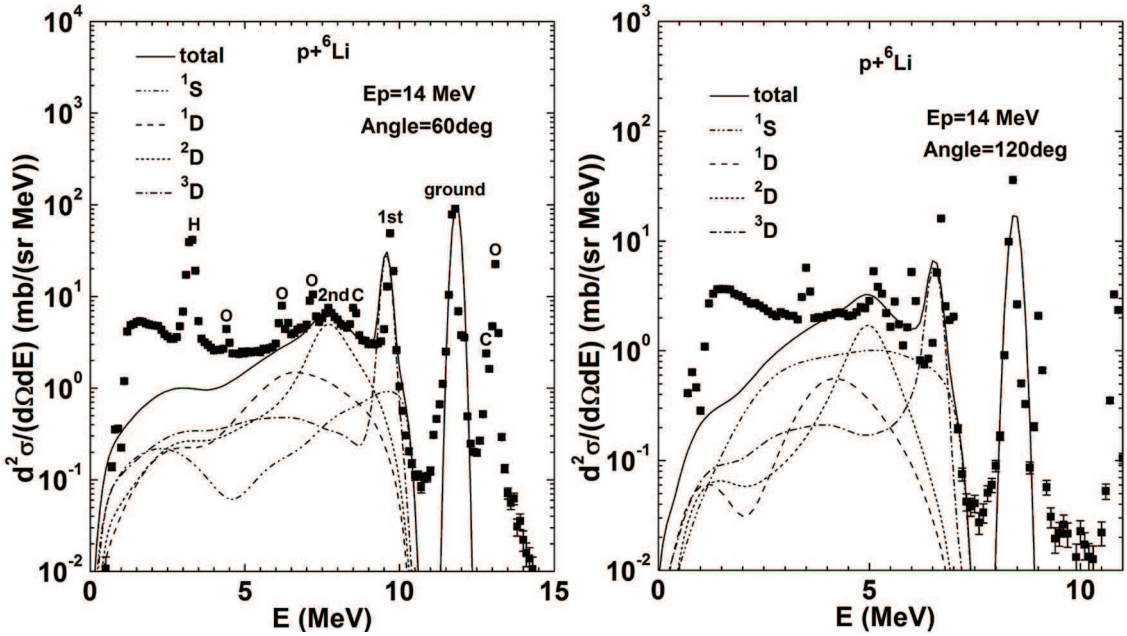

Fig. 2 Same as Fig. 1, but for proton production DDX of p+^{6}Li reaction. The experimental data are taken from Ref. [12].

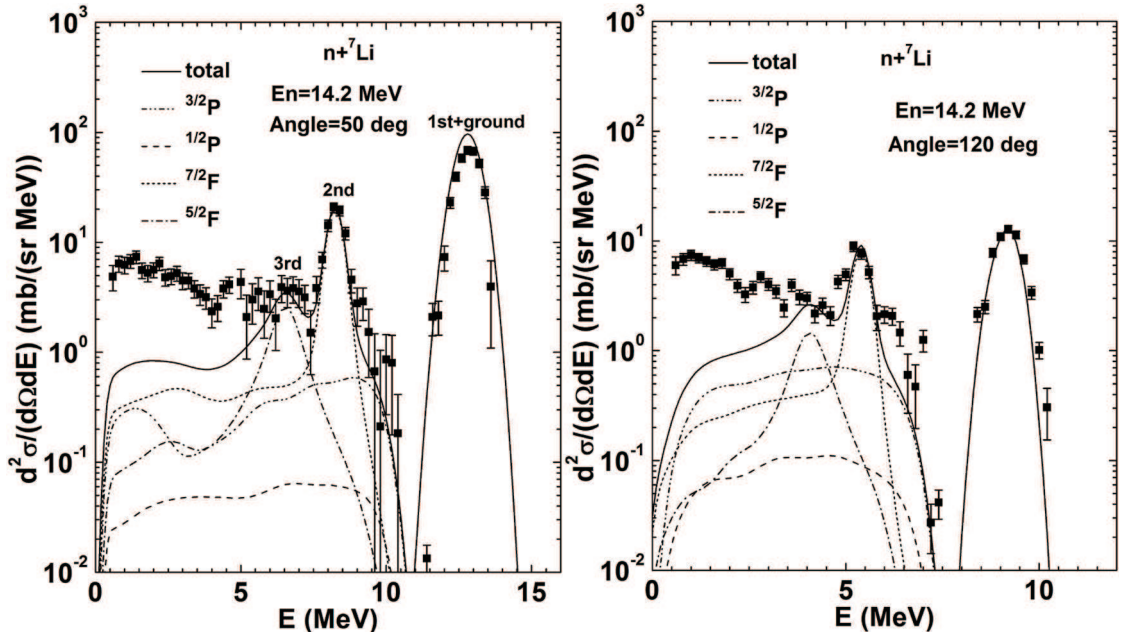

Fig. 3 The neutron production DDX (solid lines) calculated by CDCC compared with experimental data (solid squares) [13] for n+^{7}Li reaction in the laboratory system. The dash-dot-dotted, dashed, short dashed and dash-dotted lines denote the contributions corresponding to unbound $^{3/2}$P, $^{1/2}$P, $^{7/2}$F and $^{5/2}$F states of ^{7}Li, respectively.

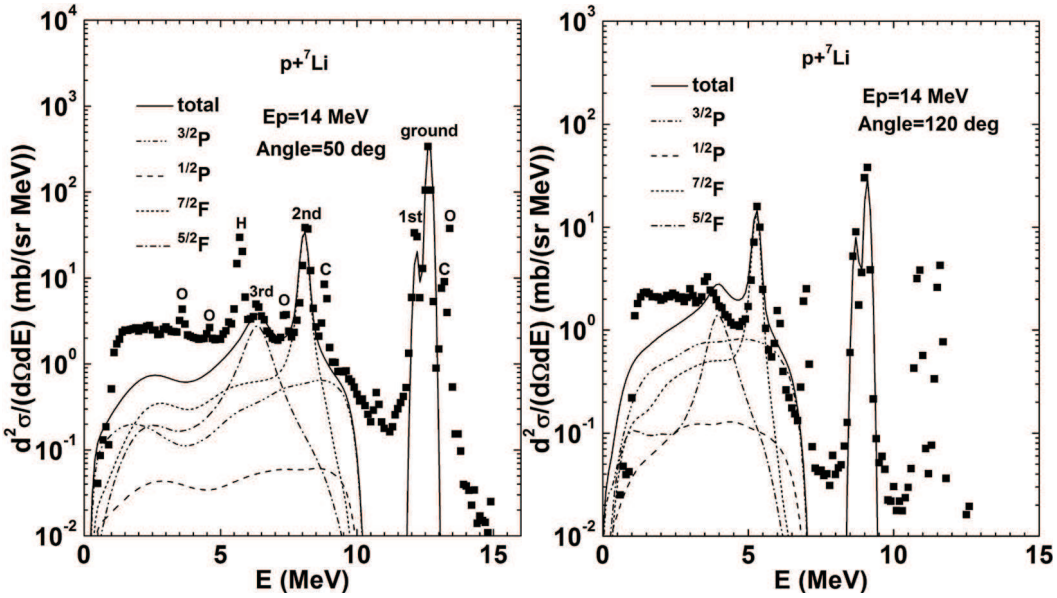

Fig. 4 Same as Fig. 3, but for proton production DDX of p+^{7}Li reaction. The experimental data are taken from Ref. [12].

Figures 3 and **4** show the comparisons of the calculated results and experimental data [12,13] of neutron and proton production DDXs for n+ ^{7}Li and p+ ^{7}Li reactions at incident

energies around 14 MeV, respectively. The contributions corresponding to unbound $^{3/2}$P, $^{1/2}$P, $^{7/2}$F and $^{5/2}$F states of ^{7}Li are denoted by dash-dot-dotted, dashed, short dashed and dash-dotted lines, respectively. For n+ ^{7}Li reaction, the first peak from high neutron emission energy denotes the summation of elastic and first inelastic scattering components because of the poor energy resolution, and the second and third peaks denote the inelastic scattering to the 7/2- and 5/2- resonance states, respectively. For p+ ^{7}Li reaction, the experimental data also include the effect of contamination in target. Four peaks seen in the calculated results represent the elastic, inelastic scattering to the first excited state, 7/2- and 5/2- resonance states, respectively, from high emission energy. The CDCC calculation gives good agreement with experimental data in the relatively high emission nucleon energy region, while the calculated results underestimate the experimental data at low emission energies. The underestimation may be due to other reaction processes, such as (n,2n) and (p,2p) reactions, which are not taken into account in the present calculation.

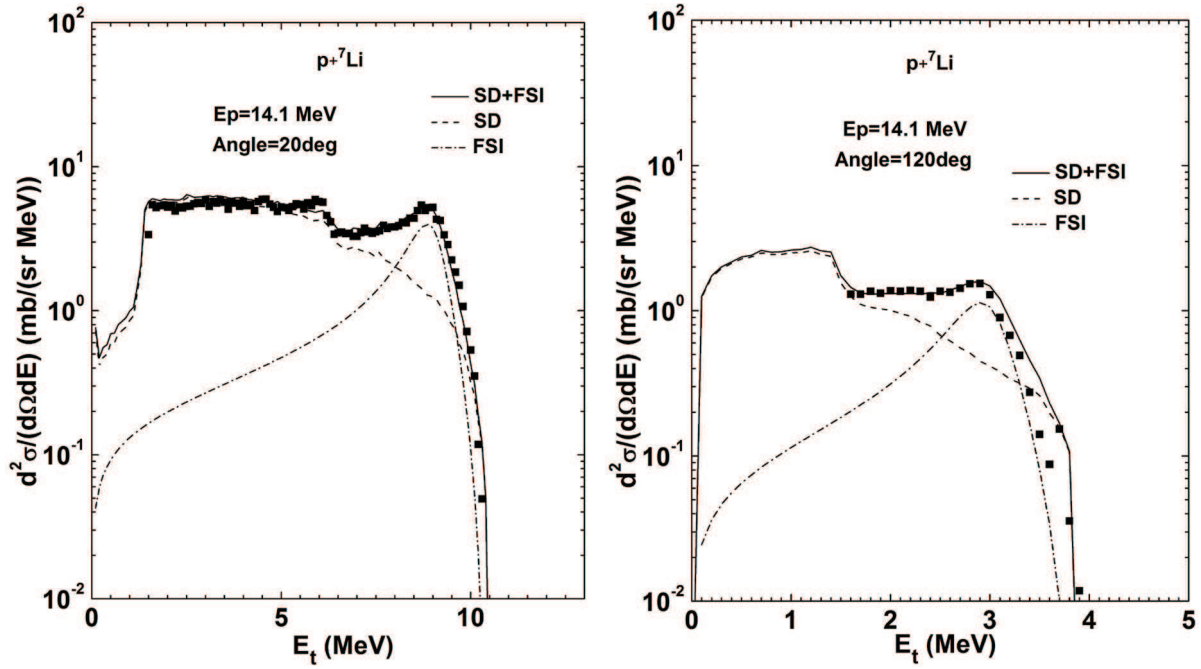

Fig. 5 The calculated triton production DDX (solid lines) compared with experimental data (solid squares) [14] for p+^{7}Li reaction in the laboratory system. The dashed lines denote the component from breakup process of ^{7}Li, while the dash-dotted lines denote the contribution from p+^{7}Li→t+^{5}Li* reaction.

Triton production from breakup of ^{7}Li* excited by nucleon inelastic scattering from ^{7}Li are calculated by the sequential decay model using the breakup cross sections obtained with CDCC. The result of the triton production DDX for p+ ^{7}Li reaction from the breakup process at incident energy of 14.1 MeV are shown by the dashed lines in **Fig. 5**. The calculated results are in good agreement with the experimental data [14] at low emission energies, while they underestimate the experimental data for relatively high emission energies. It is expected that

the discrepancy is due to another reaction process, $p+^{7}Li \rightarrow t+^{5}Li^{*}$. The contribution of this reaction is predicted by the FSI model, and shown by dash-dotted lines in Fig. 5. It can be seen that the triton emission from the latter reaction process contributes mainly to high emission energy region. The total triton production DDXs shown by the solid lines, which are the summation of the two components, can reproduce the experimental data very well.

4. Summary and conclusion

Neutron (Proton) production DDXs for $n(p)+^{6,7}Li$ reactions and triton production DDXs via breakup process of ^{7}Li for $n(p)+^{7}Li$ reactions are calculated with CDCC and sequential decay model. In order to compare the calculated results with experimental data, the triton emission from $n(p)+^{7}Li \rightarrow t+^{5}He^{*}(^{5}Li^{*})$ has also been analyzed with the final state interaction model. In most cases, the calculated results reproduce the experimental data around 14 MeV well except the nucleon production DDX for relatively low emission energies. The reason for the discrepancy is that some other reaction channels, e.g., (n,2n) and (p,2p), contribute to this energy region, which cannot be calculated with the present three-body CDCC.

REFERENCES

[1] IFMIF Comprehensive Design Report, by the IFMIF International Team. An Activity of the International Energy Agency, Implementing Agreement for a Program of Research and Development on Fusion Materials, (2004).
[2] Fusion Evaluated Nuclear Data Library FENDL 3.0: http://www-nds.iaea.org/fendl3/.
[3] M. Kamimura, M. Yahiro, Y. Iseri, Y. Sakuragi, H. Kameyama and M. Kawai, Prog. Theor. Phys. Suppl. **89**, 1 (1986).
[4] N. Austern, Y. Iseri, M. Kamimura, M. Kawai, G. Rawitscher and M. Yahiro, Phys. Rep. **154**, 125 (1987).
[5] T. Matsumoto, D. Ichinkhorloo, Y. Hirabayashi, K. Kato and S. Chiba, Phys. Rev. C **83**, 064611 (2011).
[6] T. Matsumoto, T. Kamizato, K. Ogata, Y. Iseri, E. Hiyama, M. Kamimura and M. Yahiro, Phys. Rev. C **68**, 064607 (2003).
[7] J. Jeukenne, A. Lejeune and C. Mahaux, Phys. Rev. C **16**, 80 (1977).
[8] H. Guo, Y. Watanabe, T. Matsumoto, K. Ogata and M. Yahiro, Phys. Rev. C **87**, 024610 (2013).
[9] T. Beynon and B. Sim, Ann. Nucl. Energy **15**, 27 (1988).
[10] T. Rausch *et al*., Nucl. Phys. A**222**, 429 (1974).
[11] M. Baba, S.Matsuyama, M. Fujisawa, T.Iwasaki, S. Iwasaki and R. Sakamoto, JAERI-M 90-025, 383 (1990)
[12] N. Koori *et al*., JEARI-M 89-167 (1989).
[13] S. Chiba, M. Baba, H. Nakashima, M. Ono, N. Yabuta, S. Yukinori and N. Hirakawa, J. Nucl. Sci. Tech. **22**, 771 (1985).
[14] N. Koori, I. Kumabe, M. Hyakutake, Y. Watanabe, K. Orito, K. Akagi, A. Iida, M. Eriguchi, Y. Wakuta, K. Sagara, H. Nakamura, K. Maeda and T. Nakashima, JEARI-M 91-009 (1991).

18. Neutron Total Cross-section Measurement on Sn and Ni by using Pohang Neutron Facility

Ayano Makinaga[1], Hidetoshi Akimune[2], Manwoo Lee[3], Kyung-Sook Kim[4], Kwangsoo Kim[4], Muhammad Zaman[4], Guinyun Kim[4], Eunae Kim[5], Sung-Gyun Shin[5], Mooh-Hyun Cho[5]
[1]Graduate School of Science, Hokkaido University, Sapporo 060-0810, Japan
[2]Department of Physics, Konan University, Kobe 658-8501, Japan
[3] Research Center, Dongnam Institute of Radiological and Medical Science, Busan 619-953, Korea
[4]Department of Physics, Kyungpook National University, Daegu 702-701, Korea
[5]Division of Advanced Nuclear Engineering, Pohang University of Science and Technology, Pohang 790-784, Korea
*E-mail: makinaga@nucl.sci.hokudai.ac.jp

Neutron induced reaction is one of the greatest interest to the nuclear power field, such as nuclear transmutation techniques by using accelerator-driven system (ADS), as well as nuclear astrophysics. In this work, the neutron total cross-sections for the natural Tin (^{nat}Sn) and Nickel (^{nat}Ni) were measured by using a neutron Time-of-Flight (n-TOF) technique at Pohang Accelerator Laboratory (PAL). Pulsed neutrons were produced via photo neutron of Ta-target system by using the 100-MeV electron linac. Neutrons are passed through the water moderator and moderated to its energy range between cold and thermal energy region. ^{6}LiZnS(Ag) scintillation detector was placed at the end of the n-TOF tube with about 11 m flight-path from the neutron source. We report here on the current status of the experiment and its data analysis.

1 Introduction

Measurement of neutron induced cross section is important to develop the advanced reactor system such as accelerator-driven system (ADS) to transform and recycle the nuclear wastes like long-lived fission products (LLFPs) and the minor actinides (MAs). Such nuclei are ^{79}Se, ^{93}Zr, ^{99}Tc, ^{107}Pd, ^{129}I, ^{126}Sn and ^{135}Cs. However, almost no experimental data sets are existed, because their cross section measurements are not easy due to the difficulty in preparing enriched targets and their treatments of activities. Especially, ^{126}Sn has no experimental data for neutron capture. Because activation method can't be used to ^{79}Se, ^{93}Zr, ^{107}Pd, their measurements are not existent. For other possibilities, photo nuclear reaction, which is an excellent probe of the estimation of the E1 γ strength function, a key gradient of the Hauser-Feshbach statistical model, is also used to evaluate the neutron capture cross sections for radioactive nuclei [1-3].

Measurement of the neutron induced cross section is also interested in the field of neutron imaging system because of their large transmission rate in the material. For example, large neutron transmission rates for the light nuclei like H, Li are useful to see a water or plastic material effectively. In addition, photon transmission rates decrease rapidly than that of neutron in the heavy element. For this reason, neutron is better suited for imaging in some filed.

Figure 1 shows the comparison with experimental and evaluated data for the neutron total cross section and capture cross section on ^{nat}Ni and ^{nat}Sn. Because low energy neutron cross section (below 1 eV) responds

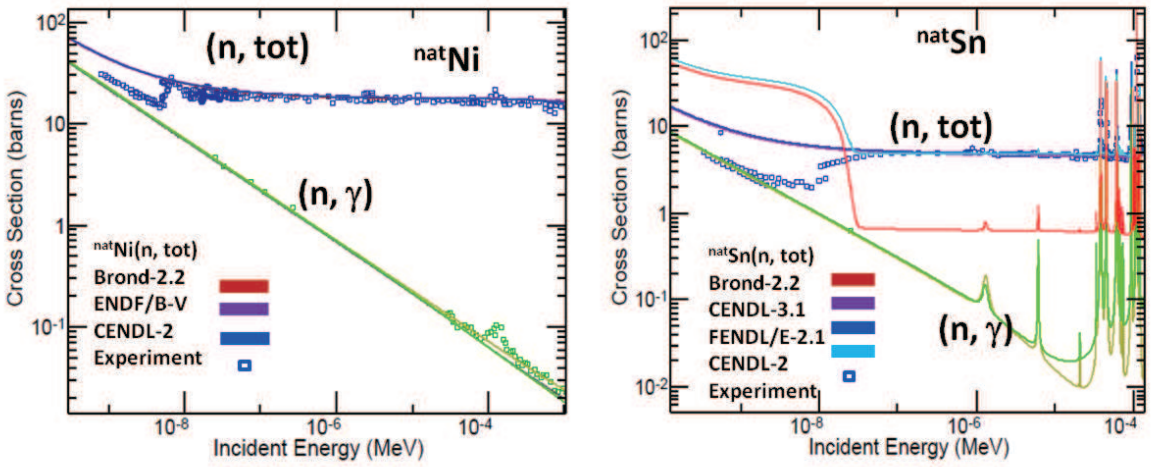

Fig 1 Comparison with the experimental data and evaluated data for the neutron total cross section and capture cross section on ^{nat}Ni and ^{nat}Sn. Experimental data sets are obtained from EXFOR Database provided by IAEA. Search system for the database is also provided by JCPRG (http://jcprg.org/exfor/index-jp.html). Evaluated Nuclear Reaction Libraries (Brond-2.2, ENDF/B-V, FENDL/E-2.1 and CENDL-2) can be obtained from the database in some nuclear data center such as JCPRG (http://jcprg.org/endf/).

sensitively to the motion of atoms or the structure of the material, precise measurement and its data analysis have usually complicate processes. As a result, only a few old experimental data sets exist in this region.

All these reasons motivated new measurement, evaluation and construction of the neutron data libraries for the total neutron cross sections. In this paper, we show the current status of the neutron transmission experiment on ^{nat}Sn and ^{nat}Ni and their data analysis at Pohang Accelerator Laboratory.

2. Neutron Transmission experiment

The total cross-section is determined by measuring the transmission of neutrons through the sample. Typically, neutron total cross section after purity correction can be written by;

$$\sigma_T(E_i) = \frac{\sigma(E_i) - M_T \cdot \sum_j P_j \sigma_j M_j^{-1} \cdot 10^{-6}}{1 - \sum_j P_j \cdot 10^{-6}} \quad , \tag{1}$$

where $\sigma(E_i)$ is the measured total cross section, M_T is the total weight of sample, M_j is the weight of impurity in the sample and P_j is the impurity in ppm.

Experimentally, the transmission rate of neutrons at the *i*-th group energy E_i is defined as the fraction of incident neutrons passing through the sample compared to that in the open beam. Thus, the neutron total cross-section is related to the neutron transmission rate $T(E_i)$ as follows:

$$\sigma(E_i) = -\frac{1}{\sum_j N_j} \ln T(E_i), \tag{2}$$

$$T(E_i) = \frac{I(E_i) - IB(E_i)/M_I}{O(E_i) - OB(E_i)/M_O}, \tag{3}$$

where N_j is the atomic density per cm^2 of the j-th isotope in the sample. $I(E_i)$ and $O(E_i)$ are the foreground counts for the sample-in and the open-beam, $IB(E_i)$ and $OB(E_i)$ are the background counts for the sample-in and the open beam, and MI and MO are monitor counts for the sample-in and the open beam, respectively [4,5]. The

neutron energy E_i is determined by using the relation between neutron time of flight T and flight path length L:

$$E_i = \left(\frac{72.3 \times L}{T}\right)^2. \quad (4)$$

2.1 Neutron Time of Flight Experiment at Pohang Accelerator Laboratory

The Pohang Neutron Facility (PNF) was proposed in 1997 and constructed at the Pohang Accelerator Laboratory in 1998 [6]. Neutron transmission experiment has been actively performed with pulsed neutrons based on a 100-MeV electron linear accelerator by using time of flight (TOF) method [7]. 100 MeV electron linac is located in the tunnel besides the 3 GeV Pohang Light Source (PLS) facility. It consists of RF-gun or by triode thermionic gun, an alpha magnet, four quadrupole magnets, two SLAC type accelerating sections, a quadrupole triplet, and a beam analyzing magnet [6-9]. The overview of the experimental set up for the neutron transmission measurements is shown in **Fig. 2**. Neutrons are produced via photo nuclear reaction of ^{181}Ta by using the bremsstrahlung photon with high energy electron. A water cooled Ta radiator system for the photo neutron source consists of ten Ta plates with a diameter of 4.9 cm and an effective thickness of 7.4 cm. There was a 0.15-cm water gap between Ta plates to cool the target effectively. Estimated neutron yield per kW of beam power on the Ta target was 2.0 ×10^{12} n/sec [6-12]. Typical neutron energy distribution by using TOF is shown in Fig.2(c).

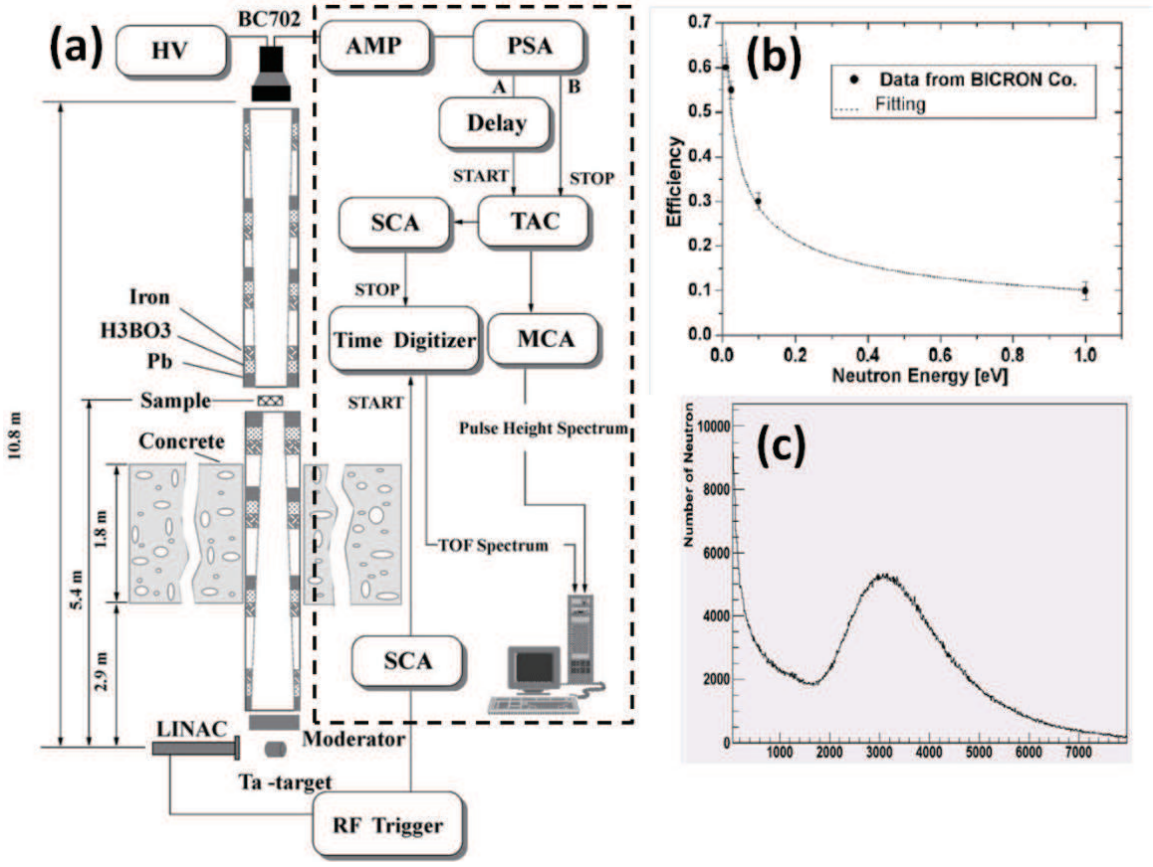

Fig. 2 (a) Experimental set up for the neutron transmission. Photo neutron sores was produced by bremsstrahlung with electron beam and cooled in the water moderator system. Ni and Sn samples are placed at the middle of the neutron guide tube. The neutron detector was located at a distance about 11 m from a water cooled Ta target system. (b) Neutron detection efficiency of the Li-ZnS(Ag) scintillator BC702 Bicron. 4 experimental data are obtained from BICRON Co. (c) Typical neutron time of flight spectrum. Horizontal axis means the neutron arrival time (μs).

Table 1. Physical parameters of the samples used in the experiment.

Sample	Purity (%)	Size (cm^2)	Thickness (mm)	Isotopic abundance (%)				
^{nat}Sn	99.9	10×10	0.20	^{112}Sn	^{114}Sn	^{115}Sn	^{116}Sn	^{117}Sn
	99.9	10×10	0.50	0.97	0.65	0.34	14.54	7.68
				^{118}Sn	^{119}Sn	^{120}Sn	^{122}Sn	^{124}Sn
				24.22	8.58	32.59	4.63	5.79
^{nat}Ni	99	10×10	0.20	^{58}Ni	^{60}Ni	^{61}Ni	^{62}Ni	^{64}Ni
				68.077	26.223	1.140	3.634	0.926

Ni and Sn samples are located at the middle of the neutron guide tube which is placed perpendicularly to the electron beam. Neutrons were collimated by using H_3BO_3, Pb and Fe in the guide tube. The neutron detector was placed at the end of the guide tube.

The characteristic parameters of the natural Ni with 0.2 mm thickness and natural Sn with 0.20 mm and 0.50 mm thickness samples are given in **Table 1**. A set of notch filter, which consists of Co, In, and Cd plates with thickness of 0.5 mm, 0.2 mm, and 0.5 mm, was also used for the energy calibration. Samples in the transmission experiment were automatically changed its position in every 5 minutes by using a sample changer.

A ^{6}Li-ZnS(Ag) scintillation counter BC702 from Bicron (Newbury, Ohio) with a diameter of 127 mm and a thickness of 15.9 mm mounted on an EMI-93090 photomultiplier was used as a detector for the neutron TOF spectrum measurement. This scintillation counter consists of a matrix of a lithium compound enriched to 95% Li dispersed in a fine ZnS(Ag) phosphor powder. Induced neutrons in the detector interact Li and occur the nuclear reaction of ^{6}Li (n, α) ^{3}H. Produced charged particles of α and ^{3}H make scintillations upon interacting with the ZnS(Ag). The detection efficiency of the neutron detector was determined by fitting the 4 experimental points from BICRON Co. Fitted efficiency curve was $\varepsilon_{eff}=1-\exp\{-N\sigma(0.0253/E_n)^{0.5}\}$ with σ=945 barn of the ^{6}Li(n, α)^{3}H reaction [5].

The electron linac was operated with a repetition rate of 10 Hz, a pulse width of 1.0 μs and the electron energy of 60 MeV. The peak current in the beam current monitor located at the end of the second accelerator section is above 50 mA. Figure 2(a) shows the data acquisition system. Usually two different data acquisition systems were used for the neutron TOF spectra measurements: one for the NIM-based system and the other for the CAMAC-based system. The main purpose of the NIM-based system was neutron-gamma separation and the parallel accumulation of the neutron TOF spectra if necessary [13, 14]. In this experiment, new data acquisition system with a 100 MHz 10-bit 8channel FADC Module on VME crate was used instead of the previous system. Separation of the gamma flash due to the bremsstrahlung and neutron signal can be performed by using software on the DAQ computer directly. For the signal and noise separation, 7 parameters are studied to find best cuts. 1) Triggering time from GATE, 2) Average ADC values, 3) Standard Error (SE) of Signals, 4) SE of pedestal in first 20 bins, 5) Average of first derivative of ADC, 6) SE of drvave and 7) Minimum value of first derivative [13,14]. Obtained neutron TOF spectrums for the notch filter, ^{nat}Ni (200 μm), ^{nat}Sn (200 μm), ^{nat}Sn (500 μm) and open spectrum are shown in **Fig. 3**, respectively.

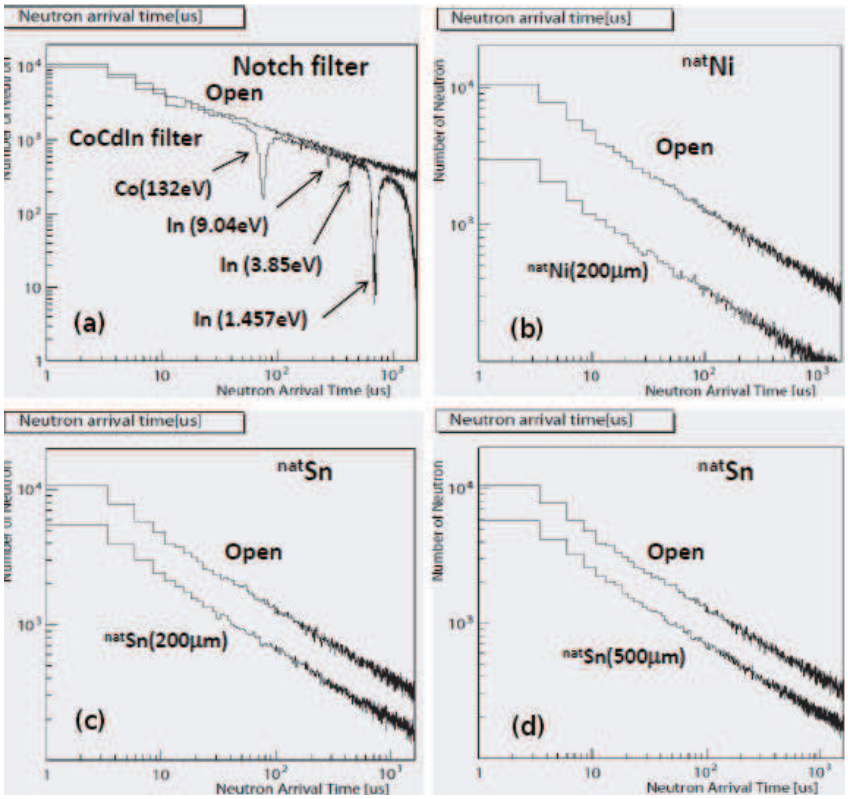

Fig. 3. Neutron TOF spectrum (a) Co-Cd-In filter, which includes 132 eV (Co), 9.04 eV and 3.85 eV (In), 1.457 eV (Cd) resonance peaks, was used to calibrate the neutron energy. (b) ^{nat}Ni sample with 200μm thick.(c) ^{nat}Sn sample with 200μm thick. (d) ^{nat}Sn sample with 500 μm. Open spectrum was obtained with no sample condition.

Summary

Neutron transmission experiments on natural Sn and Ni were performed at the Pohang Neutron Facility based on an 100-MeV electron linac in Korea. The neutrons were produced via photo nuclear reaction of Ta and cooled in the water moderator, which lead to an energy range from 0.1 eV to 100 eV. Transmitted neutrons were detected with the ^{6}Li-ZnS (Ag) scintillator BC702 by using time of flight methods. To calibrate the neutron energy, Co-In-Cd filter, which includes 132 eV (Co), 9.04 eV and 3.85 eV (In), 1.457 eV (Cd) resonance peaks, was used. Detailed experimental data analysis and evaluation will be performed in the near future.

Acknowledgments

We thank the staff of the PAL accelerator for their cooperation during the experiments. A. M also thanks Prof. K. Kato, Prof. M. Aikawa (Hokkaido Univ.) and Dr. N. Otsuka (IAEA) for their discussion of nuclear data. This research partly was supported by the Asia-Africa Science Platform Program (R&D Platform Formation of Nuclear Reaction Data in Asian Countries) of Japan Society for Promotion of Science, by the National Research Foundation of Korea (NRF) through a grant provided by the Korean Ministry of Education, Science & Technology (MEST) in 2011 (Project No.2011-0006306 and No. 2011-0025762), by the Institutional Activity Program of Korea Atomic Energy Research Institute, and by the World Class University (WCU) program (Grant No. R31-30005).

Reference

[1] A. Makinaga *et al*., Phys. Rev. C**79**, 025801 (2009).
[2] H. Utsunomiya *et al*., Phys. Rev. C**80**, 055806 (2009).
[3] H. Utsunomiya *et al*., Phys. Rev. C**84**, 055805 (2011).
[4] Guinyun Kim *et al*., Proceedings of the International Conference on Nuclear Data for Science and Technology 2007, 07739 (2008).
[5] K. Devan *et al*., Journal of the Korean Physical Society, Vol.**49**, No.1, p.88 (2006).
[6] G. N. Kim *et al*., Proceedings of the International Conference on Nuclear Data for Science and Technology, p.556 (1997).
[7] H. S. Kang *et al*., Proceedings of the First Asian Particle Accelerator Conference, p.743 (1998).
[8] G. N. Kim *et al*., Nuclear Instruments and Methods in Physics Research A **485**, p.458 (2002).
[9] A. K. M. M. H. Meaze *et al*., Journal of Korean Physics Society, Vol. **48**, No. 4, pp.827-834 (2006).
[10] Young Seok Lee *et al*., Radiation Measurements, **35**, p.321 (2002).
[11] W. Y. Baek *et al*., Proceedings of the Workshop on Nuclear Data Production and Evaluation (1998).
[12] G. N. Kim *et al*., J. Accel. Plasma Res., Vol. **3**, No. 1 (1999).
[13] Guinyun Kim, Proceedings of the 3rd Asian Nuclear Reaction Database Development Workshop, p.307 (2012).
[14] Manwoo Lee, Proceedings of the 3rd Asian Nuclear Reaction Database Development Workshop, p.339 (2012).

19. Activation Analyses for Accelerator Structural Materials by the 5-9 MeV Deuteron Beam Loss

Sunao MAEBARA[a], Hiroki TAKAHASHI[a], Hironao SAKAKI[b], Masahiro ICHIKAWA[a] and Masayoshi SUGIMOTO[a]

[a]IFMIF Accelerator Facility Development Group, Directorates of Fusion Energy Research, JAEA
[b]Photo medical research center, JAEA
e-mail:maebara.sunao@jaea.go.jp

Isotope productions in accelerator structural materials of copper and stainless steel are evaluated by the PHITS code and the DCHAIN code. In the PHITS code, the experimental data for Cu(d,nx) reaction at 5MeV and 9MeV are used as a source term in neutron transportation. Due to deuteron beam loss of 5MeV-1μA and 9MeV-1μA, it is found that ^{60}Co in the copper and ^{51}Cr, ^{54}Mn, ^{59}Fe, ^{58}Co and ^{60}Co in the stainless steel are dominant for activation after the CW operation. In the stainless steel by the 9MeV-1μA beam loss, it is evaluated that the total effective dose rate after the 1-year CW operation is to be 420[μSv/h]. From this result, it is concluded that accelerator components with a local shielding in the beam energy more than 9MeV have to be developed for maintenance works for a 20-years driving.

Keywords: Isotope production, Deuteron beam, PHITS code, DCHAIN code, Accelerator structural material

1. Introduction

An accelerator-based neutron irradiation facility is under consideration to develop materials for a demonstration fusion reactor [1-3]. To obtain a neutron flux of 10^{18} n/m^2/s or more using the neutron-generating D-Li stripping reaction, a 40MeV deuteron beam with a current of 250mA has to be injected into liquid lithium flow. Furthermore, accelerator system availability of 88% or more with CW operation mode and a 20-years driving by maintenance works are required.

Activation is caused by deuteron beam loss in beam lines and in accelerator components; an RFQ linac, a beam scraper and a drift tube linac etc. Since neutron is emitted by the (d, nx) reaction, many isotopes are produced by the (n, γ), (n, p), (n, α), (n, np) and (n, d) reaction etc., in their structural materials. The (d, nx) reaction becomes remarkable in more than the deuteron beam energy of 4MeV. In isotope productions, isotopes which have a half-life time more than a few 10 days are also included, and activation due to these isotopes must be considered for maintenance works after a CW operation. From this reason, the deuteron beam loss is critical issues in the deuteron beam accelerator.

For the order estimation in the first step, isotope productions in the accelerator structural material of copper and stainless steel due to the beam loss of 5MeV-1μA and a 9MeV-1μA are calculated, and effective dose rates due to the accumulated isotope productions during a 1-year CW operation are evaluated.

2. Analytical approach

Deuteron induced thick target neutron yield at 5 and 9MeV were measured in collaboration with Kyushu University using Tandem accelerator in 2009-2010[4-5], since there is no experimental data of Cu(d, nx) reaction in the range of 5-9 MeV. In this measurement, a 0.2 mm thick copper was used as a target, and the average beam current of 10nA was injected into the target. For the neutron distribution in all direction, the measured energy spectra at angles, 0˚, 15˚, 30˚, 45˚, 60˚, 75˚, 90˚, 120˚ and 140˚, are used for a source term.

For a simple model of accelerator component, a beam transport line of a 1m- long, a 50mm-radius and a thickness of 5mm is used, and this source is set in the inside surface of the 50mm-radius and 1m-long.

The material components of copper and stainless steel are indicated in **Table 1**. As for nuclear reaction with each material component, the JENDL 4.0 is used for nuclear cross-section library. Neutron fields with 5MeV-1μA and 9MeV-1μA deuteron bombarding copper and stainless steel are evaluated by PHITS code [6], and the isotopic productions in materials are obtained by DCHAIN code [7].

Table 1. Material components of Cu and SS

Copper	Stainless steel
^{63}Cu: 69.1%	^{56}Fe: 5.06x10^{-2}*
^{65}Cu: 30.9%	^{52}Cr: 1.35x10^{-2}*
	^{58}Ni: 6.83x10^{-3}*
	^{62}Ni: 3.45x10^{-3}*
	^{54}Fe: 3.34x10^{-3}*
	^{60}Ni: 2.55x10^{-3}*
	Mo(nat):1.24x10^{-3}*
	etc.

*Unit [10^{24} atoms/cm^3]

3. Isotope productions in copper and stainless steel

3.1 Isotope productions during 30-days CW operation

3.1.1 Copper material

In **Table 2**, Isotope productions in copper material during the 30days CW operation due to the beam loss of 5MeV-1μA and 9MeV-1μA. ^{64}Cu, ^{66}Cu, ^{60}Co and ^{63}Ni are dominant. For ^{64}Cu and ^{66}Cu, it reaches 3300 and 700 [Bq/cm^3], respectively. It is to be about 10 times higher than that of the 5MeV-1μA. These productions after the CW operation can be neglected, since ^{64}Cu and ^{66}Cu have half-lives of 12.7h and 5.12m, respectively. For ^{60}Co and ^{63}Ni, it is found that isotope productions by 9MeV-1μA after the CW operation reach 0.43 and 0.28 [Bq/cm^3], and these productions are about 29 and 19 times higher than those by 5MeV-1μA. The ^{60}Co is mainly produced by ^{63}Cu(n, α) reaction. ^{63}Ni can be neglected, since the β decay energy of 67keV does not affect for the effective dose rate at all. The activation in Cu material after the CW operation is finally decided by ^{60}Co only.

Table 2. Isotope productions in cooper material

	5MeV-1μA [Bq/cm^3]	9MeV-1μA [Bq/cm^3]	Half-lifes
^{60}Co	1.52x10^{-2}	4.45x10^{-1}	5.271y
^{60m}Co	8.75x10^{-1}	2.59x10^{-1}	10.47m
^{63}Ni	1.49x10^{-2}	2.80x10^{-1}	100.1y
^{64}Cu	3.47x10^{2}	3.32x10^{3}	12.7h
^{66}Cu	7.56x10^{1}	7.19x10^{2}	5.12m

3.1.2 Stainless steel

In **Table 3**, isotope productions in stainless steel during the 30days CW operation due to the beam loss of 5MeV-1μA and 9MeV-1μA are shown. ^{56}Mn and ^{55}Fe can be neglected, since ^{56}Mn has the short half-life time of 2.579h and ^{55}Fe has the low intensity of 1x10^{-7} for γ-ray. From these results, ^{51}Cr, ^{58}Co, ^{54}Mn, ^{59}Fe and ^{60}Co are dominant for stainless steel. ^{58}Co during the 30 days CW operation due to the beam loss of 9MeV-1μA reaches 647[Bq/cm^3], and it is to be 75.1 times much more than one of ^{60}Co. This is one of the remarkable characteristics in stainless steel. The ^{58}Co is mainly produced by ^{58}Ni(n, p) reaction in stainless steel components, and the half-life time is 70.86d. The ^{60}Co for 9MeV-1μA is to be 19.6 times more than one of Cu materials. This ^{60}Co in stainless steel is produced by ^{60}Ni(n, p) reaction.

Table 3. Isotope productions in stainless steel

	5MeV-1μA [Bq/cm^3]	9MeV-1μA [Bq/cm^3]	Half-lifes
^{51}Cr	6.39x10^1	6.00x10^2	27.7d
^{54}Mn	3.05x10^0	6.24x10^1	312d
^{56}Mn	2.38x10^2	2.52x10^3	2.579h
^{55}Fe	1.88x10^0	2.24x10^1	2.744y
^{59}Fe	7.74x10^{-1}	7.68x10^0	44.49d
^{58}Co	3.31x10^1	6.47x10^2	70.86d
^{60}Co	9.02x10^{-1}	8.62x10^0	5.27y

3.2 Effective dose rates for the CW operation

3.2.1 ^{60}Co in copper material

Figure 1 shows the effective dose rates at 1m apart from the source due to the accumulated ^{60}Co in copper material by the beam losses of the 9MeV-1μA and 5MeV-1μA during CW operation, which is calculated using the effective dose rate constant of 0.305[μSvm^{2}MBq^{-1}h^{-1}]. For both beam losses, it is to be 1.536 and 0.052 [μSv/h] after the 1-year CW operation, respectively. It is found that the maximum rate of 1.536 [μSv/h] is about one-5000th against the maximum permissible dose rate of less than 10 [mSv/h] for maintenance works. It is expected that the ^{60}Co in copper material does not affect maintenance works, even though a margin of 1000 times is assumed for the beam loss.

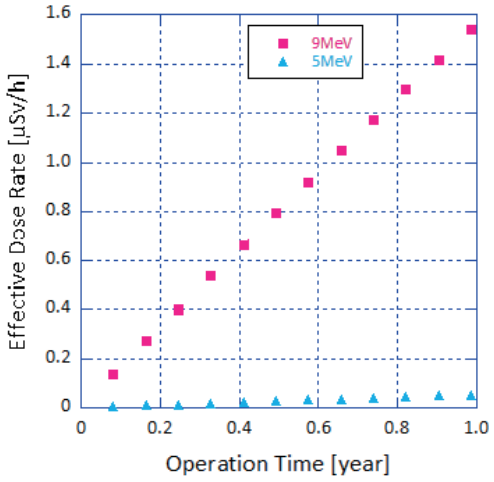

Fig.1 Effective dose rates due to the accumulated ^{60}Co during CW operation in copper material

3.2.2 ^{51}Cr, ^{58}Co, ^{54}Mn, ^{59}Fe and ^{60}Co in stainless steel

In Figure 2, the effective dose rates at 1m apart from the source due to the accumulated ^{51}Cr, ^{58}Co, ^{54}Mn, ^{59}Fe and ^{60}Co in stainless steel material by the beam losses of 5MeV-1μA during CW operation are indicated. For ^{51}Cr, ^{58}Co, ^{54}Mn, ^{59}Fe and ^{60}Co, the effective dose rate constants of 0.00458, 0.131, 0.111 and 0.305 [μSvm^{2}MBq^{-1}h^{-1}] are used, respectively. The total effective dose rate after the 1-year CW due to ^{51}Cr, ^{58}Co, ^{54}Mn, ^{59}Fe and ^{60}Co is calculated to be 23.4[μSv/h]. It is found to be about one-420th against the permissible effective dose rate for maintenance works.

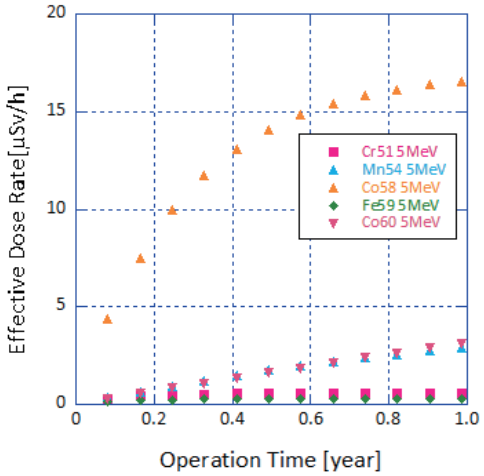

Fig.2 Effective dose rates due to the accumulated ^{51}Cr, ^{58}Co, ^{54}Mn, ^{59}Fe and ^{60}Co by the 5MeV-1μA beam loss during the CW operation in stainless steel

The effective dose rates by the 9MeV-1μA during CW operation indicate in Fig.3. The total effective dose rate after the 1-year CW due to ^{51}Cr, ^{58}Co, ^{54}Mn, ^{59}Fe and ^{60}Co is calculated to be 420[μSv/h], it is about 18 times much more than one by the 5MeV-1μA beam loss. It is also found to be about one-24th against the permissible effective dose rate for maintenance works.

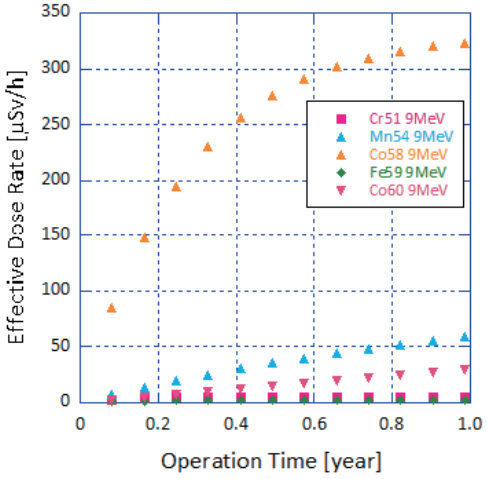

Fig.3 Effective dose rates due to the accumulated ^{51}Cr, ^{58}Co, ^{54}Mn, ^{59}Fe and ^{60}Co by the 9MeV-1μA beam loss during CW operation in stainless steel

4. Conclusion

Isotope productions in the accelerator structural materials of copper and stainless steel are evaluated by PHITS code and DCHAIN code. In these analyses, the experimental data for Cu(d,nx) reaction at the 5MeV and 9MeV are used as a source term in neutron transportation. For deuteron beam loss of 5MeV-1μA and 9MeV-1μA, it is found that ^{60}Co in the copper and ^{51}Cr, ^{54}Mn, ^{59}Fe, ^{58}Co and ^{60}Co in the stainless steel are dominant for activation after the 30-days CW operation.

For ^{60}Co in copper material due to the 9MeV-1μA beam loss, it is expected that the resulting activities do not affect maintenance works, even though a margin of 1000 times is assumed for the beam loss.

In the stainless steel by the 9MeV-1μA beam loss, it is found that the total effective dose rate after the 1-year CW is to be 420[μSv/h], and the 75% is caused by ^{58}Co production. Since the ^{58}Co has the half-life of 70.86d, and the effective dose rate strongly affects maintenance works. The ^{58}Co production cannot be avoided, since the parent nuclide of ^{58}Ni exists in stainless steel.

In the present status, we do not know how much beam loss against an accelerated current of 100-mA level can be reduced, but the beam loss could be measured at the beam energy of 5MeV and the 9MeV on the IFMIF/EVEDA prototype accelerator in future. On the other hand, neutron irradiation facility which can be driven during a 20-year, is required for a demonstration fusion reactor materials development in a final stage.

It is predicable from these results that a development of accelerator components with a local shielding is indispensable for maintenance works at the deuteron beam energy of more than 9MeV. For the shielding material, water and polyethylene may be a good candidate, since isotopes which have long half-lives of a few 10 days, are not produced. In the next step, activation analyses for a much more realistic accelerator component with the local shield are planned.

Acknowledgements

The authors would like to express their thanks to Drs. T. Fukahori, H. Nakashima, Y. Iwamoto and Y. Sakamoto of Nuclear Science and Engineering Directorate in JAEA, for their advice about nuclear-data and appropriate analysis models. We also would like to acknowledge Dr. K. Niita, Director of Research center of Research Organization for Information Science & Technology (RIST), for his continuous support of PHITS code.

References

[1] IFMIF-CDA Team (Ed.) M. Martone, IFMIF Conceptual Design Activity Final Report, ENEA Frascati Report, RT/ERG/FUS/96/17 (1996).

[2] T. Kondo, IFMIF, its facility concept and technology, Journal of Nuclear Materials258-263(1998)47-55.

[3] T. F. Shannon, R.A. Jameson, H. Katsuta, H. Maekawa, M. Martone, A. Möslang, V. Teplyakov, M.J. Rennich, Conceptual design of the international fusion materials irradiation facility (IFMIF), Journal of Nuclear Materials 258-263(1998)106-112.

[4] N. Shigyo, K.Hidaka, K.Hirabayashi, Y. Nakamura, D. Moriguchi, M. Kumabe, H.Hirano, S.Hirayama, Y. Naitou, C. Motooka, C. Lan, T. Watanabe, Y. Watanabe, K. Sagara, S. Maebara, H. Sakaki and H.Takahashi , Measurement of Deuteron Induced Thick Target Neutron Yields at 9 MeV, Journal of the Korean Physical Society, Vol. 59, No. 2, August 2011, pp. 1725-1728.

[5] K. Hirabayashi, T. Nishizawa, H. Uehara,H. Hirano, D. Moriguchi,T. Kajimoto, N. Shigyo,K.Hidaka, Y.Oshima,M.Maeda,T.Yasumune,K.Maehata,Y.Tajiri,H.Umishio,S.Hirayama,S.Abe, Y.Watanabe, K.Sagara, S.Maebara, H.Takahashi and H. Sakaki, Measurement of Deuteron Induced Thick Target Neutron Yields at 5MeV and 9MeV, JAEA-Conf 2011-002, pp.113-118.

[6] K. Niita, N. Matsuda, Y. Iwamoto, H. Iwase, T. Sato, H. Nakashima, Y. Sakamoto and L. Sihver, "PHITS: Particle and Heavy Ion Transport code System, Version 2.23", JAEA-Data/Code 2010-022 (2010).

[7] T. Kai, F. Maekawa, K. Kosako, Y. Kasugai, H.Takeda and Y. Ikeda, DCHAIN-SP 2001: High Energy Particle Induced Radioactivity Calculation Code, JAERI-Data/Code 2001-016(2001).

This is a blank page.

20. Activation Analyses of Air in the Accelerator Vault of LIPAc Building by Deuteron Beam at 5 MeV and 9 MeV

Hiroki TAKAHASHI[1*], Sunao MAEBARA[1], Hironao SAKAKI[2],
Hiromitsu SUZUKI[1], Masayoshi SUGIMOTO[1]

1. Directorates of Fusion Energy Research, Japan Atomic Energy Agency (JAEA), Rokkasho-mura, Aomori 039-3212, Japan

2. Photo Medical Research Center, JAEA, Kizugawa Kyoto 619-0215, Japan

*E-mail: takahashi.hiroki@jaea.go.jp

In the Linear IFMIF Prototype Accelerator (LIPAc), the engineering validation up to 9 MeV is planned by employing the deuteron beam of 125 mA at Rokkasho-mura, Aomori, Japan. Activation analyses of air in the accelerator vault of LIPAc building are carried out by the PHITS code and the DCHAIN code using the experimental data for neutron source of 5 MeV and 9 MeV. From these analyses, it is concluded that a cooling time of 20 hours is indispensable at least after the LIPAc commissioning on CW operation, to access into the accelerator vault for maintenance works

1. Introduction

International Fusion Materials Irradiation Facility (IFMIF) [1-3] is an accelerator-based neutron irradiation facility to develop materials for a demonstration fusion reactor next to ITER. For preparing the necessary information to make a decision of the IFMIF construction, Engineering Validation and Engineering Design Activities (EVEDA) have been started from 2007. As a part of IFMIF/EVEDA, the prototype accelerator for IFMIF, which is called Linear IFMIF Prototype Accelerator (LIPAc), is developed and its commissioning operation will be started from the middle of 2013 at Rokkasho-mura.

Since the LIPAc has a 1 MW huge beam-power due to deuteron beam, activation for the air and accelerator components due to deuteron beam loss is a critical issue. To plan the maintenance work after beam operation, the reactions of $^{14}N(n,2n)^{13}N$, $^{16}O(n,p)^{16}N$, $^{40}Ar(n,\gamma)^{41}Ar$ and etc. have to be evaluated for the air activation.

2. Linear IFMIF/EVEDA Accelerator

The LIPAc consists of an injector (output energy;100 keV), a 175 MHz RFQ linac (0.1-5.0 MeV), a medium energy beam transport, the first section of Superconducting RF linac (5-9 MeV), a high energy beam transport line and a beam dump (9 MeV-125 mA CW) [4]. The LIPAc will be installed in an accelerator vault (W: 8.0 m x D: 41.5 m x H: 7.0 m), which is surrounded by the concrete wall with

thickness of 1.5 m, in the LIPAc building (**Fig. 1**).

Three kinds of commissioning for LIPAc are planned at Rokkasho: Injector only (100 keV), Injector and RFQ (RFQ commissioning) and Whole Accelerator (LIPAc commissioning). In the RFQ commissioning, the beam maximumn power is to be 125 mA - 5 MeV and 0.1 % duty. In the LIPAc commissioning, the maximumn power is to be 125 mA - 9 MeV and Continuous Wave (CW, = 100 % duty).

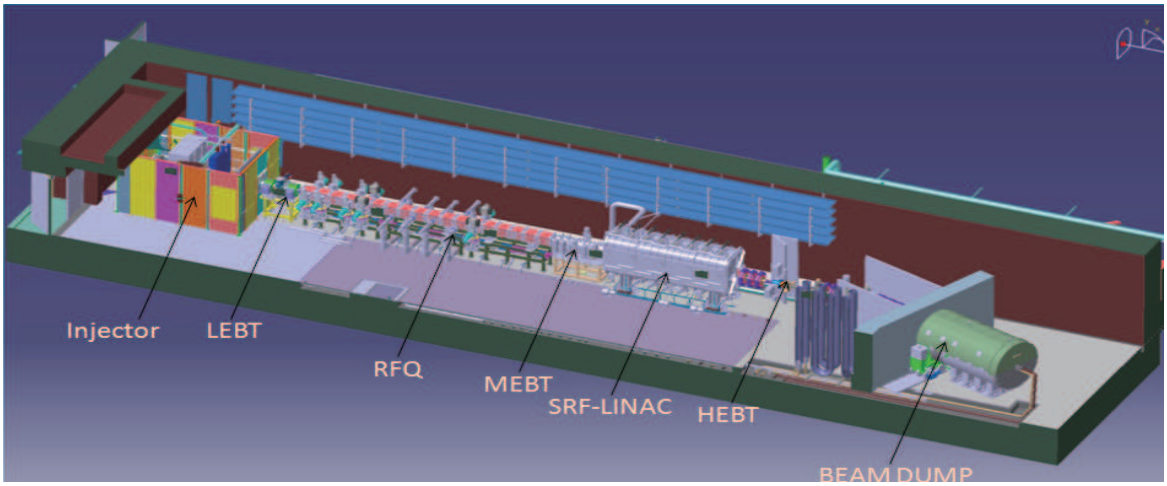

Fig. 1: LIPAc location in accelerator vault

3. Analyses

Activation analyses of air in the accelerator vault of the LIPAc building are performed for the RFQ commissioning (up to 5 MeV on pulse operation) and the LIPAc commissioning (up to 9 MeV on the CW operation). For these analyses, the experimental data for deuteron at 5 and 9 MeV [5], which have the angular distribution, are used as source term for input files of the PHITS code and its results are used for input files for the DCHAIN code.

3.1 RFQ commissioning

In the RFQ commissioning, a pulse beam operation is planned by 0.1 % duty, to avoid activation production. For this purpose, a Low Power Beam Dump (LPBD) is designed as shown in **Fig.2**. The LPBD is installed at the backside of RFQ at 50 cm distances. For the LPBD design, a disk shape is adopted for the beam target, and cupper material of 3 mm in thickness is applied for beam facing materials. Furthermore, a polyethylene material of 220 mm in thickness is surrounded around the disk shape.

For the RFQ commissioning pattern, a beam operation of 8 hours by 0.1% duty (pulse beam operation) and no beam of 16 hours are planned for one day, and the 5 days beam operation and 2 days no operation are assumed for one week.

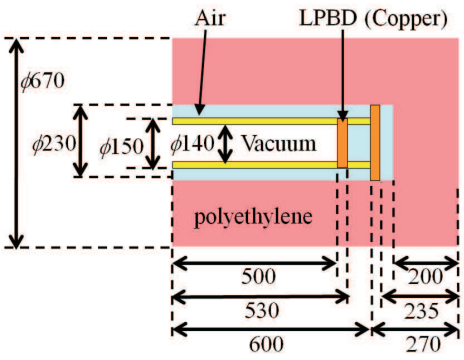

Fig. 2: LPBD model

In these analyses, neutron source of Cu(d, xn) reaction sets at the the center of LPBD (Copper) with the circle of 5 cm-radius.

3.2 LIPAc commissioning

For LIPAc commissioning up to 9 MeV-125 mA, the beam power reaches to 1.125 MW. For the CW operation, a beam dump is designed as illustrated in **Fig.3**. A cone-shaped copper with 0.5 cm in thickness is used and surrounded by the water tank of 50 cm in radius and the iron cylinder of 25 cm in radius.

It is assumed that neutron is generated at the surface of the cone-shaped copper.

For the LIPAc commissioning pattern, a beam operation of 8 hours by the CW operation and no beam of 16 hours are planned for one day, and the 5 days beam operation and 2 days no operation are assumed for one week.

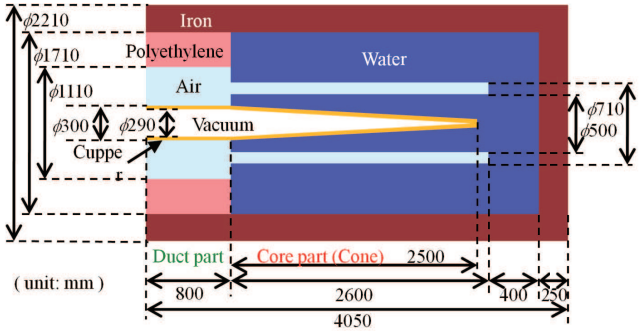

Fig. 3: Beam dump model

4. Calculations

Fig. 4 shows the LPBD installed position in accelerator vault, and the dose rate during beam operation of RFQ commissioning (125 mA - 5 MeV, 0.1 % duty) is indicated. It is found that dose rate of air area rises up to 10^5 order [μSv/h]. In **Fig 5**, it indicates the BD position and dose rate during LIPAc operation (125 mA – 9 MeV, CW). It is found that dose rate reaches up to 10^8 order [μSv/h].

About these commissioning, production isotopes after 104 hour operation are shown in **Table 1**. ("104 hour operation" means the end of beam operation of fifth day ["four

Table 1: Production isotope [Bq/cm^3] (Time = 104 h)

Isotope	RFQ commissioning	LIPAc commissioning
Total	3.31 x 10^0	1.63 x 10^2
^{3}H	8.72 x 10^{-6}	8.12 x 10^{-4}
^{14}C	5.79 x 10^{-4}	2.86 x 10^{-2}
^{13}N	-----	5.98 x 10^{-3}
^{16}N	1.09 x 10^{-4}	5.07 x 10^{-2}
^{37}S	-----	1.37 x 10^{-6}
^{37}Ar	2.78 x 10^{-3}	1.37 x 10^{-1}
^{41}Ar	**3.30 x 10^0**	**1.63 x 10^2**

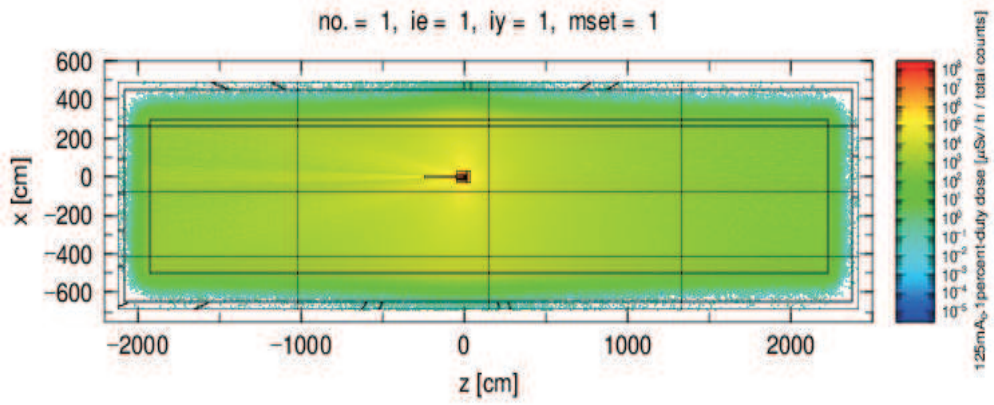

Fig. 4: Dose rate during RFQ commissioning

times of the commissioning pattern for one day" + "8 hours of fifth beam operation"]). It is found that the amount of ^{41}Ar reaches 3.3 x 10^{0} [Bq/cm^{3}] and 1.63 x 10^{2} [Bq/cm^{3}] on the RFQ commissioning and on the LIPAc commissioning, respectively. But it is to be 1000 times longer than the 0.1% duty operation for the CW operation, the ^{41}Ar for the LIPAc commissioning is about 50 times more than one on RFQ commissioning. For this difference, it is strong dependent on the LPBD design. In the LPBD, it is considered that neutron due to Cu(d, xn) reaction can't be absorbed sufficiently by the polyethylene, since it is a compact design for the pulse operation. For isotope productions in air, it is also evaluated that the ^{41}Ar is dominant, and ^{3}H, ^{14}C, ^{13}N, ^{16}N, ^{37}S and ^{37}Ar are negligible small (**Table 1**).

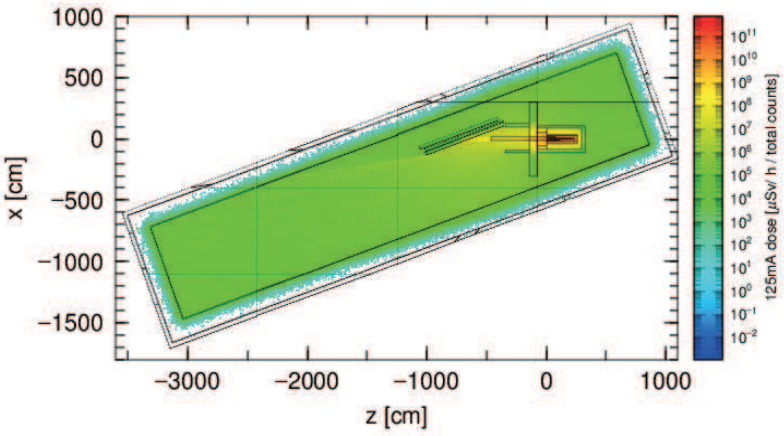

Fig. 5: Dose rate during LIPAc commissioning

5. Conclusion

An evaluation for the air activation in an accelerator vault is performed by assuming the deuteron beam at the RFQ commissioning (up to 5 MeV, 0.1 % duty) and the LIPAc commissioning (up to 9 MeV, CW). In this calculation, the PHITS code and the DCHAIN code is used, and the experimental data of Cu(d, xn) reactions due to the 5 MeV and the 9 MeV deuteron beam are applied for neutron source term.

For the isotope production in air, it is found that ^{41}Ar is dominant and ^{3}H, ^{14}C, ^{13}N, ^{16}N, ^{37}S and ^{37}Ar are negligible small. For the RFQ commissioning up to the 5MeV on the pulse operation, it is evaluated that the concentration of ^{41}Ar is to be 3.3 x 10^{0} [Bq/cm^{3}] in air, and the cooling time of 10 hours is needed to access into the accelerator vault. For the LIPAc commissioning up to the 9 MeV on the CW operation, it is evaluated to be 1.63 x 10^{2} [Bq/cm^{3}], and a cooling time of 20 hours is needed. Based on these results, a measuring method of ^{41}Ar in accelerator vault is under consideration to secure safety maintenance works after beam operation.

References

[1] IFMIF-CDA Team (Ed.) M. Martone, ENEA Frascati Report, RT/ERG/FUS/96/17 (1996)

[2] T. Kondo *et al.*, Journal of Nuclear Materials, Vol.258-263, pp.47-55(1998)

[3] T. E. Shannon *et al.*, Journal of Nuclear Materials, Vol.258-263, pp.106-112(1998)

[4] A. Mosnier *et al.*, MOPEC056, Proceedings of 1st International Particle Accelerator Conference (2010)

[5] N. Shigyo *et.al.*, Journal of the Korean Physical Society, Vol. 59, No. 2, August 2011, pp. 1725-1728.

21. Validation of CBZ Code System for Post-Irradiation Examination Analysis and Sensitivity Analysis of (n, γ) Branching Ratio

Yosuke Kawamoto, Go Chiba, Masashi Tsuji, Tadashi Narabayashi
Nuclear Reactor Engineering Laboratory, Faculty of Engineering, Hokkaido University
Kita 13 Nishi 8, Kita-ku, Sapporo, Hokkaido, 060-8628
e-mail : yohsuke@ec.hokudai.ac.jp

A code system CBZ is being developed in Hokkaido University. In order to validate it, PIE data, which are nuclide composition data of a spent fuel, have been analyzed with CBZ. The validity is evaluated as ratios of the calculation values to the experimental ones(C/E ratios). Differences between experimental values and calculation ones are smaller than 20% except some nuclides. Thus this code system is validated.

Additionally, we evaluate influence of change of (n, γ) branching ratio on inventories of fission products and actinides. As a result, branching ratios of Sb-121, Pm-147, and Am-241 influence inventories of several nuclides. We perform PIE analysis using different (n, γ) branching ratio data from the ORIGEN-2 library, JNDC-Ver.2, and JEFF-3.1A, and find that differences in (n, γ) branching ratios between different nuclear libraries have a non-negligible influence on inventories of several nuclides.

1. Introduction

A burnup calculation tool is essential to evaluate the decay heat or nuclide production accurately. For this purpose, a burnup capability has been improved in a code system CBZ, which is a multipurpose reactor physics calculation code system being developed in Hokkaido University. In the present study, we perform PIE analysis as a part of validations of this code system, and we evaluate prediction accuracy of nuclide production quantitatively. A PIE analysis is the comparison between nuclide composition data which were obtained by a chemical isotopic analysis in the spent fuel (PIE data) and calculation values. We obtain C/E ratios to compare PIE data and calculation values.

Additionally, we evaluate influence of change of (n, γ) branching ratio on inventories of fission products and actinides quantitatively. Although there have been many arguments about the influence of the nuclear data difference on the nuclide production, quite a few arguments about (n, γ) branching ratio. According to Refs. [3] and [4], a difference of (n, γ) branching ratio of Pm-147 between the ORIGEN-2 library and JNDC-Ver.2 has a relatively large influence on inventories of Sm isotopes in the burnup calculation. Thus, in the present study, we evaluate influences of branching ratios of nuclides which exist on the burnup chain using sensitivity coefficients. We also perform PIE analysis using different (n, γ) branching ratio data from the ORIGEN-2 library, JEFF-3.1A, and JNDC-Ver.2.

2. PIE analysis

2.1. PIE data

PIE data we use are taken from the high-burnup UO_2 fuels irradiated in a European commercial PWR [1] and from the MOX fuels irradiated in the Obrigheim nuclear power plant in Germany [2]. There are 4 samples, A, B, C, and D, in Ref. [1] (hereinafter referred to as UO_2A, UO_2B, UO_2C and UO_2D, respectively) and 2 samples, MOX1 and MOX2, in Ref. [2].

There are inventory data, which were obtained by chemical isotopic analysis, of FP and actinides in the UO_2 fuels, and those of only FP in the MOX fuels. In this chemical analysis, the spent fuel was dissolved in nitric acid/hydrogen fluoride. The measured data are numbers of atoms per 1g solution. Because amounts of spent fuels which were dissolved in the solution are different between samples, it is impossible to compare them simply. Thus normalization is necessary, and it will be referred in section 2.3.

2.2. Burnup calculation by CBZ code system

We perform burnup calculations whose conditions are same as UO_2A, UO_2B, UO_2C, UO_2D, MOX1 and MOX2 by the CBZ code system.

Firstly, initial composition of the UO_2 fuel is determined. Reference [5] gives nuclide number densities for a UO_2 fuel with 4.1wt% U-235 enrichment. From these data, we obtain the number densities for the UO_2 fuel we are treating assuming that number densities of O-16 and whole nuclides are not different between samples and the UO_2 fuel given in Ref. [5].

Similarly, initial composition of the MOX fuel is determined. According to Ref. [2], the Pu enrichment of the samples is 5.07wt%, and the Pu vector is Pu-238/Pu-239/Pu-240/Pu-241/Pu-242/Am-241＝1.50/59.00/24.38/9.34/4.85/0.94. There are no data about U-235 enrichment, O/M ratio and density. Thus we consider that these data of samples are same as the data given in Ref. [5]. Reference [5] provides three cases, and we adopt one whose Pu enrichment is 5wt%. The U-235 enrichment of the samples is assumed 0.2wt%. The O/M ratio and the fuel density are assumed 2.0003 and 10.131 [g/cm^3], respectively. From the above, we obtain number density of each nuclide of MOX1 and MOX2.

Because there are no data about cladding in Refs. [1] and [2], we adopt data of a PWR fuel assembly quoted from Ref. [5].

Finally, composition of moderator is determined. References [1] and [2] show temperature and boron concentration of moderator. Moderator density is determined from the steam table [6] assuming that the pressure is 15MPa. Because there are only 200℃ and 300℃ points in this table, the density is determined by linear interpolation or extrapolation. The isotopic composition ratio of boron is assumed B-10/B-11＝19.9/80.1. Fuel and cladding temperature data are also mentioned in Refs. [1] and [2]. **Table 1** shows initial nuclide number densities of fuel, cladding and moderator obtained. **Table 2** shows the temperatures.

Burnup and power history of each sample are determined as follows. According to Refs. [1] and [2], the UO_2 fuel underwent 5 cycles and the MOX fuel did 4 cycles. There are data of local burnup of each sample obtained by the chemical isotopic analysis, average power history and average burnup of each cycle. Thus, in order to obtain detailed burnup and power history of each sample and each cycle, we adjust the average power history and the average burnup to the local burnup. **Tables 3** and **4** show the detailed burnups and detailed power histories respectively. Cooling terms from ending of cycle to chemical analysis are quoted from Refs. [1] and [2]. **Table 5** shows these terms. Periodic inspection terms are assumed 90 days. Burnup calculation is performed by these data assuming the power is constant during each cycle.

Under the above conditions, we perform burnup calculations with pincell model, a 107-group cross section library, the equivalence theory for the self-shielding calculations and the collision probability method for neutron flux spectrum calculations. The burnup chain we use is the SRAC2006 detail burnup chain for developers.

Table 1 Number densities of fuel, cladding, and moderator (unit: 1/barn/cm)

	Nuclide	UO_2A	UO_2B	UO_2C	UO_2D	MOX1/2
Fuel	U-235		8.665E-4			4.345E-5
	U-238		2.166E-2			2.140E-2
	Pu-238					1.718E-5
	Pu-239					6.729E-4
	Pu-240					2.769E-4
	Pu-241					1.056E-4
	Pu-242					5.463E-5
	Am-241					1.063E-5
	O-16		4.505E-2			4.518E-2
Cladding	Cr-Nat.			6.770E-5		
	Fe-Nat.			2.382E-4		
	Zr-Nat.			3.786E-2		
Moderator	H-1	4.677E-2	4.906E-2	4.627E-2	4.816E-2	4.898E-2
	O-16	2.338E-2	2.453E-2	2.313E-2	2.408E-2	2.449E-2
	B-10	3.878E-6	4.068E-6	3.837E-6	3.994E-6	4.063E-6
	B-11	1.561E-5	1.638E-5	1.544E-5	1.608E-5	1.635E-5

Table 2 Temperatures of moderator, fuel and cladding(unit: K)

	UO_2A	UO_2B	UO_2C	UO_2D	MOX1/2
Moderator	591	568	596	577	568
Fuel			900		
Cladding			600		

Table 3 Detailed burnups (unit: GWd/t)

Cycle	UO_2A	UO_2B	UO_2C	UO_2D	MOX1	MOX2
1	12.14	9.91	11.26	11.92	9.82	10.08
2	16.01	13.07	14.85	15.72	12.30	12.55
3	13.22	10.79	12.26	12.97	12.61	12.55
4	12.14	9.91	11.26	11.92	11.27	11.42
5	11.18	9.12	10.37	10.97		

Table 4 Detailed power histories (unit: W/cm)

Cycle	UO_2A	UO_2B	UO_2C	UO_2D	MOX1	MOX2
1	236.3	192.9	219.2	232.0	192.9	198.0
2	300.6	245.3	278.7	295.0	223.7	228.1
3	253.2	206.6	234.8	248.5	231.0	229.9
4	223.2	182.2	207.0	219.1	214.7	217.8
5	204.5	166.9	189.7	200.7		

Table 5 Cooling term of each sample and nuclide

Sample	Nuclide	Period (day)
UO_2A	U, Np, Pu	1206
	Am, Cm, FP	1234
$UO_2B/C/D$	Cs-133, Cs-137, Eu-154	1625
	U, Pu	1649
	Np, other FP	1696
	Am, Cm	1706
MOX1	All FP	1636
MOX2	Ru-106, Sb-125, Cs-134, Cs-137, Ce-144, Eu-154	2275
	Other FP	2397

2.3. Comparison between PIE data and calculation values

We obtain C/E ratios to compare PIE data with calculation values obtained by the CBZ code system. It is impossible to compare them simply as mentioned in section 2.1. Thus these data are normalized by amounts of U-238, and then we obtain C/E ratios. Obtained C/E ratios are averaged ones of 4 samples in the UO_2 fuel and 2 samples in the MOX fuel.

We use JENDL-3.3 and -4.0 as cross section data in order to evaluate difference between nuclear data libraries. The data of Eu-156 is taken from JENDL-3.3 in both the cases.

Table 6 shows measurement accuracy of each sample and nuclide for the chemical isotopic analysis quoted from Refs. [1] and [2].

Figure 1 shows C/E ratio of each nuclide in the UO_2 fuel. According to Fig. 1, inventories of some nuclides are overestimated or underestimated. We take up nuclides whose C/E ratios are smaller than 0.8 or larger than 1.2.

The U-234 inventory is significantly underestimated. The C/E ratios are 0.135 with JENDL-3.3 and 0.157 with -4.0. The reason is considered that there is no U-234 in initial composition of the UO_2 fuel because Refs. [1] and [2] had no data about initial composition of U-234. Thus this underestimation is not an important issue.

The Cm-242 inventory is significantly overestimated. The C/E ratio is 1.75 in both the libraries.

C/E ratios of Cm-246, Sr-86, Sr-90, Gd-156 and Gd-160 are smaller than 0.8. Especially the Sr-86 inventory is significantly underestimated. The C/E ratio is 0.269 with JENDL-3.3 and 0.272 with -4.0.

Figure 2 shows C/E ratio of each nuclide in the MOX fuel.

C/E ratios of Gd-158 and Gd-160 are larger than 1.2. Especially the Gd-158 inventory is significantly

overestimated. The C/E ratios are 1.80 with JENDL-3.3 and 1.75 with -4.0.

C/E ratios of Sr-86, Sr-88, Sr-90, Eu-154 and Gd-155 are smaller than 0.8. Especially the Sr-86 inventory is significantly underestimated. The C/E ratio is 0.280 with JENDL-3.3 and 0.283 with -4.0. This tendency is similar to that of UO_2.

When we compare C/E ratios of the UO_2 fuel and the MOX fuel, there are generally more nuclides whose C/E ratios are close to 1.0 in the UO_2 fuel than the MOX fuel.

There are several nuclides whose C/E ratios are significantly different between JENDL-3.3 and -4.0. The ratios are generally closer to 1.0 with JENDL-4.0. However, with JENDL-4.0, the ratios of Sm-151 and Pu-238 are improved and worsened, respectively, unlike results of Ref. [7]. Thus it is impossible to determine whether the ratios of these two nuclides are improved or worsened.

We take up nuclides, Pu-238, Cm-244, -245, -246, Cs-134, Sm-152, Eu-154 and Gd-154, whose differences are larger than 5%, and investigate the cause of these differences using the sensitivity coefficients calculated by the generalized perturbation theory-based functionality of CBZ. **Table 7** shows the main cause of the difference of each nuclide. Although inventories of almost all the nuclides are influenced by the revision of capture cross sections of some nuclides, Cm-245 and -246 are influenced by the revision of fission cross section of Cm-245.

Table 6 Measurement accuracy of each sample and nuclide

Sample	Nuclide	Measurement accuracy (%)
UO_2A/B/C/D	Cm-242, Cm-244	5-10
	Ru, Cs-134, Cs-137, Ce-144, Eu-154	3-5
	U, Pu	<0.5
	Am, Cm-245, Cm-246, Nd	1
	Np-237, Rb, Sr, Y, Cs-133, Cs-135, La-139, Ce-140, -142, Pr-141, Pm-147, Sm, Eu-153, -155, Gd	2-3
MOX1/2	Ru, Sb, Cs-134, Cs-137, Ce-144, Eu-154	3-5
	Nd-142, -145, -146, -147, -148, -149, -150	1
	Rb, Sr, Y, Cs-133, Cs-135, La, Ce-140, -142, Pr, Nd-143,-144, Pm, Sm, Eu-153, -155, Gd	2-3

Table 7 Nuclides which have the differences and their causes

Nuclides which have the differences	Causal cross section of the differences
Cs-134	Cs-133
Sm-154	Sm-154
Eu-154	Eu-154
Gd-154	Eu-154
Pu-238	Pu-238
Cm-244	Pu-241, Am-243
Cm-245,-246	Pu-241, Am-243, Cm-245*

(*: fission cross section)

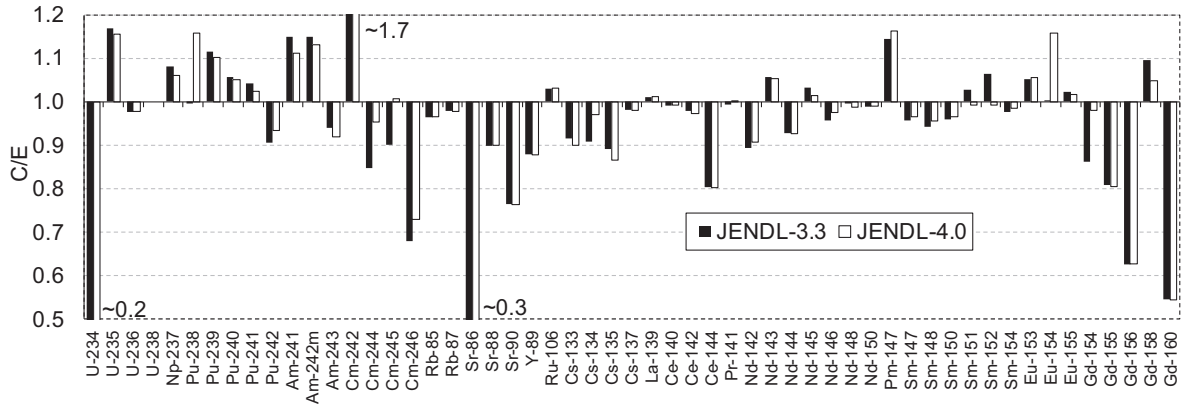

Fig.1 C/E ratio of each nuclide in the UO_2 fuel

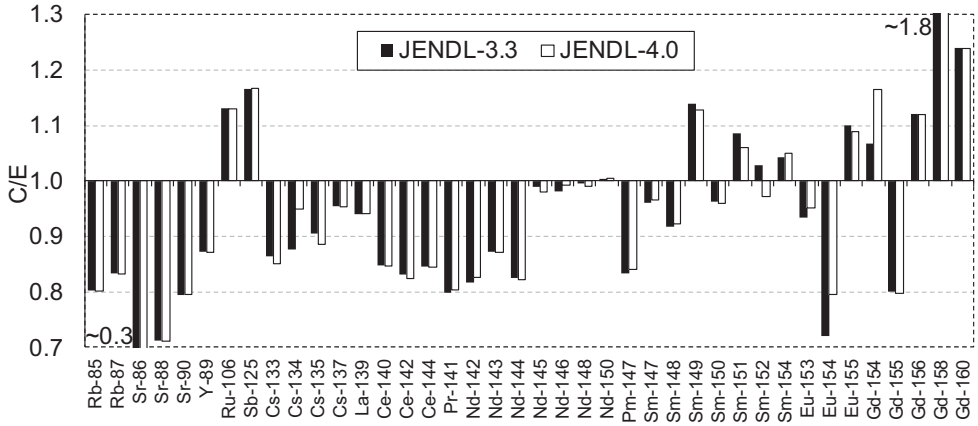

Fig.2 C/E ratio of each nuclide in the MOX fuel

3. Influence of (n, γ) branching ratio change on inventories

3.1. Sensitivity analysis of (n, γ) branching ratio

We evaluate influence of (n, γ) branching ratio on inventory of FP or actinide quantitatively with burnup calculation. The burnup chain we use include 30 nuclides which have branching in the (n, γ) reaction, and we perform sensitivity analysis of their branching ratios.

We define sensitivity as $S=(\Delta N/N)/\Delta p$, where N is an inventory of a nuclide, ΔN is a change of the inventory and Δp is a change of a nuclide's branching ratio. To calculate this sensitivity numerically, we set the Δp to 0.01. Although the sum of branching ratios should be 1.0, this normalization condition is not considered in the present sensitivity calculations. We calculate sensitivities with a burnup calculation similar to the condition of UO_2A.

Table 8 shows branching ratios which influence on inventories of more than 3 nuclides and have more than 10% sensitivities. Branching ratios from Sb-121 to Sb-122g, from Pm-147 to Pm-148m and from Am-241 to Am-242g have relatively large influence on inventories of many nuclides.

Table 8 Sensitivities of branching ratios on inventories of the nuclides (unit: %)

Sb-121→Sb-122g		Pm-147→Pm-148m		Am-241→Am-242g	
Te-122	100.0	Pm-148m	100.9	Pu-238	13.6
Te-123	100.0	Pm-149	30.3	Am-242	100.0
Te-123m	100.0	Sm-148	11.1	Cm-242	100.0
		Sm-149	30.9	Cm-243	99.9
		Sm-150	25.6		
		Sm-151	14.1		
		Eu-151	14.6		
		Eu-152	14.7		
		Gd-152	11.9		

3.2. PIE analysis using branching ratios from different libraries

We have used JNDC-Ver.2 as branching ratios data for the PIE analysis performed in section 2.3, and we perform PIE analysis similar to section 2.3 using branching ratios from the ORIGEN-2 library, JEFF-3.1A, and JNDC-Ver.2. Because energy-dependent (n, γ) branching ratios are given in JEFF-3.1A, we use energy-averaged branching ratios calculated with neutron spectrum of the UO_2 or the MOX fuel. This time only branching ratios of FP are taken from these libraries. JENDL-3.3 is used as neutron cross section data. **Figure 3** shows results of these PIE analyses. We take up nuclides whose differences of C/E ratios are larger than 1% between libraries.

As a result, differences of branching ratios between the libraries have non-negligible influence on inventories of Sm isotopes. According to Table 8, it is considered that the reason is the difference of branching ratio from Pm-147 to Pm-148m between the libraries. Moreover, there are differences between the ORIGEN-2 library and the other two, but no differences between JEFF-3.1A and JNDC-Ver.2.

According to Fig. 3, although C/E ratio of Sm-148 with ORIGEN-2 library is larger than with the other two, C/E ratios of other Sm isotopes with the ORIGEN-2 library are smaller. It is a contradiction with the sensitivities shown in Table 8. It is considered that the reason is influence of branching ratio from Pm-147 to Pm-148g on Sm-148 inventory. Although the sensitivity of Sm-148 inventory to branching ratio from Pm-147 to Pm-148m is 11.1% as mentioned in Table 8, the sensitivity of Sm-148 inventory to branching ratio from Pm-147 to Pm-148g is 64.4%. Thus it is considered that the latter sensitivity counteracts the former.

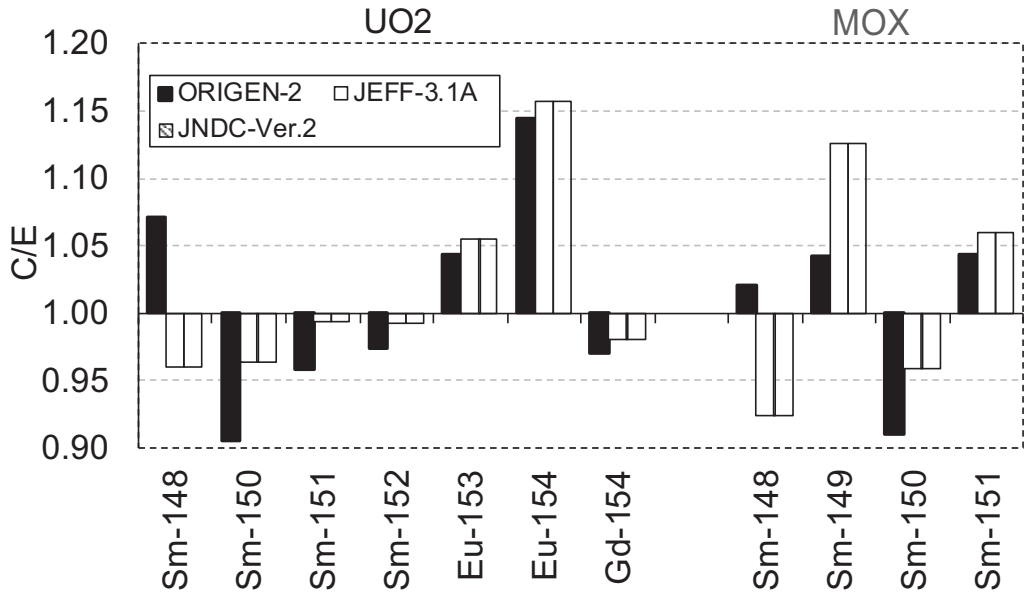

Fig.3 Results of PIE analyses using different branching ratio data

4. Conclusion

In order to validate the CBZ code system, we have performed the PIE analysis. In this analysis, differences between calculation results of the CBZ code system and experimental values have been less than 20% except 6 (UO_2) or 7 (MOX) nuclides. This code system has been validated.

When we have compared values of the UO_2 fuel and the MOX fuel, the result of the UO_2 fuel has been more accurate than the MOX fuel. The result with JENDL-4.0 has been more accurate than with -3.3.

We have also performed sensitivity analysis of (n, γ) branching ratio. It has been found that branching ratios of Sb-121, Pm-147 and Am-241 influence on inventories of several nuclides and the difference of (n, γ) branching ratio of Pm-147 between the ORIGEN-2 library and the other two libraries has a non-negligible influence on inventories of some nuclides.

References

[1] A. Sasahara, et al.: J. Nucl. Sci. Technol., 45[4], 313 (2008).
[2] A. Sasahara, et al.: J. Nucl. Sci. Technol., 45[5], 390 (2008).
[3] M. Totsuka, et al.: "Development and evaluation of SWAT library based on Evaluated Nuclear Data Library JENDL-4", 2012 Annual Meeting of AESJ, E22 (2012). [in Japanese]
[4] M. Totsuka: private communication (2012).
[5] J. Katakura, et al.: "A Set of ORIGEN2 Cross Section Libraries Based on JENDL-3.3 Library: ORLIBJ33", JAERI-Data/Code 2004-015, Japan Atomic Energy Research Institute (2004).
[6] JSME: "Thermodynamics", JSME (2002). [in Japanese]
[7] Go Chiba, et al.: J. Nucl. Sci. Technol., 48[2], 172 (2011).

22. GEANT4 Simulation Study of a Gamma-ray Detector for Neutron Resonance Densitometry

Harufumi Tsuchiya, Hideo Harada, Mitsuo Koizumi, Fumito Kitatani,
Jun Takamine, Masatoshi Kureta, Hideki Iimura
Nuclear Science and Engineering Directorate, Japan Atomic Energy Agency,
2-4 Shirakata Shirane, Tokai-mura, Naka-gun, Ibaraki 319-1195, Japan
e-mail: tsuchiya.harufumi@jaea.go.jp

A design study of a gamma-ray detector for neutron resonance densitometry was made with GEANT4. The neutron resonance densitometry, combining neutron resonance transmission analysis and neutron resonance capture analysis, is a non-destructive technique to measure amounts of nuclear materials in melted fuels of the Fukushima Daiichi nuclear power plants. In order to effectively quantify impurities in the melted fuels via prompt gamma-ray measurements, a gamma-ray detector for the neutron resonance densitometry consists of cylindrical and well type $LaBr_3$ scintillators. The present simulation showed that the proposed gamma-ray detector suffices to clearly detect the gamma rays emitted by $^{10}B(n, \alpha\gamma)$ reaction in a high environmental background due to ^{137}Cs radioactivity with its Compton edge suppressed at a considerably small level.

1. Introduction

A large earthquake and subsequent Tsunami resulted in meltdowns of nuclear fuels of reactors 1-3 in the Fukushima Daiichi Nuclear Power Plant. The melted fuels (MF) are thought to suffer from high temperature caused by their decay heat and break into pieces via phreatic explosions. Consequently, those pieces or "particle-like debris" would scatter in the pressure vessels [1]. Further, broken pieces of the MFs penetrate the bottom of the vessels and stay at the reactor containers. Presently, it is a plan that the MFs and debris are taken away from the reactors after around 10-years cooling time [1].

It is highly likely that the debris involves impurities such as boron, zirconium, concrete, and other construction materials. Moreover, it is probable that the individual debris, with a variety of their size and shape, does not have a uniform concentration of those impurities. This inhomogeneity makes it quite difficult to quantify nuclear materials in the MFs. However, from a viewpoint of nuclear safeguards and security, it is expected that conventional and accurate method to quantify nuclear material in those MFs is developed. We have proposed a concept of neutron resonance densitometry (NRD). In this paper, we discuss a design study of a gamma-ray detector used in NRCA that is one of the main techniques used for NRD.

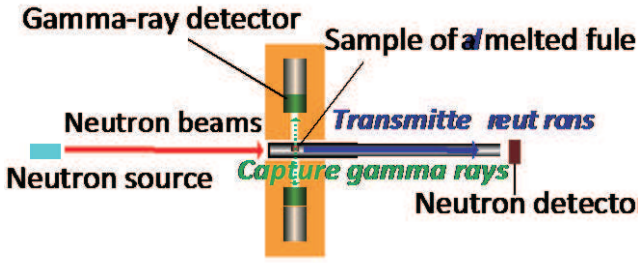

Figure 1: A conceptual view of neutron resonance densitometry

2. Neutron Resonance Densitometry

NRD is a non-destructive assay. It uses neutron resonance transmission analysis (NRTA) and neutron resonance capture analysis (NACA). **Figure 1** shows a conceptual view of NRD. As known, NRTA is used to gauge isotopic contents of fresh and spent fuel samples [2-4]. It utilizes neutron resonance reactions between nuclear materials and neutrons at energies of 0.1-40 eV. In our proposed system, pulsed neutrons propagate in a neutron flight path with length of around 5 m, to a debris sample located in the middle of the path. Then, neutrons penetrating the sample are caught by a neutron detector (e.g. a ^{6}Li glass scintillator) placed behind the sample. According to isotopic components and their quantities in the sample, some of incident neutrons are absorbed or scattered by the sample. The lack of incident neutrons causes sharp deficits in an energy spectrum of detected neutrons especially in resonance energy regions.

As described, MFs would involve various impurities as well as nuclear materials. The former, in particular, boron that is used in control rods and boronic acid initially poured on the reactors, prevents us from closely quantifying an amount of the latter. This is because ^{10}B has a large cross section to capture low-energy (<40 eV) neutrons, resulting in a heavy attenuation of transmission neutrons in the relevant energy range. Actually, it was shown in [5] that a neutron transmission spectrum for some ^{10}B concentrations in debris sharply weakens, as ^{10}B concentration is higher. Moreover, certain of impurities also have large total cross sections to diminish a transmission spectrum observed. Therefore

we need to know the amounts of impurities of individual debris to precisely analyze data of NRTA.

Generally, impurities have no resonance peaks at energies of 0.1-40 eV and hence NRTA provides little (or no) information on those impurities. For that reason, we utilize NRCA to measure prompt gamma rays that are emitted from impurities when they absorb incident neutrons. The gamma rays have characteristic energies according to isotopic nuclides. For example, ^{10}B radiates 478 keV gamma rays via the (n,αγ) reaction. Thus, NRCA would be a valuable diagnostic tool to estimate concentration of impurities in individual debris.

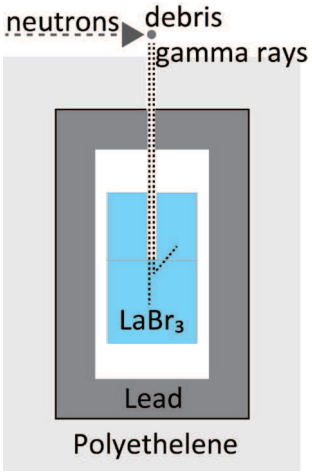

Figure 2: A schematic view of a gamma-ray detector for NRD

Figure 2 depicts a proposed gamma-ray detector, together with their shields and debris that should be measured. The gamma-ray detector is composed of a cylindrical and a tube type $LaBr_3$ scintillators. A diameter of both is 12.7 cm. Each height of the cylindrical and tube type scintillators is 12.7 cm and 10 cm, respectively. The tube type scintillator has a hole whose diameter and length are 2 cm and 10 cm, respectively. As illustrated by a black dashed-line of Fig.2, the principal function of the tube type scintillator is to collect back-scattered photons in the cylindrical one. Located outside the lead blocks, silicon rubbers including B_4C (black) and polyethylene make a role of shielding the central gamma-ray detector from neutrons coming from directions except debris.

Compared with other inorganic scintillators, a $LaBr_3$ one has a faster decay constant (<30 ns) and a better energy resolution (e.g. 2.6% at 662 keV) [6,7]. The fast response is indispensable for NRD. This is because that similar to debris samples obtained from the Three Mile Island II nuclear reactor, those for the Fukushima reactors would have a strong gamma ray background originating from ^{137}Cs. In fact, Uetsuka *et al.* [8] measured eight debris gathered from various locations in the Three Mile Island II reactor, providing that ^{137}Cs radioactivity retained by the individual debris range from 9.40×10^5 to 3.17×10^8 Bq/g. Moreover, a gamma rays detector for NRCA, compared to a neutron detector for NRTA, is placed closer to a debris sample in order to effectively detect prompt gamma rays emitted from the debris. Therefore, background level due to

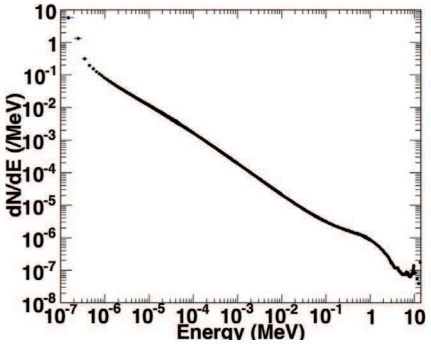

Figure 3: Neutron spectrum bombarding the debris

^{137}Cs may be so high that a gamma-ray detector needs a fast response to reduce dead time in measurement. In addition to the fast response, a good energy resolution and high photo-peak efficiency would be required for NRCA to identify isotopic compositions and determine their amounts in individual debris. Given these demands, we plan to use $LaBr_3$ scintillators in NRCA, instead of a germanium detector that is commonly used for prompt gamma-ray measurements.

3. GEANT4 simulation and its results

3.1 Simulation conditions

Using GEANT4 (ver. 9.4.p04) [9], we examined performance of the gamma-ray detector proposed. We summarize below common conditions of the present simulations. A cylindrical debris, with a height and diameter both being 1 cm, is located at 2 m away from a neutron source, which produces a neutron spectrum at the debris position as exhibited in **Figure 3**. The spectrum was calculated by MCNP5 [10]. The debris is placed at 50 cm away from the top of the cylindrical $LaBr_3$ scintillator. Based on a spent fuel composition with a burn-up of 40 GWd/t, weight ratios of ^{nat}B, ^{235}U, and ^{238}U are assumed to be 10%, 1% and 84%, respectively. Pu (1%) and O (4%) occupy the remaining 5%. A collimation diameter of polyethylene and leads is 2 cm and 1.5 cm, respectively. The polyethylene and lead blocks have 10 cm and 5 cm in thickness, respectively. We assumed 3.5% energy resolution at 662 keV for individual $LaBr_3$ crystals. Hereafter, without remarks, we presented a pulse height spectrum summed those of the cylindrical and tube type scintillators. In addition, we used ENDF-VII.0 in this work to treat nuclear interactions in an energy region of <20 MeV because emission probability of ^{10}B gamma rays (478 keV) deduced based on ENDF VII.0 [11] agreed statistically well (within 2%) with that for JENDL-4.0 [12].

3.2 Compton edge suppression

Figure 4 provides one example showing a role of the tube type $LaBr_3$ scintillator. To obtain the spectra presented in Fig. 4, a gamma-ray beam having a mono-energy of 662 keV with dimensions $\pi(1.5/2)^2$ cm^2 was uniformly irradiated from just under the debris toward the center of the cylindrical $LaBr_3$ scintillator. It is clear that the back-catcher scintillator suppresses the Compton edge (opened square), while a bump due to the Compton effect

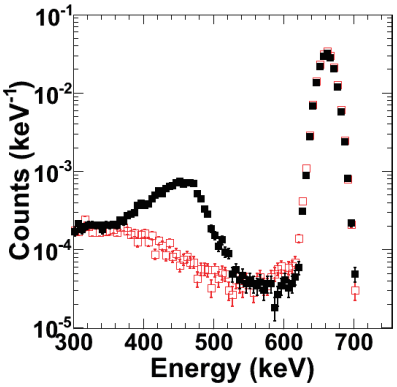

Figure 4: Comparison between pulse height spectra obtained for 662 keV gamma rays without (filled) and with (opened) the tube type scintillator. Errors denote statistical 1σ

remains at energies of 400-500 keV in case of the non-summed spectrum (filled square). Using the two spectra, we quantitatively evaluated an expected count at energies of 469-487 keV corresponding to 478 keV$\pm 1\sigma$ (σ=9 keV). Here, 2.35σ indicates a full width at half maximum at 478 keV. Consequently, it was found that an expected count of the summed spectrum (opened square) is reduced by a factor of 0.15, compared with that of the non-summed one (filled square).

3.3 Expected pulse height spectrum under ^{137}Cs background

Figure 5 represents a pulse height spectrum expected to obtain in one-hour measurement (blue). To calculate the expected spectrum, we summed a spectrum originating from ^{137}Cs (black) and that (red) derived from secondary neutrons and gamma rays that are generated from the debris via nuclear fission and room walls via nuclear interactions. Because the debris currently assumed has a weight of 8 g, we suppose that it produces 8×10^{8} Bq as ^{137}Cs radioactivity according to the measurement of [8]. Because of this radioactivity, 4.5×10^{4} photons with energy of 662 keV would enter the cylindrical $LaBr_3$ scintillator every second, after passing through the lead collimation.

As clearly seen, it was found that the gamma-ray detector is able to detect 478-keV gamma rays emitted from the debris under such a high background environment. Given these spectra, we evaluated 2160$\pm$150 (1h) as counts originating from ^{10}B in debris. This shows that one-hour measurement would be able to achieve 7% statistical accuracy. Here we assumed that a neutron production rate is 10^{12} n/s at a neutron source (10^{10} n/pulse$\times$100 pulse per second). In addition, we considered two points to derive the expected spectrum. One is that an amount of the initial neutron spectrum with the energy range of 0.1 eV – 14 MeV (Fig. 3) constitutes only 2.4% of a total of neutrons generated from the source. The other is that the Cs spectrum (black) is reduced by a factor of around 1/20, which is estimated as 0.46 ms /10 ms. Here 0.46 ms and 10 ms correspond to a flight time of 0.1 eV neutrons in the 2 m path and one cycle of the neutron production at the source, respectively.

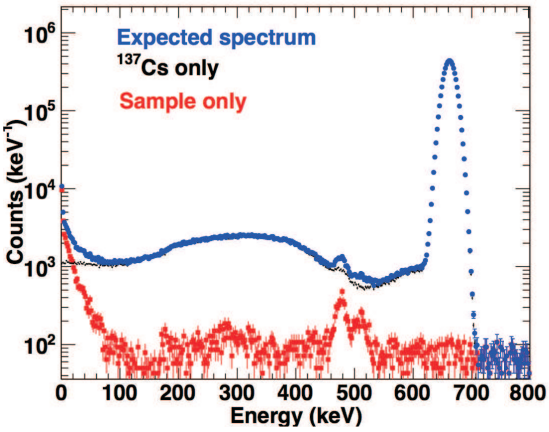

Figure 5: Expected pulse height spectrum assuming measuring time is 3600 s. Errors correspond to statistical 1σ

4. Summary

The present study shows that the $LaBr_3$-based detector proposed for NRD is capable of making an evident detection of ^{10}B signals radiated from a debris sample.

Detections of not only ^{10}B-derived gamma rays but also those from other nuclides would give an important clue to quantify nuclear materials in MFs taken from the Fukushima reactors.

Acknowledgements

This work is supported by the Japanese government: the Japan Safeguard Office (JSGO) of the ministry of education, culture, sports, science and technology in Japan (MEXT).

References

[1] Investigation Committee on the Accident at the Fukushima Nuclear Power Station, Final report, available at http://www.kantei.go.jp/jp/noda/actions/201207/23kenshou.html

[2] C.D. Bowman, R.A. Schrack, J.W. Behrens, and R.G. Johnson: “Neutron resonance transmission analysis of reactor spent fuel assemblies”, Neutron Radiography, pp.503-511 (1983).

[3] J.W. Behrens, R.G. Johnson, and R.A. Schrack: “Neutron resonance transmission analysis of reactor fuel samples”, Nucl. Tech. **67**, 161 (1984).

[4] J.W. Sterbentz and D.L. Chichester: “Further Evaluation of the Neutron Resonance Transmission Analysis (NRTA) Technique for Assaying Plutonium in Spent Fuel”, INL/ECT-11-23391 (2011).

[5] M. Koizumi, F. Kitatani, H. Harada, J. Takamine, M. Kureta, M. Senya, H. Tsuchiya, H. Iimura: “Proposal of neutron resonance densitometry for particle like debris of melted fuel using NRTA and NRCA”, Proc. of Ins. Nucl. Mat. Manag. 53th Annual Meeting (2012).

[6] E. V. D. van Loef, P. Dorenbos, C. W. E. van Eijk, K. Krämer, and H. U. Güdel:“High-energy-resolution scintillator: Ce activated LaBr,” Appl. Phys. Lett. **79**, pp.1573–1575 (2001).

[7] K. S. Shah, J. Glodo, M. Klugerman, W. M. Higgins, T. Gupta, and P. Wong: “High Energy Resolution Scintillation Spectrometers”, IEEE Tran. Nuc. Scien. **51**, pp.2395-2399 (2004).

[8] H. Uetsuka, F. Nagase, and T. Suzuki: “Gamma Spectrometry of TMI-2 Debris”, JAERI-Research 95-084 (1995).

[9] S. Agostinelli *et al*.: “GEANT4-a simulation toolkit”, Nucl. Inst. Meth. A **506**, pp.250-303 (2003).

[10] MCNP http://mcnp.lanl.gov/

[11] K. Shibata *et al*.:“JENDL-4.0: A New Library for Nuclear Science and Engineering”, J. Nucl. Sci. Technol. **48**, pp.1-30 (2011).

[12] M.B. Chadwick et al.: “ENDF/B-VII.0: Next Generation Evaluated Nuclear Data Library for Nuclear Science and Technology”, Nucl. Data Sheets **102**, pp.2931-3060 (2006).

23. Asian Collaboration on Nuclear Reaction Data Compilation

Masayuki Aikawa[1], Naoya Furutachi[1], Kiyoshi Katō[1], Ayano Makinaga[1],
Vidya Devi[2], Dagvadorj Ichinkhorloo[2], Myagmarjav Odsuren[2], Kohsuke Tsubakihara[2],
Toshiyuki Katayama[3] and Naohiko Otuka[4]
[1] Graduate School of Science, Hokkaido University, Sapporo 060-0810, Japan
[2] Meme Media Laboratory, Hokkaido University, Sapporo 060-8628, Japan
[3] School of Economics, Hokusei Gakuen University, Sapporo 004-8631, Japan
[4] Nuclear Data Section, International Atomic Energy Agency, A-1400 Wien, Austria
e-mail: aikawa@sci.hokudai.ac.jp

Nuclear reaction data are essential for research and development in nuclear engineering, radiation therapy, nuclear physics and astrophysics. Experimental data must be compiled in a database and be accessible to nuclear data users. One of the nuclear reaction databases is the EXFOR database maintained by the International Network of Nuclear Reaction Data Centres (NRDC) under the auspices of the International Atomic Energy Agency. Recently, collaboration among the Asian NRDC members is being further developed under the support of the Asia-Africa Science Platform Program of the Japan Society for the Promotion of Science. We report the activity for three years to develop the Asian collaboration on nuclear reaction data compilation.

1. Introduction

Nuclear reactions play an important role in our universe and lives. Abundance in the universe evolves with nuclear reactions in the Big Bang, supernovae, and other stellar phenomena. In the application point of view, nuclear engineering and radiation therapy are significantly improved by recent development of nuclear reaction techniques. Knowledge and precise data of nuclear reactions are therefore indispensable for such basic researches in the universe and application fields. Experiments to obtain nuclear reaction data are performed in accelerators all over the world. A large number of accelerators and experiments cause some difficulties to sort important data on nuclear reactions. Such nuclear reaction data must be compiled in a database and be accessible to nuclear data users.

One of the nuclear reaction databases is the EXFOR (EXchange FORmat) database maintained by the International Network of Nuclear Reaction Data Centres (NRDC) under the auspices of the International Atomic Energy Agency (IAEA). NRDC collaborates to compile experimental nuclear reaction data and

maintain the compiled data in the EXFOR database. NRDC has 14 nuclear data centres around the world, and one of them is the Hokkaido University Nuclear Reaction Data Centre.

The former organization, Japan Charged-Particle Nuclear Reaction Data Group (JCPRG), was established in 1974 and joined the NRDC in 1975. In 2011, the Nuclear Reaction Data Centre was established in the Faculty of Science, Hokkaido University and succeeded the abbreviation, JCPRG. Its objectives are: 1) Compilation of charged-particle and γ induced nuclear reaction data obtained in Japan, 2) Evaluation of light nuclei reaction, especially astrophysically important, data, 3) Promotion of collaboration within Asia and the NRDC, and 4) Education for graduate school students. We report here the activities related to the objectives, 1) compilation and 3) collaboration.

2. Compilation in the Hokkaido University Nuclear Reaction Data Centre (JCPRG)

Under the objective 1), JCPRG compiles nuclear reaction data from refereed journals into the original database, Nuclear Reaction Data File (NRDF). The scope of compilation in NRDF is charged-particle and γ induced nuclear reaction data obtained in Japan. The compilation process in JCPRG is shown in Fig. 1. The information to compile is the bibliographic information, experimental setup, physical quantities and numerical data, respectively. Such information is retrieved from papers and input into databases. If there are questions about any information on the paper and requests for numerical data, we have contacts with the authors. The number of compiled articles is over two thousand and the compiled data are accessible on the website (http://www.jcprg.org).

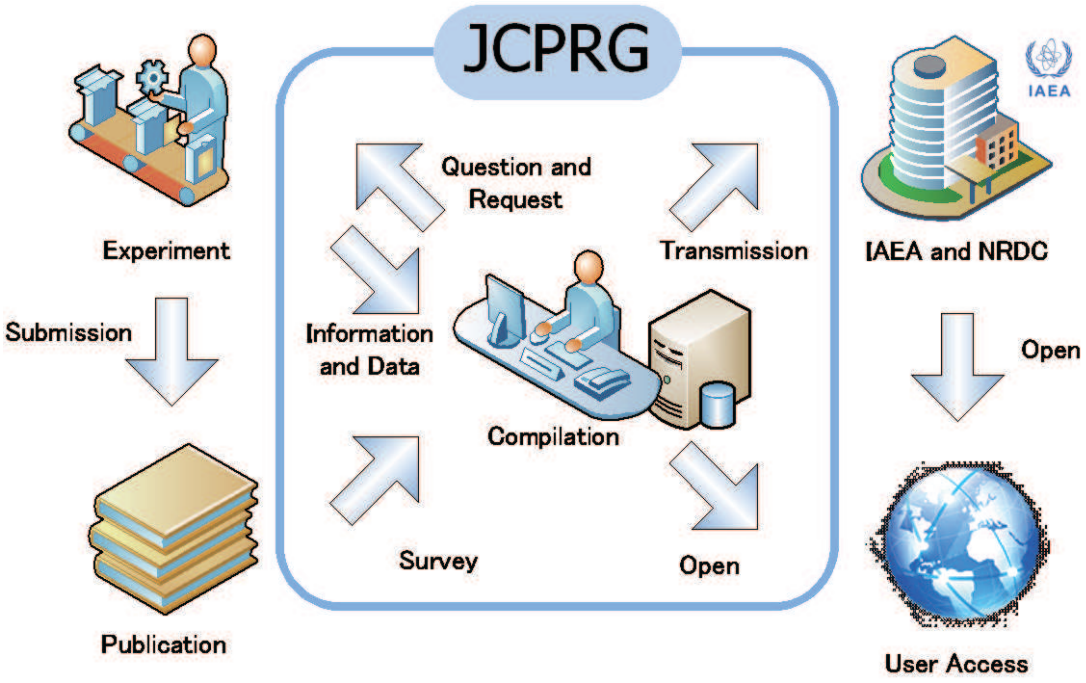

Fig. 1: Schematic view of the compilation process in JCPRG

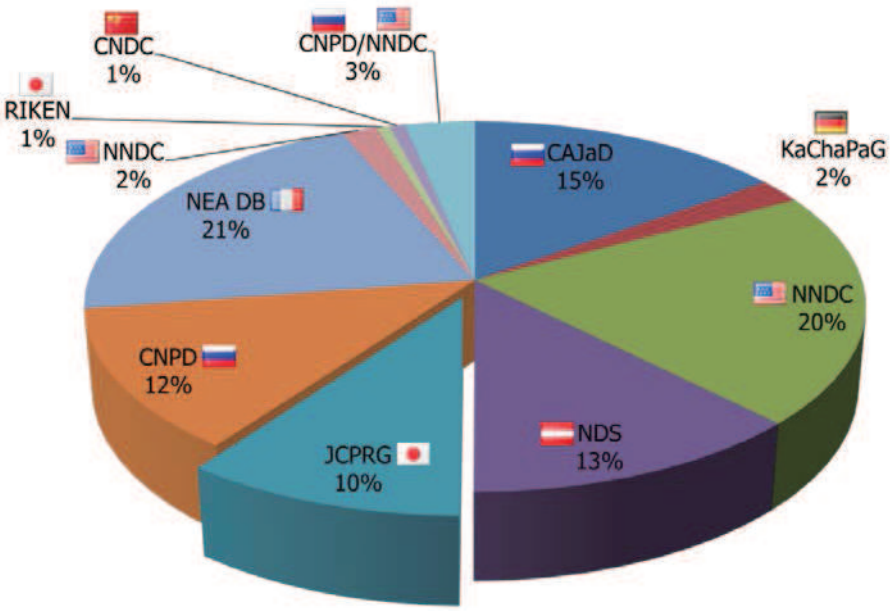

Abbreviation	Nuclear Reaction Data Centre	
NDS	IAEA Nuclear Data Section, Austria	Core Centres
NEA DB	OECD NEA Data Bank, France	
NNDC	National Nuclear Data Center, USA	
CAJaD	Nuclear Structure and Nuclear Reaction Data Centre, Russia	Regional, National and Specialized Centres
CNDC	Chinese Nuclear Data Center, China	
CNPD	Center for Nuclear Physics Data, Russia	
JCPRG	Nuclear Reaction Data Centre, Japan	
KaChaPaG	Charged Particle Nuclear Data Group, Germany	
RIKEN	RIKEN, Japan	

Fig. 2: Ratio of the numbers of entries compiled in each centre

Most part of the data compiled in NRDF is converted into the EXFOR format and transmitted to NRDC. Fig. 2 shows the ratio of the entry numbers of charged-particle induced nuclear reaction data provided by each data centre. We found that the contribution of JCPRG is about 10% and comparable to the activity of Core Centres.

In addition to the compilation and the transmission, retrieval systems for application and software for compilation were developed. One of them is the digitization software “GSYS”, which is freely available on the JCPRG website. As a result, GSYS was propagated to other NRDC members due to its availability.

3. Asian Collaboration

Recently, collaboration with the NRDC members in Asia was developed under the support of “R&D”

Platform Formation of Nuclear Reaction Data in Asian Countries (FY2010-FY2012), Asia-Africa Science Platform Program, the Japan Society for the Promotion of Science. Since 2010, annual workshops, named as Asian Nuclear Reaction Database Development Workshop, were held at Sapporo, Japan in 2010, Beijing, China in 2011, and Pohang, Korea in 2012, respectively. The workshops were devoted to sharing information about their activities, to strengthen collaboration among the NRDC members in Asia and to promote the dissemination and improvement of data compilation techniques. In order to improve compilation techniques, educational sessions for digitization and compilation took place.

There are many participants from the NRDC members in Asia, such as Japan, China, India and South Korea. In addition to the NRDC members, researchers belonging to institutes in other Asian countries, such as Kazakhstan, Mongolia, and Vietnam, also participated in the workshops and discussed topics in compilation and their own research. The workshops were very fruitful for all participants.

Among the participants in the 3rd workshop at Pohang, Korea in 2012, the following consensuses could be reached. The workshop must be continued 1) to share information on compilation and research activity, 2) to enhance nuclear data activities, 3) to promote collaboration of compilation and evaluation, and 4) to encourage and educate young researchers.

4. Summary

Nuclear data are indispensable for basic researches, nuclear physics and astrophysics, and for application fields, nuclear engineering and radiation therapy. Compilation of the data requires broad and long-term efforts due to the large number and variety of experiments worldwide. In order to sustain and develop such efforts, international collaboration must be promoted. Under the support of the Japan Society for the Promotion of Science, the annual workshops since 2010 were held to promote the dissemination and improvement of data compilation techniques, to share information about their own research activities, and to strengthen collaboration among the NRDC members in Asia.

Under the consensuses in the 3rd workshop in Pohang, Korea in 2012, we will continue to develop Asian collaboration in nuclear data.

Acknowledgement

This work was supported by the Asia-Africa Science Platform Program and Grant-in-Aid for Publication of Scientific Research Results (No. 248029) of the Japan Society for the Promotion of Science (JSPS).

24. JENDL-4.0 Benchmarking For Effective Delayed Neutron Fraction with a Continuous-energy Monte Carlo Code MVP

Yasunobu NAGAYA

Japan Atomic Energy Agency
Tokai-mura, Naka-gun, Ibaraki-ken 319-1195 Japan
email: nagaya.yasunobu@jaea.go.jp

Benchmark calculations with a continuous-energy Monte Carlo code have been performed for delayed neutron data of JENDL-4.0. JENDL-4.0 gives good prediction for the effective delayed neutron fraction in the present benchmarks but further detailed analysis is required for some cores.

1. Introduction

The effective delayed neutron fraction, which is commonly denoted as β_{eff}, is a very important parameter in criticality safety. It is not only a key parameter in the point-reactor kinetic equation but is also a reactivity unit to convert between dollar and $\Delta k/k$. Therefore, some methods based on the continuous-energy Monte Carlo method have been developed for accurate estimation of the β_{eff} value [1-4]. Benchmark calculations have been also done for the delayed neutron data of recent evaluated nuclear data[5-6].

Recently Nagaya and Mori proposed a new method to calculate the β_{eff} value with continuous-energy Monte Carlo[7]. This method has an advantage that it theoretically gives an exact β_{eff} value. In addition, the method has been well verified for the β_{eff} values of simple geometries, for which the deterministic results can be considered the reference values. Therefore it serves as a useful procedure to benchmark delayed neutron data in evaluated nuclear data files.

The objective of this paper is the validation of the delayed neutron data in the new version of Japanese nuclear data library JENDL-4.0[8], which has been recently released. To this end, we perform benchmark calculations with the new method for various systems for which measured β_{eff} values are given.

2. Benchmark

The following cores are selected for benchmarking the delayed neutron data in the present analysis.

- Jezebel: 95 at.% Pu-239
- Godiva: 94 wt.% U-235
- Jezebel-23: 98 at.% U-233
- Flattop-Pu: 94 at.% Pu-239
- Flattop-25: 93 wt.% U-235
- Flattop-23: 98 at.% U-233
- TCA: 2.6 wt% UO_2, light-water moderated[9]
- IPEN/MB-01: 4.35 wt% UO_2, light-water moderated

Jezebel, Godiva cores are bare fast systems and Flattop cores are a uranium-reflected fast system. On the other hand, TCA and IPEN/MB assemblies are thermal systems. Calculation geometries are described in the ICSBEP handbook[10].

Table 1 shows the comparison of the calculated β_{eff} values with the experimental ones for the above systems. Monte Carlo calculations are performed for 20 million histories with the MVP code[11]. The calculated values agree with the experimental ones almost within the experimental and statistical uncertainties except for Godiva and Flattop-23. The calculated result for Godiva underestimates the experimental one by ~4%, while the calculated result for Flattop-23 overestimates by ~7%. These are the same trend as Chiba et al. obtained with the deterministic code[12]; the C/E values are 0.964 and 1.054, respectively.

Table 1 Comparison of the calculated β_{eff} values with the experimental ones

System	Experimental β_{eff} (pcm)	Calculated β_{eff} (pcm)	C/E
Jezebel	194(10)	185(3)	0.95
Godiva	659(10)	629(5)	0.96
Jezebel-23	290(10)	293(4)	1.01
Flattop-Pu	276(7)	278(3)	1.01
Flattop-25	665(13)	685(5)	1.03
Flattop-23	360(9)	385(4)	1.07
TCA	771(17)	774(8)	1.00
IPEN/MB-01	739(7)	755(7)	1.02

* The values in the parentheses show the experimental and statistical uncertainties (1 standard deviation).

3. Comparison between JENDL-4.0 and ENDF/B-7.1

To compare the prediction accuracy for the β_{eff} value, we performed the benchmark calculations with ENDF/B-7.1 for the same problems listed in Table 1. **Figure 1** shows the comparison of JENDL-4.0 and ENDF/B-7.1 results for β_{eff} benchmark calculations. One can observe that ENDF/B-7.1 yields very good results for all the benchmark problems; the calculated results agree with the experimental ones within the experimental and statistical uncertainties. Comparing with the JENDL-4.0 results, better results can be obtained for Godiva and Flattop-23.

To investigate the contribution of each nuclide to the β_{eff} value for Flattop-23 and Jezebel-23, we perform simple sensitivity calculations by changing each uranium cross section of JENDL-4.0 to that of ENDF/B-7.1. **Table 2** shows the results of the sensitivity calculations. For Flattop-23, the contribution of the dominant nuclide (uranium-233) in the core is the largest but that of uranium-238 in the reflector is not negligible. On the other hand, no significant difference can be observed between JENDL-4.0 and ENDF/B-7.1. This is a different trend from Flattop-23, but the statistical uncertainties are still large for further discussion.

4. Conclusion

Benchmark calculations have been performed for the delayed neutron data of JENDL-4.0 in the present work. From overall results, it has been confirmed that JENDL-4.0 yields reasonable β_{eff} values for a wide range of systems. It is also found that further detailed analysis is required for some cores such as Flattop-23 and Godiva. To assure the accuracy and reliability of the delayed neutron data in JENDL, extensive benchmarks are necessary for β_{eff} values. Currently, a new method to calculate the neutron generation time Λ is under development. Benchmark calculations will be performed not only for β_{eff} values but also β_{eff}/Λ values.

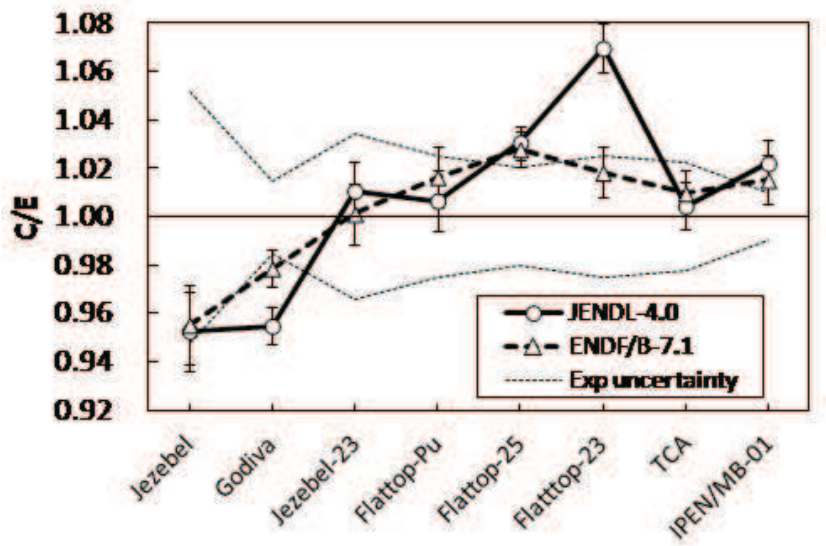

Fig 1 Comparison of JENDL-4.0 and ENDF/B-7.1 results for β_{eff} benchmark calculations

Table 2 Contribution to discrepancy for Flattop-23 and Jezebel-23

	Flattop-23		Jezebel-23	
Experiment	360(9)*		290(10)	
Calculated	β_{eff} (pcm)	Diff. from J-4.0(pcm)	β_{eff} (pcm)	Diff. from J-4.0(pcm)
JENDL-4.0	385(4)*	0	293(4)	0
JENDL-4.0+B7.1(U233)	372(4)	-13	290(4)	-3
JENDL-4.0+B7.1(U238)	378(4)	-7	296(4)	3
JENDL-4.0+B7.1(U235)	384(4)	-1	290(4)	-3
ENDF/B-7.1	367(4)	-18	290(4)	-3

References

[1] R. K. Meulekamp, S. C. Van der Marck, "Calculating the effective delayed neutron fraction with Monte Carlo", Nucl. Sci. Eng., **152**, pp.142–148 (2006).

[2] Y. Nauchi, T. Kameyama, "Proposal of direct calculation of kinetic parameters β_{eff} and Λ based on continuous energy Monte Carlo method", J. Nucl. Sci. Technol., **42**, pp.503–514 (2005).

[3] Y. Nauchi, T.Kameyama, "Development of calculation technique for iterated fission probability and reactor kinetic parameters using continuous-energy Monte Carlo method", J. Nucl. Sci. Technol., **47**, pp.977–990 (2010).

[4] B. C. Kiedrowski, F. B. Brown, P. P. H. Wilson, "Adjoing-Weighted Tallies for *k*-Eigenvalue Calculations with Continuous-Energy Monte Carlo", Nucl. Sci. Eng., **168**, pp.226-241 (2011).

[5] S.C. Van der Marck, "Benchmarking ENDF/B-VII.0", Nucl. Data Sheets, **107**, pp.3061-3118 (2006).

[6] A. C. Kahler, *et al*., "ENDF/B-VII.1 Neutron Cross Section Data Testing with Critical Assembly Benchmarks and Reactor Experiments", Nucl. Data Sheets, **112**, pp.2997-3036 (2011).

[7] Y. Nagaya, T. Mori, "Calculation of effective delayed neutron fraction with Monte Carlo perturbation techniques", Ann. Nucl. Energy, **38**, pp.254-260 (2011).

[8] K. Shibata, *et al*., "JENDL-4.0: A New Library for Nuclear Science and Engineering", J. Nucl. Sci. Technol., **48**, pp.1-30 (2011).

[9] K. Nakajima, "Re-evaluation of the Effective Delayed Neutron Fraction Measured by the Substitution Technique for a Light Water Moderated Low-enriched Uranium Core", J. Nucl. Sci. Technol., **38**, pp.1120-1125 (2001).

[10] OECD/NEA Nuclear Science Committee, "International Handbook of Evaluated Criticality Safety Benchmark Experiments", NEA/NSC/DOC(95)03, September 2008 Edition (2008) [CD-ROM].

[11] Y. Nagaya, *et al.*, "MVP/GMVP II: General Purpose Monte Carlo Codes for Neutron and Photon Transport Calculations based on Continuous Energy and Multigroup Methods", JAERI 1348 (2005).

[12] G. Chiba, *et al*., "JENDL-4.0 Benchmarking for Effective Delayed Neutron Fraction of Fast Neutron Systems", J. Nucl. Sci. Technol., **48**, pp.1471-1477 (2011).

25. Measurement of Capture Cross Section of ^{142}Nd with the Accurate Neutron-Nucleus Reaction Measurement Instrument (ANNRI) at J-PARC

Taihei MATSUHASHI[1)], Masayuki IGASHIRA[1)], Tatsuya KATABUCHI[1)], Motoharu MIZUMOTO[1)], Kazushi TERADA[1)], Kentaro HIROSE[2)], Atsushi KIMURA[2)], Kazuyoshi FURUTAKA[2)], Kaoru HARA[2)], Hideo HARADA[2)], Mitsuo KOIZUMI[2)], Fumito KITATANI[2)], Shoji NAKAMURA[2)], Masumi OSHIMA[2)], Yosuke TOH[2)], Takashi KAMIYAMA[3)], Koichi KINO[3)], Yoshiaki KIYANAGI[3)], Jun-ichi HORI[4)]

1) Research Laboratory for Nuclear Reactors, Tokyo Institute of Technology, 2-12-1-N1-26 O-okayama, Meguro-ku, Tokyo 152-8550, Japan
2) Nuclear Science and Engineering Directorate, Japan Atomic Energy Agency, 2-4 Shirakata Shirane, Tokai-mura, Naka-gun, Ibaraki 319-1195, Japan
3) Graduate school of Engineering, Hokkaido University, Kita 13 Nishi8, Kita-ku, Sapporo, Hokkaido 060-8628, Japan
4) Research Reactor Institute, Kyoto University, Kumatori, Sennan, Osaka, 590-0494, Japan
e-mail : matsuhashi.t.aa@m.titech.ac.jp

A project to measure the neutron capture cross section of ^{142}Nd using the Accurate Neutron Nucleus Reaction Measurement Instrument (ANNRI) in J-PARC is ongoing. Measurement was made by the time-of-flight method with a pulsed neutron beam from a spallation neutron target. Neutron capture gamma-rays were detected with an NaI(Tl) spectrometer. Preliminary experimental results are presented.

1. Introduction

In the current nucleosynthesis scenario, elements heavier than ^{56}Fe were mainly synthesized by successive neutron capture reactions in stellar environments. The neutron-capture nucleosynthesis is categorized into two processes, depending on neutron capture rate relative to beta-decay rate, s-process (slow) and r-process (rapid). The s-process is relatively well understood than the r-process because capture reactions and beta-decays in the s-process occur along the valley of stability. However, in late 1990's, the classical model that is based on simultaneous equations of simple reaction flow in the reaction network and had been accepted to describe the s-process for more than 30 years [1] was denied. The classical model failed to reproduce s-process abundances when using revised neutron capture cross section of Nd isotopes as input parameters [2,3]. Instead, stellar model calculations successfully reproduced the abundances [4]. Reliable capture cross section data of Nd isotopes, in particular, ^{142}Nd are very important for building the stellar models. However capture measurements of ^{142}Nd in the resolved resonance region are still very poor. The resonance parameters below 2.6 keV are based on only one transmission experiment. In the present work, we carried out neutron capture cross section measurements using an intense pulse neutron beam from a spallation neutron source of the Japan Proton Accelerator Research Complex (J-PARC).

2. Experiment

Experiments were carried out with the Accurate Neutron Nucleus Reaction Measurement Instrument (ANNRI) in J-PARC (**Fig.1**). The pulsed neutron beam was produced by the spallation reaction with a 3-GeV proton beam on a Hg target. The proton beam power was about 200 kW and the repetition rate was 25Hz. The produced neutrons

were moderated with a liquid hydrogen moderator kept at a temperature below 20 K. The measurement was made with an NaI(Tl) spectrometer in Experimental Area 2. The sample position of the NaI(Tl) spectrometer is 27.92 m away from the moderator. The detection angle of NaI(Tl) detector was 90° with respect to the neutron beam.

An isotopically enriched ^{142}Nd sample was used for the measurement. The chemical form was neodymium oxide (Nd_2O_3). The net weight of ^{142}Nd was 1.49 g. The isotope enrichment of the sample was 95.7%. The sample was pressed and sintered to form a pellet. Moisture in the sample was removed in the sintering process. This process is very important since Nd_2O_3 is very hygroscopic. The ^{142}Nd sample contained isotope impurities of ^{143}Nd and ^{145}Nd that have considerably larger capture cross sections than ^{142}Nd. Despite small amounts of the impurities, capture events of those isotopes are sizable. Thus, measurements with ^{143}Nd and ^{145}Nd enriched samples were also made. Samples of boron, gold, carbon and lead were also used in the experiments. A relative neutron spectrum was determined from the ^{10}B(n,αγ)^{7}Li reaction, detecting 478 keV γ-rays from the reaction. The saturated resonance method using the 4.9 eV resonance of ^{197}Au was used for normalization. Background from scattered neutrons at the sample was estimated from measurements of ^{nat}C and ^{nat}Pb samples.

A new signal processing technique was developed to reduce count loss and baseline shift caused by high counting rate events due to the intensive neutron beam of J-PARC. Negative anode signals from the photomultiplier tubes of the NaI(Tl) spectrometer were fed into a fast multiple event time digitizer (FAST ComTec MCS6A) directly without any analog shaping amplifiers. The time digitizer can detect timing for signals to cross a threshold with identification of falling or rising edges. The edge identification allows for calculating the pulse width of the signals as time duration under the threshold. The time differences from the start trigger to detected events were recorded sequentially in a list-data format. Signals from a current transformer picking up the incident proton beam pulses were used as the start trigger. The pulse heights of the signals were reconstructed offline from the pulse width using an energy calibration curve obtained from calibration measurements of standard γ-ray sources and discrete γ-rays from the neutron capture reactions, ^{1}H(n,γ)^{2}H ^{14}N(n,γ)^{15}N, ^{28}Si(n,γ)^{29}Si and ^{127}I(n,γ)^{128}I. The obtained calibration curve is shown in **Fig. 2**.

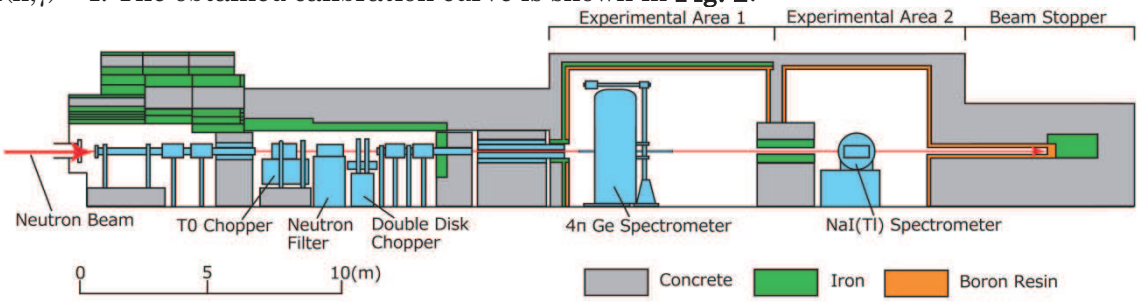

Fig. 1： Accurate Neutron-Nucleus Reaction measurement Instrument(ANNRI).

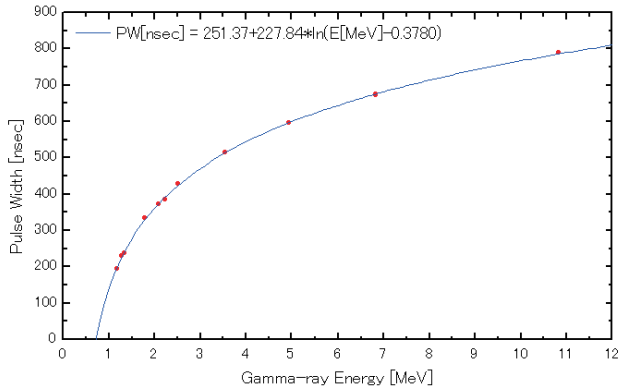

Fig. 2：Energy calibration curve

3. Results

TOF spectra of capture events for the ^{142}Nd, ^{143}Nd and ^{145}Nd samples are shown in **Fig. 3**. Previously reported resonances of ^{142}Nd [5] were observed in the keV region (labeled with solid arrows). Resonances of contaminant of ^{143}Nd (dashed arrows) and ^{145}Nd (dotted arrows) were also observed and confirmed from measurements of the ^{143}Nd and ^{145}Nd samples. Data analysis to derive the neutron capture cross section of ^{142}Nd is underway. Pulse-height weighting technique will be applied. Resonance analysis to the observed resonances is planned.

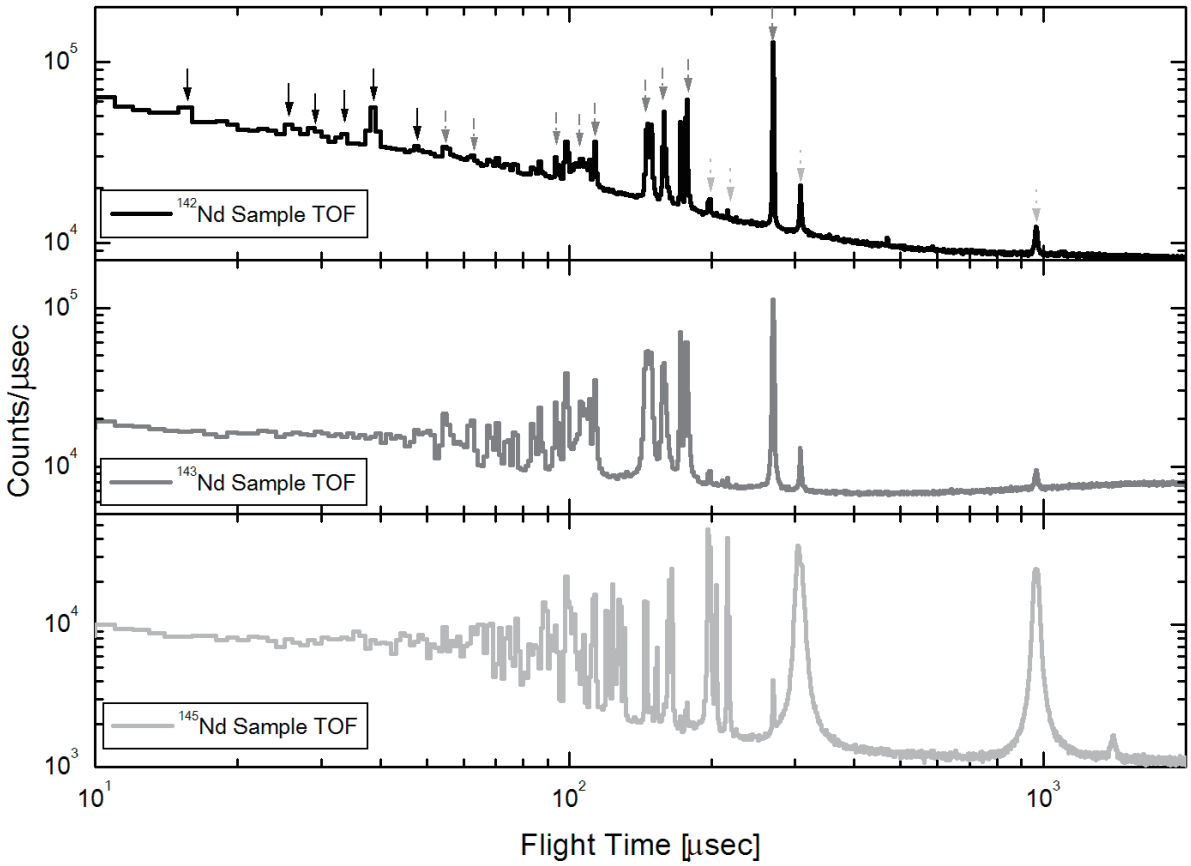

Fig. 3 : TOF spectrum of ^{142}Nd sample (upper), ^{143}Nd sample (middle), and ^{145}Nd sample (bottom).

4. Conclusion

We carried out capture experiments for ^{142}Nd using the NaI(Tl) spectrometer of ANNRI in J-PARC. Preliminary results were given in the present report. To derive the capture cross section of ^{142}Nd, data analysis of the experimental data is ongoing.

Reference

[1] F. Käppeler *et. al.*, Rep. Prog. Phys. **52**, pp.945-1013 (1989).
[2] C. Arlandini *et. al.*, J. Astrophys. **525**, pp.886-899 (1999).
[3] K. Wisshak, K *et. al.*, Phys. Rev. C **57**, pp.391-408 (1998).
[4] F. Käppeler *et. al.*, Rev. Mod. Phys. **83**, pp.157-193 (2011).
[5]JENDL-4.0 data file for ^{142}Nd (MAT = 6025), evaluated by N. Iwamoto, A. Zukeran (2009).

This is a blank page.

26. Measurement of 100 MeV/u carbon incident neutron production cross sections on a carbon target

Nobuhiro SHIGYO[1], Yusuke UOZUMI[1], Haruhiko UEHARA[1], Tomoya NISHIZAWA[1], Takafumi MIZUNO[1], Daiki SATOH[2], Toshiya SANAMI[3], Yusuke KOBA[4], Masashi TAKADA[4] and Naruhiro MATSUFUJI[4]
[1] *Kyushu University, Fukuoka, 819-0395, Japan*
[2] *Japan Atomic Energy Agency, Ibaraki-ken, 319-1195, Japan*
[3] *High Energy Accelerator Research Organization, Tsukuba, 305-0801, Japan*
[4] *National Institute of Radiological Sciences, Chiba, 263-8555, Japan*
e-mail: shigyo@kune2a.nucl.kyushu-u.ac.jp

Double differential neutron production cross sections down to 0.6 MeV of neutron energy from 100 MeV/u carbon ion incidence on a carbon target were measured at HIMAC facility. Two sizes of NE213 organic scintillators were adopted to detect neutrons in a wide energy range. Measurement angles were 15°, 30°, 45°, 60°, 75° and 90°. Neutron energy was determined by the time-of-flight technique between the target and the detector. Neutron flight paths were 1.7 to 3.7 m. In order to reduce neutrons from the beam dump, an iron and a concrete shield was placed between the detectors and the beam dump. The measured neutron energy spectra were compared with calculation results by the PHITS code.

1 Introduction

Heavy ion cancer therapy has been increased by reason of its clinical advantages. During the treatment, the secondary particles such as neutron and γ-ray are produced by nuclear reactions of a heavy ion incidence on a nucleus in a patient body. It has become essential to estimate the risk of secondary cancer from recent survey[1, 2]. In particular, it is important to know contribution of secondary neutrons for the estimation of risk assessment of extra dose to organs in the vicinity of the irradiated tumor because the secondary neutron has a strong penetrability and gives undesired dose to normal tissues in a wide area. Estimation of the secondary neutrons yields data is critical for assessment of radiation safety on both of workers and public in treatment facilities.

The experimental data of neutron yields are required to be simulated with high accuracy. Especially, the accurate data around neutron energy of 1 MeV is required because the 1 MeV neutron has a large relative biological effectiveness (RBE). The exposure dose from secondary neutrons is predicted by simulation codes. 290 MeV/u carbon ion incident neutron double differential cross sections for bio elements have been measured down to 0.6 MeV of neutron energy using NE213 liquid organic scintillators[3, 4]. Monte-Carlo simulation code, PHITS[5] reproduced the measured neutron spectra well in both the magnitude and shape.

In this study, to have knowledge of neutron production by deceleration stage of 290 MeV/u carbon in a human body, we measured double differential thick target neutron yields down to 0.6 MeV of neutron energy from 100 MeV/u carbon ion incidence on a carbon target which is one of the elements of human tissue in wide angular range from 15° to 90° using NE213 scintillators. The experimental data are compared with calculated results by the PHITS code.

2 Experiment

The measurement of neutron energy spectra was carried out at the PH2 course of Heavy Ion Medical Accelerator in Chiba (HIMAC), National Institute for Radiological Sciences. The experimental setup is illustrated in **Figure 1**. Incident ^{12}C beam energy was 100 MeV/u. The beam spot size was less than

10 mm in diameter at the target position. Since the synchrotron was operated in a pulse mode (0.3 Hz repetition cycle) and incident carbon beam intensity was very weak in level of 5 x 10^5 particles / 3.3 sec, the number of incident carbons can be individually counted. The carbon ions came from a vacuum duct through a 100 μm thick aluminum window. Before bombardment on a target, the beam passed a beam pick-up detector. The beam pick-up detector was a 0.5 mm thick NE102A plastic scintillator and provided the signal for the time-of-flight (TOF) measurement and the number of incident particles.

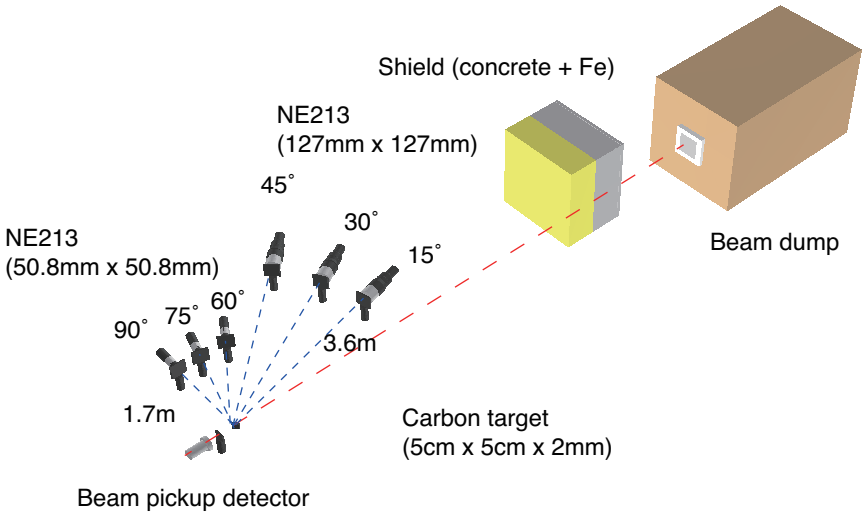

Figure 1. Experimental setup at the PH2 course of HIMAC.

The carbon target was 50 mm x 50 mm x 2 mm and rotated 45° with respect to the beam direction to suppress neutron multiple scattering to about 90°. The 100 MeV/u carbon give about 15 % of its energy in the medium.

Emitted neutrons were detected with NE213 liquid organic scintillators. Two sizes of scintillators were used to cover wide neutron energy range. Large and small detector sizes were 127 mm in diameter and 127 mm long and 50.8 mm in diameter and 50.8 mm long, respectively. The scintillators were placed at 15, 30, 45, 60, 75 and 90. Scintillation lights from the NE213 liquid organic scintillators are originated from neutrons as well as γ-rays. Distance between the target and NE213 scintillators were varied from 1.8 m to 3.6 m for large scintillators and from 1.7 m to 2.1 m for small ones, respectively. The light outputs of the neutron detectors were calibrated by using photons from γ-ray sources of ^{241}Am (E_γ = 0.060 MeV), ^{137}Cs (E_γ = 0.661 MeV), ^{60}Co (E_γ = 1.22 MeV) and ^{241}Am-Be (E_γ = 4.33 MeV) to determine the threshold level in the data analysis. The kinetic energy of neutron was obtained by TOF technique using the time difference between the beam pickup scintillator and the neutron detector. A veto detector, 2 mm thick NE102A plastic scintillator, was put in front of each NE213 scintillator to separate charged particle events.

In order to reduce neutrons from the beam dump, a couple of an iron of 63 cm thick and a concrete of 50 cm thick shields was placed between the neutron detectors and beam dump as shown in Figure 1. For measurement of neutrons from floor or other items in the experimental room, the measurement with a 110 cm long iron shadow bar put between a target and a neutron detector were also done.

Data on the signal charge integrated with a specific gate width, and flight time triggered by the beam pick up scintillator and the neutron detectors were recorded event by event via a NIM and CAMAC electronic circuit connected to a personal computer.

3 Data Analysis

The light-output distribution of the beam pickup scintillator is shown in **Figure 2**. To determine the number of heavy ions bombarding the target, the incident beam was monitored ion by ion. Events that two or more heavy ions were incident simultaneously were designated as multiple incident events shown

in the region above 550 ch in the figure, give larger light outputs compared with the single incident events which is a region between 250 and 550 ch. The beam intensity was controlled to keep the condition that the number of the multiple incident events is 10 % or less than that of the single ones.

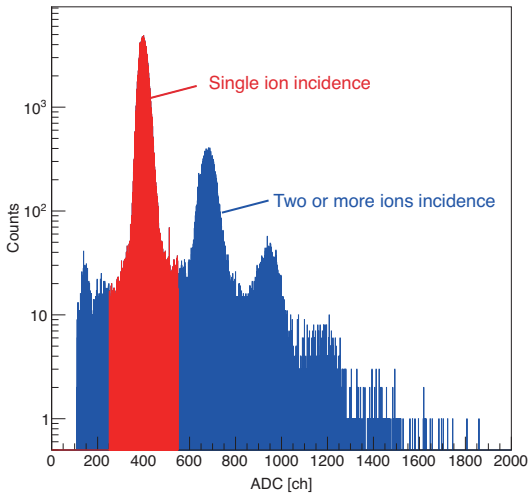

Figure 2. Light output spectrum of the beam pickup scintillator.

A typical result of separation of neutron and γ-ray events using light output data with total and slow gates for the small NE213 scintillator is demonstrated in **Figure 3**. One can see that neutron events designated as the middle line were clearly separated from photon events shown as lower dark gray point region above 200 ch of the light output with the total gate.

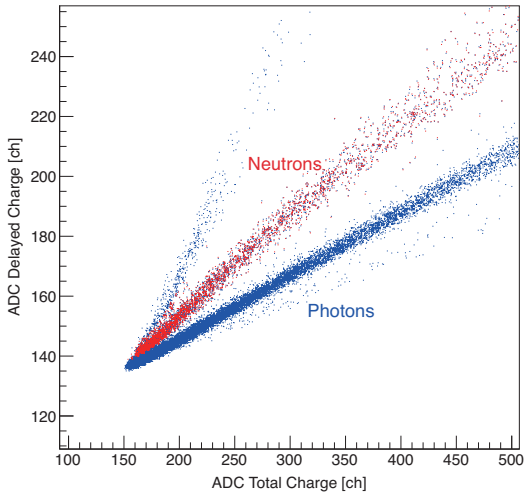

Figure 3. Separation of neutron and γ-ray events of a small NE213 scintillator using two gate integration method.

Neutron detection efficiencies of the NE213 scintillators were obtained using a computer simulation code named SCINFUL-QMD[6]. The threshold levels were set at the position of half height with respect to a Compton edge in light output spectra with photons from the γ-ray sources. The neutron detection efficiencies of both size of scintillators calculated by SCINFUL-QMD with some threshold levels were

shown in **Figure 4**.

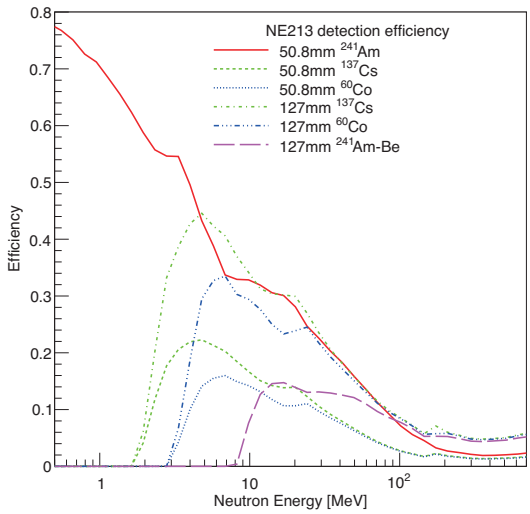

Figure 4. Neutron detection efficiencies of two sizes of NE213 scintillators calculated by SCINFUL-QMD.

An example of the TOF spectra without and with a shadow bar of a large NE213 scintillator is illustrated in **Figure 5**, where the charged particle events were removed. Both spectra are normalized by the number of incident ions. The horizontal axis of the TOF spectra is reversed, because the stop signal of the TOF measurement was taken by the beam pickup scintillator. The sharp peak of prompt γ-ray appears at about 2600 ch of the spectrum.

The neutron energy was deduced from the TOF data. The results of the neutron production double differential cross sections were obtained by subtracting the background data measured with the shadow bars from the ones of foreground measurement.

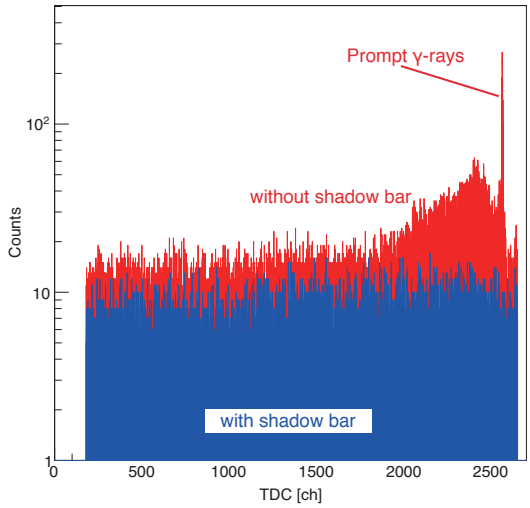

Figure 5. An example of time-of-flight spectra of a large NE213 scintillator.

4 Results

Experimental data of double differential neutron thick target yields are shown as circles in **Figure 6**. Error bars include only statistical errors. Calculation results by PHITS code with different switching time from Quantum Molecular Dynamics (QMD)[7] to Generalized Evaporation Model (GEM)[8] processes are also indicated in the same figure. PHITS reproduce the shape of experimental data above 10 MeV in all directions. Especially, calculation with the switching time of 100 and 150 fm/c simulates experimental neutron spectra well above several MeV. It means that the minimum switching time time from QMD to GEM process is 100 fm/c to calculate neutron production double differential cross sections. However, all calculations underestimate experimental data below a few MeV.

We adopted 150 fm/c as the switching time from QMD to GEM in the case of 290 MeV/u ^{12}C incidence. PHITS gives good agreements with experimental data for this incident energy[3]. The results of these two cases show that the default switching time (150 fm/c) is acceptable to simulate neutron production double differential cross sections in the incident ion energy between 100 and 290 MeV/u.

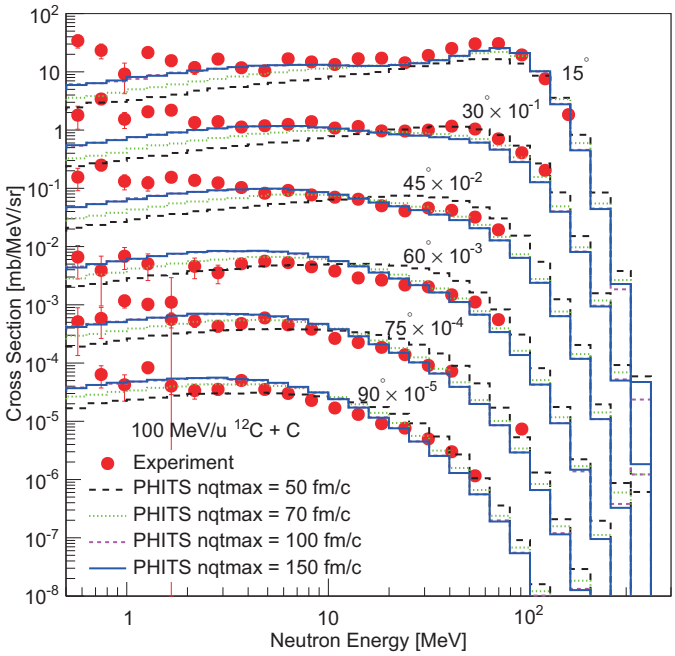

Figure 6. Experimental data of neutron production double differential cross sections of 100 MeV/u carbon incidence on a carbon target. Calculated results by PHITS with different switching time from QMD to GEM are also indicated as lines.

5 Summary

In order to have knowledge of neutron production by deceleration stage of 290 MeV/u carbon in a human body, neutron production double differential cross sections from a carbon target by 100 MeV/u carbon beam were measured from 15° to 90° by the TOF method using two sizes of NE213 liquid organic scintillators down to 0.6 MeV. PHITS calculation with 150 fm/c switching time from QMD to GEM processes reproduces experimental data above several MeV in all measurement directions.

Acknowledgement

This work is supported by grand-aid of ministry of education (KAKENHI 22360406) in Japan and was performed as a Research Project with Heavy Ions at NIRS-HIMAC.

References

[1] B. Clasie, A. Wroe, H. Kooy, N. Depauw, J. Flanz, H. Pa-ganetti and A. Rosenfeld, Assessment of out-of-field absorbed dose and equivalent dose in proton fields, *Med. Phys.* 37 (2010), pp. 311-321.

[2] E. J. Hall, Intensity-modulated radiation therapy, protons, and the risk of second cancers, *Int. J. Radiat. Oncol. Biol. Phys.* 65 (2006) pp. 1-7.

[3] D. Satoh, D. Moriguchi, T. Kajimoto, H. Uehara, N. Shigyo, M. Ueyama, M. Yoshioka, Y. Uozumi, T. Sanami, Y. Koba, M. Takada, and N Matsufuji, Measurement of neutron-production double-differential cross-sections on carbon bombarded with 290-MeV/nucleon carbon and oxygen ions, *Nucl. Instrum. Meth.* A644 (2011), pp. 59-67.

[4] D. Moriguchi, Y. Nakamura, T. Kajimoto, Y. Koba, M. Ueyama, M. Yoshioka, N. Shigyo, Y. Uozumi, D. Satoh, T. Sanami, M. Takada and N. Matsufuji, Measurement of Neutron-Production Cross Sections for 290 MeV/u Carbon Ion Incidence, *J. Korean Phys. Soc.* 59 (2011), pp. 1789-1792.

[5] K. Niita, N. Matsuda, Y. Iwamoto, H. Iwase, T. Sato, H. Nakashima, Y. Sakamoto and L. Sihver, PHITS: Particle and Heavy Ion Transport code System, Version 2.23, JAEA-Data/Code 2010-022, Japan Atomic Energy Agency, (2010).

[6] D. Satoh, T. Satoh, N. Shigyo, K. Ishibashi, SCINFUL-QMD: Monte Carlo Based Computer Code to Calculate Response Function and Detection Efficiency of a Liquid Organic Scintillator for Neutron Energies up to 3 GeV, JAEA-Data/Code 2006-023, Japan Atomic Energy Agency, (2006).

[7] K. Niita, S. Chiba, T. Maruyama, T. Maruyama, H. Takada, T. Fukahori, Y. Nakahara, and A. Iwamoto, Analysis of the (N,xN) reactions by quantum molecular dynamics plus statistical decay model, *Phys. Rev.* C52 (1995), pp. 2620-2635.

[8] S. Furihata, Statistical analysis of light fragment production from medium energy proton-induced reactions, *Nucl. Instrum. Meth.* B171 (2000), pp. 251-258.

27. Evaluation of Neutron Induced Reaction Cross Sections on Re Isotopes

Nobuyuki Iwamoto
Nuclear Data Center, Nuclear Science and Engineering Directorate,
Japan Atomic Energy Agency, Tokai, Ibaraki 319-1195, Japan
e-mail: iwamoto.nobuyuki@jaea.go.jp

Evaluation of neutron nuclear data on ^{185,186,187}Re in the incident energies up to 20 MeV was performed, using theoretical nuclear reaction calculation code CCONE. The calculated cross sections are in good agreement with measured total, elastic scattering, inelastic scattering, capture, $(n, 2n)$, (n, p) and (n, α) reaction cross sections, angular distributions of scattered neutrons and gamma-ray emission spectrum of ^{185,187}Re or natural Re. The derived Maxwellian averaged capture cross sections have similar values as KADoNiS at around the temperature of 30 keV, but have stronger temperature-dependences for ^{185,186}Re.

1 Introduction

Natural rhenium with atomic number 75 comprises two stable isotopes ^{185,187}Re (natural abundances 37.4 and 62.6%, respectively). Neutron nuclear data on Re are included in the latest ENDF/B-VII.1 [1], JEFF-3.1.2 [2] and TENDL-2011 [3]. However, JENDL-4.0 [4] does not have the data on Re. JENDL/A-96 [5] opened in 1996 includes activation cross sections of only selected reactions for ^{185,187}Re, and becomes out-of-date when radioactivity for decommissioning of reactor and the produced amounts of radioisotopes (e.g., ^{186}Re and ^{184}Ta) for possible use of nuclear medicine are estimated. Rhenium is recently considered as structural materials in Fusion reactor. Radiative neutron capture cross section on unstable ^{186}Re as well as ^{185,187}Re has also attracted interests in an astrophysical point of view (Re/Os cosmochronology) for almost half a century. It becomes important to provide neutron nuclear data on stable and unstable Re isotopes, taking account of recent experimental efforts. In this work, new evaluation of ^{185,186,187}Re was made with theoretical nuclear reaction calculation code CCONE [6].

2 Optical Model Calculation

Total cross section was calculated by using a coupled-channels optical model with deformation parameters $\beta_2 = 0.22$, 0.207 and 0.195 for ^{185,186,187}Re, respectively, and $\beta_4 = -0.04$ for those isotopes. The form and parameters of optical model potential (OMP) for Re targets were adopted from Kunieda et al.[7], in which potential parameters were modified to get better agreement with measured total cross section and angular distribution of emitted neutrons. The $5/2^+$ (g.s.)- to $11/2^+$-levels and the 1^- (g.s.)- to $(5)^-$-levels in ground-state band were coupled for ^{185,187}Re and ^{186}Re, respectively. The evaluated result of total cross section is shown in **Fig. 1**, in which total cross sections of ENDF/B-VII.1 and JEFF-3.1.2 are also illustrated. The present one is in good agreement with measured data. The neutron OMP of the other nuclides was employed from Koning and Delaroche [8]. The OMPs for the other particle emissions were taken from Koning and Delaroche for protons, Lohr and Haeberli [9] for deuterons, Becchetti and Greenlees [10] for tritons and ^{3}He, and McFadden and Satchler [11] for α-particles.

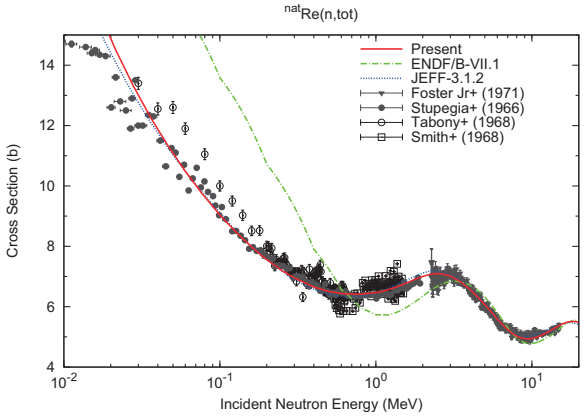

Figure 1: Total cross section of natural Re.

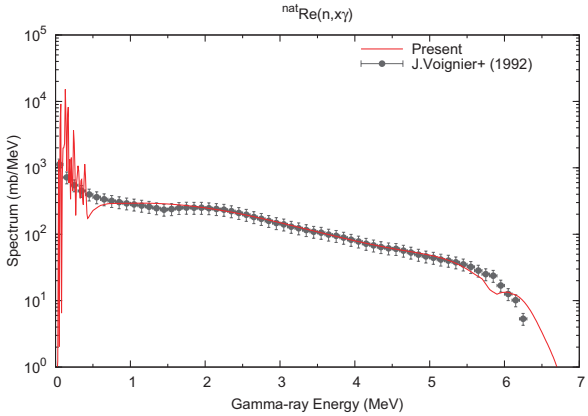

Figure 2: Gamma-ray emission spectrum of natural Re at 500 keV incident energy.

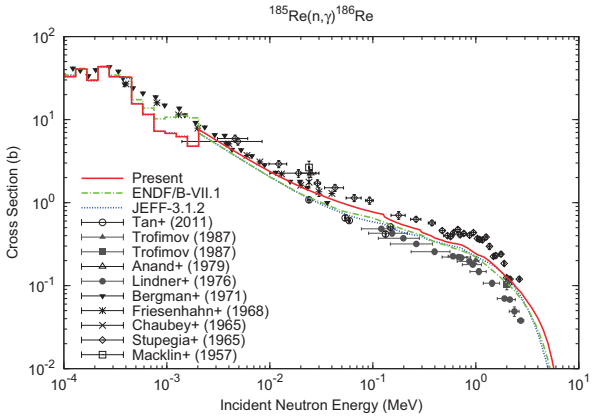

Figure 3: Radiative capture cross section of ^{185}Re.

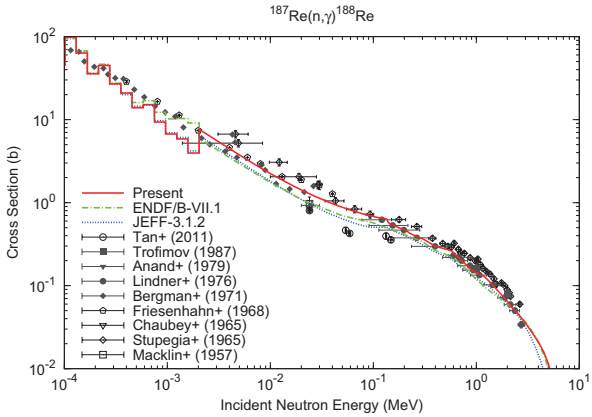

Figure 4: Radiative capture cross section of ^{187}Re.

3 Evaluated Results

Reaction cross sections were derived by theoretical nuclear reaction calculation code CCONE, which is composed of Hauser-Feshbach statistical model and preequilibrium two-component exciton model. Information of discrete levels was taken from RIPL-3 [12]. Level density was adopted from the formulation of Mengoni and Nakajima [13]. The level density parameter a was re-fixed so as to reproduce experimental average level spacings of s-wave resonances. Gamma-ray strength function for E1 transition consists of giant dipole resonance (GDR) and pygmy resonance, which were represented by Generalized and Standard Lorentzian forms, respectively. The resonance energy, width and cross section of GDRs were determined by reproducing measured photoneutron cross sections of ^{185,187}Re. The pygmy resonances for ^{186,188}Re were needed to explain measured gamma-ray emission spectrum of natural Re [14], since they gave additional increase of E1 gamma-ray strength function below neutron separation energy. The present evaluation obtains good match with the measured data as shown in **Fig. 2**.

The radiative capture cross sections of ^{185,187}Re are illustrated in **Figs. 3** and **4**, respectively. The calculated result for ^{185}Re contradicts measured data above the neutron energy of 0.03 MeV above which measured data bifurcates. The other evaluated cross sections as well as

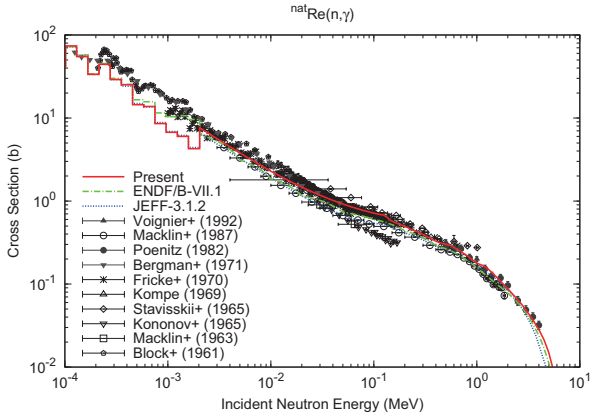

Figure 5: Radiative capture cross section of natural Re.

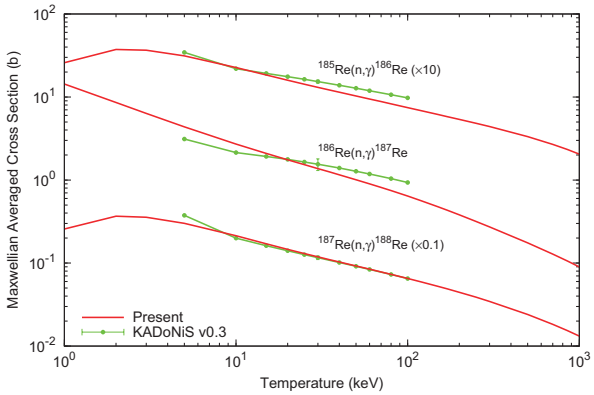

Figure 6: Maxwellian averaged capture cross section of ^{185,186,187}Re.

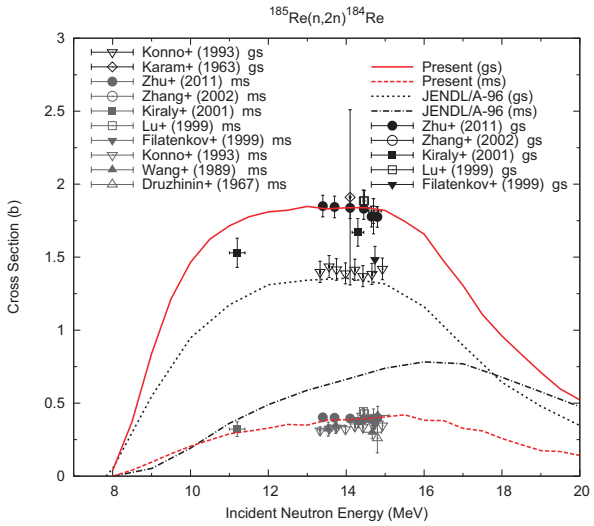

Figure 7: Production cross sections of $3^{(-)}$-ground- and $8^{(+)}$-meta-states of ^{184}Re by ^{185}Re$(n, 2n)$ reaction.

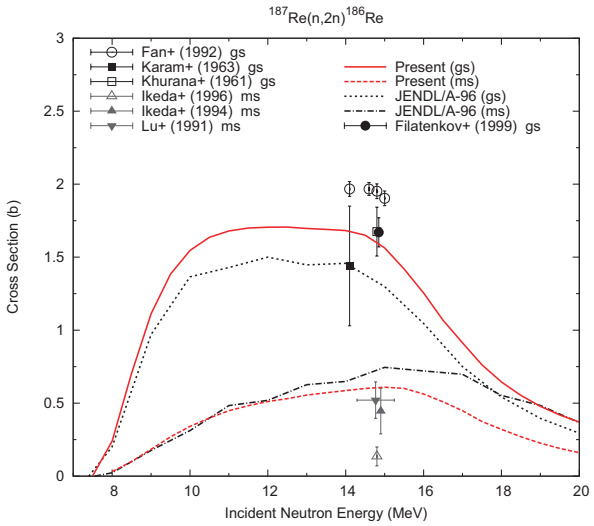

Figure 8: Production cross sections of 1^--ground- and (8^+)-meta-states of ^{186}Re by ^{187}Re$(n, 2n)$ reaction.

the present one are between two branches of the measured data. The calculated gamma-ray strength functions for s-wave resonances ($S_{\gamma 0} = \langle \Gamma_{\gamma 0} \rangle / \langle D_0 \rangle$) in unit of 10^{-4} are 185 and 159 for ^{185,187}Re, respectively. These values are in good agreement with compiled ones ($S_{\gamma 0} = 195 \pm 14$ and 155 ± 10 [15] for ^{185,187}Re, respectively). Resulting radiative capture cross section of natural Re generated from the evaluated results of two stable ^{185,187}Re shows consistency with experimental data as shown in **Fig. 5**. **Figure 6** presents the Maxwellian averaged capture cross sections derived from the present results together with resonance cross sections. The calculated results of ^{185,186}Re have almost the same values as KADoNiS[16] at around the temperatures of 30 keV, at which it is considered that slow neutron capture process (s-process) takes place in a low-mass, thermally pulsing asymptotic giant branch star. They, however, show stronger temperature dependences than those of KADoNiS.

Figures 7 and **8** illustrate the production cross sections of $3^{(-)}$-ground- and $8^{(+)}$-meta states of ^{184}Re by ^{185}Re$(n, 2n)$ reaction and those of 1^--ground- and (8^+)-meta states of ^{186}Re

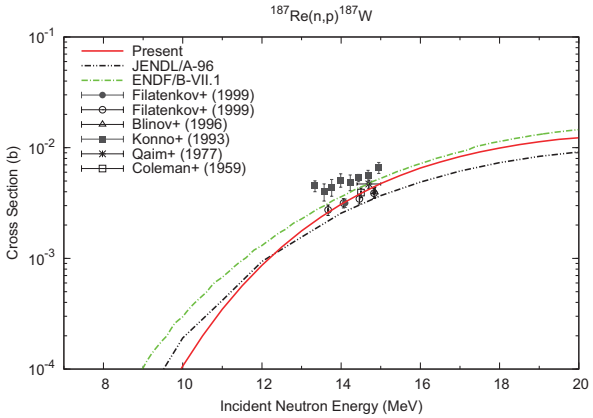

Figure 9: ^{187}Re(n,p) reaction cross section.

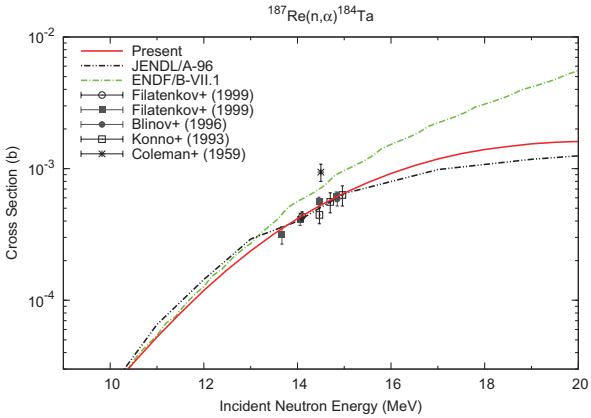

Figure 10: ^{187}Re(n,α) reaction cross section.

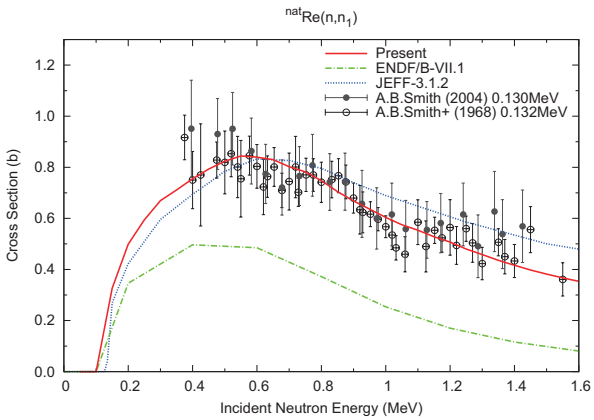

Figure 11: Inelastic scattering cross sections to each first excited level (excitation energy of $\sim$ 130 keV) of ^{185,187}Re using natural Re target.

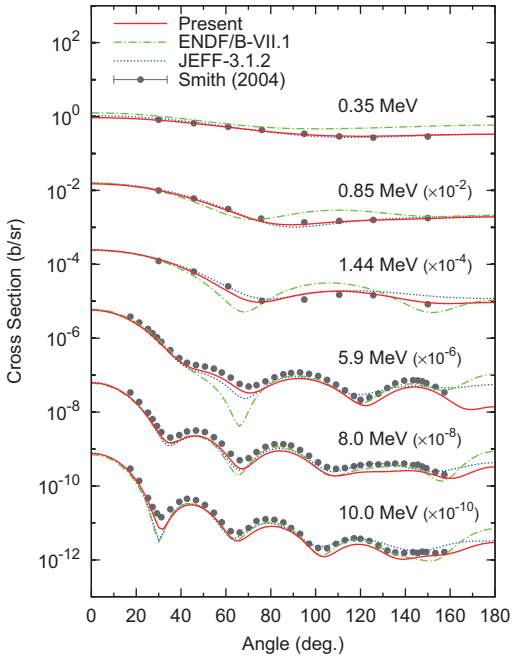

Figure 12: Angular distribution of scattered neutrons in the energy range from 0.35 to 10 MeV.

by ^{187}Re$(n,2n)$ reaction. The present evaluation is consistent with the latest measured data. In contrast, it is found that the production cross sections of ^{184g,186g}Re in JENDL/A-96 are significantly small, compared with the latest ones, and that those of ^{184m,186m}Re are larger than measured ones.

The cross sections of ^{187}Re(n,p) and ^{187}Re(n,α) reactions are shown in **Figs. 9** and **10**, respectively. Both of evaluated results agree with the data of Filatenkov et al. [17] and Blinov et al. [18] at around 14 MeV. For the ^{187}Re(n,p) reaction the ENDF/B-VII.1, JENDL/A-96 and present evaluations gave almost the same cross sections. The data of Konno et al. [19] are larger than the evaluated and the other experimental data.

Inelastic scattering cross sections to each first excited level (excitation energy of $\sim$ 130 keV) of two stable isotopes for natural Re target were reported by Smith et al. [20, 21]. **Figure 11** represents that the present calculation is in good agreement with the measured data. This result indicates that the deformation parameters β_2 adopted for ^{185,187}Re were appropriate. The ENDF/B-VII.1 evaluation provides relatively small cross section. This may be due to no or underestimated contributions of direct inelastic scattering components. **Figure 12** illustrates angular distributions of neutrons elastically scattered from natural Re. The angular distributions above 5.9 MeV incident energies are contaminated by inelastic scattering components below excitation energies of 300 keV. The present evaluation was performed, including the contaminants. The calculated results are consistent with the data of Smith [20].

4 Conclusion

Neutron nuclear data on ^{185,186,187}Re were evaluated in the fast energy region up to 20 MeV by using the theoretical nuclear reaction calculation code CCONE. The present evaluation well reproduces the available measurements on total, elastic scattering, inelastic scattering, capture, $(n, 2n)$, (n, p) and (n, α) reaction cross sections, angular distributions of scattered neutrons, and gamma-ray emission spectrum of ^{185,187}Re or natural Re. The Maxwellian averaged capture cross sections for Re isotopes were derived with using cross sections in resolved resonance region, and were almost the same as those of KADoNiS at around the temperature of 30 keV. However, it is found that the temperature-dependence of the calculated cross sections is stronger for ^{185,186}Re. The production cross sections of radioactive nuclides obtained in this evaluation will be included to a new activation cross section file.

Acknowledgments

This work was supported by JSPS KAKENHI Grant Number 23602015.

References

[1] M.B. Chadwick, M. Herman, P. Oblozinský, M.E. Dunn, Y. Danon, et al., "ENDF/B-VII.1 Nuclear Data for Science and Technology: Cross Sections, Covariances, Fission Product Yields and Decay Data," *Nucl. Data Sheets*, **112**, 2887-2996 (2011).

[2] JEFF project, online at http://www.oecd-nea.org/dbdata/jeff/ (2012).

[3] A.J. Koning, D. Rochman, "TENDL-2011: TALYS-based Evaluated Nuclear Data Library", online at ftp://ftp.nrg.eu/pub/www/talys/tendl2011/tendl2011.html (2011).

[4] K. Shibata, O. Iwamoto, T. Nakagawa, N. Iwamoto, A. Ichihara, et al., "JENDL-4.0: A New Library for Nuclear Science and Engineering," *J. Nucl. Sci. Technol.*, **48**, 1-30 (2010).

[5] Y. Nakajima, JNDC WG on Activation Cross Section Data, "JENDL Activation Cross Section File," Proc. the 1990 Symposium on Nuclear Data, JAERI-M 91-032, p. 43 (1991).

[6] O. Iwamoto, "Development of a Comprehensive Code for Nuclear Data Evaluation, CCONE, and Validation Using Neutron-Induced Cross Sections for Uranium Isotopes," *J. Nucl. Sci., Technol.*, **44**, 687-697 (2007).

[7] S. Kunieda, S. Chiba, K. Shibata, A. Ichihara, E.Sh. Sukhovitskii, "Coupled-channels Optical Model Analyses of Nucleon-induced Reactions for Medium and Heavy Nuclei in the Energy Region from 1keV to 200 MeV," *J. Nucl. Sci. Technol.*, 44, 838 (2007).

[8] A. Koning, J.-P. Delaroche, "Local and global nucleon optical models from 1 keV to 200 MeV," *Nucl. Phys.*, **A713**, 231 (2003).

[9] J.M. Lohr, W. Haeberli, "Elastic scattering of 9-13 MeV vector polarized deuterons," *Nucl. Phys.*, **A232**, 381-397 (1974).

[10] F.D. Becchetti Jr., G.W. Greenlees, "Polarization Phenomena in Nuclear Reactions", Univ. of Wisconsin Press, p.682 (1971).

[11] L. McFadden, G.R. Satchler, "Optical-model analysis of the scattering of 24.7 MeV alpha particles," *Nucl. Phys.*, **84**, 177 (1966).

[12] R. Capote, M. Herman, P. Oblozinsky, P.G. Young, S. Goriely et al., "RIPL - Reference Input Parameter Library for Calculation of Nuclear Reactions and Nuclear Data Evaluations," *Nucl. Data Sheets*, **110**, 3107-3214 (2009).

[13] A. Mengoni, Y. Nakajima, "Fermi-Gas Model Parametrization of Nuclear Level Density," *J. Nucl. Sci., Technol.*, **31**, 151-162 (1994).

[14] J. Voignier, S. Joly, G. Grenier, "Capture cross sections and gamma-ray spectra from the interaction of 0.5 to 3.0 MeV neutron with nuclei in the mass range A=63 to 209," *Nucl. Sci. Eng.*, **112**, 87 (1992).

[15] S.F. Mughabghab, "Atlas of Neutron Resonances - Resonance Parameters and Thermal Cross Sections $Z = 1 - 100$", Elsevier (2006).

[16] I. Dillmann, M. Heil, F. Käppeler, R. Plag, T. Rauscher, F.-K. Thielemann, "KADoNiS - The Karlsruhe Astrophysical Database of Nucleosynthesis in Stars," AIP Conf. Proc. 819, 123; online at http://www.kadonis.org (2006).

[17] A.A. Filatenkov, S.V. Chuvaev,V.N. Aksenov, V.A. Yakovlev, A.V. Malyshenkov et al., "Systematic Measurement of Activation Cross Sections At Neutron Energies from 13.4 to 14.9 MeV," RI-252 (1999).

[18] M.V. Blinov, A.A. Filatenkov, S.V. Chuvaev, V.A. Yakovlev, A.A. Rimskiy-Korsakov, "Systematic Measurement of Activation Cross Sections At Neutron Energies from 13.4 to 14.9 MeV," INDC(NDS)-342, 53 (1996).

[19] C. Konno, Y. Ikeda, K. Oishi, K. Kawade, H. Yamamoto et al., "Activation Cross section measurements at neutron energy from 13.3 to 14.9 MeV," JAERI-1329 (JAERI) (1993).

[20] A.B. Smith, "Fast-neutron scattering from elemental rhenium," *J. Phys.*, **G30**, 407 (2004).

[21] A.B. Smith, P.T. Guenther, J.F. Whalen, "Fast-Neutron Scattering from Ta, Re, and Pt," *Phys. Rev.*, **168**, 1344 (1968).

28. Influences of Differences in Nuclear Data Libraries on Important Back-end Parameters

Shota YOSHIDA, Go CHIBA, Masashi TSUJI, Tadashi NARABAYASHI
Graduate School of Engineering, Hokkaido University,
Kita13-Nishi8, Kita-ku, Sapporo-shi, Hokkaido
e-mail: mellow.amber@eng.hokudai.ac.jp

It is considered that some evaluated values such as decay heat, decay chain and fission yield show differences among evaluated nuclear data libraries developed and released by several communities. This paper describes quantitative comparisons of calculated important back-end parameters among several different nuclear data libraries such as ENDF, JEFF and JENDL. We change fission product yield data and fission product decay data and focus on differences of decay heat and inventories of molybdenum, noble metals and I-129. Comparisons of decay heat and inventories of molybdenum and noble metals show no visible differences. By contrast, I-129 inventory has about 20% difference at maximum because of difference in fission product yields of Sn-129 and Sn-129m.

1. Introduction

It is important to accurately evaluate radionuclide waste inventories on back-end analysis. On the other hand, the inventories depend on the evaluated nuclear data library used for the evaluation. The evaluated nuclear data libraries have been developed and released in several countries for working up and using nuclear technology. ENDF (USA), JEFF (Europe) and JENDL (Japan) are commonly used as nuclear data libraries. Dependence of nuclear data libraries on back-end analysis has not been evaluated so far. It is considered that some evaluated values such as decay heat, decay chain and fission yield show difference among these evaluated nuclear data libraries. Therefore, quantitative comparisons of back-end parameters among these libraries are important.

The objectives of the present study are 1) to provide comparisons of decay heat and inventories of molybdenum, noble metals and other major nuclides among each result by using ENDF, JEFF and JENDL and 2) to investigate differences in these back-end parameters calculated with each library.

2. Parameters for comparison

Decay heat and inventories of molybdenum, noble metals and I-129 are adopted for comparison parameters. The reasons are as follows. High decay heat causes increase in the number of high-level-radionuclide-waste (HLW) canister due to heat generation limit of a HLW canister. This is because temperature of HLW glass should be maintained 750-800K to prevent the

deterioration of the chemical durability in storage period [1]. Separated molybdenum rich phase called “yellow phase” is formed in borosilicate waste glass when the MoO_3 density is more than 2 wt% [2]. This yellow phase consists of water-soluble compounds and deteriorates chemical durability of the glass. Noble metals such as ruthenium, rhodium, and palladium are insoluble in the borosilicate waste glass. These metals tend to form separate phase of alloy or oxide, accumulate at the melter bottom and form electrical short circuit in the liquid fed ceramic melter. It can cause melting capability decrease and electrode corrosion making the melter lifetime short [3]. I-129 is the key nuclide on the safety assessment for the geological disposal because of mobility in groundwater and long half life of about 16 million years.

3. Calculation

We use a code system CBZ which is being developed in Hokkaido University in the present study. We produce several burn-up chains by BurnupChainGenerator of CBZ. **Figure 1** shows utilized code system in the present study. We utilize JENDL-3.3[4], JENDL-4.0[5], JENDL/FPY-2011[6], JEFF-3.1.1[7] and ENDF/B-VII.1[8] for fission product yield data and JENDL/FPD-2011[6], JEFF-3.1.1 and ENDF/B-VII.1 for fission product decay data. Five chains are produced by combination of the above libraries. **Table 1** shows these chains. JEFF-3.1.1 is used for decay heat data of heavy metal in all the chains. PWR fuel pin-cell model is adopted for calculation model. UO_2 fuel is chosen for fuel type and burn-up is 45 GWd/tHM. U-235 enrichment is assumed to be 4.5 wt%. Conditions for burn-up calculation are summarized in **Table 2**.

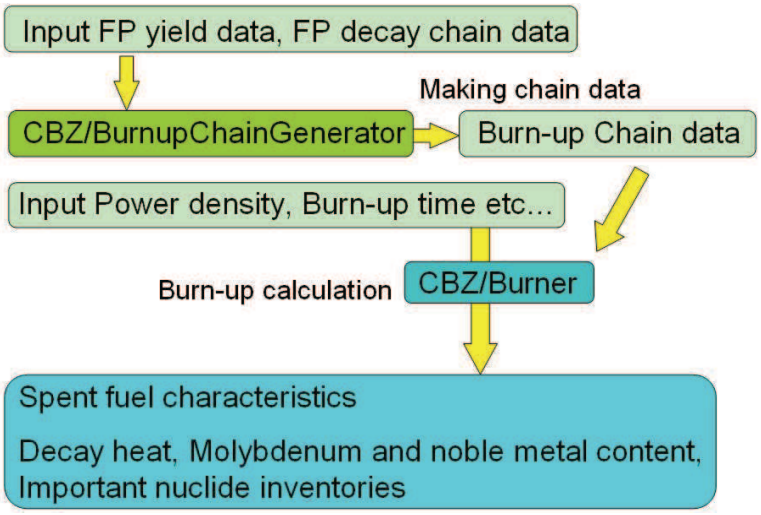

Figure 1 Code system CBZ

Table 1 Utilized Chains

Chain name	Fission product yield data	Fission product decay data
JEN33	JENDL-3.3	JENDL/FPD-2011
JEN40	JENDL-4.0	JENDL/FPD-2011
JENFPY11	JENDL/FPY-2011	JENDL/FPD-2011
JEF311	JEFF-3.1.1	JEFF-3.1.1
ENDFB71	ENDF/B-VII.1	ENDF/B-VII.1

Table 2 Calculation conditions

Calculation model	PWR fuel pin-cell model
Fuel type	UO_2 fuel
Burn-up [GWd/tHM]	45
Uranium enrichment [wt%]	4.5
Cooling time after burning [yr]	4 to 1000

4. Comparisons among calculation results

We compared decay heat calculated over 1000 years and inventories of molybdenum, noble metal and I-129 at 4 years cooling, by using the above five chains. Differences from JEN40 result among each result are expressed as

$$D = \frac{X_i - X_{JEN40}}{X_{JEN40}},$$

where

$X_{JEN40} = calculation\ \ value\ by\ the\ JEN40\ chain$

$X_i = calculation\ value\ by\ the\ i\ chain\ where\ i = JEN33, JENFPY11, JEF311, ENDFB71.$

Figure 2 shows comparisons of integrated decay heat for 1000 years. HM and FP in this figure denote heavy metal and fission products, respectively. Integrated fission product decay heat calculated by using the JEF311 chain is about 1.5 % smaller than JEN40. In contrast, there is no visible difference in HM integrated decay heat. **Figure 3** shows decay heat rate differences from JEN40 at 4, 10, 100 and 1000 years. Decay heat calculated by using the JEN33 chain is about 1 % bigger than the JEN40 result at 10 year cooling, since some nuclide inventories with high heat generation, such as Ba-137m and Y-90, are bigger. There are differences between the JEF311 and JEN40 results at 4, 10 and 100 year cooling. It is considered that one reason is difference in decay energy of Ba-137m. **Figure 4** shows inventory differences of molybdenum and noble metals including ruthenium, rhodium and palladium. The biggest difference is about 1.5 % between the JEN33 and JEN40 results. The I-129 inventory differences are shown in **Figure 5**. The I-129 inventory calculated by JEN33 is bigger by about 20 % from JEN40 and the JEF311 result is also bigger by about 10 %. These differences can influence back-end planning. For instance, it can lead to increase waste container and space for storage or disposal.

5. Analyzing I-129 inventory difference

In this section, differences in the I-129 inventory are investigated with a focus on fission yield data. Nuclide with large yield from U-235 and Pu-239 fission on the decay route to I-129 is Tin as shown in **Figure 6**. **Table 3** shows cumulative fission yields of I-129 and independent fission yields of Sn-129 and Sn-129m from U-235 and Pu-239 fission at thermal energy region. Cumulative fission yields of I-129 from U-235 fission in JENDL-3.3 and JEFF-3.1.1 are evaluated by about 30% bigger than the value of JENDL-4.0. In JENDL-3.3 and JEFF-3.1.1, independent fission yields of Sn-129 and Sn-129m from U-235 fission, which are parent nuclides of I-129, are also bigger than JENDL-4.0. These differences have mainly impact on cumulative fission yield of I-129. The I-129 inventory calculated by ENDF/B-VII.1 does not differ much from the JEN40 result, but independent fission yields of Sn-129 and Sn-129m show difference from evaluated values in other nuclear data libraries.

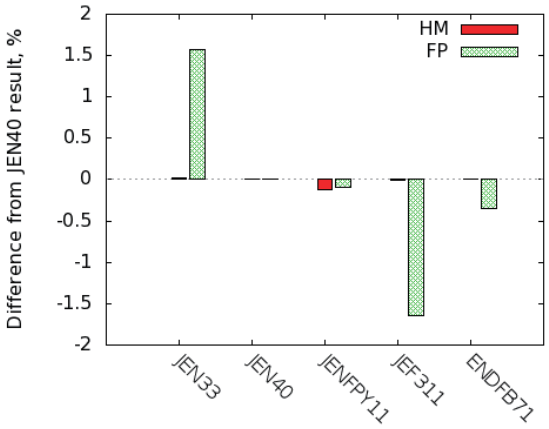

Figure 2 Integrated decay heat differences

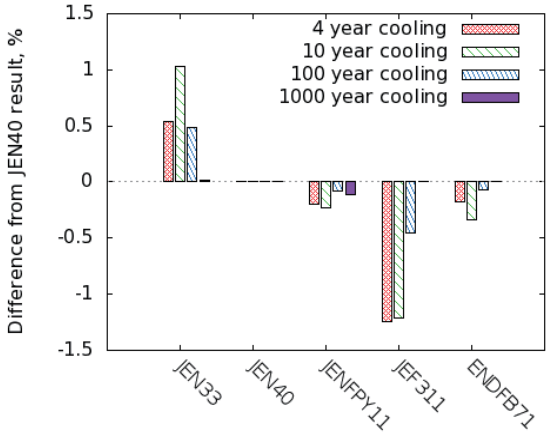

Figure 3 Decay heat rate differences

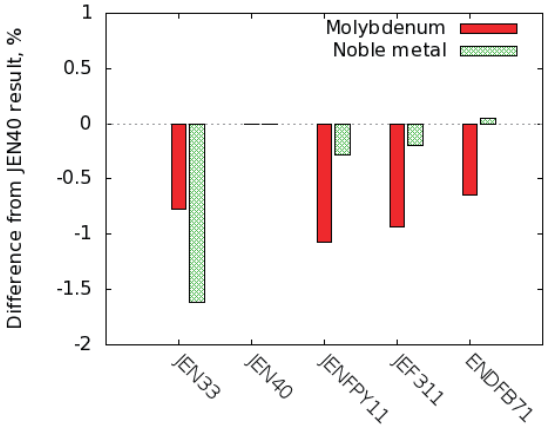

Figure 4 Molybdenum and noble metals inventory differences

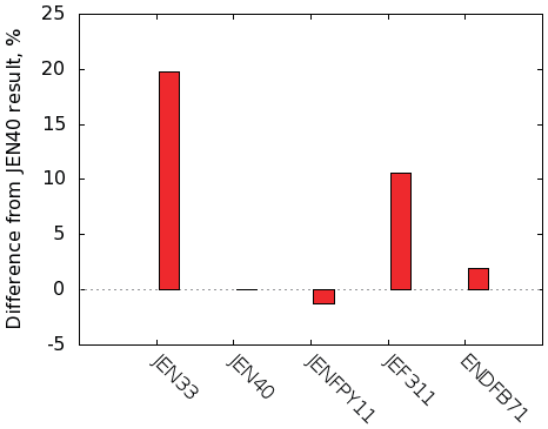

Figure 5 I-129 inventory differences

Table 3 Fission yields of I-129, Sn-129 and Sn-129m from U-235 and Pu-239 fission

Data library	Cumulative FYs of I-129 from U-235 / Pu-239 (0.025eV)	Independent FYs of Sn-129 from U-235 / Pu-239 (0.025eV)	Independent FYs of Sn-129m from U-235 / Pu-239 (0.025eV)
JENDL-3.3	**7.178E-03** / 1.393E-02	**1.639E-03** / 2.590E-03	**3.957E-03** / 6.253E-03
JENDL-4.0	5.432E-03 / 1.321E-02	1.247E-03 / 2.870E-03	3.008E-03 / 6.925E-03
JENDL/FPY-2011	5.376E-03 / 1.321E-02	1.247E-03 / 2.870E-03	3.009E-03 / 6.925E-03
JEFF-3.1.1	**7.061E-03** / 1.407E-02	**1.758E-03** / 2.409E-03	**4.243E-03** / 5.815E-03
ENDF/B-VII.1	5.433E-03 / 1.371E-02	2.303E-03 / 6.906E-03	1.959E-03 / 2.891E-03

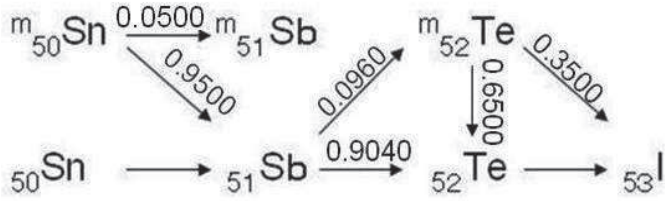

Figure 6 Decay route to I-129 [9]

6. Conclusion

Important back-end parameters, such as decay heat and inventories of molybdenum, noble metals and I-129, have been compared by using five chains. Visible differences among results of each chain are almost none except the I-129 inventory. The I-129 inventory in the JEN33 chain is about 20% bigger than the result inthe JEN40 chain due to difference in fission yields of Sn-129 and Sn-129m, which are parent nuclides of I-129, from U-235 and Pu-239 fission at thermal energy region. The I-129 inventory has small difference of 2 % between JEN40 and ENDF/B-VII.1, while fission yields of Sn-129 and Sn-129m in ENDF/B-VII.1 show different values from other nuclear data libraries.

References

[1] Second Progress Report on Research and Development for the Geological Disposal of HLW in Japan; H12 Project to Establish the Scientific and Technical Basis for HLW Disposal in Japan, Supporting Report 2: Repository Design and Engineering Technology, JNC TN1410 2000-003, JNC, Japan (2000)

[2] W. Luze, R. C. Ewing (Eds), Radioactive Waste Forms for the Future, North-Holland Physics Publishing (1988)

[3] H. Ikeda, N. Endo, *et al.*, “Cold test for improvement of the glass melter performance,” JNC Technical Reviews, No. **14**, 25 (2002), [in Japanese]

[4] K. Shibata, T. Kawano, *et al.*,"Japanese Evaluated Nuclear Data Library Version 3 Revision-3: JENDL-3.3", J. Nucl. Sci. Technol. **39**, 1125 (2002).

[5] K. Shibata, O. Iwamoto, *et al.*,"JENDL-4.0: A New Library for Nuclear Science and Engineering," J. Nucl. Sci. Technol. **48**(1), pp.1-30 (2011)
[6] J. Katakura, "JENDL FP Decay Data File 2011 and Fission Yields Data File 2011", JAEA-Data/Code 2011-025 (March 2012)
[7] A. Santamarina, D. Bernard, Y. Rugama: "The JEFF-3.1.1 Nuclear Data Library", JEFF Report 22 (2009).
[8] M.B. Chadwick, M. Herman, *et al.*, "ENDF/B-VII.1 Nuclear Data for Science and Technology: Cross Sections, Covariances, Fission Product Yields and Decay Data", Nucl. Data Sheets, **112**, pp.2887-2996 (2011).
[9] K. Tasaka, J. Katakura, *et al.*, "JNDC Nuclear Data Library of Fission Products, - Second Version -", JAERI 1320 (1990)

Appendix

Independent fission yields of parent nuclides of I-129 except Sn-129 and Sn-129m shown in Figure 6 are shown in **Table 4**.

Table 4 Independent fission yield of Sb-129, Te-129 and Te-129m

	Sb-129		Te-129		Te-129m	
Fissile (thermal)	U-235	Pu-239	U-235	Pu-239	U-235	Pu-239
JENDL-3.3	7.89E-03	1.47E-05	3.56E-05	4.30E-03	1.10E-04	2.66E-04
JENDL-4.0	2.47E-04	5.77E-08	1.39E-07	1.46E-03	1.98E-06	4.77E-06
JENDL/FPY-2011	2.47E-04	5.77E-08	1.39E-07	1.47E-03	1.98E-06	4.77E-06
JEFF-3.1.1	2.83E-04	1.78E-08	4.30E-08	2.69E-03	7.76E-05	1.87E-04
ENDF/B-VII.1	6.41E-04	5.73E-08	1.40E-07	3.81E-03	1.96E-06	4.79E-06

29. Study on keV-neutron Capture Cross Sections and Capture Gamma-ray Spectra of Pd Isotopes

K. Terada, T. Matsuhashi, T. Katabuchi, M. Igashira,

Research Laboratory for Nuclear Reactors, Tokyo Institute of Technology, 2-12-1 Ookayama, Meguro-ku, Tokyo 152-8550

E-mail: terada.k.aa@m.titech.ac.jp

The capture cross sections and capture gamma-ray spectra of ^{104,105,106,108,110}Pd were measured in the neutron energy region of 15-100 keV. A neutron time-of-flight method was utilized by means of an anti-Compton NaI(Tl) spectrometer and a nsec pulsed neutron source via the ^{7}Li(p,n)^{7}Be reaction. The capture yields were obtained by applying a pulse-height weighting technique to the net capture gamma-ray pulse-height spectra. The capture cross sections of ^{104,105,106,108,110}Pd were derived with errors of less than 6%, using the standard capture cross sections of ^{197}Au. The capture gamma-ray spectra of ^{104,105,106,108,110}Pd were also derived by unfolding the respective observed capture gamma-ray pulse-height spectra. Additionally, the theoretical calculation was made by means of the CCONE computer code.

1 Introduction

The nuclear transmutation of long-lived fission products (LLFPs) into stable or short-lived nuclides by neutron capture reaction is expected to reduce the impact on the environment by nuclear waste disposal on the environment. Palladium-107 (half life: 6.5×10^{6} y) is one of the most important LLFPs, and its neutron capture cross sections are important for the study of LLFP transmutation systems. On the other hands, the capture cross sections of stable Pd isotopes also affect the performance of a transmutation system without isotope separation. Therefore, their capture cross sections as well as those of ^{107}Pd are important for the R&D of nuclear transmutation systems. Additionally, capture gamma-ray spectra contain much information on important physical quantities such as gamma-ray strength function, and the information is quite useful for theoretical calculation of neutron capture cross sections of Pd isotopes, especially ^{107}Pd. From the viewpoint mentioned above, we started a systematic series of studies on keV-neutron capture cross sections and capture gamma-ray spectra of Pd isotopes (^{104,105,106,108,110}Pd and ^{107}Pd), using a time-of-flight method with a pulsed ^{7}Li(p,n)^{7}Be neutron source and a large anti-Compton NaI(Tl) gamma-ray spectrometer. We completed measurement for ^{104,105,106,108,110}Pd in the neutron energy of 15-100 keV. Moreover, the theoretical calculations of capture cross sections and capture gamma-ray spectra were made by using the CCONE[1)] computer code.

2 Experimental Procedure and Analysis

The keV-neutron capture cross sections and capture gamma-ray spectra were measured in the neutron energy region of 15-100 keV by means of the 3 MV Pelletron accelerator at the

Research Laboratory for Nuclear Reactors of the Tokyo Institute of Technology.

Pulsed proton beams from the accelerator produce a 1.5 nsec pulsed neutron beam via the ^{7}Li(p,n)^{7}Be reaction.

We used isotopically enriched Pd and standard ^{197}Au samples. The distance between the neutron source and the sample was 12 cm. The capture gamma-rays emitted from the sample were measured with an anti-Compton NaI(Tl) spectrometer. The signals from the spectrometer were accumulated event by event as time-of-flight (TOF) and Pulse Height(PH) data. The incident neutron energy spectra were measured by a time-of-flight method with a ^{6}Li-glass scintillation detector.

Table 1 shows details of samples. Pd samples had chemical purities of higher than 99.97% and isotopic purities of higher than 93%. The ^{104,108,110}Pd samples were formed into disks by using a pressing machine and were then sealed with Mylar films. The ^{105,106}Pd samples were sealed in a graphite case. Two standard Au samples which respectively matched the dimensions of the Pd samples were also used.

We carried out the measurements cyclically for the Pd sample, the Au sample, and a blank run, in order to average experimental conditions.

The incident neutron energy spectra were obtained from the TOF spectra measured with a ^{6}Li-glass detector from the no sample measurement. Four neutron energy regions were set in the incident neutron energy spectrum, and average capture cross sections were derived for these neutron energy regions, respectively.

Four gates, corresponding to the four neutron energy regions, were set in the foreground region of the TOF spectra measured with the NaI(Tl) spectrometer, and one gate was set in the time-independent background region in the TOF spectra. Then the foreground and background PH spectra were obtained from the Pd and Au measurements.

A pulse height weighting technique[2] was applied to the net PH spectra in order to obtain the capture yields of Pd and Au. Finally, the capture cross sections of ^{104,105,106,108,110}Pd were derived with the standard capture cross sections of ^{197}Au[3]. Moreover, the capture gamma-ray spectra were derived by unfolding the net capture gamma-ray PH spectra with the FERDOR computer code[4] and the response matrix of the NaI(Tl) spectrometer.

Table 1: Characteristics of samples

Sample	^{104}Pd	^{105}Pd	^{106}Pd	^{108}Pd	^{110}Pd	^{197}Au
Form	Metal powder	Metal powder	Metal powder	Metal powder	Metal powder	Metal
Purity [%]	99.97	99.97	99.97	99.97	99.97	99.99
Net weight [g]	0.690	0.487	0.853	0.657	0.686	3.42 or 6.02
Composition [%]						
^{102}Pd	< 0.03	< 0.03	< 0.03	< 0.02	< 0.05	
^{104}Pd	98.35	0.16	0.06	4.83	0.10	
^{105}Pd	1.05	98.4	0.68	0.15	0.35	
^{106}Pd	0.35	1.24	98.4	0.90	0.50	
^{108}Pd	0.18	0.15	0.80	93.8	0.70	
^{110}Pd	< 0.05	0.05	0.06	0.30	98.3	
^{197}Au						100
Diameter [mm]	15	20	15	15	15	15 or 20.1
Thickness [mm]	0.5	2.22	2.3	0.5	0.5	1.0 or 1.05
Case	Mylar	Graphite	Graphite	Mylar	Mylar	

3 Theoretical Calculation

Theoretical calculations were performed by using the CCONE[1)] computer code. First, coupled channel optical calculation was applied to reproduce the total cross sections and elastic scattering angular distribution for natural palladium, and the neutron transmission coefficients were obtained which are used in statistical model calculations by CCONE. Next, the calculation of capture cross sections and capture gamma-ray spectra for palladium isotopes were made by using CCONE code based on the Hauser-Feshbach statistical model.

The generalized Lorentzian was used as the gamma-ray strength functions in order to obtain the neutron capture cross sections and capture gamma-ray spectra of ^{104,105,106,108,110}Pd. The gamma-ray strength functions were adjusted to reproduce the present experimental results both capture cross sections and capture gamma-ray spectra. The data of discrete level and decay branching ratio were adopted from Reference Input Parameter Library for Calculation of Nuclear Reactions and Nuclear Data Evaluations (RIPL-3)[5)]. The nuclear level density was derived from the constant temperature model and Fermi-Gas model that is predicated on the systematics of Mengoni-Nakajima[6)].

4 Results

4.1 Capture Cross sections

The capture cross sections of ^{104,105,106,108,110}Pd were derived with errors of less than 6% in the neutron energy region of 15-100 keV. Figure 1 shows the present experimental results together with previous measurements, evaluated values, calculation results.

For ^{104}Pd, there are two previous measurements: those of Macklin[7)] and Cornelis *et al.*[8)]. Their measurements are in good agreements with the present measurements. The evaluations of JENDL-4.0[3)] and ENDF/B-Ⅶ.1[9)] are also in good agreement with the present measurements. For ^{105}Pd, there are four previous measurements: Ro *et al.*[10)], Cornelis *et al.*[8)], Macklin[7)], and Hockenbury *et al.*[11)]. Comparing the previous measurements with the present results, the previous measurements are larger than the present measurements by 10-20%. The evaluations of JENDL-4.0 and ENDF/B-Ⅶ.0 are also larger than the present results by 6-10%. For ^{106}Pd, there are two previous measurements: those of Macklin[7)] and Cornelis *et al.*[8)]. The previous measurements are larger than the present measurements by 15-22%. For ^{108}Pd, there are two previous measurements: those of Macklin[7)] and Cornelis *et al.*[8)]. Their measurements are in good agreements with the present measurements. For ^{110}Pd, there are two previous measurements: those of Macklin[7)] and Cornelis *et al.*[8)]. Measurements of Macklin are in good agreements with the present measurements.

4.2 Capture Gamma-ray Spectra

The keV-neutron capture gamma-ray spectra of ^{104,105,106,108,110}Pd were derived from the present measurements. Figure 2 shows the present measurements and calculations, respectively. The calculations of the gamma-ray strength functions were made by using the Giant Dipole Resonance (GDR) parameters of RIPL-3. Additionally, the gamma-ray strength functions were adjusted in order to reproduce the present experimental results.

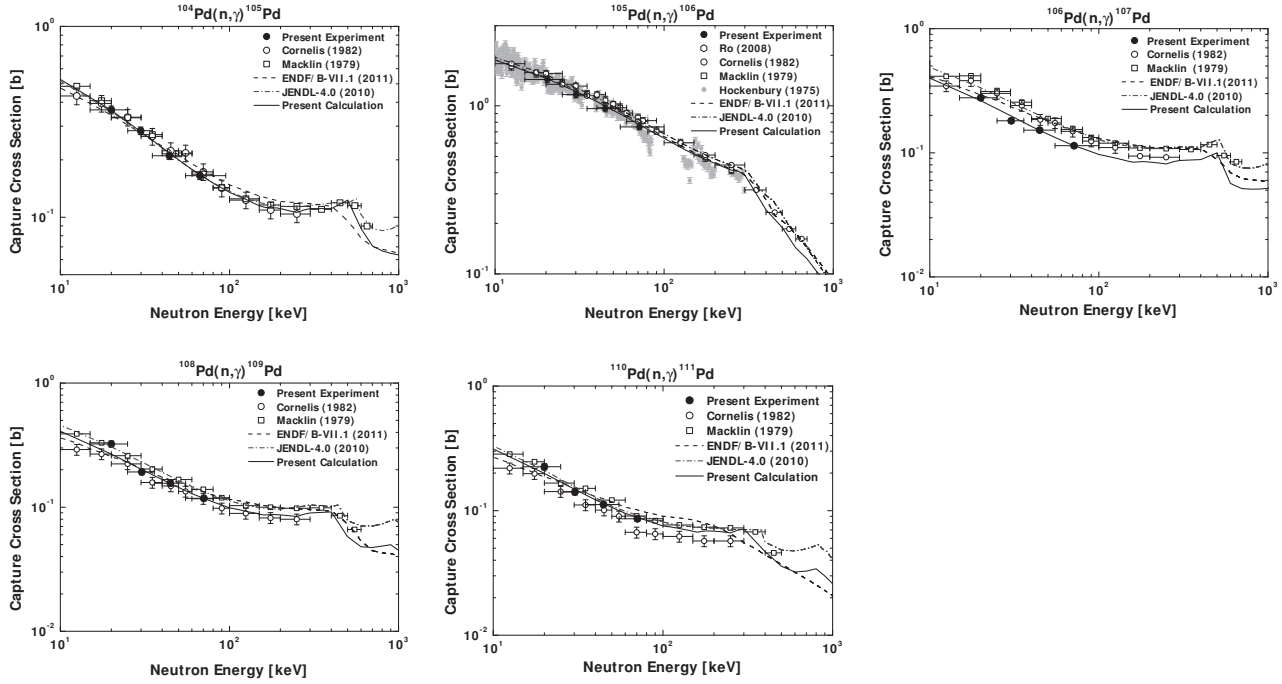

Figure 1: The keV-neutron capture cross sections of ^{104,105,106,108,110}Pd. Circles indicate the present measurements. Those are plotted at the average neutron energies, and the horizontal bars indicate the neutron energy regions. Solid lines indicate the calculation results by using the CCONE. Dashed lines indicate the evaluations of JENDL-4.0 and ENDF/B-VII.1.

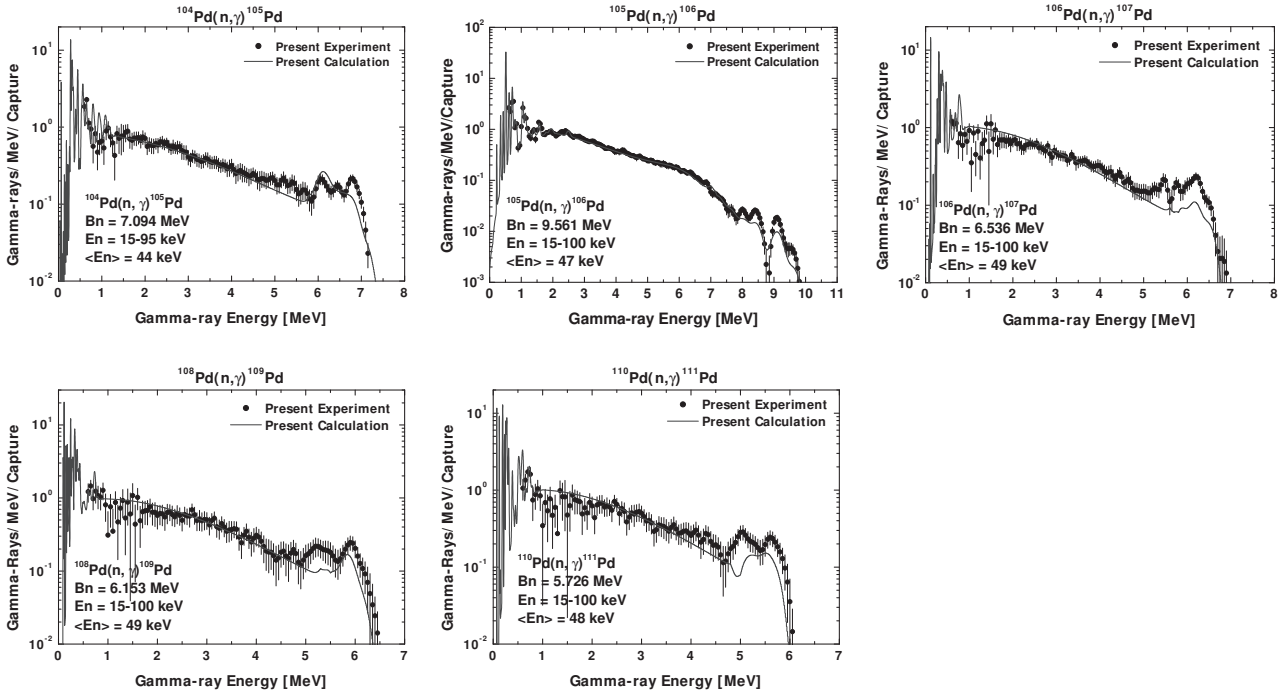

Figure 2: The keV-neutron capture gamma-ray spectra of ^{104,105,106,108,110}Pd. Circles indicate the present measurements. Solid lines indicate the calculation results.

5 Conclusion

We have measured the keV-neutron capture cross sections and capture gamma-ray spectra of ^{104,105,106,108,110}Pd in the neutron energy region of 15-100 keV. The neutron capture cross sections of ^{104,105,106,108,110}Pd have been derived with errors of less than 6%. The keV-neutron capture gamma-ray spectra of ^{104,105,106,108,110}Pd were derived for the first time. In addition, a calculation of capture cross sections and capture gamma-ray spectra has been performed to reproduce the present results.

Acknowledgments

This work was supported by KAKENHI (22226016).

References

1) O. Iwamoto, *J. Nucl. Sci. Technol*, **44**, 687-697 (2007).

2) R. L. Macklin and J. H. Gilbbons, *Phys. Rev.*, **159**, 1007-1012 (1967).

3) K. Shibata *et al.*, *J. Nucl. Sci. Technol.*, **48**, 1-30 (2011).

4) H.Kendrick *et al*, *Gulf Radiation Technology*, **GA-9882**, (1970).

5) R. Capote *et al.*, Reference Input Parameter Library (RIPL-3), http://www-nds.iaea.org/RIPL-3, (2009)

6) A. Mengoni and Y. Nakajima, *J. Nucl. Sci. Technol.*, **31**, 151-162 (1994).

7) R. L. Macklin, *Nucl. Sci. Eng.*, **71**, 181-191 (1979).

8) E. Cornelis *et al.*, *Proc. Int. Conf. Nuclear Data for Science and Technology, 1982, Antwerp, Belgium*, p.222 (1982).

9) M. B. Chadwick *et al.*, (CSEWG collaboration), *Nucl. Data Sheets*, **102**, 2931-3060 (2006).

10) T. I. Ro *et al.*, *Journal of the Korean Physical Society*, **5**, 1598-1603, (2007).

11) R. W. Hockenbury *et al.*, *Proc. Int. Conf. on Nucl. Cross-Sect. and Techn., 1975, Washington, USA*, **2**, p.905 (1975).

This is a blank page.

30. Measurements and Simulations of the Responses of the Cluster Ge Detectors to Gamma Rays

Kaoru Y. HARA*, Shinji GOKO†, Hideo HARADA, Kentaro HIROSE, Atsushi KIMURA, Tadahiro KIN‡, Fumito KITATANI, Mitsuo KOIZUMI, Shoji NAKAMURA and Yosuke TOH

Nuclear Science and Engineering Directorate, Japan Atomic Energy Agency

Tokai-mura, Naka-gun, Ibaraki-ken 319-1195 Japan

Present address: †Japan Nuclear Energy Safety Organization, Tokyo 105-0001 Japan

‡Kyushu University, Fukuoka 816-8580 Japan

*e-mail: hara.kaoru@jaea.go.jp

Responses of cluster Ge detectors have been measured with standard γ-ray sources and the $^{35}Cl(n,\gamma)^{36}Cl$ reaction in ANNRI at J-PARC/MLF. Experimental results and simulations using the EGS5 code are compared.

1. Introduction

Responses of 2 cluster Ge detectors have been measured in the Accurate Neutron-Nucleus Reaction Measurement Instrument (ANNRI) [1, 2] at the Materials and Life Science Experimental Facility (MLF) of the Japan Proton Accelerator Research Complex (J-PARC). And the simulations have been made using the Monte Calro simulation code, EGS5 [3]. The responses will be used for the data analysis for measurements of neutron capture cross sections in ANNRI with the pulse-height weighting technique [4].

2. Measurement and simulation

The schematic view of the experimental setup is shown in **Fig. 1**. The Ge detector system which comprises 2 cluster Ge detectors with BGO anti-coincidence detectors is placed at the neutron flight length of 21.5 m. Each cluster Ge detector consists of 7 pure germanium crystals. Each crystal has a hexagonal shape with a distance between sides of hexagon of 58 mm, an external diameter of 70 mm, and a depth of 78 mm. The distance is 125 mm from a sample to the front of the cluster Ge detector. The setup of the neutron and γ-ray shields (^{6}LiH, Pb, and borated silicone rubber) between the sample and each detectors is at the same position in Ref. [5] except for the position of Pb plate of 3-mm thick.

In the response measurements with/without the rejection of events with signals in BGO detectors (“BGO anti-coincidence”), γ-ray from standard sources of ^{60}Co and ^{137}Cs were used for a

low-energy region (E_γ<2 MeV), while prompt γ-rays emitted from the ^{35}Cl(n,γ) reactions were used for a high-energy region (E_γ=7.5-8.6 MeV). The sample was a 0.5-g NaCl crystal (natural abundance). Also a 3-g ^{208}Pb pellet was used as a sample to estimate the background caused by the nuclear reactions of the structural materials with the scattering neutrons from the NaCl sample. In addition, ^{133}Ba and ^{152}Eu standard sources were used in the measurements of the full-energy peak efficiencies.

The γ-ray detection signals from each Ge crystals are recorded with a data acquisition system (DAQ) [6] based on a digital data processing technique. Random timing pulses from a random pulse generator were input to the pre-amplifiers of every Ge crystals for dead time correction of the DAQ. Therefore the events of the random timing pulses and γ-ray detection signals were recorded with the DAQ. At the same time, the number of the random timing pulse was counted with a scaler module (N_s). The pulse rate was approximately 1 kcps. For example, the pulse-height spectrum of the ^{35}Cl(n,γ) reaction measured with one Ge crystal is shown in Fig. 2. The pulse height of the random timing pulse is adjusted above 10 MeV to avoid overlap the spectrum of the ^{35}Cl(n,γ) reaction. The live-time rate of DAQ (D) is estimated as N_D/Ns, where N_D is the number of counts of the random timing pulse in the spectrum.

In order to reproduce the measurement results, the pulse-height spectra were calculated using the EGS5 code in the γ-ray energy region of 0.2-10 MeV, where a γ-ray source was a point source at the sample position. In this work, we report about the spectra measured and simulated without BGO anti-coincidence.

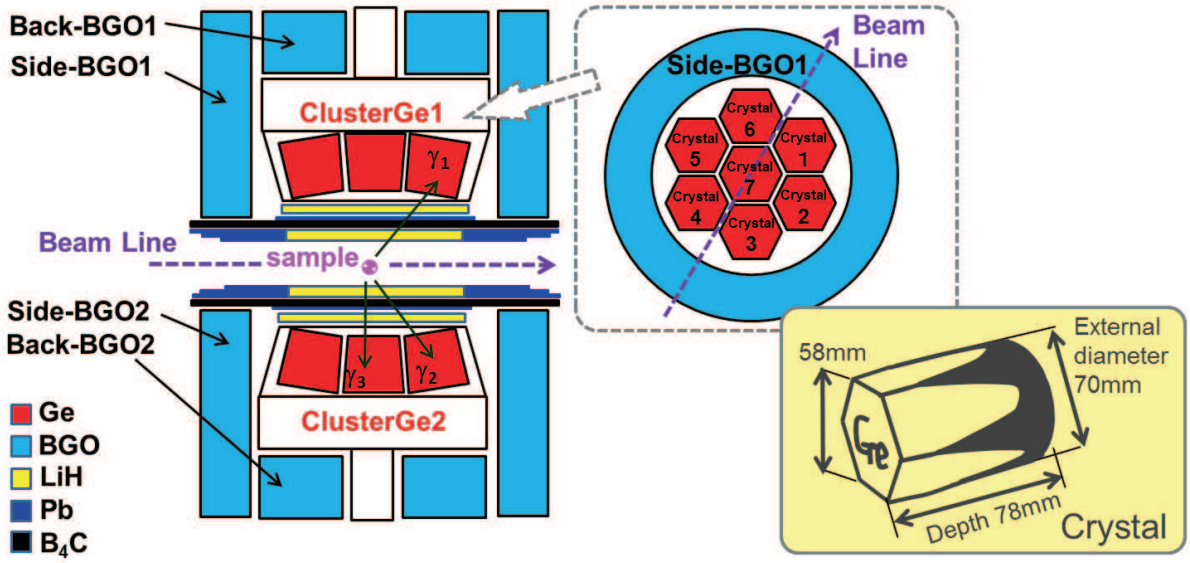

Figure 1: Schematic illustration of the experimental setup of the cluster Ge detectors with the BGO anti-coincidence detectors. The upper and lower Ge detectors are called as “cluster1” and “cluster2”, respectively.

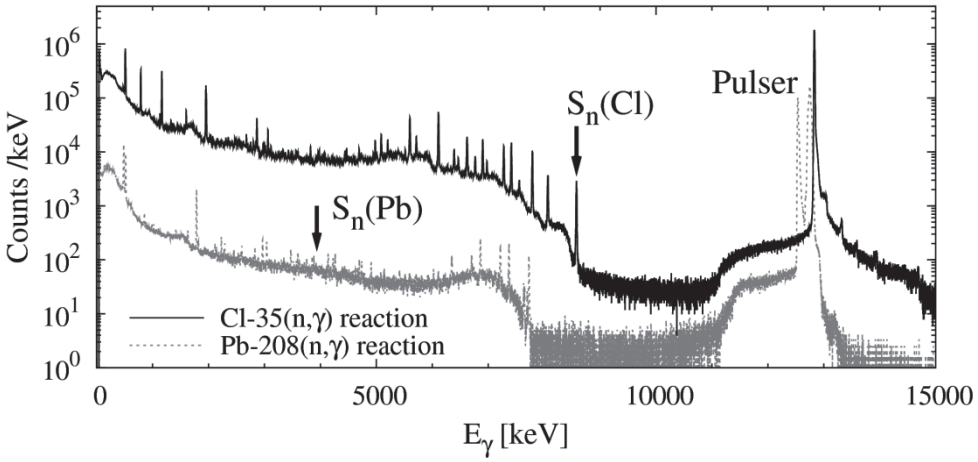

Figure 2: γ-ray pulse-height spectra of the ^{35}Cl(n,γ) and ^{208}Pb(n,γ) reactions measured in the neutron energy range of 0.01-16 eV with one of the Ge crystals. The peak at 12-13 MeV is pulser signals. The arrows indicate the separation energies of ^{36}Cl (S_n=8.6 MeV) and ^{209}Pb (S_n=3.9 MeV). Most of the gray line shows background specrum since the capture cross section of ^{208}Pb is very small.

3. γ-ray pulse-height spectra for ^{137}Cs and ^{60}Co sources and ^{35}Cl(n,γ) reaction

The measured pulse-height spectra for the ^{137}Cs and ^{60}Co sources are plotted by the black circles in **Figs. 3** and **4**, respectively. Figs. 3 (a) and (b) (or Figs. 4 (a) and (b)) show the spectra that were measured by the "cluster1" and "cluster2" detectors, respectively. After the dead time correction and the background subtraction, 7 spectra of Ge crystals in cluster1 (or cluster2) are summed into a "single" spectrum. For comparison, the spectra which are calculated with the EGS5 code are plotted by the gray lines.

In this data analysis, the area of the full-energy peak (P) is obtained by a following procedure because the full-energy peak has an asymmetry shape with a tail at the high energy side. Firstly, the full-energy peak in the measured spectrum is fitted by a gauss function. Secondly, the number of counts in the spectrum from E_m-W to E_m+3W is integrated in N_0, where E_m and σ are the peak energy and width of the gauss function, respectively, and W is 3.5σ. Then the numbers of counts in the spectrum from E_m-1.5W to E_m-W and from E_m+3W to E_m+3.5W are integrated in N_1 and N_2, respectively. Finally,

$$P = N_0 - 4(N_1 + N_2) \quad (1)$$

is calculated. The total area (T) is defined as the total number of counts in the spectrum from an experimental discrimination level (100 keV) to E_m+3W. The experiment-to-calculation ratios (E/C) of the peak-to-total ratio (P/T),

$$R = [E/C] = [P/T]_{exp} / [P/T]_{cal} \quad (2)$$

are 0.94 (cluster1)/0.93 (cluster2) for the γ-rays of the ^{137}Cs source (662 keV) and 0.96 (cluster1)/0.93 (cluster2) for the γ-rays of the ^{60}Co source (1173 and 1332 keV). As shown in Figs. 3 and 4, these

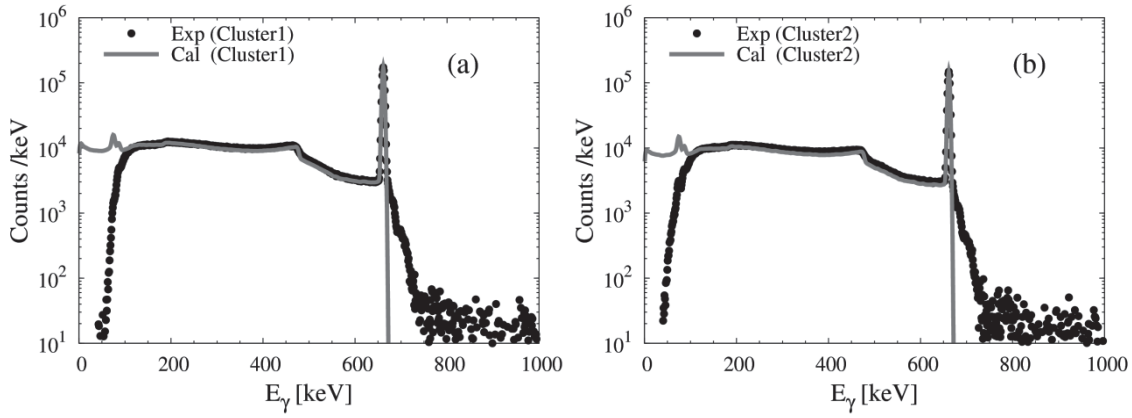

Figure 3: γ-ray pulse height spectra for the ^{137}Cs source were measured by the cluster1 (a) and cluster2 detectors (b), respectively (black circles). The simulated spectra are shown by the gray lines.

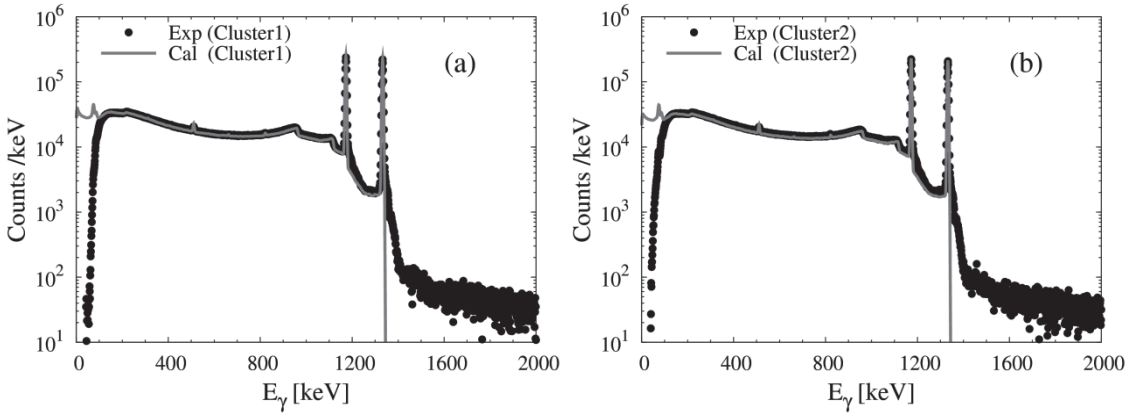

Figure 4: γ-ray pulse height spectra for the ^{60}Co source were measured by the cluster1 (a) and cluster2 detectors (b), respectively (black circles). The simulated spectra are shown by the gray lines.

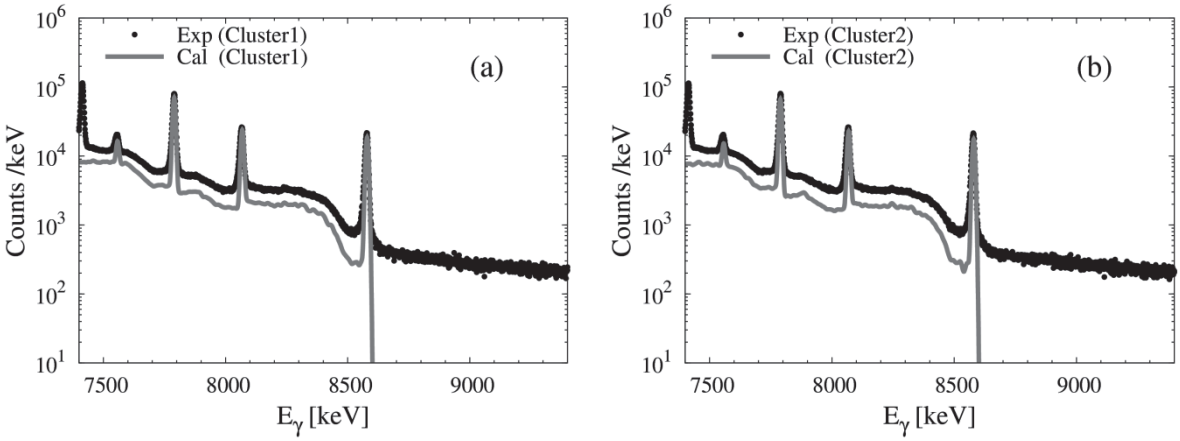

Figure 5: γ-ray pulse height spectra for the ^{35}Cl(n,γ) reaction were measured by the cluster1 (a) and cluster2 detectors (b), respectively (black circles). The simulated spectra are shown by the gray lines.

simulated spectra are reasonable agreement with the measured spectra. The full-energy peak area of the simulated spectrum is normalized by one of the measured spectrum and the spectrum is degraded by the gauss function.

In the similar way, the measured spectrum of the ^{35}Cl(n,γ) reaction in the neutron energy region of 0.01-16 eV is plotted in **Fig. 5**. In Fig. 5, the background is subtracted with the measured spectrum for the ^{208}Pb(n,γ) reaction (see Fig. 2). However the residual component due to pile-up is shown above 8.7 MeV. For the spectrum of the ^{35}Cl(n,γ) reaction, the simulation is needed to reflect on a counting rate. Further fitting for simulation parameters are in progress including the data are measured with BGO anti-coincidence.

4. Full-energy peak efficiencies

The γ-rays of the standard sources (^{60}Co, ^{133}Ba, ^{137}Cs, and ^{152}Eu) and the prompt γ-ray from the ^{35}Cl(n,γ) reaction are used to determine the full-energy peak efficiencies. In the data analysis to obtain the area of the full-energy peak, Eq. (1) is replaced as

$$P' = N_3 - 2(N_1 + N_4), \quad (3)$$

because it is not easy to apply Eq. (1) to neighboring peaks, where N_3 and N_4 are the numbers of counts in the spectrum from E_m-W to E_m+W and from E_m+W to E_m+1.5W, respectively. Although this procedure underestimates P' due to the tail of the full-energy peak, the systematic uncertainty in P' is estimated to less than 3% based on P'/P for the 662, 1173, and 1333-keV γ-rays.

The efficiencies for the measurements with the cluster1 and cluster2 detectors are shown in **Fig. 6(a)** and **(b)**, respectively. The data of the ^{60}Co, ^{133}Ba, ^{137}Cs, and ^{152}Eu source are shown as the square, triangle, diamond, and circle, respectively. The plotted error bar has the following sources in quadrature; the statistical uncertainty in P', the uncertainty of emitted γ-ray intensity, and the uncertainty of standard source activity. The data of the ^{35}Cl(n,γ) reaction (inverted triangle) are normalized to the data of the standard sources, where the γ-ray pulse-height spectrum for the ^{35}Cl(n,γ) reaction gated in the neutron energy region 0.01-16 eV were used. The simulated result (gray line) is normalized to the datum of ^{137}Cs source. As shown in Fig. 6, the energy dependence of the simulated efficiencies reproduces the measurement results.

5. Conclusion

To obtain the responses, the γ-rays from the standard sources (^{60}Co, ^{133}Ba, ^{137}Cs, and ^{152}Eu) and the prompt γ-ray from the ^{35}Cl(n,γ) reaction were measured with the cluster Ge detector system at ANNRI in J-PARC/MLF. The γ-ray pulse-height spectra, peak efficiencies, and peak-to-total ratio were compared with the simulations using the EGS5 code. The simulations are in reasonable agreement with the experimental results without BGO anti-coincidence. Further fitting for simulation parameters are currently in progress including the data measured with BGO anti-coincidence.

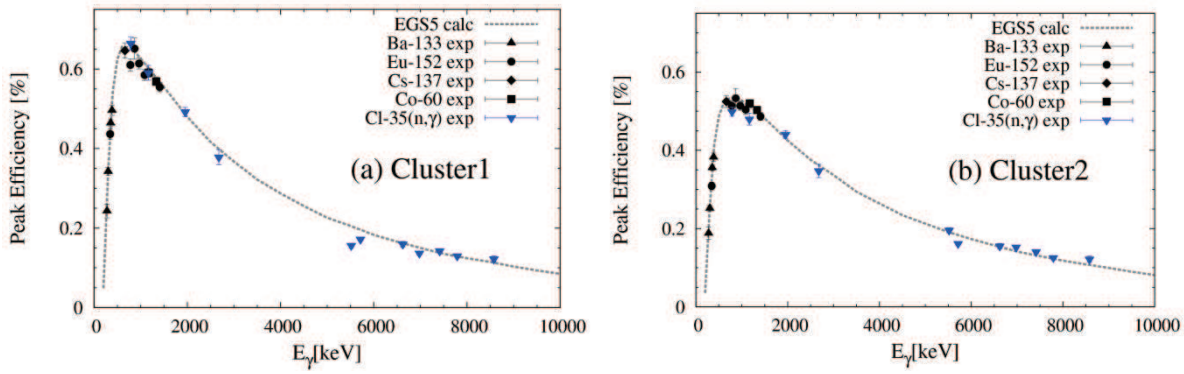

Figure 6: Full-energy peak efficiencies for the γ-rays from the standard sources (^{60}Co, ^{133}Ba, ^{137}Cs, and ^{152}Eu) and the prompt γ-rays from the ^{35}Cl(n,γ) reaction. The data points are measured with the cluster1 (a) and cluster2 detectors (b), respectively. The lines are the simulations.

Acknowledgements

The authors would like to thank the staffs of J-PARC and MLF for their operations of the accelerators and the neutron production target. This work was supported by JSPS KAKENHI Grant Number 22226016.

References

[1] Igashira M, Kiyanagi Y, Ohshima M. Nculear data study at J-PARC BL04. Nucl. Instr. Methods, 2009; A**600**: pp.332-334.

[2] Kimura A, Fujii T, Fukutani S, Furutaka K, Goko S, Hara KY, Harada H, Hirose K, Hori J, Igashira M, Kamiyama T, Katabuchi T, Kin T, Kino K, Kitatani F, Kiyanagi Y, Koizumi M, Mizumoto M, Nakamura S, Ohta M, Oshima M, Takamiya K, Toh Y. Neutron-capture cross-sections of ^{244}Cm and ^{246}Cm measured with an array of large germanium detectors in the ANNRI at J-PARC/MLF. J. Nucl. Sci. Technol., 2012; **49**: pp.708-724.

[3] Hirayama H, Namito Y, Bielajew AF, Wilderman SJ, Nelson WR. 2005. The EGS5 Code Systems. KEK Report 2005-8, SLAC-R-730. High Energy Accelerator Research Organization (KEK), Stanford Linear Accelerator Center (SLAC).

[4] Abbondanno U (n_TOF Collaboration) New experimental validation of the pulse height weighting technique for capture cross-section measurements. Nucl. Instr. Methods, 2004; A**521**: pp.454-467.

[5] Goko S, Kimura A, Harada H, Oshima M, Ohta M, Furutaka K, Kin T, Kitatani F, Koizumi M, Nakamura S, Toh Y, Igashira M, Katabuchi T, Mizumoto M, Kiyanagi Y, Kino K, Furusaka M, Hiraga F, Kamiyama T, Hori J, Fijii T, Fukutani S, Takamiya K. Measurement of neutron capture cross section ratios of ^{244}Cm resonances using NNRI. J. Nucl. Sci. Technol. 2010;**47**: pp.1097-1100.

[6] Kimura A, Toh Y, Koizumi M, Furutaka K, Kin T, Ohshima M. Performance of a High Density Data Acquisition System for Multiple Gamma-Ray Detection, NSS-MIC 2008, Dresden, Germany 19-25 October 2008, pp. 2107-2111, 2009.

31. Development of keV region neutron spectrometer using ^{3}He proportional counter

Tsubasa Obata, Masao Ito,and Isao Murata,
Division of Electrical, Electronic and Information Engineering, Graduate School of Engineering,
Osaka University, Yamada-oka 2-1, Suita, Osaka 565-0871, Japan
E-mail: tobata@ef.eie.eng.osaka-u.ac.jp

At present, measurement of energy spectrum for thermal and epi-thermal neutrons becomes crucial to apply to the medical, as well as physical applications. We have been carrying out the series of studies concerning the thermal/ep-ithermal spectrometer especially for BNCT. In the present paper, we described the preliminary result of ongoing development of a new thermal and epi-thermal neutron spectrometer using the detection depth information measured by a commercially available ^{3}He position sensitive proportional counter. From the measurement, the detection position distribution were obtained as a two dimensional spectrum. And the detector was confirmed to detect coincident signals appropriately at Z=6~34cm. It means in other words that the measurable energy range was thus from around 0.005eV to 1keV.

In the next phase, we will carry out the real detection depth distribution measurement and confirming reproduction of the neutron spectrum in thermal / epi-thermal neutron fields by using the present spectrometer.

1. Introduction

Boron neutron capture therapy (BNCT) is a new radiation cancer therapy which can destroy selectively tumor cells, simultaneously suppress influence against healthy cells. In BNCT, only the case using a nuclear reactor is reported now because of requiring strong low-energy neutron sources. Nowadays, Neutron sources based on accelerators which can be constructed in medical facilities such as hospitals have being developed, which supply an effective remedy and reduce a patient's burden. However, patients should be positioned very close to the accelerator target because the source strength is quite weak. This leads to a problem that the spectrum is distorted and becomes different from the standard field. And it means accordingly that the shape of the spectrum varies depending on kind of accelerator. Therefore we should measure accurately the neutron field for each accelerator equipped with a different moderator system. Development of low-energy neutron spectrometers is thus required now.

In the author's laboratory, the ^{3}He position sensitive proportional counter was developed to estimate the detection depth distribution which was derived from the measured detection position information. Until now reproduction of thermal neutron(Maxwellian distribution) have been already confirmed. We have been progressing to test measuring of epi-thermal neutron spectrum. However, due to so-called ^{3}He crisis, we could

not refill ^{3}He gas to the detector and decided to use a commercially available position sensitive ^{3}He proportional counter instead as an alternative spectrometer, because it is cheaper and more stable though it is a little thin. The objectives of the present study are to develop a low energy neutron spectrometer based on a commercially available ^{3}He position sensitive proportional counter to measure neutrons from thermal (0.01eV) to 10 keV by one detector.

2. Measuring Technique and Equipments

2.1 Principles

There is no direct method to measure the low energy neutron spectrum, because generally neutron energy is so smaller than the Q value of reaction used to detect neutrons. The important point is to find a certain and large difference of physical quantity to expand and view small energy difference in the low-energy region. The difference should make neutrons to be identified via one-to-one correspondence. Practically in the present method it is based on the fact that some nuclides have a feature that lower energy neutrons have a larger reaction cross section value and high energy neutrons have a smaller one. And in addition, there is clear one-to-one correspondence between energy and cross section value in the nuclides. The reaction cross section difference is exhibited as the detection position (depth) changes, i.e., low energy neutrons can transmit to deeper places until captured. We measure reaction depth distribution possessing the energy information. The neutron spectrum could be reproduced from the measured reaction depth distribution with the response function, that is, the reaction depth distribution for energy. The response matrix **R(E,r)dr** can theoretically be deduced as $\sum(E)\exp(-\sum(E)\cdot r)\cdot dr$, where $\sum(E)$[1/cm] is the macroscopic cross section and **E** is the neutron energy. Measured detection depth distribution **y(r)** and neutron energy spectrum **x(E)** are related by the next equation, $y(r)= R(E,r)\cdot x(E)$. Thus, the measured reaction position distribution could be unfolded with an appropriate unfolding code in order to estimate the neutron energy spectrum. For the unfolding process, we adopted the Bayes theorem[2][3].

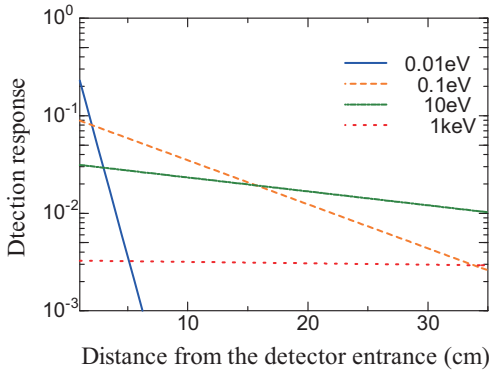

Fig.1 Response function of detector: R(E,r)

2.2 Detector

We used a commercially available position sensitive ^{3}He proportional counter shown in **Fig.2**. The length and diameter of the detector are 40cm and 2.5cm, respectively. The ^{3}He gas pressure is 0.5 MPa.

The practical technique to measure the detection position (depth) distribution of an incident low-energy neutron is in the following manner: The position sensitive proportional counter has two output BNC connectors at both ends to identify where the incident neutron reacts with inner gaseous material. The induced charge in the counter is conveyed to two directions according to the ratio of distances to both side edges of the detector. Two output

signals are amplified adequately by two pairs of pre- and main-amplifiers, and fed to a multi-parameter system (MPS-1600 (Laboratory Equipment Corporation)) to obtain a two dimensional spectrum for coincident two signals. **Figure 3** shows the block diagram of the measurement circuit.

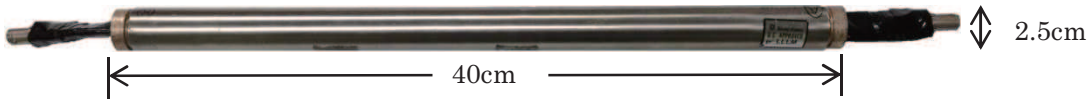

Fig.2 ^{3}He position sensitive proportional counter

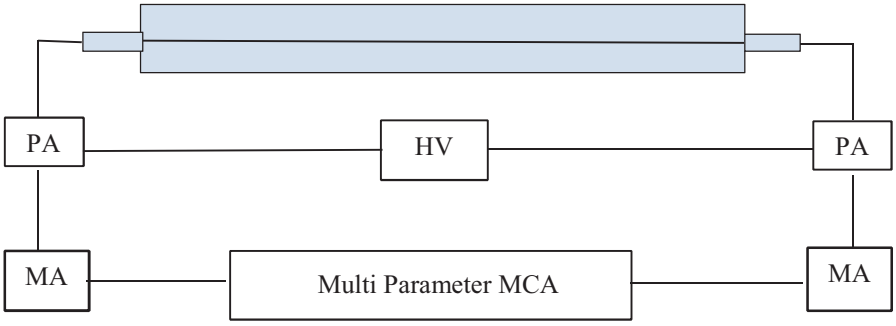

PA: Preamplifier (703-1C, OKEN)

HV: High voltage power supply (714-1E, OKEN)

MP: Amplifier (571, ORTEC)

Fig.3 Schematic block diagram of measuring system

2.3 Calculation and Setting

Experiments were carried out at OKTAVIAN facility of Osaka University, Japan. For measurement of thermal/epithermal neutrons, we designed a graphite thermal column with an AmBe source by MCNP5 calculations. The calculation model is shown in **Fig.4**. Using graphite as neutron moderator, a rectangular shape (100 x 100 x 100 cm) graphite thermal column was constructed. The AmBe neutron source was located at several distances, D [cm], from the thermal column surface. The neutron spectrum at the ^{3}He proportional counter positioned at 100cm from the thermal column was calculated and the most reasonable setting was examined from the calculation results. The key point is that the ^{3}He proportional counter was arranged vertically against the beam direction in the measurement so that we can ascertain the detection position of neutron in the detector using an appropriate neutron absorber and to confirm detection position dependence of the detection efficiency. But in a real application, the incident neutron direction must be parallel to the detector axis. Therefore, we have calculated both of these cases. **Figure 5** shows one of the MCNP calculation results in distances, D; 20cm,40cm,60cm,80cm and 100cm. From the results, we set the moderator thickness D to 50cm. At the distance of 50cm, the ratio between Thermal/MeV is enough high and the neutron number density is not so low. The calculated spectrum will be used to verify the unfolded result obtained from a parallel incidence experiment.

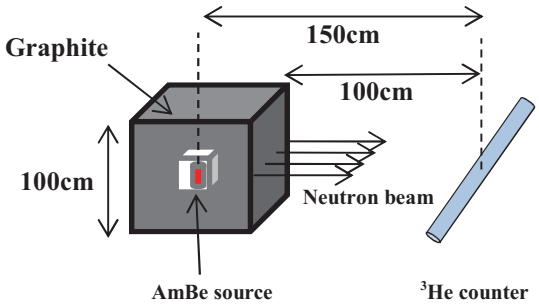

Fig.4 Calculation model

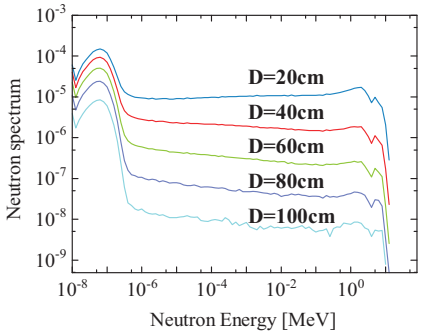

Fig.5 MCNP calculation results

3. Experiments and results

3.1 Two-dimensional spectrum

A two-dimensional spectrum measured by the ^{3}He position sensitive proportional counter is shown in **Fig.6**. In the figure, the horizontal axis shows one of the two signals and the vertical axis shows the other. It was confirmed that the detection position information could successfully be extracted. In this measurement, no cadmium collimators were used. It means that neutrons enter the detector from the side surface uniformly. Now, we have to connect between the two-dimensional spectrum and the detection depth spectrum. It means that it is necessary to make one-to-one correspondence between the position (coordinates) in **Fig.6** and the real detection position in the detector. And also it is quite important to fix the detectable reaction depth to define the measurable neutron energy range. For these requirements, in the next step, we carried out measurements with a cadmium collimator put around the detector.

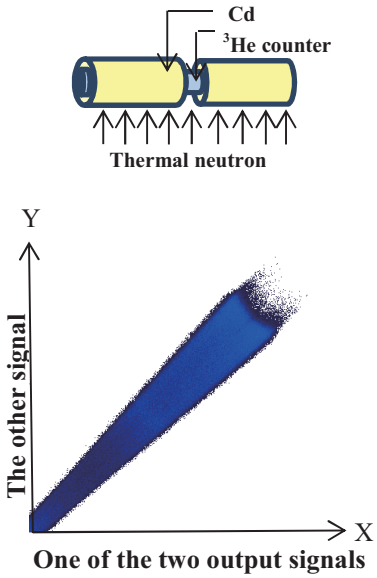

Fig.6 Two dimensional MCA result

3.2 Detection position identification

As a collimator we used a cadmium sheet because cadmium has a large (n,γ) reaction cross section for thermal neutrons. Incident thermal neutrons are mostly blocked by the collimator and detected only from an open window of 1cm in width. The schematic view for the measurement is shown in the upper figure in Fig.7. To establish the one-to-one correspondence between the real detection position and the coordinates of the measured two-dimensional spectrum, we have measured several times by moving the open window from the one edge to the other by 1cm. As in the upper figure, several cadmium collimators were rolled around the detector to fix the open position . The center positions of two open windows (A and B in the figure) were 9.5cm, 29.5cm from the one side edge (X), at which each spectrum was expected to be observed. For spectra in the two open positions, the signals from X and Y are proportional with each other. We thus projected the counts of the two-dimensional

spectrum along a line starting from the origin as a function of angle to x-axis as shown in **Fig.7**. We could successfully obtain the projected spectrum shown in **Fig. 8**, which shows two peaks corresponding to the positions where no Cd covers exist. By repeating this experiment, we could assign the detection position from 0 cm to 40 cm in the detector and normalize the detection depth in the measured depth distribution. From the result s, it was found that the detectable position is at Z=6cm~34cm.

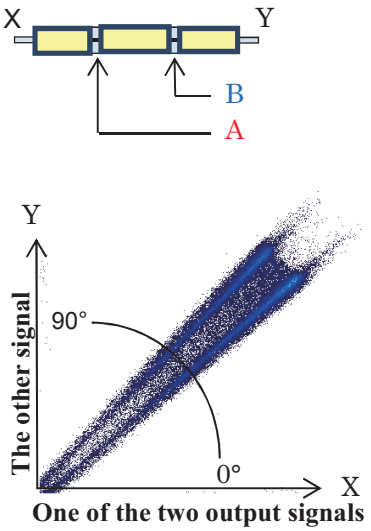

Fig.7 Position detection by the Cd collimator

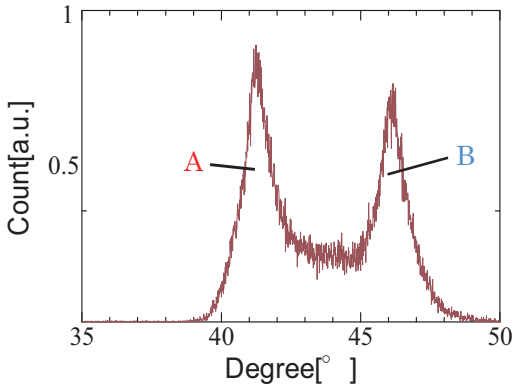

Fig.8 numerical result

3.3 Measurable neutron energy range

Limit of measureable detection depth can affect the measurable neutron energy range. The measurable energy range was examined by the experimental results described in Sec. 3.2 and the response matrix of the detector. At the depth of 6cm, there exists an enough large value in the response matrix for neutrons with energy of over 0.005eV. And over 1keV, the response difference for neutron energy is getting too small to discriminate the energy. Consequently, this detector can be expected to measure neutrons of 0.005eV~1keV, which mostly cover energy region from thermal to epi-thermal. For the BNCT facilities these neutrons will be used and this spectrometer can obtain the crucial information of the neutrons.

4. Future works

In the present study, we made it appear that the detection position could be distinguished in the test measurement using a commercially available position sensitive ^{3}He proportional counter. In the next phase, the incident direction of neutrons is changed to be parallel to the detector axis, as shown in **Fig. 9**, in order to check how well the neutron spectrum could be reproduced from the measured detection depth distribution. For this purpose, several neutron sources having different neutron spectra are to be utilized, i.e., mono-energetic thermal neutrons at JRR-3M of JAEA, thermal/epi-thermal neutrons at OKTAVIAN and 8 keV neutrons at FRS facility of JAEA. We will use them to check one-to-one correspondence between the direction depth distribution and the incident neutron energy through measuring the response

function. Finally we will confirm whether the thermal / epi-thermal neutron energy spectrum will be reproduced by unfolding the detection depth distribution with the response matrix using the Bayes theorem.

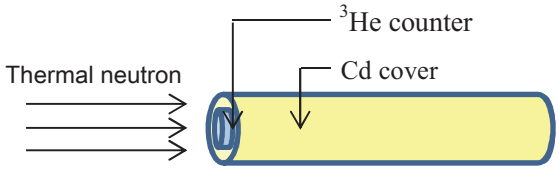

Fig.9 Schematic view of parallel incidence experiment

5. Conclusion

We have been carrying out the series studies concerning the thermal/epithermal spectrometer especially for BNCT. In the present study, we tested a commercially available position sensitive ^{3}He proportional counter as a thermal/epithermal neutron spectrometer. For this purpose, the measurement system with a multi parameter MCA was designed and developed for the measurement. Also, a thermal neutron field was designed by MCNP5 calculation and constructed for the detector test measurement. From the measurement, the detection position distribution could be obtained as a two dimensional spectrum. And the detector was confirmed to detect coincident signals appropriately at Z=6~34cm. It means in other words that the measurable energy range was thus from 0.005eV to 1keV.

In the next phase, we will carry out the real detection depth distribution measurement with incident neutrons being incident parallel to the detector axis. For this purpose, several neutron sources are taken into consideration to be utilized for confirming one-to-one correspondence between the detection depth distribution and the neutron energy by measuring the response of the detector, and for confirming reproduction of the neutron spectrum in thermal / epi-thermal neutron fields by using the present spectrometer.

References

[1] X-5 Monte Carlo Team: MCNP-A General Monte Carlo N-Particle Transport Code(2003) N-particle transport code, version 5(2003).

[2] I,Murata, H.Miyamaru, “Low-energy neutron spectrometer using position s ensitive proportional counter —Feasibility study based on numerical analysis” Nuclear Instruments and methods in Physics Research A 589,445-454(2008).

[3] S.Iwasaki: “A new approach for unfolding PHA problems based only the Bayes’ Theorem”, Proc. 9 th International Symposium on Rector Dosimetry, Prague, Chezk Republic, pp. 245-252 (1996).

32. Cross Section Measurement of ^{117}Sn(n,γ) using ANNRI-NaI(Tl) Spectrometer at J-PARC

K. Hirose[1,*], K. Furutaka[1], K. Y. Hara[1], H. Harada[1], A. Kimura[1], F. Kitatani[1], M. Koizumi[1], S. Nakamura[1], M. Oshima[1], Y. Toh[1], M. Igashira[2], T. Katabuchi[2], T. Matsuhashi[2], M. Mizumoto[2], K. Terada[2], T. Kamiyama[3], K. Kino[3], Y. Kiyanagi[3] and J. Hori[4]

[1] *Japan Atomic Energy Agency*

[2] *Research Laboratory for Nuclear Reactors, Tokyo Institute of Technology*

[3] *Graduate School of Engineering, Hokkaido University*

[4] *Research Reactor Institute, Kyoto University*

*email:hirose.kentaro@jaea.go.jp

Abstract

A cross section measurement for ^{117}Sn(n,γ) was performed using the ANNRI-NaI(Tl) spectrometer at J-PARC/MLF. The relative cross section was normalized to JENDL-4.0 at the first resonance. All s −wave resonances below 1.5 keV listed in JENDL-4.0 were observed. This report shows a data analysis and a preliminary result of the measurement in a neutron energy region of about 1 eV to 2 keV.

1. Introduction

To evaluate the feasibility of development of nuclear transmutation technology and advanced nuclear system, precise nuclear data of neutron-induced reactions for minor actinides (MAs) and long-lived fission products (LLFPs) are indispensable. Precise nuclear data for stable isotopes of LLFPs are also needed as well as those for LLFPs themselves, because there are sizable yields for stable isotopes in ^{235}U(n,f). For example, tin isotopes produced in ^{235}U(n,f) amount to 20-30% for $^{115,117-120}$Sn and about 50% for ^{124}Sn as compared to ^{126}Sn which is one of the LLFPs. In the present study, the cross section measurement has been performed for ^{117}Sn(n,γ) using the ANNRI-NaI(Tl) spectrometer at J-PARC/MLF.

2. Experiment

The experiment was performed using the ANNRI-NaI(Tl) spectrometer of the Beam Line 04 at J-PARC/MLF. Neutron energy was determined by the TOF method.

Neutrons were produced by spallation reaction of mercury irradiated with 3-GeV pulsed proton beam which was accelerated by LINAC and Rapid Cycling Synchrotron (RCS). The beam power and repetition were 200 kW and 25 Hz, respectively. The proton pulses from RCS were transported to MLF and/or another synchrotron called MR for high energy physics experiments. In the present experiment, 58 proton pulses were transported to MLF and remained 6 pulses were transported to MR for every 64 pulses. To keep the proton intensity as high as possible, a double-bunch operation is used at J-PARC. In the double-bunch operation, a proton pulse consists of two bunches separated 600-ns interval. This causes a split of resonance structure in the TOF spectrum as described later.

Prompt γ rays emitted in capture reactions were detected using the ANNRI-NaI(Tl) spectrometer. The spectrometer was located at 28-m flight length and consists of two sets of an NaI(Tl) and plastic scintillators. The plastic scintillators are annular shaped and surrounding the NaI(Tl) scintillators. These plastic scintillators are used as veto counters for cosmic-ray events. The two sets of NaI(Tl) and plastic scintillators are located at the angles of 90° and 125°with respect to the neutron beam line. In the present experiment, only the NaI(Tl) and the plastic scintillators located at 90° were used. The size of the NaI(Tl) was 30.3 cm diam.× 20.3 cm.

The sample used in the present experiment was enriched by 87% in ^{117}Sn. The impurities of ^{116}Sn and ^{118}Sn were 9.3% and 3%, respectively. Tin powder of 88.9 mg was pressed into pellet shape with diameter of 5 mm.

Dynode signals from three photo-multiplier tubes attached to the NaI(Tl) scintillator were used for pulse height measurement. The sum of these signals was amplified (ORTEC113 and ORTEC572A) and input to a 7072 Dual ADC module (Fast ComTec). The sum of the anode signals was amplified (ORTEC472), discriminated (ORTEC584) and input to a multi-stop TDC (Daiei Musen Denki). The digitized data of ADC and TDC were handled by a data acquisition system of MPA-3 (Fast ComTec).

3. Data analysis

A fixed dead time of 3.00 μs is imposed to the DAQ system for each accepted signal. Signals arriving during dead time which is imposed by the prior accepted signal are not accepted and do not impose dead time to the DAQ system. In other words, the non-extended dead time model is applied to the DAQ system. In the non-extended dead time model, the true counting rate is expressed by

$$R_0(t) = \frac{R(t)}{1 - \int_{t-3\mu s}^{t} R(t')dt'} \quad , \qquad (1)$$

where $R(t)$ is the measured counting rate at TOF t. The spectrum shown by a gray line in

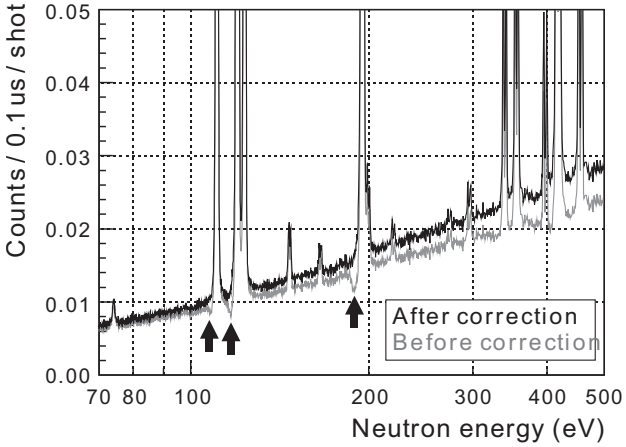

Figure 1 The spectrum shown by a gray line is corrected to that shown by a black line.

Fig.1 is the TOF spectrum for the ^{117}Sn sample before the dead time correction. The dips just below the strong resonances are because of dead time (see arrows in the figure). After the dead time correction by Eq.(1), these dips disappear as shown by a black line.

In the present analysis, we consider three backgrounds; frame overlap, blank and scattering neutrons. Slow neutrons produced by a proton pulse reach the sample position after fast neutrons produced by the next proton pulse. The energy of these slow neutrons cannot be determined because the start signal of TOF is updated for the neutrons produced by the next proton pulse. The events due to these slow neutrons are the frame-overlap background. This background was estimated in the same manner as described in Ref.[1].

The second background is blank, i.e., events observed even without any sample. This background can be obtained by a measurement for no sample. The third background is events due to scattered neutrons. Some scattered neutrons from the sample are captured by materials around the sample and subsequently produce capture γ rays. These undesirable γ rays make background events. This background was estimated by an auxiliary measurement of carbon sample. The neutron capture cross section of ^{12}C is much smaller than that of the elastic scattering. Hence the carbon can be used as a scatterer. Letting $C(t)$ be a count rate at TOF t after the background subtraction for frame-overlap background, the background subtraction is expressed as

$$C_{\mathrm{Sn}}^{\mathrm{cap}}(t) = \left\{C_{\mathrm{Sn}}(t) - C_{\mathrm{Blank}}(t)\right\} - \frac{\{\sigma^{ela}(t)\rho T\}_{\mathrm{Sn}}}{\{\sigma^{ela}(t)\rho T\}_{\mathrm{C}}}\left\{C_{\mathrm{C}}\ (t) - C_{\mathrm{Blank}}(t)\right\}$$

$$= C_{\mathrm{Sn}}(t) - \left\{\alpha C_{\mathrm{C}}\ (t) + (1-\alpha)C_{\mathrm{Blank}}(t)\right\} \qquad \left(\because \alpha(t) \equiv \frac{\{\sigma^{ela}(t)\rho T\}_{\mathrm{Sn}}}{\{\sigma^{ela}(t)\rho T\}_{\mathrm{C}}}\right), \qquad (2)$$

where $C_{\mathrm{Sn}}^{\mathrm{cap}}$ is the counting rate due only to the capture reaction on ^{117}Sn. The factor α is needed to normalize the background of scattered neutrons estimated using ^{12}C to that for ^{117}Sn. The background subtraction is shown in Fig.2, where the counting rate observed in the measurement of ^{117}Sn, $C_{\mathrm{Sn}}(t)$, is depicted by a black line and the background spectrum, the second term in Eq.(2), is depicted by a gray line.

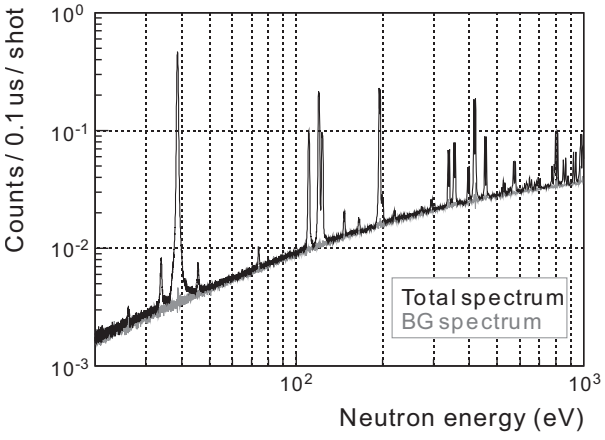

Figure 2 Background subtraction

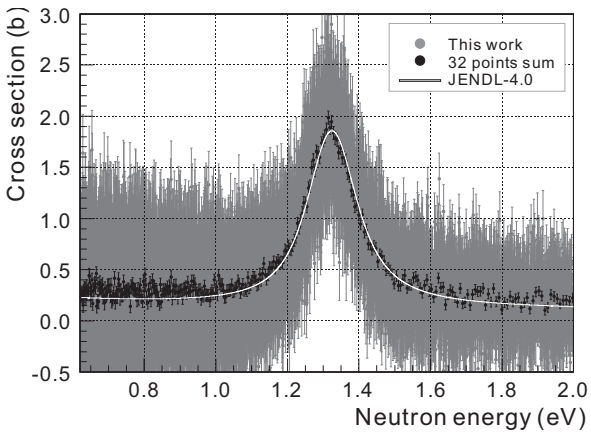

Figure 3 Cross section normalization

4. Results and discussion

The relative cross section value, i.e. the neutron energy dependence of the cross section, was obtained from $C_{\mathrm{Sn}}^{\mathrm{cap}}$ in Eq.(2) divided by the neutron spectrum. The neutron spectrum is well expressed by $\alpha E^{-\beta}$(E is neutron energy) [2]. In the neutron energy range above 1 eV, the parameter is obtained as $\beta \approx 1$. The obtained relative cross section was normalized to the evaluated value of ENDF/B-VII.1 at the first resonance. Figure 3 shows the cross section normalization. The gray plots are the relative cross section. The sums of every 32 points are shown by the black plots. The white solid curve is JENDL-4.0 [3].

The evaluation is broadened by the resolution function of the neutron beam. The broadening result is shown in Fig.4. The thin black line is the original data of JENDL-4.0 at $T = 300$ K. The thick black line is JENDL-4.0 broadened according to the resolution function and the double-bunch structure of the proton pulse. Therefore, each resonance splits into two peaks with a certain energy interval corresponding to 600 ns in TOF.

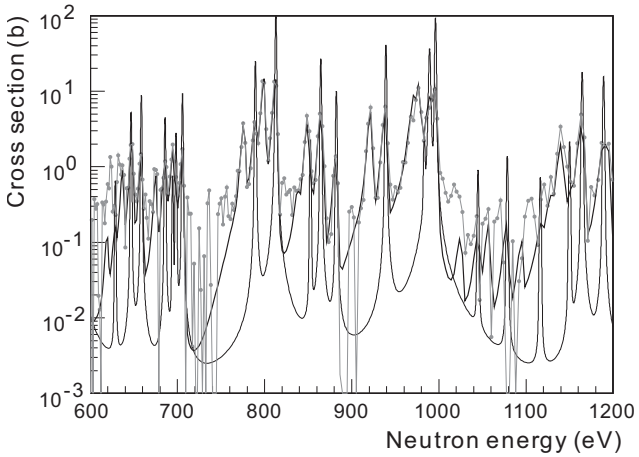

Figure 4 JENDL-4.0 evaluation (thin black line) is broadened into the thick black line considering the neutron resolution function and the double-bunch structure of the proton pulse.

The cross section in higher energy region is shown in Fig.5 and Fig.6. The gray plots are the result of this work without error bars for easy-viewing. The solid and dashed curves are broadened JENDL-4.0 and ENDF/B-VII.1 [4]. It should be noted that the result of this work has been obtained without any correction for the self-shielding effect. Hence, at this moment, the evaluations shown in Fig.5 and Fig.6 are decreased by a self-shielding factor instead. The self-shielded cross section σ' is given by

$$\sigma'(E) = \frac{1 - \exp\{-\sigma(E)\rho T\}}{\rho T}, \qquad (3)$$

where ρ and T are the number density of the ^{117}Sn nucleus and the sample thickness, respectively.

Resonances indicated by black stars and an gray star in Fig.5 and Fig.6 are supposed to be backgrounds from ^{116}Sn and ^{118}Sn. The resonances at around 581, 996 and 1359 eV are clearly seen in the present result, which are also seen in JENDL-4.0 whereas the ENDF/B-VII.1 does not include these resonances. Difference between these two evaluations seems to be whether the experimental data obtained by Smith *et al.* [5] was considered or not. In the experiment of Smith, enrichment of the ^{117}Sn sample was 87.6% which is nearly same as that used in the present experiment (87%), and not so highly enriched. In order to confirm whether these resonances are belong to the $^{117}\mathrm{Sn}(n,\gamma)$ reaction or not, a measurement is needed for $^{116,118}\mathrm{Sn}(n,\gamma)$ which are included in the ^{117}Sn sample.

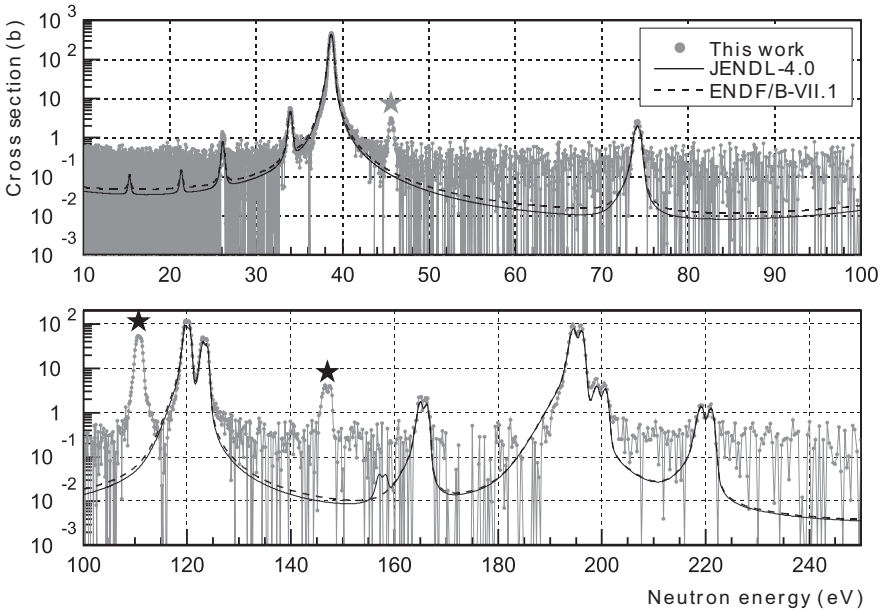

Figure 5 [*PRELIMINARY RESULT*] The result of this work shown by gray plots is compared to evaluations. The solid and dashed curves are JENDL-4.0 and ENDF/B-VII.1 which are broadened by the neutron resolution function and double-bunch structure of the proton pulse.

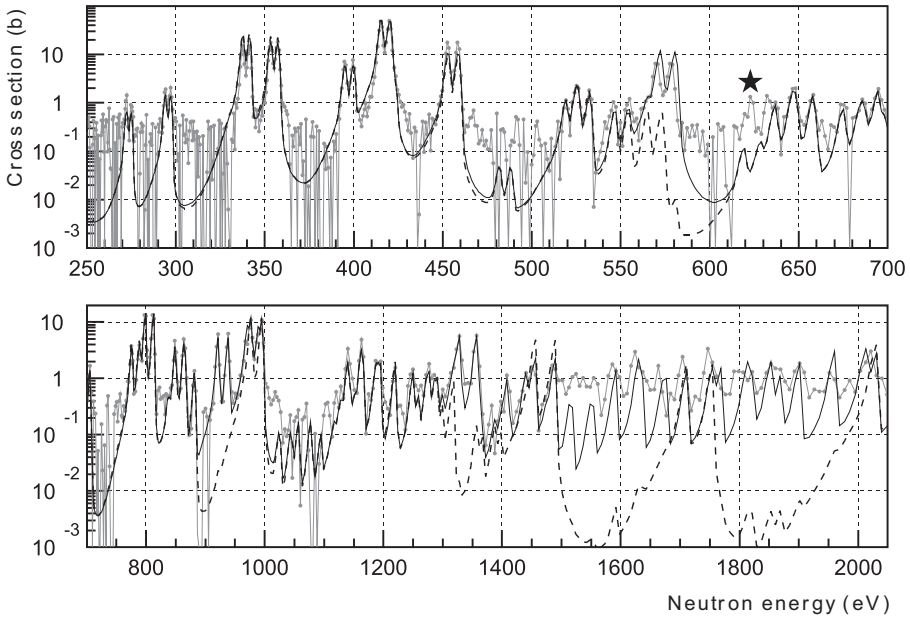

Figure 6 [*PRELIMINARY RESULT*] (same as Fig.5)

5. Summary

The cross section measurement for $^{117}\mathrm{Sn}(n,\gamma)$ was performed using the ANNRI-NaI(Tl) spectrometer at J-PARC/MLF. The obtained relative cross section was normalized to JENDL-4.0 at the first resonance. It should be noted that, up to now, the correction of the self-shielding effect and the pulse-height weighting technique have not been applied yet. The result of this work is compared to

JENDL-4.0 and ENDF/B-VII.1 which are broadened by the neutron resolution function and the double-bunch structure of the proton beam. JENDL-4.0 reproduces the present data better than ENDF/B-VII.1, especially at the resonance around 581, 996 and 1359 eV. These resonances, however, should be confirmed by another measurement for ^{116,118}Sn. For the final result, further analysis is needed such as the self-shielding correction, pulse-height weighting technique and uncertainty evaluation. We are planning to measure the other tin isotopes including ^{116,118}Sn.

Acknowledgements

The authors would like to thank the staffs of J-PARC and MLF for their operations of the accelerators and the neutron production target. This work was supported by JSPS KAKENHI Grant Number 22226016.

References

[1] K.Hirose, K.Furutaka, K.Y.Hara, H.Harada, A.Kimura, T.Kin, F.Kitatani, M.Koizumi, S.Nakamura, M.Oshima, Y.Toh, M.Igashira, T.Katabuchi, M.Mizumoto, T.Kamiyama, K.Kino, Y.Kiynagi, and J.Hori, Cross section measurement of ^{237}Np(n,γ) from 10meV to 1keV at J-PARC, *J. Nucl. Sci. Technol.* **50**, pp.188-200 (2013).

[2] K.Kino, M.Furusaka, F.Hiraga, T.Kamiyama, Y.Kiyanagi, K.Furutaka, S.Goko, H.Harada, M.Harada, T.Kai, A.Kimura, T.Kin, F.Kitatani, M.Koizumi, F.Maekawa, S.Meigo, S. Nakamura, M.Ooi, M.Ohta, M.Oshima, Y.Toh, M.Igashira, T.Katabuchi, M.Mizumoto, Measurement of energy spectra and spatial distributions of neutron beams provided by the ANNRI beam line for capture cross-section measurements at the J-PARC/MLF, *Nucl. Instr. Meth.* A 626–627 (2011) pp.58-66.

[3] K.Shibata, O.Iwamoto, T.Nakagawa, N.Iwamoto, A.Ichihara, S.Kunieda, S.Chiba, K.Furutaka, N.Otuka, T.Ohsawa, T.Murata, H.Matsunobu, A.Zukeran, S.Kamada, and J.Katakura, JENDL-4.0: A New Library for Nuclear Science and Engineering, *J. Nucl. Sci. Technol.* **48** (2011) pp.1-30.

[4] M.B.Chadwick, M.Herman, P.Oblozinsky, M.E.Dunn, Y.Danon, A.C.Kahler, D.L.Smith, B. Pritychenko, G.Arbanas, R.Arcilla, R.Brewer, D.A.Brown, R.Capote, A.D.Carlson, Y.S.Cho, H.Derrien, K.Guber, G.M.Hale, S.Hoblit, S.Holloway, T.D.Johnson, T.Kawano, B.C.Kiedrowski, H.Kim, S.Kunieda, N.M.Larson, L.Leal, J.P.Lestone, R.C.Little, E.A.McCutchan, R.E.MacFarlane, M.MacInnes, C.M.Mattoon, R.D.McKnight, S.F.Mughabghab, G.P.A.Nobre, G.Palmiotti, A.Palumbo, M.T.Pigni, V.G.Pronyaev, R.O.Sayer, A.A.Sonzogni, N.S.Summers, P.Talou, I.J.Thompson, A.Trkov, R.L.Vogt, S.C.van der Marck, A.Wallner, M.C.White, D.Wiarda, and P.G.Young, ENDF/B-VII.1 Nuclear Data for Science and Technology: Cross Sections, Covariances, Fission Product Yields and Decay Data, *Nucl. Data Sheets* **112** (2011) pp.2887-2996.

[5] D.A.Smith, J.D.Bowman, B.E.Crawford, C.A.Grossmann, T.Haseyama, Mikkel B.Johnson, A.Masaike, Y.Matsuda, G.E.Mitchell, V.A.Nazarenko, S.I.Penttila, N.R.Roberson, S.J.Seestrom, E.I.Sharapov, L.M.Smotritsky, S.L.Stephenson, and V.Yuan, Neutron resonance spectroscopy of ^{117}Sn from 1 eV to 1.5 keV, *Phys. Rev. C**59*** (1999) p.2836.

33. Estimation of Reaction Rate in Subcritical System by Gamma Ray Spectrum Measurement

*Yasushi NAUCHI[a], Hirokazu OHTA[a], Hironobu UNESAKI[b], Tsuyoshi MISAWA[b], Tadafumi SANO[b], Takahiro YAGI[b], Takanori KAMEYAMA[c]

[a] Central Research Institute of Electric Power Industry, 2-11-1, Iwado Kita, Komae-shi, Tokyo 201-8511.

*e-mail: nauchi@criepi.denken.or.jp

[b] Kyoto University Research Reactor Institute, 2, Asashiro-Nishi, Kumatori-cho, Sennan-gun, Osaka 590-0494.

[c] Tokai University, 4-11-1, Kita Kaname, Hiratsuka, Kanagawa 259-1292.

A quantification method of reaction rates in multiplication systems by γ ray spectrum measurements is studied. Light water moderated subcritical cores are mocked up with uranium (U) - aluminum (Al) alloy fuels in KUCA and high energy (>3MeV) γ rays are measured with a BGO scintillator. The response functions and the detection efficiencies are calculated for γ rays from ^{235}U(n,fis), Al(n,γ), and SUS(n,γ) reactions. With calculated ones and the measured pulse height spectra, the reaction rates are unfolded. For the Al(n,γ) reaction, the deduced reaction rates agree with those deduced by neutronics calculations.

I. Introduction

When nuclear fuel is stored in a dense transport cask or a storage rack taking the burn-up credit (BUC), it is required to certify whether the nuclide composition of the fuel is conservatively evaluated from a criticality safety viewpoint[1)]. To take the burn-up credit for the transport and the storage of an intact fuel assembly, the burn-up of the assembly has been evaluated based on the passive measurements of neutrons and γ rays from the assembly with FORK, PYTHON, and BUM detectors, etc[2)]. The neutron induced reaction rates of the burnt fuel assemblies have not yet been measured directly.

In many cases, neutron absorption reactions are associated with emission of γ rays. The emission spectrum of the γ rays is intrinsic to the reaction. By a spectrum measurement of the γ rays, the absorption rate could be quantified. The quantified absorption rates would be useful to know the subcriticality margin by the absorption. Focusing on it, Nauchi et al. have proposed the "capture credit" (CapC)[3)]. To take CapC means to enable increment of the storage density of the fuel in the range of the negative reactivity of the capture reactions confirmed by the γ ray measurements. CapC would enhance the range of BUC. Besides, it could be useful to quantify the negative reactivity effect of stainless steels (SUS) mixed with the melted fuels after severe accidents of LWRs.

In the present work, the concept of CapC is described[4)]. Then the quantification of the capture reactions is demonstrated by subcritical experiments in Kyoto University Critical Assembly facility (KUCA) and by processing of the obtained data. The current status of the nuclear data used for the processing is also discussed.

II. Capture Credit

The concept of the CapC is shown in **Fig. 1**. The target fuel is irradiated by neutrons then the γ rays are radiated. Those γ rays are measured with a spectrometer such as a BGO scintillator or a HP-Ge

detector. The obtained pulse height spectrum consists of the γ ray components from the fission and the capture reactions. Assuming kinds of reaction and their spatial distributions in the fuel, the pulse height response of the reactions and the detection efficiencies of them are simulated by the photon-electron coupled transport calculations. By using the responses, the efficiencies and the measured pulse height spectrum, the reaction rates are unfolded.

Suppose we do not know any information of a fuel assembly but its initial nuclide composition. Then the infinite multiplication factor is conservatively evaluated as

$$k_{\infty} = \frac{\langle \nu_t \Sigma_f \phi \rangle}{\langle \Sigma_c \phi \rangle + \langle \Sigma_f \phi \rangle} \quad . \tag{1}$$

Here the brackets mean the integration over the position, the flying direction, and the energy of neutrons. ν_t is the total neutron yield per fission. ϕ is the angular neutron flux. Σ_c and Σ_f are the capture and the fission cross sections of the fresh fuel in the water, respectively. By quantifying the ratio of a capture reaction i to ^{235}U fission, $< \phi\Sigma_{c,i} > / < \phi\Sigma_f >$, the multiplication factor can be evaluated as

$$k_{\infty,CapC} = \frac{\langle \nu_t \Sigma_f \phi \rangle}{\langle \Sigma_c \phi \rangle + \langle \Sigma_f \phi \rangle \left\{ 1 + \alpha \frac{\langle \Sigma_{c,i} \phi \rangle}{\langle \Sigma_f \phi \rangle} \right\}} \quad . \tag{2}$$

Where α is a kind of engineering parameter which satisfies

$$0 < \alpha < 1 \tag{3}$$

The difference of the two kinds of the infinite multiplication factor is the confirmed subcriticality margin by the capture reaction.

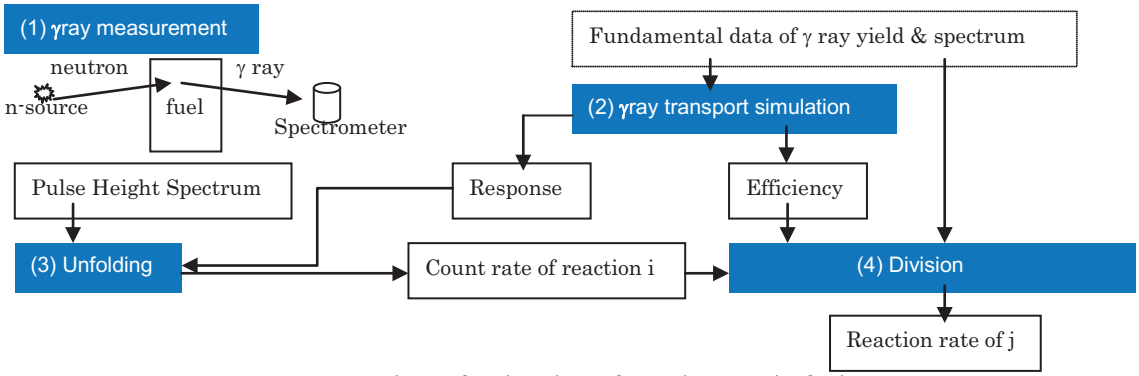

Fig. 1 Procedure of estimation of reaction rate in fuel

III. Experiment

A demonstration measurement was performed in the C-core of KUCA. Fuel plates of U – Al alloy covered by Al cladding were used. The ^{235}U enrichment of the fuel is 93wt-%. Fuel plates were inserted in frames and the frames were loaded onto the bottom grid made of SUS as shown in **Fig. 2**. The reactivity was inserted by feeding the water moderator from the bottom of the core tank. However, the amount of fuels loaded for the present work was less than the minimum number of plates to attain the criticality. The core was driven subcritically by a ^{252}Cf neutron source. The γ rays radiated from absorption reactions of hydrogen, Al, ^{235}U, and SUS were measured with a BGO scintillator which is located 40cm from the outer surface of the core. The BGO scintillator is covered with a water-tight tube made of Al-alloy. γ rays were measured for 3 cores varying the number of fuel plates. The duration time for the measurements are 2 ~ 4h for each core. A slight increment of count rate (<2%) was observed as the detection duration time increases due to decay of short lived fission products (FP). Background γ rays from long-lived FP accumulated in the fuel plates by other experiments and from the experimental room were quantified by measurements without

the ^{252}Cf source. By the ^{252}Cf source in / out measurements, the net pulse height spectra originated in the ^{252}Cf source were obtained. The thermal neutron flux distributions inside the cores were measured vertically by the activation method with ^{115}In wire.

To determine the intensity of the ^{252}Cf neutron source and its activity, 2.223 MeV γ rays were measured for geometries in which any fuel plate was discharged and the only the source was set in the water moderator. In a similar geometry, only an Am-Be neutron source was set and the radiated γ rays of 4.437 MeV were measured for the pulse height calibration and for an evaluation of the resolution of the BGO scintillator (see **Fig. 3**).

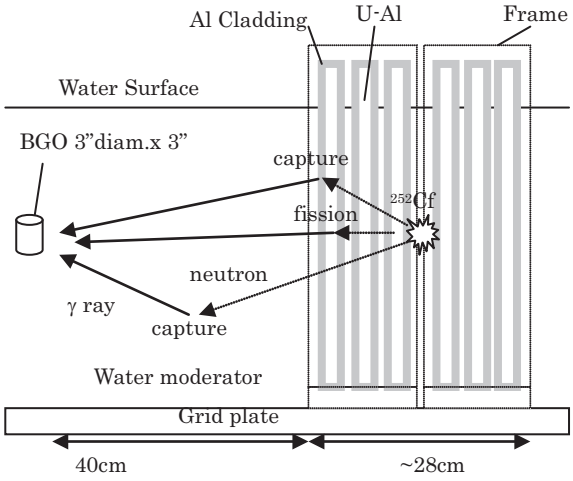

Fig. 2 Experimental geometry

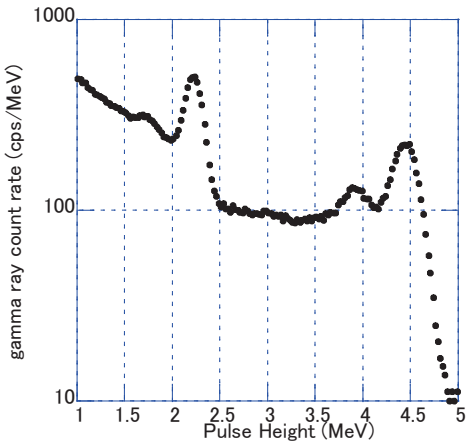

Fig. 3 γ ray spectrum measured for Am-Be source in water

IV. Data Processing

The net spectrum obtained for a core is shown in **Fig. 4.** It consists of a 2.223MeV peak, a continuum part (3 - 6 MeV) and peak structures in 7~8MeV energy region. The background components were not observed for the energy region above 3MeV. In the present work, the authors focused on the energy region above 3MeV.

The authors assumed that the γ ray pulse height spectra consist of the 4 components: 1) the spontaneous fission of ^{252}Cf and the decay of its FP, 2) the fission of ^{235}U and the decay of its FP, 3) (n,γ) reactions of Al, 4) (n,γ) reactions of SUS. The authors assumed that the measured γ rays were radiated by reactions induced by the thermal neutrons and surveyed evaluations of the γ ray spectrum and of the number of γ ray emission per reaction for each reaction. For the prompt γ ray emission by the spontaneous fission of ^{252}Cf and by the fission of ^{235}U, an evaluation by Verbeck[5] is adopted. In his evaluation, the relative spectrum is identical for the two reactions although the number of γ ray emission per reaction is different. The FP decay γ ray was evaluated with the FPGS-90[6] code with the JNDC-2000 decay chain data file[7]. For the ^{235}U fission, the average intensity of the FP decay γ ray emission was calculated taking the duration time for the measurement into account. For the capture reactions, γ ray emission data presented in the CapGam database[8] were adopted. Capture reactions of ^{27}Al, ^{55}Mn, ^{56}Fe and ^{58}Ni were considered. That of ^{235}U was neglected since the number of higher energy (>3MeV) γ ray emission per capture listed in CapGam is small. $^{52 \text{ and } 53}$Cr are also major nuclides in SUS, but the numbers of the absolute values of γ ray emission per capture are unknown. For the reason, they were neglected. For SUS, γ ray emission data for ^{55}Mn, ^{56}Fe and ^{58}Ni were averaged after weighted by their number densities and the thermal cross sections.

With the γ ray emission spectra, the pulse height response and the efficiency for the reactions were calculated. The vertical distributions of those reactions were assumed similar to the measured

^{115}In(n,γ) reaction rates. The horizontal one is assumed a cosine shape function. The responses were calculated in three steps with the MCNP-5 code. At first, photon transport calculations were performed and the inner current of photons on the surface of the water-tight tube covering the BGO scintillator was calculated with the cutoff energy of 1.0 MeV. Then the photon-electron coupled transport calculations were done inside the tube with cutoff energy of 0.1MeV. Those energies are carefully determined to predict the ratio of the single escape events to the photo peak ones. By the procedure, pulse height responses were tallied. The responses *r*s were smeared taking the measured resolution into account. Then detection efficiencies *ε*s were also obtained.

With the calculated response and the efficiency for the case where only ^{252}Cf was loaded in water, the intensity of the source was determined. Then, the pulse height spectrum components of the direct γ rays from ^{252}Cf were quantified for the subcritical systems where the fuel plates were loaded. The spectra C_is were obtained by subtracting the direct components from the net pulse height spectra. The reaction rates of the fission of ^{235}U, Al(n,γ), and SUS(n,γ), *p*s were unfolded from C_i by inversely solving the following equation.

$$\begin{pmatrix} \vdots \\ C_i \\ \vdots \end{pmatrix} = \begin{pmatrix} \vdots & \vdots & \vdots \\ r_{fis\to i} & r_{Al(n,\gamma)\to i} & r_{SUS(n,\gamma)\to i} \\ \vdots & \vdots & \vdots \end{pmatrix} \begin{pmatrix} \varepsilon_{fis} & 0 & 0 \\ 0 & \varepsilon_{Al(n,\gamma)} & 0 \\ 0 & 0 & \varepsilon_{SUS(n,\gamma)} \end{pmatrix} \begin{pmatrix} p_{fis} \\ p_{Al(n,\gamma)} \\ p_{SUS(n,\gamma)} \end{pmatrix} \quad (4)$$

For the unfolding, the spectrum type Bayesian unfolding method proposed by Iwasaki[9] is adopted.

The unfolded pulse height components are shown in **Fig. 4**. The summation of the unfolded components well predicts the measured data. In the energy region above 8MeV, only the SUS(n,γ) component exists. The prominent peak structure in 6.5-8MeV is mainly dominated by the Al(n,γ) reactions. A major component in 3-5MeV region is fission of ^{235}U.

The unfolded reaction rates are listed in the **Table 1** and compared to those deduced by neutronics calculations using the MCNP-5 code with the FSXLIB-J4 library [10) †]. For the Al(n,γ) reaction, the deduced reaction rates by the γ ray measurements agree with the calculated values within 7% accuracy. However, the fission reactions rates by the γ ray measurements are larger than the calculated values by 50~58% by the present method.

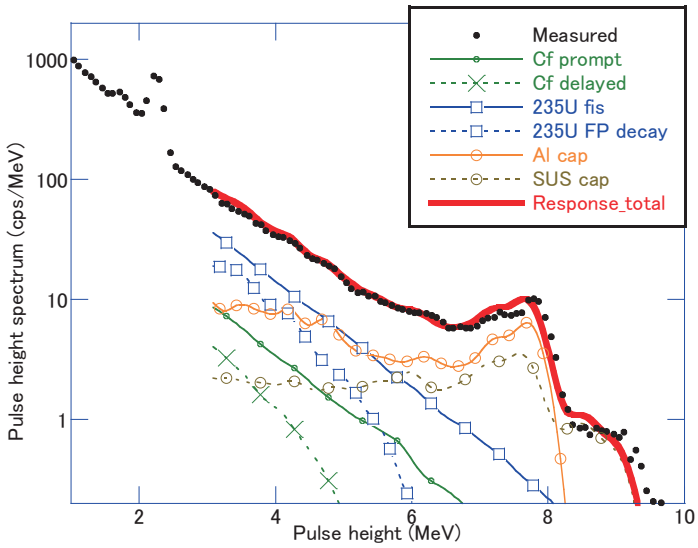

Fig. 4 Measured pulse height spectrum and unfolded components

Table 1 Reaction rate based on the γ ray measurements (E) and the neutronics calculations (C)

Reaction	Geom.	Measured(E)	Calc.(C)
Al(n,γ)	2x2	1.43E+05	1.42E+05
	3x2	2.59E+05	2.65E+05
	4x2	4.28E+05	4.55E+05
^{235}U fis	2x2	1.54E+06	1.02E+06
	3x2	2.95E+06	1.94E+06
	4x2	5.27E+06	3.33E+06

† FSXLIB-J4 is not based on JENDL-4u but JENDL-4 published in 2010.

V. Discussion

The γ ray emission data used in section IV are compared to those listed in JENDL-4 [10].

Absolute γ ray emission data for the thermal fission of ^{235}U are shown in **Fig. 5**. In JENDL-4, the prompt γ ray spectrum is evaluated in coarse energy meshes so it is difficult to apply it for CapC. The spectrum of JENDL-4 is flat from 6.3 to 10.3MeV and differs from the Verbeke's evaluation. It should be investigated whether the flat spectrum is adequate or not against the experimental data.

In **Fig. 6**, γ ray data of ^{235}U(n,γ) reactions for thermal neutrons are compared to CapGam data. The yield data are given for the discrete energy γ rays in CapGam and in a part of JENDL-4. However, the data in the other part of JENDL-4 are given as the continuous energy distribution. The yield data for the discrete energy gamma rays were divided by the energy width of the mesh used for the evaluation of the continuous energy distribution in JENDL-4. Then the data were compared. It is noteworthy that significant amount of γ rays are radiated in 3-4.5MeV region in the JENDL-4. The amount is comparable for the prompt γ rays per fission (see Fig. 5). In CapGam, yields of experimentally observed γ rays are listed. In contrast, calculated values by the CCONE code[11] is used in JENDL-4. Although discrete gamma ray yields have not been observed, the spectra are evaluated continuously in the energy region 3-4.5MeV in JENDL-4. If the data in JENDL-4 are accurately evaluated, the neglect of the capture reactions of ^{235}U might cause the overestimation of the fission of ^{235}U in the unfolding from the measured pulse height spectra in section IV.

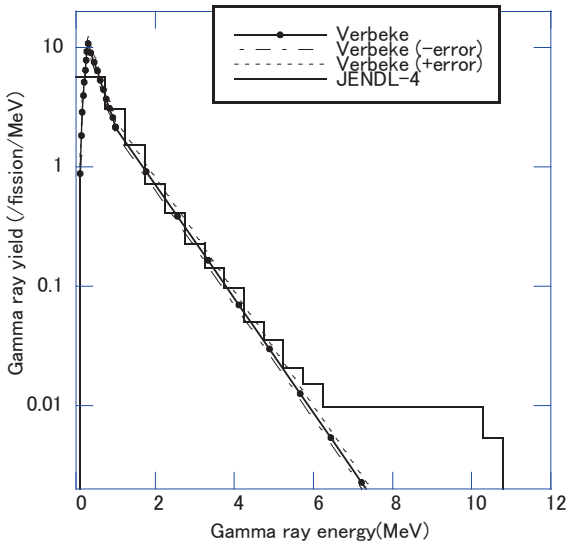

Fig.5 Evaluations of prompt γ ray spectra of ^{235}U fission for thermal neutron[5),10)]

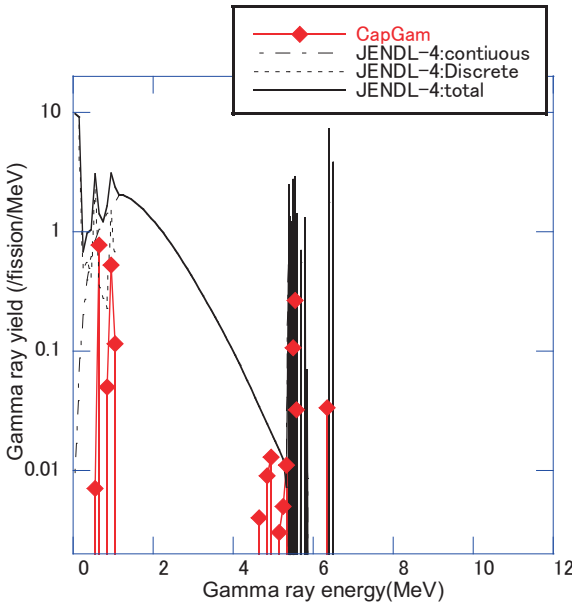

Fig. 6 Evaluations of γ ray spectra of ^{235}U capture reaction for thermal neutron [8),10)]

VI. Summary and Future Work

In order to determine the subcriticality margin of capture reactions in a sub-critical system, the gamma ray measurements and the numerical analyses have been conducted. For the 3 subcritical assemblies mocked up in the C-core tank of KUCA, the higher energy γ ray spectra (> 3MeV) were observed with a BGO scintillator. The authors assumed the spectra consist of γ rays from capture reactions of Al and SUS and fission of ^{235}U. By using the fission spectrum by Verbeke and the capture γ ray spectra by CapGam, those reaction rates were unfolded. The unfolded Al(n,γ) reaction rates agree with neutronics

calculations. This result demonstrates the possibility of CapC. However, the fission rate of ^{235}U was overestimated. By the comparison of the γ ray data from the capture of ^{235}U in CapGam with those in JENDL-4, the former gives smaller yields since CapGam presents only discrete energy γ rays experimentally observed. Accordingly, the neglect of ^{235}U capture in the unfolding might cause the overestimation of fission of ^{235}U.

In order to develop the CapC technique, revisions of the γ ray spectra and the yields are essential. For the purpose, the integral type experiments with various kinds of fuel and structural materials shall be done as well as the differential type experiments.

Acknowledgement

The authors would like to express their thanks to Dr. O. Iwamoto of JAEA and Dr. J. K. Tuli of BNL for their comments on γ ray emission data in JENDL-4 and CapGam.

References

1) TS-R-1, Regulations for the Safe Transport of Radioactive Material, 2005 Edition, International Atomic Energy Agency, (2005).
2) Proc. Advances in Applications of Burnup Credit to Enhance Spent Fuel Transportation, Storage, Reprocessing and Disposition, London, 29, August – 2, September, 2005, IAEA-TECDOC-1547, p.58.
3) Y. Nauchi, T. Kameyama, H. Unesaki, *et al*., Preprints 2012 Fall Meeting of Atomic Energy Soc. of Japan, Hiroshima Univ., Japan, Sep. 19-21, Q32 (2012), [on CD-ROM, in Japanese]
4) Y. Nauchi, T. Kameyama, H. Unesaki *et al*., KURRI Progress Report 2011, p.224, 2012.
5) J. M. Verbeke, C. Hagmann, D. Wright, UCRL-AR-228518, Lawrence Livermore National Laboratory, 2010
6) H. Ihara, J. Katakura and T. Nakagawa, JAERI-Data/Code 95-014, 1995.
7) J. Katakura, T. Yoshida, K. Oyamatsu *et al*., JAERI 1343 (2001).
8) J. K. Tuli ed. "Thermal Neutron Capture γ's (CapGam)", National Nuclear Data Center, Brookhaven National Laboratory, http://www.nndc.bnl.gov/capgam/, 2012.
9) Y. Nauchi, M. Baba, Y. Hirasawa *et al.*, Proceedings 1998 Symposium on Nuclear Data, JAERI-Conf 99-002, 1999, pp.274-279.
10) K. Shibata, O. Iwamoto, T. Nakagawa *et al*., J. Nucl. Sci. Technol. **48**(1), pp.1-30 (2011).
11) O.Iwamoto, J. Nucl. Sci. Technol., **44**, p.687 (2007).

34. Target Dependency of Light Mass Fragment Production DDX for 6 MeV/u Carbon Induced Reaction

T. Sanami

Applied research laboratory, High energy accelerator research organization,

Oho 1-1, Tsukuba, Ibaraki 305-0801 JAPAN

Email: toshiya.sanami@kek.jp

Double differential cross section (DDX) data of light mass fragment (LMF) production for 6 MeV/n carbon induced reaction have been measured for light to medium mass targets for evaluation of LMF production model at tens of MeV energy region. The data are useful not only to understand contribution of nuclear reactions during slowing down process of incident energetic ions in a matter, but also to study cluster like behavior of nucleus that was observed for proton induced LMF production around reaction threshold energy. The experiments were carried out at cyclotron facility of national institute of radiological sciences. Bragg curve counters at 30, 60 and 90 degrees were employed as fragment detector. DDXs for Li, Be, B, C, N, O production were measured for Be, C, Al, Ti and Cu targets. From the obtained DDXs, several features on DDX become obvious for description of LMF production in this energy range.

1. Introduction

Double differential cross section (DDX) is key parameter to describe secondary particle production and transportation. Regarding recent progress of high-energy ion beam application for tumor therapy, precise calculation and measurement are required for energy deposition distribution due to ionization by primary particle as well as secondary particles. For this purpose, several Monte-Carlo codes have been developed and utilized with fine particle tracking under actual three-dimensional structure and material. The codes use nuclear reaction models to describe secondary particle generation. The models are originally developed for nuclear reaction with several hundred of MeV/n projectiles. Because of the energy, the model calculates reaction products based on nucleon-nucleon reaction cross section. From application point of view, a primary ion impinging in a matter slowdowns continuously, which means reaction models are required for not only several hundred of MeV/n but also down to few MeV/n with considering nucleon binding energy. One idea is simply use the reaction model based on nucleon-nucleon reaction cross section for low energy ion reaction, however the applicability of this model must be carefully assessed though comparison with experimental data.

Especially, for several MeV/n energy region, experimental data are not available for not only LMF production DDX but also total reaction cross section that is indispensable parameter to determine absolute value of reaction products. Therefore, experimental data for LMF production DDX are requested for low energy range.

Experimental data of LMF production DDX for low energy range are generally not sufficient. Until now, several data have been taken for special reaction channel or much higher energy, thus systematic data have not been available covering wide target mass, entire fragment types, energy and emission angles, which allow us to assess applicability of calculation model with regarding this energy range.

From this standpoint, experimental data for carbon induced reaction on carbon target for 6 MeV/n and 12 MeV/n impinging energy were measured using Bragg Curve Counter [1]. The experimental data were in fairly agreement with calculation results with QMD model, except for fragments belonging to the low-lying levels of the residual nuclei, however it is still not clear about the applicability for another target nuclei. In this study, fragment DDXs were measured for several target nuclei to study target dependency on fragment production. The target nuclei were Be, C, Al, Ti and Cu, to cover light to medium nuclei. Results of fragment DDX as well as outline of data taking procedure are presented in the following sections.

2. Experiment

Details of experimental apparatus and procedure were same as one for proton induced reaction measurement described in references [1-8]. The experiments were performed using the NIRS 930 cyclotron in National Institute of Radiological Science (NIRS). **Figure 1** shows a picture of the experimental setup.

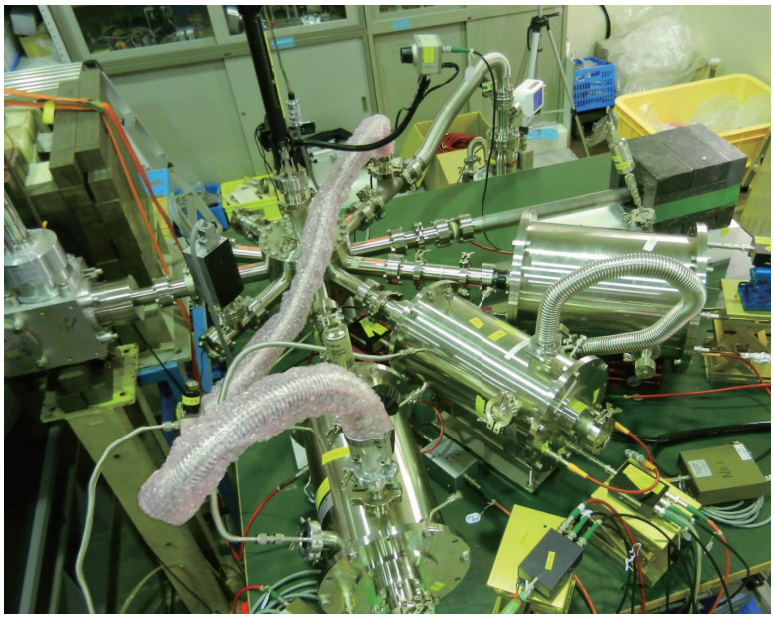

Fig. 1 Experimental setup

Carbon beam of 6 MeV/n was focused to 5 mm in diameter spot size on the target foil that was mounted on a target changer. The target changer mounts blank, ZnS viewer as well as less than 1 μm in thickness C, Al, Ti, Cu and Ta targets. Fragments from the target were measured by the BCCs mounted on the 30, 60 and 90 ports of the scattering chamber.

The BCC is a parallel plate ionization chamber with a grid. The details of BCC, operation parameters and readout electronics are already described in reference [1]. **Figure 2** shows Two dimensional spectrum of Bragg Peak vs Energy at 30 degree laboratory angle for 6 MeV/n carbon on beryllium target. As shown in this figure, very clear separation was derived for He to O fragments. In addition, the low energy events shown in this figure as (i), which were too low energy to form Bragg peak, were also separated using range-energy plot that can be derived from time-difference between signals from cathode and anode [1]. The events shown in this figure as (ii), which were too high energy to stop within BCC length, were used as data points with compensating missing energy by calculation [2]. It should be stressed that these two techniques are essential to cover required energy range for fragment measurement in this energy range.

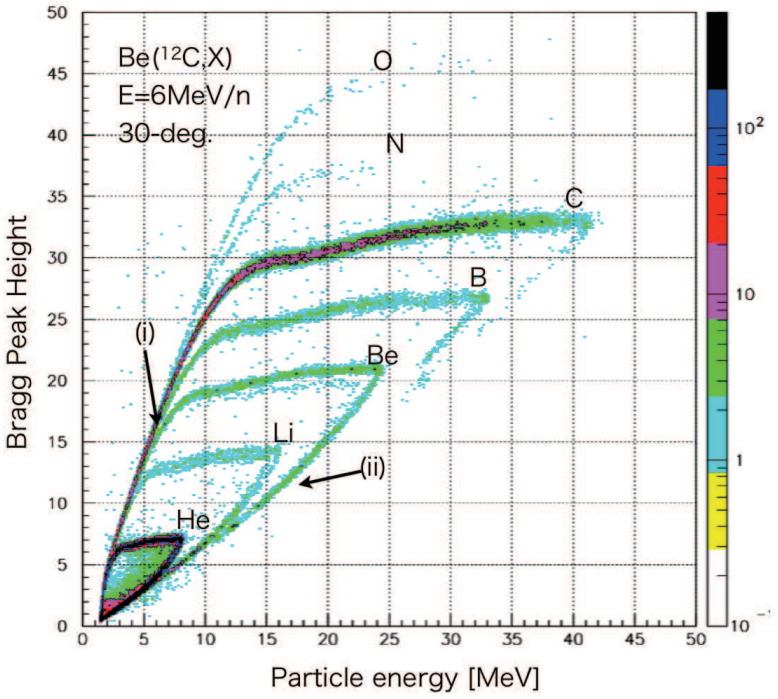

Figure 2 Two dimensional spectrum of Bragg Peak vs Energy at 30 degree laboratory angle for 6 MeV/n carbon on Beryllium

After particle identification according to Bragg peak vs energy plot, pulse height spectra were converted to energy spectra for each fragment. The energy spectra were normalized by number of incident carbons and solid angle. The number of carbon was obtained from Faraday cup measurement during each run. Solid angle was deduced analytically and confirmed through α-particle counting from ^{241}Am check source placed instead of the target.

3. Result and discussion

Figures 3-8 show experimental results of DDX for lithium, beryllium, boron, carbon nitrogen and oxygen emission at 30 degree, 6 MeV/n carbon on various targets. The experimental data covers energy ranges up to 30 MeV for lithium, 45 MeV for beryllium, 60 MeV for boron and more than 70 MeV for carbon, nitrogen and oxygen spectra. Therefore, part of energy spectrum was covered for lithium and beryllium emission. The missed energy range for lithium and beryllium could be covered by using a silicon surface barrier detector just behind the BCC.

As shown in these figures, the highest of DDXs are given for the carbon emission, Fig. 6,

which means most of projectile carbons are scattered from target nuclei with keeping their structure. The comparison between boron (Fig.5) and nitrogen (Fig.7) emission DDXs tells difference between proton stripping and attachment probabilities of projectile carbon on various targets. The same comparison can be done for alpha-particle stripping and attachment using beryllium (Fig.4) and oxygen (Fig.8) emission DDXs. For proton stripping/attachment, similar spectra are obtained for boron and nitrogen emission for carbon and aluminum target except for low energy side of boron emission from carbon. For the other targets, Be, Ti and Cu, boron emission spectra show one order of magnitude higher than nitrogen emission. For alpha stripping/attachment, only aluminum shows similarity in comparison between beryllium and oxygen spectra. In the comparison between proton/alpha attachment, i.e, Fig. 7 and 8, almost same spectra are given each other, which means that the attachment probability of proton and alpha -particle is almost same for all the target nuclei. These features should be considered to describe reaction models in this energy range.

Acknowledgements

The authors wish to thank operators and supporting crew of NIRS cyclotron for their help to perform beam experiment. The BCC was originally developed with support of Grant-in-aid of ministry of education "KAKENHI(15360499, M.Baba, Tohoku University)". The experiment was performed with support of Grant-in-aid of ministry of education "KAKENHI(24561051, T.Sanami, KEK)".

References

[1] T. Sanami *et al.*, “Measurement of fragment production DDX of 72 and 144 MeV ^{12}C beam induced reaction on carbon using Bragg Curve Counter”, *Proc. 2009 Symp. Nucl. Data,* JAEA-Conf 2010-005 (2010).

[2] T. Sanami *et al.*, *Nucl. Instrm. Meth.* A589, 193 (2008).

[3] M. Hagiwara *et al.*, *Nucl. Instrm. Meth*. A592, 73 (2008).

[4] M. Hagiwara *et al.*, "Measurements of double differential fragment production cross sections of silicon for 70 MeV protons”, *Proc. 2005 Symp. Nucl. Data*, JAEA-Conf 2006-009 (2006), pp.78-83.

[5] T. Sanami *et al.*, “Recent progress of fragment measurement from tens of MeV proton induced reaction using Bragg Curve Counter”, *Proc. 2008 Symp. Nucl. Data,* JAEA-Conf 2009-004 (2009), pp.111-116.

[6] T. Sanami *et al.*, "Fragment DDX measurement of proton induced reactions on light-medium nuclei for energy range from reaction threshold to a few hundred MeV ", *Journal of Korean Physics Society* **59**, pp.1805-1808 (2011).

[7] T. Sanami *et al.*, “Experimental studies of light fragment production cross section for nucleon induced reaction at intermediate energies”, *Proc. 2010 Symp. Nucl. Data,* JAEA-Conf 2011-002 (2011).

[8] M. Hagiwara *et al.*, *Journal of Nuclear Science and Technology*, **49**(6), pp.571-587 (2012).

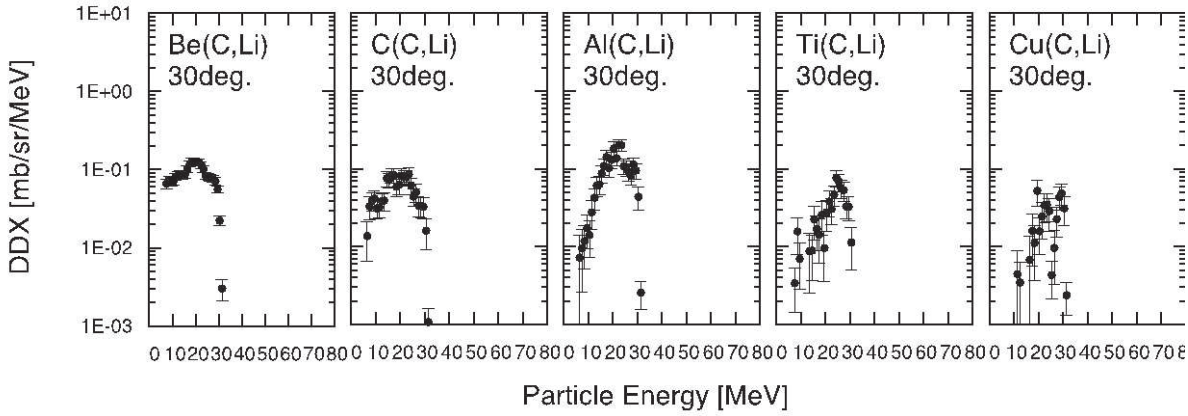

Figure 3 DDXs of lithium emission at 30 degree for various samples

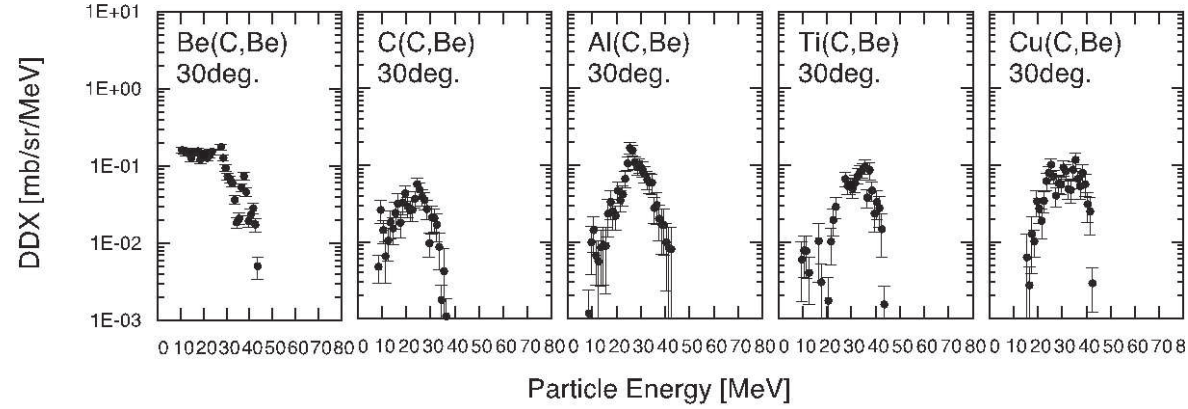

Figure 4 DDXs of beryllium emission at 30 degree for various samples

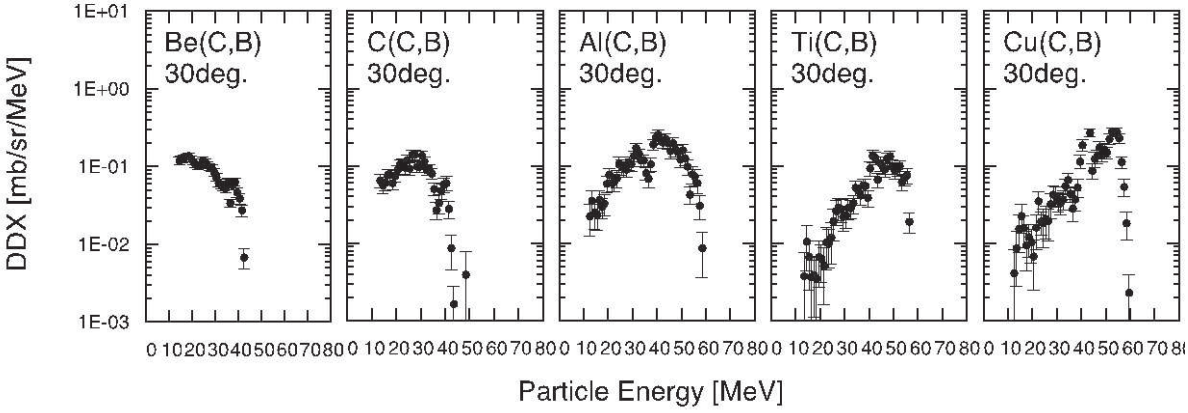

Figure 5 DDXs of boron emission at 30 degree for various samples

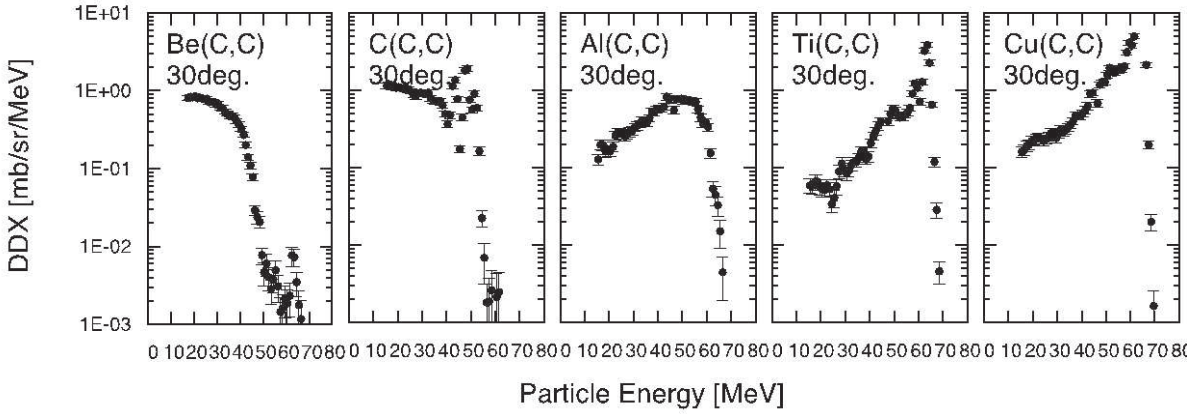

Figure 6 DDXs of carbon emission at 30 degree for various samples

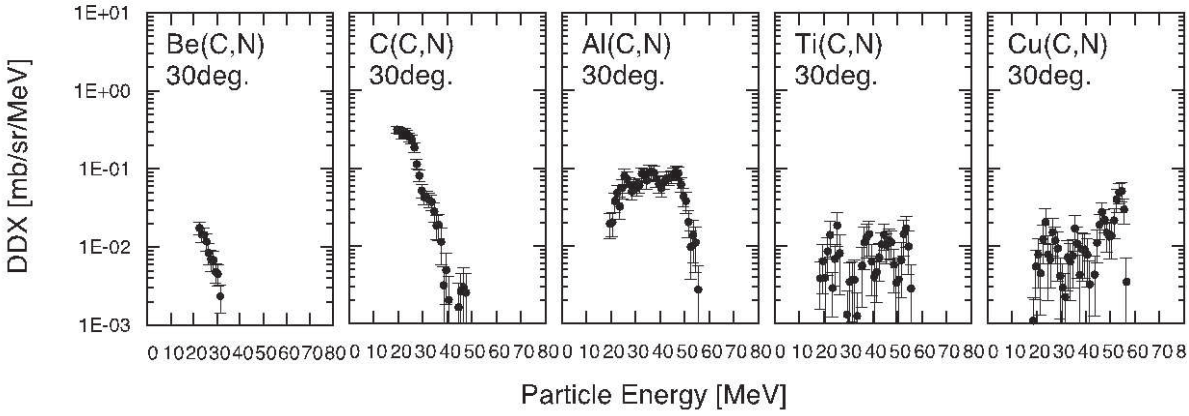

Figure 7 DDXs of nitrogen emission at 30 degree for various samples

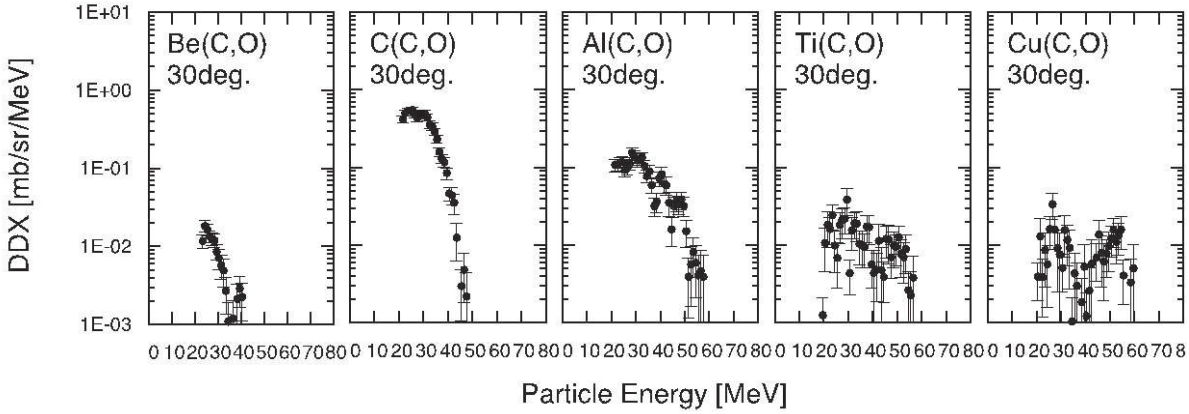

Figure 8 DDXs of oxygen emission at 30 degree for various samples

35. Validity of Covariance Data of ^{232}Th in JENDL-4.0 and ENDF/B-VII.1

Tatsuya KOJIMA, Takashi FUJII, Takanori KITADA
Osaka University, 2-1 Yamadaoka, Suita-shi, Osaka, Japan, 565-0871
t-kojima@ne.see.eng.osaka-u.ac.jp

Reliability of ^{232}Th cross section is not so high because of less experience in real core than uranium etc, and the cross section and its uncertainty show remarkable difference among JENDL-4.0, ENDF/B-VII.1 and JENDL-3.3. Validity of the covariance data of ^{232}Th capture reaction in JENDL-4.0 and ENDF/B-VII.1 was investigated by calculating the uncertainty of ^{232}Th replacement reactivity worth in KUCA experiments. An error bar for ENDF/B-VII.1 does not cover the value (C/E = 1) with considering 3σ and this shows underestimation of the covariance data in ENDF/B-VII.1. Although variance of JENDL-4.0 at 1 eV to 10 eV is 40 %, the difference in cross section between JENDL-4.0 and JENDL-3.3 is more than 100% in maximum. Although the variance of JENDL-4.0 may be underestimated in this energy range, the error bar for JENDL-4.0 covers the value (C/E = 1) in 1σ and this shows the validity of covariance data in JENDL-4.0.

1. Introduction

Thorium has various advantages and many researches have been performed. The reliability of ^{232}Th cross section is not so high because of less experience in real core than uranium etc, and the cross section and its uncertainty show the remarkable difference among JENDL-4.0[1], ENDF/B-VII.1[2] and JENDL-3.3[3]. Figure 1 shows ^{232}Th capture cross sections of JENDL-4.0, and relative difference between JENDL-4.0, ENDF/B-VII.1 and JENDL-3.3.

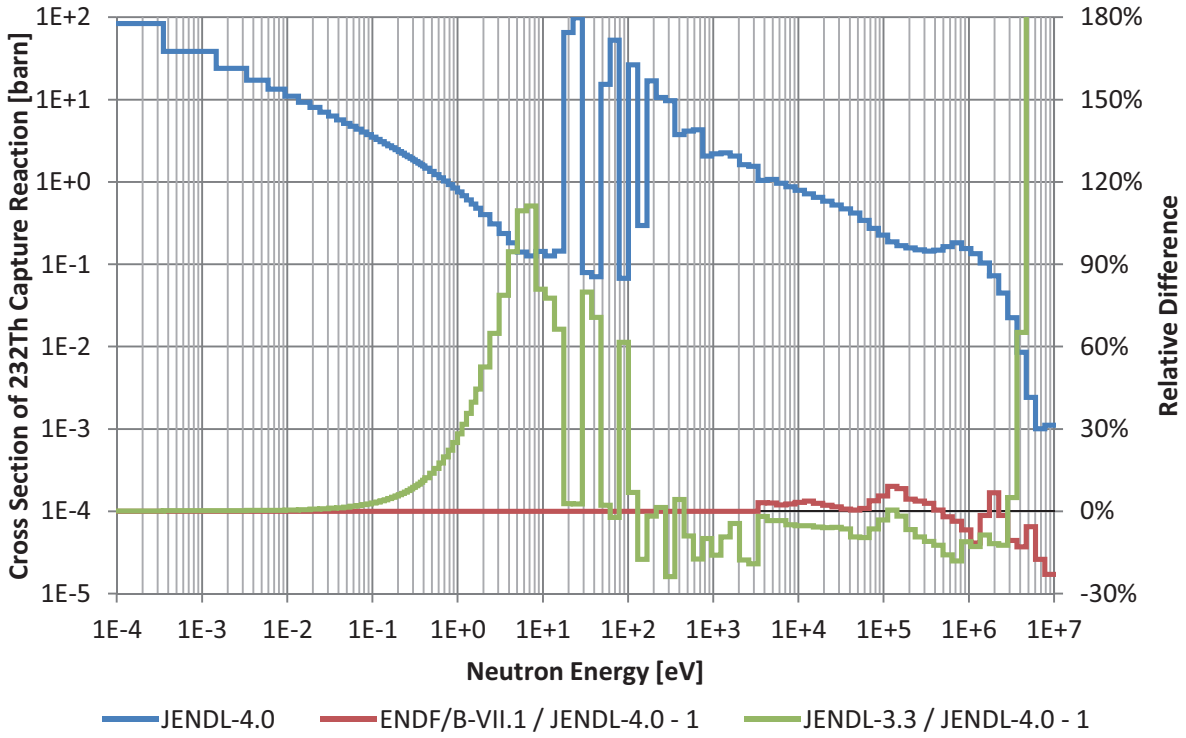

Fig. 1 ^{232}Th Capture Cross Sections of JENDL-4.0, and Relative Difference among JENDL-4.0 and ENDF/B-VII.1 and JENDL-3.3

Covariance values of JENDL-4.0 are larger than those of ENDF/B-VII.1 in energy groups from 53 to 96 (from 22.6 eV to 0.05 eV) as shown in Fig. 2 and 3. The object of this study is to clarify the reliability of the covariance data of ^{232}Th through the evaluation of ^{232}Th replacement worth measured at KUCA in 2011.

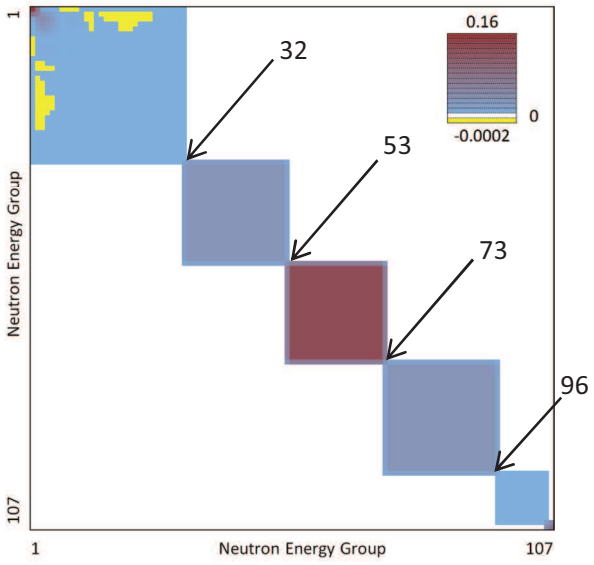

Fig. 2 ^{232}Th Covariance Matrix of (n,γ) Reaction of JENDL-4.0

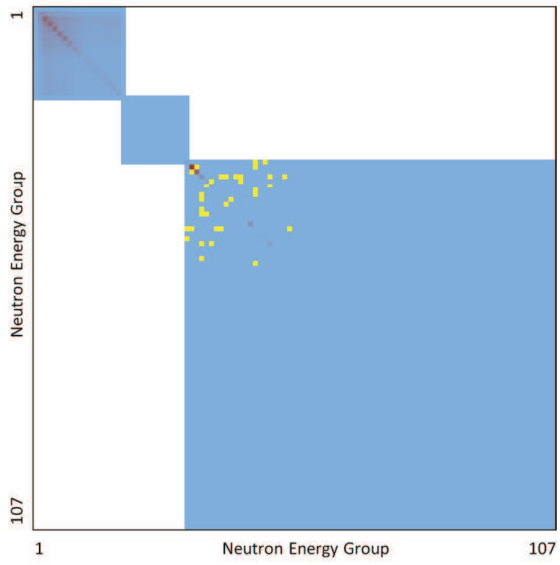

Fig. 3 ^{232}Th Covariance Matrix of (n,γ) Reaction of ENDF/B-VII.1

2. Experiment and Analysis

In KUCA experiments, two cores were assembled; B7/8”P12ETEETEE and B10/8”P9ETEETEE in 2011. Table 1 shows ^{232}Th/^{235}U and H/^{235}U ratio of the two cores.

Fuel cells of the cores are composed of thorium plate, enriched uranium plate, and polyethylene plates, and the difference between the cores is the width of polyethylene plates (7/8” and 10/8” in one unit fuel cell, respectively.) A neutron spectrum at fuel region is shown in Fig.4, and the difference in neutron spectrum is observed especially at around 0.1 eV. Th replacement worth was evaluated as the change of excess reactivity between the two states: with and without Th sample plates, for both cores. Th replacement worth were evaluated by continuous energy Monte Carlo code MVP[4] with 1 billion history, and the error caused by the uncertainty in ^{232}Th cross section was evaluated by using the covariance data with sensitivity coefficient for Th replacement worth. Sensitivity coefficients were evaluated by SAGEP[5] code with the cross section data obtained by SRAC2006[6]. The covariance data was evaluated by NJOY99[7]. Results are summarized in Fig.5.

Table 1 H/^{235}U and ^{232}Th/^{235}U Ratio

	B7/8”P12ETEETEE	B10/8”P9ETEETEE
^{232}Th/^{235}U	15.2	
H/^{235}U	140	210

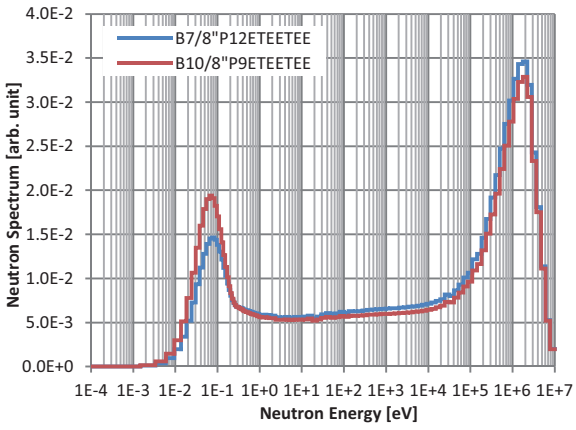

Fig. 4 Neutron Spectrum of Two Cores, B7/8"P12ETEETEE and B10/8"P9ETEETEE

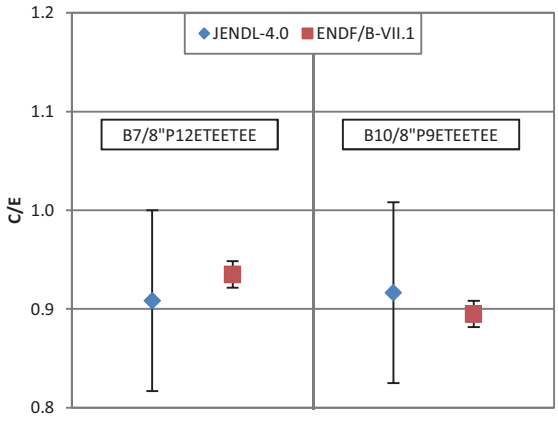

Fig. 5 C/E Value of Th Replacement Worth of JENDL-4.0 and ENDF/B-VII.1 at B7/8"P12ETEETEE and B10/8"P9ETEETEE

3. Discussions

To investigate the ^{232}Th cross section of JENDL-4.0 in detail, comparison between JENDL-4.0 and JENDL-3.3 was performed. Figure 6 shows C/E value of Th replacement worth of JENDL-4.0 and JENDL-3.3 at B7/8”P12ETEETEE core and B10/8”P9ETEETEE core. JENDL-3.3 shows better results than JENDL-4.0. C/E value is 0.91 with JENDL-4.0 and 0.94 with JENDL-3.3. Figure 7 shows the energy breakdown of the Th replacement worth between JENDL-4.0 and JENDL-3.3 for both cores.

Figure 8 shows the sensitivity coefficient of Th replacement worth of JENDL-4.0 for both cores. Figure 9 shows standard deviations of ^{232}Th capture cross sections in JENDL-4.0. Main contribution to the difference in C/E comes from the energy range below 10 eV, and one remarkable point is observed at around 61.4 eV where the 2nd resonance peak is. Energy range from 0.2 eV to 10 eV has small sensitivity coefficient but the difference in the cross section is remarkable. Although the variance of JENDL-4.0 at 1 eV to 10 eV is 40 %, the difference in cross section between JENDL4.0 and 3.3 is more than 100% in maximum. The variance of JENDL-4.0 may be small in this energy range.

Figure 5 shows that the error bar for ENDF/B-VII.1 does not cover the value (C/E = 1) with considering 3σ and this shows underestimation of covariance data in ENDF/B-VII.1. The error bar for JENDL-4.0 covers the value (C/E = 1) in 1σ and this shows the validity of covariance data in JENDL-4.0.

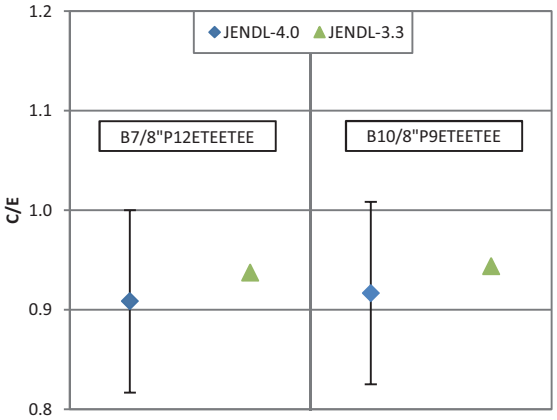

Fig. 6 C/E Value of Th Replacement Worth of JENDL-4.0 and JENDL-3.3 at B7/8"P12ETEETEE and B10/8"P9ETEETEE

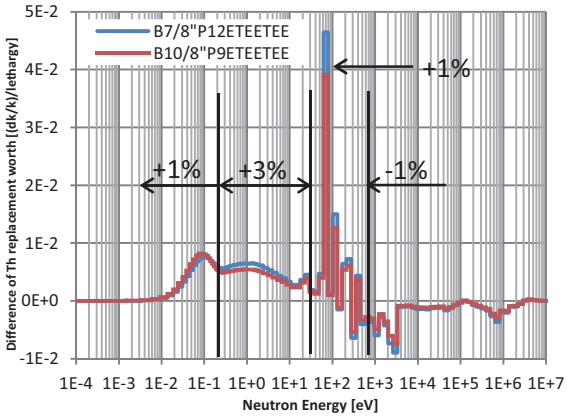

Fig. 7 Energy Breakdown of the Th Replacement Worth between JENDL-4.0 and JENDL-3.3 at B7/8"P12ETEETEE and B10/8"P9ETEETEE

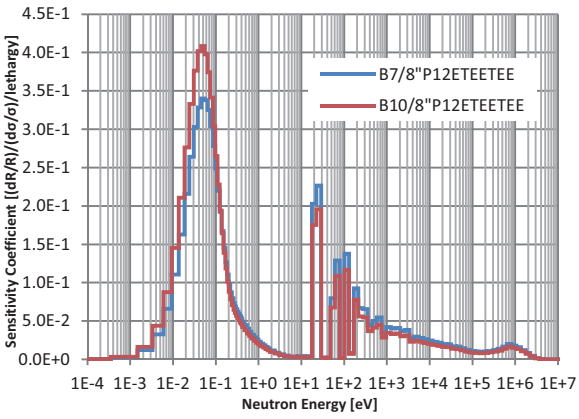

Fig. 8 Sensitivity Coefficient of Th Replacement Worth of JENDL-4.0 at B7/8"P12ETEETEE and B10/8"P9ETEETEE

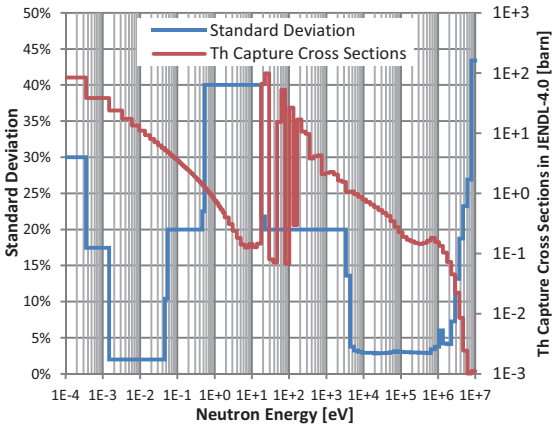

Fig. 9 Standard Deviations of ^{232}Th Capture Cross Sections in JENDL-4.0

4. Future Works

In order to investigate the validity of cross section and covariance of ^{232}Th in detail, the experiments at softest and/or hardest spectrum core are being planned in the future.

References

[1] K. Shibata, O. Iwamoto, T. Nakagawa, N. Iwamoto, A. Ichihara, S. Kunieda, S. Chiba, K. Furutaka, N. Otuka, T. Ohsawa, T. Murata, H. Matsunobu, A. Zukeran, S. Kamada, and J. Katakura: "JENDL-4.0: A New Library for Nuclear Science and Engineering," J. Nucl. Sci. Technol. 48(1), 1-30 *(2011)*.

[2] M.B. Chadwick, M. Herman, P. Oblozinský, M.E. Dunn, Y. Danon, A.C. Kahler, D.L. Smith, B. Pritychenko, G. Arbanas, R. Arcilla, R. Brewer, D.A. Brown, R. Capote, A.D. Carlson, Y.S. Cho, H. Derrien, K. Guber, G.M. Hale, S. Hoblit, S. Holloway, T.D. Johnson, T. Kawano, B.C. Kiedrowski, H. Kim, S. Kunieda, N.M. Larson, L. Leal, J.P. Lestone, R.C. Little, E.A. McCutchan, R.E. MacFarlane, M. MacInnes, C.M. Mattoon, R.D. McKnight, S.F. Mughabghab, G.P.A. Nobre, G. Palmiotti, A. Palumbo, M.T. Pigni, V.G. Pronyaev, R.O. Sayer, A.A. Sonzogni, N.C. Summers, P. Talou, I.J. Thompson, A. Trkov, R.L. Vogt, S.C. van der Marck, A. Wallner, M.C. White, D. Wiarda, P.G. Young: "ENDF/B-VII.1 Nuclear Data for Science and Technology: Cross Sections, Covariances, Fission Product Yields and Decay Data," Nucl. Data Sheets, 112, 2887-2996 *(2011)*.

[3] K. Shibata, T. Kawano, T. Nakagawa, O. Iwamoto, J. Katakura, T. Fukahori, S. Chiba, A. Hasegawa, T. Murata,H. Matsunobu, T. Ohsawa, Y. Nakajima, T. Yoshida, A. Zukeran, M. Kawai, M. Baba, M. Ishikawa, T. Asami, T. Watanabe, Y. Watanabe, M. Igashira, N. Yamamuro, H. Kitazawa, N. Yamano and H. Takano: "Japanese Evaluated Nuclear Data Library Version 3 Revision-3: JENDL-3.3," J. Nucl. Sci. Technol. 39, 1125 *(2002)*.

[4] Y. Nagaya, K. Okumura, T. Mori et al., "MVP/GMVP Version 2: General Purpose Monte Carlo Codes for Neutron and Photon Transport Calculations based on Continuous Energy and Multigroup Methods," JAERI 1348 *(2005)*.

[5] A. Hara, T. Takeda, Y. Kikuchi, "SAGEP: Two-dimensional sensitivity analysis code based on generalized perturbation theory," JAERI-M 84-027, Japan Atomic Energy Research Institute (JAERI) *(1984)* [in Japanese].

[6] K. Okumura, T. Kugo, K. Kaneko and K. Tsuchihashi, "SRAC2006: A Comprehensive Neutronics Calculation Code System, " JAEA-Data/Code 2007-004 *(2007)*.

[7] R. E. MacFarlane, D. W. Muir, R. M. Boicourt, "The NJOY nuclear data processing system, Volume I: User's manual", LA-9303-M (ENDF-324) *(1982)*.

This is a blank page.

36. Measurement of High Energy Neutron Induced Cross Sections for Terbium

Hirohito SUZUKI[1], Shun SEKIMOTO[1], Hiroshi YASHIMA[1], Kazuki NISHIMURA[1], Kazuhiko NINOMIYA[2], Yoshitaka KASAMATSU[2], Tatsushi SHIMA[3], Naruto TAKAHASHI[2], Atsushi SHINOHARA[2], Hiroshi MATSUMURA[4], Masayuki HAGIWARA[4], Kunihiko NISHIIZUMI[5], Marc W.CAFFEE[6], Seiichi SHIBATA[1]

[1] Research Reactor Institute, Kyoto University, Kumatori, Osaka 590-0494, Japan

[2] Graduate School of Science, Osaka University, Toyonaka, Osaka 560-0043, Japan

[3] Research Center for Nuclear Physics, Osaka University, Suita, Osaka 567-0047, Japan

[4] High Energy Accelerator Research Organization, Tsukuba, Ibaraki 305-0801, Japan

[5] Space Sciences Laboratory, University of California, Berkeley, CA 94720-7450, USA

[6] Department of Physics, Purdue University, West Lafayette, IN 47907, USA

e-mail: sekimoto@rri.kyoto-u.ac.jp

Reaction cross sections for Tb induced by neutrons at 197 and 386 MeV were measured by using ^{7}Li(p,n) reaction at N0 beam line in the Research Center for Nuclear Physics (RCNP), Osaka University. To estimate quasi-monoenergetic neutron cross sections, Tb samples were irradiated on the two angles of 0°and 25° for the axis of the primary proton beam. The measured cross section data in the ^{159}Tb(n,x) reactions are compared with values calculated by using the particles and heavy ion transport code system (PHITS). The proton cross sections for Tb at 400 MeV were also measured, and then neutron cross sections obtained are compared to the proton ones.

1. Introduction

Neutron cross sections are important as basic nuclear data for the estimation of residual radioactivities in the accelerator facility and even for cosmochemistry [1-2]. Although the high-energy neutron cross sections from C, Cu, Pb and Bi have already been published [3-4], neutron cross sections in the energy range above 100 MeV have scarcely been measured experimentally. Therefore, those evaluated from calculation codes are utilized and proton cross section data are also utilized on the basis of the assumption that neutron cross sections in higher energies than 100 MeV approximately equal to proton ones in the same energy range. Recently, cross section measurements for quasi-monoenergetic neutron induced reactions for the basic nuclear data as well as the cosmochemical application have been commenced by our group [2,5-8].

In this work, we measured reaction cross sections of radionuclides produced through nuclear spallation reaction of Tb, induced by neutrons at 197 and 386 MeV, which have never been reported. Furthermore, proton cross sections for Tb at E_p = 400 MeV were also measured to compare with the neutron ones.

2. Experimental procedure

2.1. Neutron irradiation

The irradiations were carried out using neutrons produced through ^{7}Li(p,n) reaction at N0 beam line in the Research Center for Nuclear Physics (RCNP), Osaka University. To estimate quasi-monoenergetic neutron cross sections, the sample stack of Tb was irradiated on the two angles of 0° and 25° for the axis of the primary proton beam. The schematic view of these irradiation configurations is shown in **Fig. 1**.

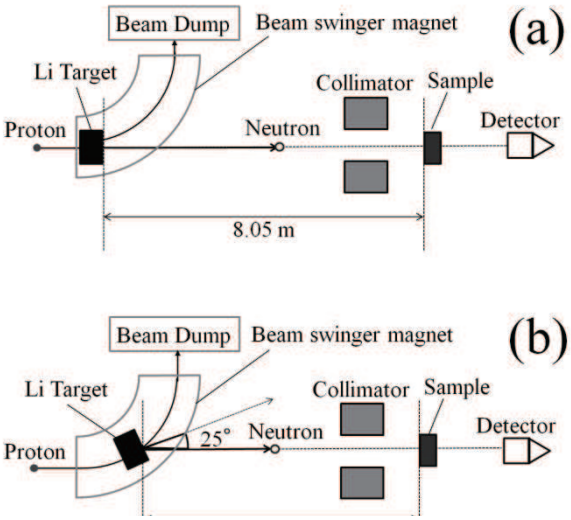

Figure 1. Schematic view of irradiation configurations; (a) 0° and (b) 25°.

This irradiation method referred to the method by Sisterson *et al*. [9]. Since peak energy neutrons produced by ^{7}Li(p,n) reaction are tend to be emitted in the forward direction and low energy neutrons isotropically, the irradiation on the angle of 0° was performed by peak and low energy neutrons, whereas the irradiation on 25° by low energy ones only. Therefore, neutron cross sections were able to be estimated by subtracting the activities produced in the samples placed on 25° from those on 0° to correct the contribution of the low energy tail in the neutron spectrum.

The neutron energy spectra were measured by the time-of-flight method using a NE213 liquid scintillation detector. The neutron spectra obtained in the irradiations on the angle of 0° and 25° are shown in **Fig. 2(a)**. The quasi-monoenergetic neutron spectrum obtained by subtracting the spectrum on 25° from the one on 0° is shown in **Fig. 2(b)**. The samples were placed at 8.05 or 7.20 m from the Li-target in the forward direction at 0° or 25° for the axis of the primary proton beam, respectively (shown in Fig. 1). The samples induced by 386 MeV neutron on the angle of 0° and 25° were irradiated for 31.6 and 23.0 h, respectively and the samples by 197 MeV on 0° and 25° were for 52.7 and 41.3 h, respectively.

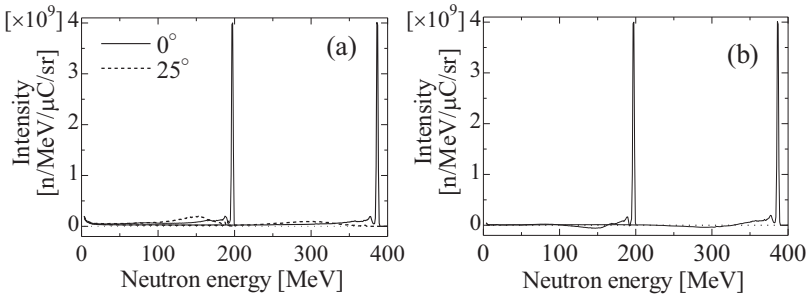

Figure 2. (a) Neutron spectra of the 0° and 25° irradiations measured with the TOF method, (b) Quasi–monoenergetic neutron spectra obtained from the spectra of the 0° and 25° irradiations.

2.2. Proton irradiation

Terbium foil with a thickness of 21 mg cm^{-2} was mounted in the holder where the Li target was mounted in the neutron irradiation. The Tb foil was irradiated with protons having a mean current of approximately 100 nA for 183.8 s. The average beam current in this irradiation was 101.5±4.5 nA, which was determined by the ^{27}Al(p,3pn)^{24}Na monitor reaction. The Tb foil was sandwiched by guard foils of identical material to monitor

recoil losses and to prevent cross contamination between the samples.

2.3. Gamma-ray spectrometry

After the irradiation, gamma-rays emitted from the irradiated samples were measured with a high-purity germanium (HPGe) detector. The neutron-irradiated samples were counted for 1000－610000 seconds more than ten times, and the proton-irradiated ones for 2000－1700000 seconds several times. The measured nuclides in the neutron- and proton- irradiated samples are listed in **Table 1** with their nuclear properties.

Table 1. Relevant nuclear properties of measured nuclides. Each nuclide is either independent (*I*) or cumulative (*C*).

Target nuclides	Reaction	Measured nuclides	Half-life	Gamma-ray energy [keV]	Branching ratio [%]
^{159}Tb	(p,x), (n,4n)	^{156}Tb (*I*)	5.35 d	534	67
^{159}Tb	(p,x), (n,5n)	^{155}Tb (*I*)	5.32 d	106	25
^{159}Tb	(p,x), (n,7n)	^{153}Tb (*I*)	2.34 d	212	31
^{159}Tb	(p,x), (n,8n)	^{152}Tb (*I*)	17.5 h	345	65
^{159}Tb	(p,x), (n,9n)	^{151}Tb (*I*)	17.6 h	288	28
^{159}Tb	(p,x), (n,x)	^{149}Gd (*C*)	9.3 d	150	48
^{159}Tb	(p,x), (n,x)	^{147}Gd (*C*)	38.1 h	230	63
^{159}Tb	(p,x), (n,x)	^{146}Gd (*C*)	48.3 d	155	47
^{159}Tb	(p,x), (n,x)	^{148}Eu (*I*)	54.5 d	550	99
^{159}Tb	(p,x), (n,x)	^{145}Eu (*C*)	5.93 d	1659	15

3. Data analysis

3.1. Reaction rate in neutron-irradiated sample

Activation reaction rates were estimated by considering the peak counts of gamma-ray spectra measured with the HPGe detector, the peak efficiency of the HPGe detector calculated by the EGS4 code [10], the self-absorption of gamma-rays in the samples also corrected by the EGS4 code and the beam current fluctuation during the irradiation.

The reaction rates (R) per beam current, corrected for the above-mentioned effects, are given as follows:

$$R = \frac{\lambda C}{N\varepsilon\gamma e^{-\lambda t_c}(1-e^{-\lambda t_m})\sum_{i=1}^{n}\{Q_i(1-e^{-\lambda i\Delta t})e^{-\lambda(n-i)\Delta t}\}} \quad (1)$$

where λ is a decay constant (s^{-1}), C is a total counts of gamma-ray peak area, ε is a peak efficiency, N is a number of atoms in the target (atom), t_c is a cooling time (s),γ is a branching ratio of gamma rays, t_m is a measurement time (s), and Q_i is a beam current for irradiation time interval Δt.

3.2. Cross section estimation in neutron-irradiated sample

The activation cross section (σ) can be determined in principle as follows:

$$\sigma = \frac{R}{\varphi} \quad (2)$$

where φ is a neutron fluence rate per beam current.

Since neutron cross sections were estimated by subtracting the reaction rate in the irradiation on the angle of 25° from that in 0°. In this work, the cross sections were estimated as follows:

$$\sigma = \frac{R_0 - R_{25}f}{\varphi} \quad (3)$$

where R_0 and R_{25} are the reaction rate in the irradiation on the angles of 0° and 25°, respectively and f is a factor for the correction in subtraction of neutron spectrum, and the one due to the variation from 8.05 to 7.20 m in the distance between the Li-target and the samples.

3.3. Cross section estimation in proton-irradiated sample

The proton cross sections were able to be estimated as follows:

$$\sigma = \frac{A}{IN_d x\left(1-e^{-\lambda t_i}\right)} \tag{4}$$

where I is a mean beam intensity during the proton irradiation (s^{-1}), N_d is an atomic density in the irradiated samples (atom・cm^{-3}), x is a thickness of the irradiated samples (cm), t_i is an irradiation time (s), λ is a decay constant (s^{-1}), A is an activity produced in the on-beam sample (Bq). Those activities were estimated as follows:

$$A = \frac{\lambda C}{\varepsilon\gamma e^{-\lambda t_c}\left(1-e^{-\lambda t_m}\right)} \tag{5}$$

where symbols used in the Eq. (5) denote the same physical quantities as those used in the Eq. (1).

4. Results and discussion

4.1. Neutron cross sections in Terbium

The cross sections obtained for ^{159}Tb(n,4n)^{156}Tb, ^{159}Tb(n,9n)^{151}Tb, ^{159}Tb(n,x)^{149}Gd, and ^{159}Tb(n,x)^{145}Eu reactions are shown in **Fig. 3(a-d)**, respectively. Since neutron cross section data in this energy range have never been reported, the obtained values are compared with neutron cross sections at 197, 287 and 385 MeV, which were calculated with the Monte-Calro simulation of PHITS code [11]. It is apparent from Fig.3 that the

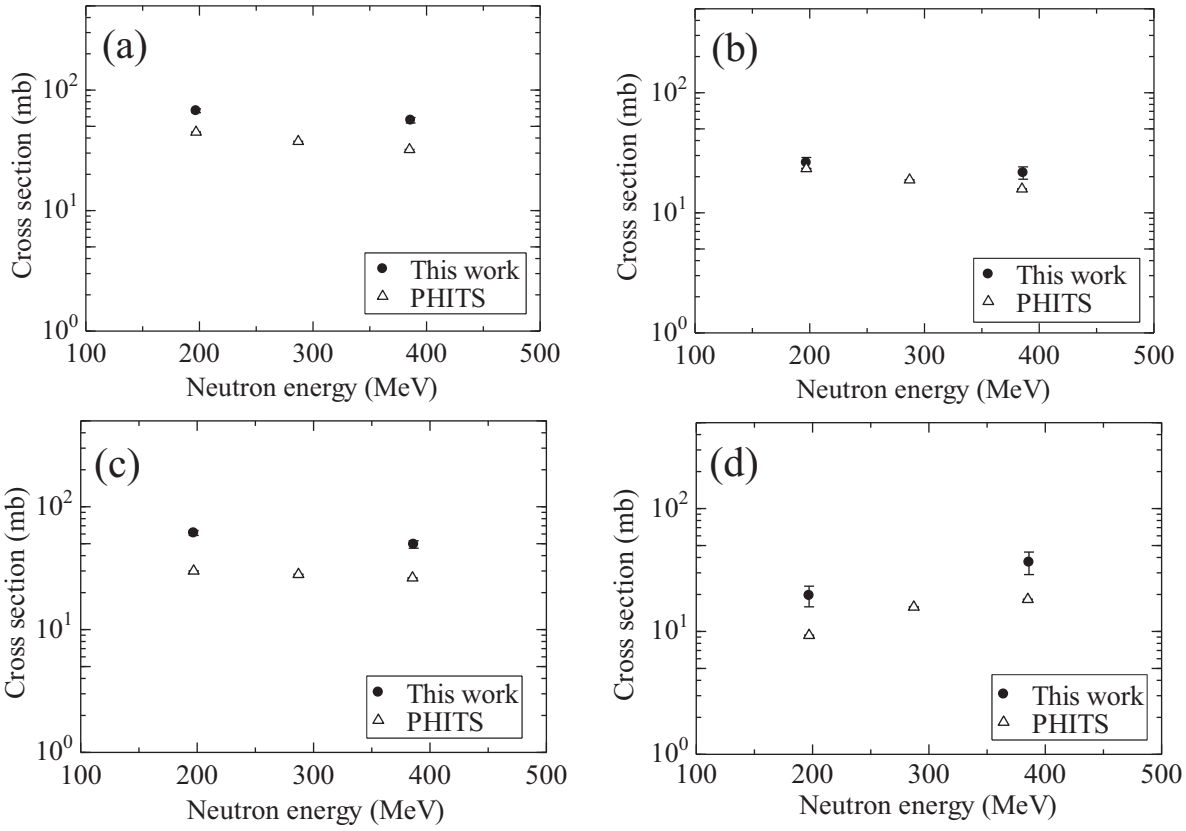

Figure 3. Excitation functions for (a) ^{159}Tb (n,4n) ^{156}Tb, (b) ^{159}Tb (n,9n) ^{151}Tb, (c) ^{159}Tb (n,x) ^{149}Gd, (d) ^{159}Tb(n,x)^{145}Eu.

experimental values in this work tend to be higher than calculated values by PHITS code. It is also found that the similar trend that the cross section values decrease or increase with higher neutron energy can be seen between experimental values and calculated values. Such tendencies as described above are also the case for not only the four reactions shown in Fig. 3 but also the all reactions interested in this work (shown in **Table 1**).

4.2. Comparison of neutron cross sections with proton ones

The cross sections of ^{159}Tb(n,x) and ^{159}Tb(p,x) reactions (E_n=386 MeV, E_p=400 MeV) shown in **Table 1** are illustrated in **Fig. 4**. The measured neutron cross sections agree well with the measured proton ones in the neutron- and proton-induced reactions whose products are ^{155}Tb, ^{153}Tb, ^{152}Tb, ^{149}Gd, ^{146}Gd and ^{145}Eu. On the other hand, the neutron cross sections are higher than proton ones in those reactions whose products are ^{156}Tb and ^{148}Eu, and the neutron ones are lower than proton ones in those reactions whose products are ^{151}Tb and ^{147}Gd. To evaluate those experimental neutron data in detail, further studies along this line are in progress.

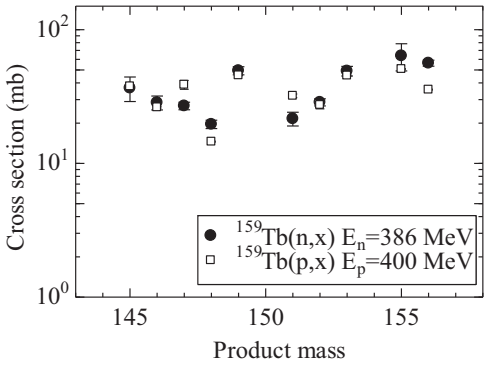

Figure 4. Cross sections obtained for ^{159}Tb (n,x) and ^{159}Tb(p,x) reactions.

5. Conclusion

Reaction cross sections for Tb induced by quasi-monoenergetic 197 and 386 MeV neutrons and 400 MeV protons were measured. The measured neutron cross sections at 386 MeV are compared with the measured proton cross sections at 400 MeV.

The measured cross sections for the ^{159}Tb (n,x) reactions in this work tend to be higher than the cross sections calculated by PHITS code. The similar trend of increasing or decreasing cross section with increasing neutron energy can be seen between experimental values and calculated values.

Acknowledgments

The authors express their gratitude to the accelerator staff of RCNP for their generous supports in this experiment (RCNP-E298 and E361). This work was supported by embryonic research project support in Kyoto University Global COE Program "International Center for integrated Research and Advanced Education in Materials Science", Kansai Research Foundation for technology promotion for SS, and National Science Foundation for KN and MWC.

References

[1] H. Yashima, K. Terunuma, T. Nakamura, M. Hagiwara, N. Kawata and M. Baba, Mesurements of neutron activation cross sections for major elements of water, air and soil between 30 and 70 MeV, *J. Nucl. Sci. Technol. Suppl.* 4 (2004), pp. 70-73.

[2] K. Nishiizumi, K.C. Welten, H. Matsumura, M.W. Caffee, K. Ninomiya, T. Omoto, R. Nakagaki, T.

Shima, N. Takahashi, S. Sekimoto, H. Yashima, S. Shibata, K. Bajo, K. Nagao, N. Kinoshita, M. Imamura, J. Sisterson and A. Shinohara, Measurements of high-energy neutron cross sections for accurate cosmogenic nuclide production rates, *Geochim. Cosmochim. Acta* 73 (2009), pp. A945.

[3] E. J. Kim, T. Nakamura, A. Konno, Y. Uwamino, N. Nakanishi, M. Imamura, N. Nakao, S. Shibata and S. Tanaka, Measurements of neutron spallation cross sections of ^{12}C and ^{209}Bi in the 20- to 150-MeV energy range, *Nucl. Sci. Eng.* 129, (1998), pp. 209-223.

[4] E. J. Kim, T. Nakamura, Y. Uwamino, N. Nakanishi, M. Imamura, N. Nakao, S. Shibata and S. Tanaka, Measurements of activation cross sections on spallation reactions for ^{59}Co and ^{nat}Cu at incident neutron energies of 40 to 120 MeV, *J. Nucl. Sci. Technol.* 36 (1999), pp. 29-40.

[5] S. Sekimoto, T. Utsunomiya, H. Yashima, K. Ninomiya, T. Omoto, R. Nakagaki, T. Shima, N. Takahashi, A. Shinohara, N. Kinoshita, H. Matsumura, D. Satoh, Y. Iwamoto, M. Hagiwara, K. Nishiizumi and S. Shibata, Measurement of Neutron Cross Sections for Yttrium and Terbium at 287 MeV, *Prog. Nucl. Sci. Technol.* 1 (2011), pp. 89-93.

[6] K. Ninomiya, T. Omoto, R. Nakagaki, N. Takahashi, A. Shinohara, S. Sekimoto, T. Utsunomiya, H. Yashima, S. Shibata, T. Shima, N. Kinoshita, H. Matsumura, M. Hagiwara, Y. Iwamoto, D. Satoh, M. W. Caffee, K. C. Welten, M. Imamura and K. Nishiizumi, Cross sections of ^{7}Be, ^{22}Na and ^{24}Na for geochemical and cosmochemical important elements by monoenergetic 287 and 370 MeV neutrons, *Proc. Radiochim. Acta* 1 (2011), pp. 123-126.

[7] H. Yashima, S. Sekimoto, T. Utsunomiya, K. Ninomiya, T. Omoto, R. Nakagaki, T. Shima, N. Takahashi, A. Shinohara, H. Matsumura, D. Satoh, Y. Iwamoto, M. Hagiwara, K. Nisiizumi and S. Shibata, Measurements of the neutron activation cross sections for Bi at 287 and 370 MeV, *Proc. Radiochim. Acta* 1 (2011), pp. 135-139.

[8] J. M. Sisterson, F. D. Brooks, A. Buffler, M. S. Allie, D.T. L. Jones and M. B. Chadwick, Cross-section measurements for neutron-induced reactions in copper at neutron energies of 70.7 and 110.8 MeV, *Nucl. Instrum. Methods Phys. Res. B* 240 (2005), pp. 617-624.

[9] S. Sekimoto, T. Utsunomiya, H. Yashima, H. Joto, S. Shibata, K. Ninomiya, D. Satoh, Y. Iwamoto, T. Omoto, R. Nakagaki, N. Takahashi, A. Shinohara, T. Shima, M. Hagiwara, H. Matsumura, K. Nishiizumi, Y. Matsushi and H. Matsuzaki, Measurement of High Energy Neutron Induced Cross Sections for Chromium, *J. Korean Phys. Soc.* 59 (2011), pp. 1916-1919.

[10] W. R. Nelson, H. Hirayama and D. W. O. Rogers, “The EGS4 code system” , SLAC-265, Stanford linear Accelerator Center, Stanford University, (1985).

[11] K. Niita, N. Matsuda, Y. Iwamoto, H. Iwase, T. Sato, H. Nakashima, Y. Sakamoto and L. Sihver, *PHITS: Particle and Heavy Ion Transport code System, Version 2.23,* JAEA-Data/Code 2010-022, Japan Atomic Energy Agency, (2010).

国際単位系（SI）

表１．SI 基本単位

基本量	SI 基本単位	
	名称	記号
長さ	メートル	m
質量	キログラム	kg
時間	秒	s
電流	アンペア	A
熱力学温度	ケルビン	K
物質量	モル	mol
光度	カンデラ	cd

表２．基本単位を用いて表されるSI組立単位の例

組立量	SI 基本単位	
	名称	記号
面積	平方メートル	m^2
体積	立法メートル	m^3
速さ，速度	メートル毎秒	m/s
加速度	メートル毎秒毎秒	m/s^2
波数	毎メートル	m^{-1}
密度，質量密度	キログラム毎立方メートル	kg/m^3
面積密度	キログラム毎平方メートル	kg/m^2
比体積	立方メートル毎キログラム	m^3/kg
電流密度	アンペア毎平方メートル	A/m^2
磁界の強さ	アンペア毎メートル	A/m
量濃度(a)，濃度	モル毎立方メートル	mol/m^3
質量濃度	キログラム毎立法メートル	kg/m^3
輝度	カンデラ毎平方メートル	cd/m^2
屈折率(b)	（数字の） 1	1
比透磁率(b)	（数字の） 1	1

(a) 量濃度（amount concentration）は臨床化学の分野では物質濃度（substance concentration）ともよばれる。
(b) これらは無次元量あるいは次元１をもつ量であるが、そのことを表す単位記号である数字の１は通常は表記しない。

表３．固有の名称と記号で表されるSI組立単位

組立量	SI 組立単位			
	名称	記号	他のSI単位による表し方	SI基本単位による表し方
平面角	ラジアン(b)	rad	1 (b)	m/m
立体角	ステラジアン(b)	sr(c)	1 (b)	m^2/m^2
周波数	ヘルツ(d)	Hz		s^{-1}
力	ニュートン	N		m kg s^{-2}
圧力，応力	パスカル	Pa	N/m^2	m^{-1} kg s^{-2}
エネルギー，仕事，熱量	ジュール	J	N m	m^2 kg s^{-2}
仕事率，工率，放射束	ワット	W	J/s	m^2 kg s^{-3}
電荷，電気量	クーロン	C		s A
電位差（電圧），起電力	ボルト	V	W/A	m^2 kg s^{-3} A^{-1}
静電容量	ファラド	F	C/V	m^{-2} kg^{-1} s^4 A^2
電気抵抗	オーム	Ω	V/A	m^2 kg s^{-3} A^{-2}
コンダクタンス	ジーメンス	S	A/V	m^{-2} kg^{-1} s^3 A^2
磁束	ウエーバ	Wb	Vs	m^2 kg s^{-2} A^{-1}
磁束密度	テスラ	T	Wb/m^2	kg s^{-2} A^{-1}
インダクタンス	ヘンリー	H	Wb/A	m^2 kg s^{-2} A^{-2}
セルシウス温度	セルシウス度(e)	℃		K
光束	ルーメン	lm	cd sr(c)	cd
照度	ルクス	lx	lm/m^2	m^{-2} cd
放射性核種の放射能(f)	ベクレル(d)	Bq		s^{-1}
吸収線量, 比エネルギー分与, カーマ	グレイ	Gy	J/kg	m^2 s^{-2}
線量当量, 周辺線量当量, 方向性線量当量, 個人線量当量	シーベルト(g)	Sv	J/kg	m^2 s^{-2}
酸素活性	カタール	kat		s^{-1} mol

(a)SI接頭語は固有の名称と記号を持つ組立単位と組み合わせても使用できる。しかし接頭語を付した単位はもはやコヒーレントではない。
(b)ラジアンとステラジアンは数字の１に対する単位の特別な名称で、量についての情報をつたえるために使われる。実際には、使用する時には記号radおよびsrが用いられるが、習慣として組立単位としての記号である数字の１は明示されない。
(c)測光学ではステラジアンという名称と記号srを単位の表し方の中に、そのまま維持している。
(d)ヘルツは周期現象についてのみ、ベクレルは放射性核種の統計的過程についてのみ使用される。
(e)セルシウス度はケルビンの特別な名称で、セルシウス温度を表すために使用される。セルシウス度とケルビンの単位の大きさは同一である。したがって、温度差や温度間隔を表す数値はどちらの単位で表しても同じである。
(f)放射性核種の放射能（activity referred to a radionuclide）は、しばしば誤った用語で"radioactivity"と記される。
(g)単位シーベルト（PV,2002,70,205）についてはCIPM勧告2（CI-2002）を参照。

表４．単位の中に固有の名称と記号を含むSI組立単位の例

組立量	SI 組立単位		
	名称	記号	SI 基本単位による表し方
粘度	パスカル秒	Pa s	m^{-1} kg s^{-1}
力のモーメント	ニュートンメートル	N m	m^2 kg s^{-2}
表面張力	ニュートン毎メートル	N/m	kg s^{-2}
角速度	ラジアン毎秒	rad/s	m m^{-1} s^{-1}=s^{-1}
角加速度	ラジアン毎秒毎秒	rad/s^2	m m^{-1} s^{-2}=s^{-2}
熱流密度，放射照度	ワット毎平方メートル	W/m^2	kg s^{-3}
熱容量，エントロピー	ジュール毎ケルビン	J/K	m^2 kg s^{-2} K^{-1}
比熱容量，比エントロピー	ジュール毎キログラム毎ケルビン	J/(kg K)	m^2 s^{-2} K^{-1}
比エネルギー	ジュール毎キログラム	J/kg	m^2 s^{-2}
熱伝導率	ワット毎メートル毎ケルビン	W/(m K)	m kg s^{-3} K^{-1}
体積エネルギー	ジュール毎立方メートル	J/m^3	m^{-1} kg s^{-2}
電界の強さ	ボルト毎メートル	V/m	m kg s^{-3} A^{-1}
電荷密度	クーロン毎立方メートル	C/m^3	m^{-3} sA
表面電荷	クーロン毎平方メートル	C/m^2	m^{-2} sA
電束密度，電気変位	クーロン毎平方メートル	C/m^2	m^{-2} sA
誘電率	ファラド毎メートル	F/m	m^{-3} kg^{-1} s^4 A^2
透磁率	ヘンリー毎メートル	H/m	m kg s^{-2} A^{-2}
モルエネルギー	ジュール毎モル	J/mol	m^2 kg s^{-2} mol^{-1}
モルエントロピー, モル熱容量	ジュール毎モル毎ケルビン	J/(mol K)	m^2 kg s^{-2} K^{-1} mol^{-1}
照射線量（X線及びγ線）	クーロン毎キログラム	C/kg	kg^{-1} sA
吸収線量率	グレイ毎秒	Gy/s	m^2 s^{-3}
放射強度	ワット毎ステラジアン	W/sr	m^4 m^{-2} kg s^{-3}=m^2 kg s^{-3}
放射輝度	ワット毎平方メートル毎ステラジアン	$W/(m^2$ sr)	m^2 m^{-2} kg s^{-3}=kg s^{-3}
酵素活性濃度	カタール毎立方メートル	kat/m^3	m^{-3} s^{-1} mol

表５．SI 接頭語

乗数	接頭語	記号	乗数	接頭語	記号
10^{24}	ヨタ	Y	10^{-1}	デシ	d
10^{21}	ゼタ	Z	10^{-2}	センチ	c
10^{18}	エクサ	E	10^{-3}	ミリ	m
10^{15}	ペタ	P	10^{-6}	マイクロ	μ
10^{12}	テラ	T	10^{-9}	ナノ	n
10^9	ギガ	G	10^{-12}	ピコ	p
10^6	メガ	M	10^{-15}	フェムト	f
10^3	キロ	k	10^{-18}	アト	a
10^2	ヘクト	h	10^{-21}	ゼプト	z
10^1	デカ	da	10^{-24}	ヨクト	y

表６．SIに属さないが、SIと併用される単位

名称	記号	SI 単位による値
分	min	1 min=60s
時	h	1h =60 min=3600 s
日	d	1 d=24 h=86 400 s
度	°	1°=(π/180) rad
分	’	1’=(1/60)°=(π/10800) rad
秒	”	1”=(1/60)’=(π/648000) rad
ヘクタール	ha	$1ha=1hm^2=10^4m^2$
リットル	L, l	$1L=11=1dm^3=10^3cm^3=10^{-3}m^3$
トン	t	$1t=10^3$ kg

表７．SIに属さないが、SIと併用される単位で、SI単位で表される数値が実験的に得られるもの

名称	記号	SI 単位で表される数値
電子ボルト	eV	$1eV=1.602\ 176\ 53(14)\times10^{-19}J$
ダルトン	Da	$1Da=1.660\ 538\ 86(28)\times10^{-27}kg$
統一原子質量単位	u	1u=1 Da
天文単位	ua	$1ua=1.495\ 978\ 706\ 91(6)\times10^{11}m$

表８．SIに属さないが、SIと併用されるその他の単位

名称	記号	SI 単位で表される数値
バール	bar	1 bar=0.1MPa=100kPa=10^5Pa
水銀柱ミリメートル	mmHg	1mmHg=133.322Pa
オングストローム	Å	1 Å=0.1nm=100pm=10^{-10}m
海里	M	1 M=1852m
バーン	b	$1\ b=100fm^2=(10^{-12}cm)2=10^{-28}m^2$
ノット	kn	1 kn=(1852/3600)m/s
ネーパ	Np	SI単位との数値的な関係は、対数量の定義に依存。
ベル	B	
デジベル	dB	

表９．固有の名称をもつCGS組立単位

名称	記号	SI 単位で表される数値
エルグ	erg	$1\ erg=10^{-7}$ J
ダイン	dyn	$1\ dyn=10^{-5}$N
ポアズ	P	1 P=1 dyn s cm^{-2}=0.1Pa s
ストークス	St	1 St =$1cm^2$ s^{-1}=$10^{-4}m^2$ s^{-1}
スチルブ	sb	1 sb =1cd cm^{-2}=10^4cd m^{-2}
フォト	ph	1 ph=1cd sr cm^{-2} 10^4lx
ガル	Gal	1 Gal =1cm s^{-2}=$10^{-2}ms^{-2}$
マクスウェル	Mx	1 Mx = 1G cm^2=10^{-8}Wb
ガウス	G	1 G =1Mx cm^{-2} =10^{-4}T
エルステッド(c)	Oe	1 Oe≙ $(10^3/4\pi)$A m^{-1}

(c) ３元系のCGS単位系とSIでは直接比較できないため、等号「 ≙ 」は対応関係を示すものである。

表10．SIに属さないその他の単位の例

名称	記号	SI 単位で表される数値
キュリー	Ci	$1\ Ci=3.7\times10^{10}Bq$
レントゲン	R	$1\ R = 2.58\times10^{-4}C/kg$
ラド	rad	$1\ rad=1cGy=10^{-2}Gy$
レム	rem	$1\ rem=1\ cSv=10^{-2}Sv$
ガンマ	γ	1γ=1 nT=10-9T
フェルミ		1フェルミ=1 fm=10-15m
メートル系カラット		1メートル系カラット = 200 mg = 2×10-4kg
トル	Torr	1 Torr = (101 325/760) Pa
標準大気圧	atm	1 atm = 101 325 Pa
カロリー	cal	1cal=4.1858J（「15℃」カロリー），4.1868J（「IT」カロリー）4.184J（「熱化学」カロリー）
ミクロン	μ	1 μ =1μm=10^{-6}m

（第8版，2006年改訂）

この印刷物は再生紙を使用しています